CORROSION CELL FORMATION ON A BAR EMBEDDED IN CONCRETE EXPOSED TO CHLORIDES

A Thesis

Submitted to the College of Graduate Studies and Research

In Partial Fulfillment of the Requirements

for the

Degree of Doctor of Philosophy

in the

Department of Civil and Geological Engineering

University of Saskatchewan

Saskatoon

By

James Anthony Zacaruk

PERMISSION TO USE

In presenting the thesis in partial fulfillment of the requirements for a postgraduate degree from the University of Saskatchewan, I agree that the libraries of this University may make it freely available for inspection. I further agree that permission for copying of this thesis in any manner, in whole or in part, for scholarly purposes may be granted by the professor who supervised my thesis work or, in his absence, by the Head of the Department or the Dean of the College in which my thesis work was done. It is understood that any copying or publication or use of this thesis or parts thereof for financial gain shall not be allowed without my written permission. It is also understood that due recognition shall be given to me and to the University of Saskatchewan in any scholarly use which may be made of any material in my thesis.

Requests for permission to copy or to make other use of material in this thesis in whole or part shall be addressed to:

Head of the Department of Civil and Geological Engineering
University of Saskatchewan
Saskatoon, Saskatchewan, S7N 5A9, Canada

ABSTRACT

This thesis investigated corrosion of a reinforcing steel bar embedded in concrete and the effect of corrosion coupling on the bar/concrete interface induced by the variation of corrosion potentials with concrete depth. Two separate numerical models were used to simulate the corrosion process which included: a two-dimensional finite element model for mass transport of oxygen and chloride to the bar/concrete interface; and, a one-dimensional model for the corrosion current flow through the electrolyte induced by corrosion potential differences on the bar/concrete interface.

A novel approach to corrosion modeling in reinforced concrete that had not been identified in the literature was used. This new approach, incorporated: variable solution conductivity developed from concentrations within the pore solution; anodic and cathodic areas modified to maximize corrosion current through the electrolyte; and, kinetics of corrosion set by the pore solution chemistry.

Various reinforcing configurations and moisture conditions were evaluated within the simulation to obtain insight into the effect these variables have on corrosion potentials measured on the concrete surface and the corresponding corrosion currents generated on the bar/concrete interface. Variables related to bar diameter, concrete cover, and bar spacing where all shown to affect corrosion potentials and current densities on the bar/concrete interface and the concrete surface where field measurements are obtained.

Moisture conditions were found to have the largest impact on corrosion potentials and current density's on the bar/concrete interface. When relative humidity's of 90% or higher were used, simulated corrosion potentials on the concrete surface under high chloride conditions were found to reach values identified in ASTM C876 and Alberta Transportations Deck Testing Guidelines that indicate active corrosion. However, when moisture conditions were reduced to below 90% relative humidity, simulated corrosion potentials on the concrete surface for high chloride concentrations did not achieve values that indicate a high probability of corrosion. This result suggests a secondary mechanism must be present on the bar/concrete interface that changes the chemical composition within the pore solution to shift the kinetics of corrosion to an environment that will produce the negative corrosion potentials recognized as indicating a high probability of corrosion.

Therefore, a new mechanism is proposed that outlines the process necessary for the pore solution on the bar/concrete interface to transition the kinetics of corrosion to an actively corroding state at low relative humidity. This mechanism requires local acidification of the pore solution along portions of the bar where anodic processes are increased due to the presence of chloride and reduced oxygen availability. Reaching this environment requires free OH^- to be consumed without replenishment from the surrounding environment by either diffusion from high pH areas or dissolution of the hardened portions of the pore structure. The proposed mechanism begins with corrosion by-products formed when Fe^{2+} reacts with free OH^-, precipitates from the pore solution onto the pore structure as $Fe(OH)_2$. Once precipitated, the contact area between pore solution and hardened portions of the pore structure are reduced which restricts the dissolution process for restoring OH^- removed from the electrolyte. Additionally, precipitation of $Fe(OH)_2$ reduces the flow of OH^- from the surrounding high pH zones as the pore structure is restricted. Both mechanisms result in a pH gradient being formed with acidified zones created on the bar/concrete interface in the anodic regions. These acidified zones cause the kinetics of corrosion to transition from a passivated state, towards an environment similar to carbonation.

ACKNOWLEDGEMENTS

I wish to express my appreciation to my supervisors and committee members, Dr. Bruce Sparling, Dr. Lisa Feldman, Dr. Gordon Sparks, Dr. Richard Evitts, and Dr. Moh Boulfiza for their invaluable guidance, suggestions, encouragement, and continuous assistance throughout the present study.

Also, I would like to express my deepest and sincerest gratitude to my family, especially my wife, Kim Zacaruk, who put up with my life goal of learning for the fun of learning.

TABLE OF CONTENTS

LIST OF TABLES

LIST OF FIGURES

LIST OF SYMBOLS

A	Amps or concentration of reactant in mol/m^3.
A_{bar}	Area of the bar surface (mm^2).
a	Stoichiometric coefficient of species A or aggregate content (kg/m^3).
a_i	Fitting parameters.
B_L	Width of element (mm).
B	Concentration of reactant B in mol/m^3.
b	Stoichiometric coefficient of species B.
b_i	Fitting parameters.
C	Concentration of a species within the electrolyte or concentration of the product (mol/mm^3).
C^*	Oxygen solubility (mol/kg) at 1 atm of pressure.
C_{bc}	Concentration of bound chloride.
C_f	Concentration of free chloride within the pore electrolyte.
C_i	Concentration of species i in the electrolyte (mol/mm^3).
$Cl_{decanted}$	Chloride concentration in the bulk concrete in percent by weight of cement.
$Cl_{expressed}$	Chloride concentration in the pore solution (mmol/mm^3).
C_{O_2}	Oxygen concentration on the concrete surface or bulk electrolyte above the diffusion layer (mol/mm^3).
c	Stoichiometric coefficient of species C, or cement content (kg/m^3).
c_i	Fitting parameters.
c_{g,O_2}	Oxygen concentration in the gas phase (mol/mm^3).
c_{mg,O_2}	Oxygen concentration in the gas phase converted to the total material volume (mol/mm^3).
c_l	Oxygen concentration in the liquid phase (mol/mm^3).
c_{ml}	Oxygen concentration in the liquid phase converted to the total material volume (mol/mm^3).
D	Diffusion coefficient in mm^2/s or concentration of reactant D in mol/m^3.
d	Stoichiometric coefficient of species D or concrete cover thickness in metres.
d_x	Control volume width along the circumference of the reinforcing steel bar (mm).
d_y	Control volume width along the longitudinal axis of the reinforcing steel bar (mm).
d_z	Control volume width perpendicular to the reinforcing steel bar (mm).

D_C	Chloride diffusion coefficient (mm^2/s).
$D_{C,rev,\infty}$	Chloride diffusion coefficient (mm^2/s).
D_{O_2}	Oxygen diffusion coefficient (mm^2/s).
D_{d,O_2}	Dissolved oxygen diffusion coefficient (mm^2/s).
D_{g,O_2}	Gaseous oxygen diffusion coefficient (mm^2/s).
D_{H_2O}	Oxygen diffusion coefficient of chloride in an infinite solution (1.6×10^{-3} mm^2/s for NaCl).
D_i	Diffusion coefficient of species i (mm^2/s).
D_j	Diffusion coefficient of species j (mm^2/s).
E	Apparent activation energy (KJ/mol).
e_{pp}	Primary passive potential (V).
e_{rev}	Reversible corrosion potential at a specific temperature and species concentration (V).
e^o_{rev}	Reversible corrosion potential of the reaction at standard temperature and species concentration of unity (V).
$e_{n,coupled,overpotential}$	Coupled corrosion potential evaluated at the bar/concrete interface at segment n (V).
$e_{n,coupled,solution}$	Coupled corrosion potential evaluated through the solution at segment n (V).
$e_{n,uncoupled}$	Uncoupled corrosion potential at segment n (V).
$e_{transition}$	Uncoupled corrosion potential at the transition point between the cathodic and anodic zones (V).
$\Delta e_{i,j}$	Potential difference between elements i and j (Volts).
Δe_{corr}	Maximum corrosion potential difference between the uncoupled anodic and cathodic zones (Volts).
F	Faraday's constant = 96,485 C/mol.
$F_1(h)$	Chloride diffusion coefficient modification factor for relative humidity.
$F_2(T)$	Chloride diffusion coefficient modification factor for temperature.
$F_3(t)$	Chloride diffusion coefficient modification factor for age.
g	Oxygen consumption rate on the bar/concrete interface $mol/m^2/s$, or a coefficient represented by Equation 2.30.
g_{blend}	Blended oxygen consumption rate on the bar/concrete interface $mol/m^2/s$.
g_{new}	New oxygen consumption rate on the bar/concrete interface $mol/m^2/s$.
g_{old}	Old oxygen consumption rate on the bar/concrete interface $mol/m^2/s$.
$g_{original}$	Original oxygen consumption rate on the bar/concrete interface $mol/m^2/s$.
h	Constants of the Freundlich isotherms represented by Equation 2.31, or relative humidity as a value between 0 and 1.

h_c	Material parameter for developing the modification factor $F_1(h)$.
H	Henry's constant.
H_{O_2}	Henry's constant for dissolved oxygen in an electrolyte.
i	Current density (A/mm^2), current flow through the electrolyte (A/mm^2), or element.
i_{anode}	Incremental corrosion current density created due to coupling in the anodic zone (A/mm^2).
$i_{coupled}$	Total corrosion current density created due to coupling in the anodic zone (A/mm^2).
i_{crit}	Critical corrosion current density (A/mm^2).
i_{corr}	Corrosion current density (A/mm^2).
i_{lim}	Limiting corrosion current density (A/mm^2).
$i_{microcell}$	Corrosion current density for a microcell corrosion cell (A/mm^2).
i_{pass}	Passive corrosion current density (A/mm^2).
$i_{uncoupled}$	Uncoupled corrosion current (A/mm^2).
Δi_n	Corrosion current contribution from each control segment (A/mm^2).
J_{O_2}	Dissolved oxygen flux (g/mm^2).
j	Species under consideration, or element.
k_{adj}	Modification factor used to adjust the oxygen consumption rate on the bar/concrete interface.
l_m	Free path length of a molecule of gas (m).
ΔL_i	Length of element i (mm).
ΔL_j	Length of element j (mm).
$\Delta L_{i,j}$	Distance between element i and element j (mm).
M_{O_2}	Molecular density of oxygen (32 g/mol).
m	Stoichiometric constant for H^+, or number of species in electrolyte.
N	Counter used in the algorithms.
N_k	Knudsen number.
n	Number of electrons transferred in the half-cell reaction.
n_h	Material parameter for developing the modification factor $F_1(h)$.
n_i	Number of electrons transferred in the half-cell reaction for species i.
n_j	Number of electrons transferred in the half-cell reaction for species j.
n_{O_2}	Number of electrons transferred when oxygen is reduced to OH^- (4).
O_2	Oxygen.

$[O_{2_d}]$	Concentration of oxygen in the dissolved phase (mol/mm^3).
$[O_{2_g}]$	Concentration of oxygen in the gaseous phase (mol/mm^3).
$[O_2]_d$	Concentration of dissolved oxygen within the pore solution within the pore phase of the concrete (mol/mm^3).
$[O_2]_{bulk}$	Concentration of oxygen within the concrete including both solid and pore phases (mol/mm^3).
PS	Degree of pore saturation.
P_{O_2}	Partial pressure of oxygen in the gaseous phase.
P_v	Pore volume per m^3 of concrete.
Q_{O_2}	Sink term representing the consumption of oxygen on the corroding surface (mol/mm^2).
R	Universal gas constant = 8.314 J/K/mol, or reaction term.
RH	Relative humidity in percent.
r_e	Actual pore radius minus the thickness of the adsorbed water (m).
S	Salinity of the total quantity of dissolved solids (g/kg).
S_r	Degree of water saturation.
$S_{g,c}$	Specific gravity of cement.
$S_{g,a}$	Specific gravity of aggregate.
T	Temperature in Kelvin.
T_{ref}	Reference curing temperature in Kelvin.
t	Age of concrete in days or time.
V_{elem}	Referential finite volume (mm^3).
w	Specific resistance of concrete (ohms).
w/c	Water to cement ratio.
Greek Letters	
β_3	Material parameter for developing the modification factor $F_3(t)$.
γ	Material parameter for developing the modification factor $F_1(h)$.
ε_c	Concrete porosity.
ε_e	Electrolyte permittivity (Farad/m).
κ	Solution conductivity (1/Ω)
μ_i	Ionic mobility of species i (m^{2}mol/J/s).
μ_j	Ionic mobility of species j (m^{2}mol/J/s).
μ_v	Darcy's velocity.
ρ_{gO_2}	Density of gaseous oxygen (g/mm^3).

ρ_{dO_2}	Density of dissolved oxygen (g/mm^3).
Φ	Porosity in percent, or potential difference between two locations (V).
Φ_{Anode}	Overpotential at the anode (V).
$\Phi_{Cathode}$	Overpotential at the cathode (V).
$\Phi_{conc,Anode}$	Concentration potential drop through the electrolyte within the anode (V).
$\Phi_{conc,Cathode}$	Concentration potential drop through the electrolyte within the cathode (V).
Φ_n	Overpotential created by coupling (V).
Φ_Ω	Ohmic potential drop through the electrolyte (V).
$\Phi_{\Omega,j}$	Ohmic potential drop through the electrolyte at segment j (V).
$\Phi_{\Omega,Anode}$	Ohmic potential drop through the electrolyte within the anode (V).
$\Phi_{\Omega,Cathode}$	Ohmic potential drop through the electrolyte within the cathode (V).
Φ_w	Water saturated porosity in percent.
Ω	Resistance (ohms).
Ω_1	Coefficient that accounts for the average tortuosity of a single pore which is set to be $(\pi/2)^2$.

Subscripts/Superscripts

a	Anode.
c	Cathode.
i	Chemical species or reaction.
j	Chemical species.

LIST OF ABBREVIATIONS

ASTM	American Society of Testing and Materials
AT	Alberta Transportation
BFSC	Blast Furnace Slag Cement
CSE	Copper Sulfate Electrode
CHBDC	Canadian Highway Bridge Design Code
HSC	High Strength Concrete
MSC	Medium Strength Concrete
OPC	Ordinary Portland Cement
PD	Pourbaix Diagram
PMA	Polymer Modified Asphalt
SCE	Saturated Calomel Electrode
SHE	Standard Hydrogen Electrode

1 INTRODUCTION

1.1 Background

A recent report published by Transportation for America (Shoup et al. 2011) stated that 1 in 9 bridge structures in the United States of America have sustained a major defect requiring closure, significant maintenance, rehabilitation, or replacement of one of the major components. Combined with these structural deficiencies, the inventory's average age is reaching the nominal design life of 50 years. To combat this situation, significant funds have been invested in repair, rehabilitation, and replacement but, despite this, it is generally conceded that current efforts are not sufficient to meet future replacement or expansion needs.

In Canada, the Council of Ministers publishes an annual report on the state of the National Highway System (Canadian Council of Ministers Responsible for Transportation and Highway Safety, 2012). The most recent annual report identified that, between 2006 and 2011, the number of structures less than 10 years old increased by 50% while the number of bridges older than 50 years increased by 60%. Similar to the United States, it would appear that Canada's infrastructure replacement policy is unable to keep pace at current funding levels.

These statistics suggest the model currently used for funding and assessment of existing infrastructure is unsustainable. Therefore, if funding levels cannot increase, opportunities exist for developing improved methods related to:

- Construction materials and techniques for new structures or the rehabilitation of existing infrastructure to increase the expected life of the facility; and
- Alternative assessment and prediction methods that increase our understanding of the deterioration process in order that the remaining service life of existing infrastructure can be extended.

In Canada, most jurisdictions have adopted the Canadian Highway Bridge Design Code (CHBDC) and referenced standards for the design of new or replacement transportation infrastructure. This code employs detailed mechanistic models for assessing vehicle loads and component capacities to support these loads. Durability aspects of the design, however, employ a "deemed to comply" methodology that is based on empirical evidence obtained from in-service structures rather than mechanistic models that simulate physical and chemical

processes that may be present at a particular site (fib bulletin 34, 2006). The deemed-to-comply methodology essentially states that, if minimum code requirements are met related to cover and concrete type, that the structure will achieve the expected design life, which, for Canadian structures, is 75 years.

CHBDC requirements are intended to produce a long-lasting, durable design for new and rehabilitated structures. However, the CHBDC does not provide extensive guidance to the designer for determining the extent of a rehabilitation or maintenance plan given visual or test data obtained from a particular site. Therefore, transportation authorities have developed guidelines for inspection and testing to ensure public safety and to gather relevant information that can be used to minimize the life cycle cost of their inventory. Most jurisdictions use the results of their testing program immediately prior to the rehabilitation in order to confirm quantities and extent of repair (Alberta Transportation 2007). However, since 1977, Alberta Transportation (AT) has been using data collected from their testing program to develop service life estimates and predict the effect different levels of repair could have on the service life of an element (Skeet et al. 1994). These models rely exclusively on corrosion potential testing as a key indicator of when a rehabilitation or repair should be scheduled.

AT's model has been used in other jurisdictions by the author, specifically for the City of Saskatoon and City of Regina, on various bridge rehabilitations conducted over the past 15 years. Observations from these rehabilitations indicate that, while test data suggests the deck is heavily corroding, once the concrete covering the reinforcing steel was removed, minimal corrosion was observed. This outcome implies that the AT model for corrosion potential prediction may only be relevant to the structures and environment for which it was developed. However, if the underlying corrosion principles that create the measured corrosion potentials could be understood, a mechanistic model for predicting corrosion potentials for various bridge configurations and environments could be developed for use in any jurisdiction.

Several efforts have been expended in developing mechanistic models for describing the corrosion processes on the bar/concrete interface (Maruya et al. 2007,Isgor and Razaqpur 2006a and 2006b, Hussain and Ishida 2010a, Soleimani et al. 2010). Each of these models were successfully validated against laboratory test data; however, both the test and simulation limited the environmental conditions experienced on the bar/concrete interface by simplifying:

- Electrolyte chemistry so that chlorides were uniform around the bar circumference but variable along the length (Hussain and Ishida 2010, Soleimani et al. 2010); and

- Model geometry to limit mass transport of oxygen and chloride to the corroding surface in one dimension (Isgor and Razaqpur 2006, Maruya et al. 2007, and Soleimani et al. 2010).

Both of these simplifications limited coupling between points on the bar induced by variations in corrosion potential to the longitudinal axis of the bar.

These assumptions employed in the development of the preceding models are not consistent with some field observations such as that shown in Figure 1.1, which shows exposed reinforcing steel located on the splash side of a concrete barrier from the Arcola Avenue Overpass in Regina, Saskatchewan. The unique aspect of this photograph is that it was taken immediately following removal of the concrete, thereby creating a snapshot of the corrosion conditions around the bar without these conditions being influenced by atmospheric corrosion. This photo exhibits several corrosion characteristics that current models do not address, such as:

- Concentration of corrosion by-product at the bar face closest to the concrete surface;

- Corrosion by-product present at the interface between horizontal and vertical reinforcement; and

- Limited corrosion by-product evident on sides of the vertical bar even though chlorides have reached the deeper horizontal bar, as evident by the visual signs of corrosion.

Similar observations to the corrosion features identified in Figure 1.1 have been identified in carbonation research where bars embedded in carbonated concrete were extracted, with the visual evidence of corrosion limited to the side closest to the surface where carbonation originated (Ji et al. 2011). Additionally, research conducted in chloride-induced corrosion of prestressing steel strand observed localized corrosion at contact points between individual strands even when chlorides had encapsulated the entire cable (Moser et al. 2011).

The most common method for monitoring the condition of a reinforced concrete element is the half-cell or corrosion potential test which measures the corrosion potential of the bar below the concrete surface by placing a reference half-cell on the concrete surface. Recorded values are used as an indication of corrosion occurring at the bar/concrete interface and, as such, are believed to provide a powerful predictive tool for scheduling interventions. However, the corrosion potential results recorded at the concrete surface can produce misleading results as current practices do not address variability introduced by concrete cover, bar diameter, bar spacing, or moisture conditions within the concrete, nor do they consider the kinetics of corrosion created by the materials employed, the geometric conditions, or the changing

Figure 1.1. Exposed reinforcing steel from a concrete barrier.

electrolyte chemistry as corrosion by-products are produced.

Current reinforced concrete corrosion models can simulate the complex corrosion geometry observed in the field by adopting techniques developed from research related to crevice corrosion, given that many similarities exist between these two forms of corrosion due to diffusion barriers that:

- Limit the movement of oxygen to portions of the corroding surface, thereby creating corrosion potential differences between discrete points on the same surface; and

- Delay the arrival of chlorides to the corroding surface, thereby creating a variable chemical composition within the electrolyte at different points on the same surface.

Once built and validated, this mechanistic corrosion model will enable bridge engineers to understand the corrosion processes occurring on a bar embedded in concrete. With this improved understanding, the potential exists to implement these findings for:

- New and rehabilitation work to improve the corrosion durability of corrodible materials; and

- Assessments of existing infrastructure to potentially delay major rehabilitation if alternative forms of maintenance can be implemented.

1.2 Objectives

The main objective of this research is to develop a multi-mechanistic model for predicting the evolution of corrosion potentials on a bar embedded in concrete as chlorides diffuse to the bar/concrete interface that will simulate:

- The transport of chloride to the bar/concrete interface, creating a variable chloride concentration around the bar with higher concentrations initially occurring at the bar surface closest to the concrete surface;

- Transport of oxygen under different boundary conditions on the bar/concrete interface caused by kinetics of corrosion established by the electrolyte chemistry;

- Modification of the anodic and cathodic half-cell processes on the bar surface according to the kinetics of corrosion and corrosion potential differences created by the varying

concentrations of chloride and oxygen within the electrolyte around the bar circumference; and

- Current flow through the electrolyte to complete the corrosion cell circuit formed on the bar/concrete interface.

This mechanistic model will permit detailed simulations to be conducted that will allow investigation into:

- Corrosion cell development on the bar/concrete interface and whether corrosion potential differences of sufficient magnitude are created to cause current flow through the pore solution;

- Development of spatially separated cathodic and anodic half-cell processes on the bar circumference and the relative size of each contributing half-cell;

- The influence of system geometry such as bar spacing, cover, and bar diameter, along with moisture conditions, on the corrosion processes occurring on the bar/concrete interface and the resulting corrosion potentials measured on the concrete surface; and

- The mechanisms that cause localized high corrosion rates resulting in damaging formation of corrosion by-product.

1.3 Contributions to Original Knowledge

The creation and development of the multi-mechanistic corrosion model described previously enabled detailed study of the corrosion processes occurring on the bar/concrete interface. Results from this study have identified unique aspects of the corrosion process for a reinforcing steel bar embedded in concrete that have not been reported in previous studies which include:

- Spatially separated corrosion cells can be produced on the bar circumference which create current flow through the connecting pore solution. The resulting configuration closely matches field observed corrosion patterns;

- A unique methodology for identifying the size of the anode and cathode was developed and implemented in the model created as part of this study. Included was a unique approach for simulating current flow through the pore solution which allowed portions of

the bar circumference to decouple when current flows produced potential drops through the electrolyte that exceeded the corrosion potential differences present;

- The influence of system geometry such as cover, bar spacing, and bar diameter on the development and formation of corrosion potentials on the bar/concrete interface and concrete surface; and

- A mechanism for describing the changes to pore solution chemistry which cause the kinetics of corrosion for reinforcing steel embedded in concrete to transition from an initial high alkalinity state to a localized acidified state. Past studies have set this transition based on a chloride concentration level which has been shown in this study to be dependent on the system geometry and the chemical equilibrium between the pore solution and hardened pore structure.

1.4 Scope and Methodology

The current research is focused on developing a numerical model that simulates the corrosion processes occurring on a bar embedded in concrete subjected to various chloride and oxygen concentrations within the concrete pore solution. Initially, the model focuses on uncoated, smooth reinforcing steel bars embedded in concrete that is not protected from chloride ingress with membranes, sealers, or concrete overlays. However, these features can be easily added.

The model was developed using principles of corrosion that describe crevice corrosion and calibrated using test data obtained from electrochemical studies of reinforcing steel in simulated concrete pore solutions. Two distinct models are required to describe the processes occurring on the bar surface. The first simulates the transport of chloride and oxygen to the bar/concrete interface while the second simulates the electrochemistry, corrosion potential drops, and current flow through the electrolyte on the bar surface. Simulation results produced by this model are compared to the relevant standards and experiences obtained by the author from in-service bridge structures.

1.5 Layout of the Thesis

This thesis is organized into six chapters with additional information provided in the appendices. A brief outline of each chapter is described below.

This chapter presents an overview of the research background, showing the need for this research.

Chapter 2 contains the detailed literature review, which encompasses the state of the art for corrosion of reinforcing steel in concrete from research targeted at civil engineering and corrosion engineering applications.

Chapter 3 outlines the detailed research methodology based on the gaps identified from the literature review completed in Chapter 2.

Chapter 4 presents the numerical model developed as part of this research, which describes the corrosion processes that occur on the bar/concrete interface under different chloride and oxygen concentration conditions.

Chapter 5 presents the results from the numerical model with comparisons to photographs of corrosion and test data obtained from in-service structures.

Chapter 6 contains the summary and conclusions along with recommendations for future research.

2 LITERATURE REVIEW

2.1 Overview

Deterioration of reinforced concrete is a complex process as several mechanisms can be present, each of which attack concrete differently. While covering a wide range of deterioration, these mechanisms can be combined into the following major groups:

- Corrosion of embedded reinforcement followed by surface cracking, delamination, and spalls; and
- Concrete degradation as a result of physical deterioration of the cement/aggregate interface.

For reinforced concrete structures in North America, the primary cause of deterioration has been reported as chloride induced reinforcement corrosion (Wang et al. 2005, Zhou et al. 2005, Williamson et al. 2009), which has similar corrosion characteristics to that observed in concentration cell corrosion. For this type of corrosion, diffusion barriers on the corroding surface cause localized changes to the environment (Jones 1996) that create a local reduction in pH (Garćes et al. 2005). This localized change in pH creates a similar effect to that produced when reinforcing steel is exposed to carbonated concrete. These observations have led to a significant amount of research in corrosion deterioration of reinforced concrete for the purpose of developing mechanistic models for chloride and carbon dioxide diffusion, corrosion initiation, and spalling of concrete.

Two forms of corrosion in reinforced concrete have been identified, which are micro-cell and macro-cell corrosion (Hansson et al. 2006, Rodriguez et al. 1999). Micro-cell corrosion occurs when half-cell reactions required to form a corrosion cell occur on the same bar, while macro-cell corrosion occurs when half-cell reactions are coupled between discrete points within an element (Hansson et al. 2006). Examples of macro-cell corrosion include:

- A bridge deck where the top mat of reinforcement is encapsulated in chloride contaminated concrete coupling with the bottom mat of steel that is in chloride free concrete; or

- Reinforcement passing from repaired to un-repaired concrete creating a couple where steel in the un-repaired concrete corrodes at a higher rate with the offsetting cathodic reactions occurring in the repaired concrete (Soleimani et al. 2010).

While both macro and micro cell corrosion are present in reinforced concrete, measuring techniques cannot differentiate between the two forms. Therefore, micro-cell corrosion is generally neglected (Hansson et al. 2006) even though it may represent the larger contribution to the overall corrosion rate (Zhang and Mailvaganam 2006, Ji et al. 2011).

Therefore, a detailed literature review was performed with the intent of capturing the current knowledge base in:

- Corrosion processes that occur on reinforcing steel embedded in concrete, including, corrosion cells, thermodynamics, and kinetics of corrosion;
- Mass transport of oxygen and chloride and how these species affect the corrosion process;
- Chloride concentrations required to initiate corrosion of reinforcing steel embedded in concrete;
- Current models that have adapted corrosion theory to simulate the initiation and development of corrosion on reinforcing steel embedded in concrete; and a
- Brief overview of the current practice employed by practicing engineers for obtaining corrosion data from in-service structures.

2.2 Reinforcement Corrosion

From an electrochemical standpoint, the terms micro-cell or macro-cell corrosion does not readily describe the specific corrosion processes occurring on a metal surface embedded in concrete. Rather, the terms describe whether the corrosion process is localized (micro) or causing ionic flow through the electrolyte creating a corrosion cell with half-cell processes at two distinct areas (macro). Using terminology from corrosion science, the following forms of corrosion can occur:

- Uniform corrosion resulting from reinforcing steel embedded in carbonated concrete (Raupach and Schiessl 1997, Steffens et al. 2002);

- Pitting corrosion when chlorides reach the reinforcing steel bar surface (Wang et al. 2005, Zhou et al. 2005, Williamson et al. 2009); and

- Concentration cell corrosion caused by variations in electrolyte concentration or oxygen supply from one part of the reinforcing steel bar to another.

The formation of a micro-cell or macro-cell is dependent on potential differences created along and around each bar when these forms of corrosion are initiated. Initially, uniform and pitting corrosion form on the bar surface closest to the surface from which the respective contaminant arrives (Ji et al. 2011). For pitting corrosion, separation of the anodic and cathodic processes can occur, creating a localized increase in the rate of metal dissolution, while increased oxygen reduction occurs in the area immediately surrounding the pit (Jones 1996, Revie 2004). The development and balance between these two major processes is a complex problem requiring an understanding of mass-transport as well as thermodynamics and the kinetics of corrosion. Therefore, in the following sections, the literature review focuses on the corrosion cell, thermodynamics and kinetics and how they interact to influence the corrosion process of reinforcing steel embedded in concrete.

2.2.1 Corrosion Cell

For corrosion to occur, a corrosion cell must form which consists of two half-cells on the steel surface, namely the cathode and anode. At the anode, steel dissolution occurs, which is described by:

$$Fe \Leftrightarrow Fe^{2+} + 2e^{-} \qquad [2.1]$$

Meanwhile at the cathode, either oxygen reduction (Equation 2.2) or the creation of hydrogen gas (Equation 2.3) occurs, described by:

$$O_2 + 2H_2O + 4e^{-} \Leftrightarrow 4OH^{-} \qquad [2.2]$$

$$2H_2O + 2e^{-} \Leftrightarrow H_2 + 2OH^{-} \qquad [2.3]$$

Once corrosion is initiated, steel is oxidized at the anode (Equation 2.1), creating electrons and positively charged ions, while oxygen is reduced or hydrogen is generated at the cathode

(Equation 2.2 and 2.3) consuming electrons. Electrons produced at the anode flow through the steel to the cathode where they provide the electrons necessary for completing the cathodic reaction. Ions created at the two half-cells are attracted to each other through the electrolyte (pore water solution) and recombine according to:

$$Fe^{2+} + 2OH^{-} \Leftrightarrow Fe(OH)_2 \qquad [2.4]$$

Figure 2.1 represents the electrical circuit created by the flow of electrons and ions between the anodic and cathodic sites. The current flow shown in Figure 2.1 produces a potential field that can be measured when a reference half-cell is placed against the concrete surface (Elsener 2001). Of note is that corrosion cells can range in size from microscopic in the case of uniform corrosion to several millimeters in area for pitting corrosion or concentration cell corrosion (Jones 1996).

2.2.2 Thermodynamics of Corrosion

Normally, reinforcing steel embedded in concrete remains passive due to the high pH provided by concrete and the formation of a passive iron oxide layer (Alonso et al. 2002), which reduces

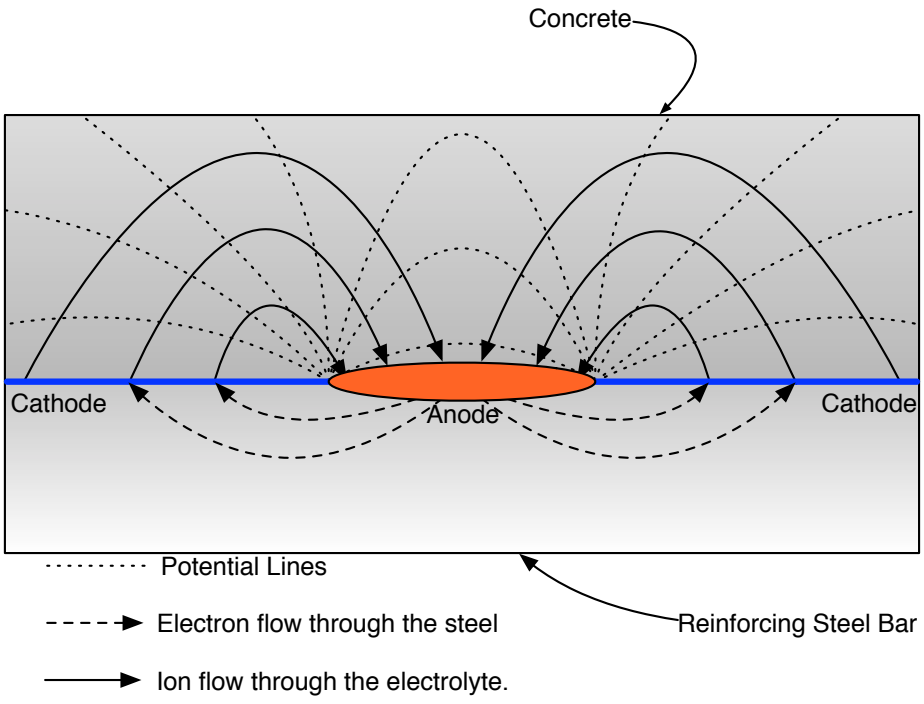

Figure 2.1 Idealized corrosion cell with current flow and potential lines (Elsener 2001).

the corrosion rate to very low levels (Millard et al. 2001). This passivity is represented in a potential versus pH diagram (Pourbaix Diagram) (Moreno et al. 2004 and Jones 1996) as shown in Figure 2.2 which graphically presents whether a metal is stable, corroding or passive in an aqueous environment once it has achieved equilibrium under a specific potential and pH. Solid lines shown in Figure 2.2 represent transitions between states that are developed using the general equation for a half-cell (Equation 2.5):

$$aA + mH^{+} + ne^{-} = bB + dH_2O \qquad [2.5]$$

and the Nernst Equation (Equation 2.6) that describe the relationship between concentration, pH, and potential for each given reaction (Jones 1996):

$$e_{rev} = e^{o}_{rev} + \frac{2.303RT}{nF}\log\frac{[A]^a[B]^b}{[C]^c[D]^d} \qquad [2.6]$$

where e_{rev} is the reversible corrosion potential of the reaction in volts, e^{o}_{rev} is the reversible corrosion potential of the reaction at standard temperature and a concentration of unity in volts, R is the gas constant which is equal to 8.314 J/k/mol, T is the temperature in degrees Kelvin, n is the number of electrons exchanged in the reaction, F is Faraday's constant which is 96,485 C/mol, A and B are concentrations of the reactant in mol/m^3, C and D are concentrations of the products in mol/m^3, and the values a, b, c and d are stoichiometric coefficients of each species involved in the reaction.

Within this diagram, three distinct regions are identified representing immunity, passivity, and corrosion. Immunity represents the zone where steel cannot corrode while the corrosion zone represents an area where steel freely corrodes. The area of interest for reinforced concrete, however, is the passivity zone. In this zone, a corrosion by-product layer is formed which creates a stable diffusion barrier that reduces the corrosion rate to very low values (Jones 1996).

For reinforcing steel embedded in concrete, the corrosion potential reported in the literature is between 0.15 and 0.20 volts versus the standardized hydrogen electrode (SHE) (Stratfull 1973, Skeet and Kriviak 1994) while the range of pH for concrete is from 11 to 14 (Macias and Andrade 1987, Huet et al. 2005). These values are represented on the PD in Figure 2.2 as the shaded area, which falls completely in the passive region. This passivity reduces the corrosion rate to a very low level until an external contaminant is introduced, such as carbonation and/or

chlorides (Saetta and Vitaliani, 2004). While carbonation is not specifically considered in this research, chloride induced corrosion is believed to cause localized reductions in pH on the reinforcing steel bar surface, thereby creating a similar effect to that observed with carbonation (Garćes et al. 2005).

For the case of carbonation, CO_2 diffuses from the atmosphere into the concrete, which then interacts with the cement paste in contact with the pore network according to (Hartt et al. 2004),

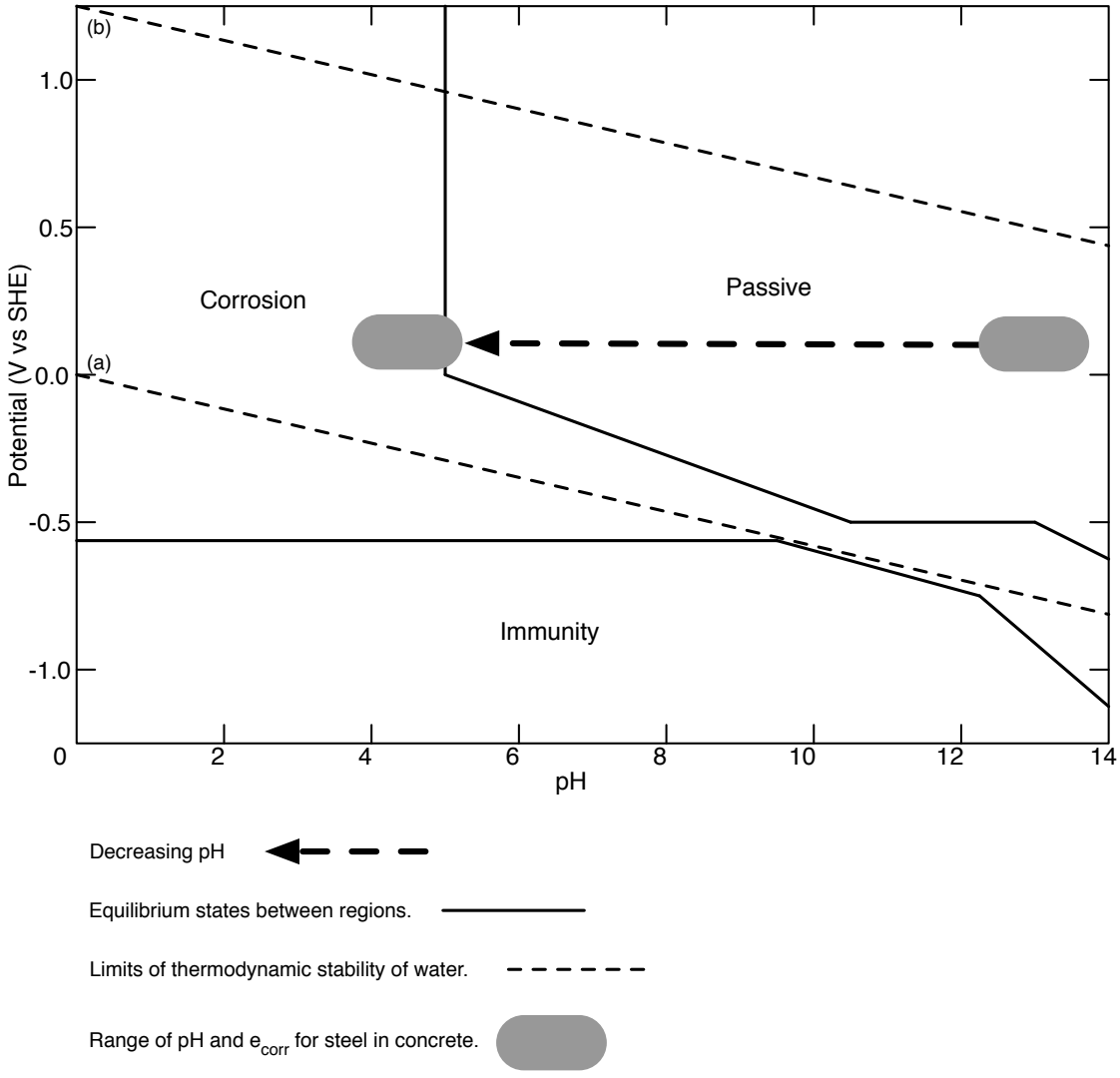

Figure 2.2. Idealized Pourbaix Diagram for Iron in Water (Pourbaix, 1973) with identification of passivated steel potential in concrete and pH range for concrete. Lines denoted as (a) and (b) represent stability lines for water and its decomposition products of hydrogen and oxygen respectively. (Pourbaix (1973), Moreno et al. (2004))

Huet et al. 2005):

$$Ca(OH)_2 + CO_2 \Leftrightarrow CaCO_3 + H_2O \qquad [2.7]$$

This reaction consumes free OH^- thereby lowering pH until the reinforcing steel is no longer in the passive region and corrosion can initiate (Bentour et al. 1997; Steffens et al. 2002; Hartt et al. 2004). Thermodynamically, the carbonation process is represented in Figure 2.2 by the heavy dashed line, which represents decreasing pH as carbonation develops. Depending on the magnitude of carbonation, the pH can be reduced until the reinforcing steel transitions into the corrosion zone and uniform corrosion occurs. Under uniform corrosion, anodic and cathodic sites are microscopic in size and constantly changing locations resulting in the uniform dissolution of iron and ultimately the formation of various forms of iron oxide.

For chloride-induced corrosion, the thermodynamic process is different than carbonation, as the pH surrounding the reinforcing steel does not initially change with the introduction of chloride. When chlorides are present, the form of corrosion changes from uniform to pitting corrosion (Raupach and Schiessl 1997, Steffens et al. 2002), which is a localized form of corrosion (Jones 1996) where high rates of metal dissolution can occur in a localized area.

In order for the pit to form, sufficient oxygen must be present to initially passivate and maintain the passive surface, followed by chloride that reaches the passivated surface. Figure 2.3 presents a simple schematic of the processes occurring on the steel once a pit is formed. The main difference between uniform and pitting corrosion is the presence of the porous cap that restricts movement of ions from the anodic pit to the surrounding bulk electrolyte. This restriction allows the anodic pit to become more acidic due to consumption of free OH^-, as described by Equation 2.4. This increase in acidity results in an increase in the corrosion rate as the thermodynamics dictated by the pit chemistry move into the same general area as that represented by carbonation in Figure 2.2. Therefore, pitting corrosion has similar characteristics to carbonation corrosion within the pit, as the local electrolyte chemistry created is similar to that produced under carbonation.

When chlorides are introduced into the concrete/steel system, the Pourbaix Diagram shown in Figure 2.2 is modified to produce Figure 2.4 (Pourbaix 1973, Moreno et al. 2004). Chlorides at the reinforcing steel level create two new regions identified as “pitting corrosion” and “partial passivation”. Depending on the concentration of chlorides within the electrolyte, these new

regions may cause the steel to exhibit pitting corrosion even though the electrolyte has not changed its pH and steel has not change its potential.

Figure 2.4 shows chlorides are required to produce an environment whereby corrosion is possible. However, if pH is low due to carbonation or pit acidification and chlorides are present, corrosion can proceed even if chloride levels are low or non-existent. This observation from the PD is consistent with relationships comparing chloride levels required to initiate corrosion with the pH of concrete (Thangavel and Rengaswamy 1998, Hurley and Scully 2002). In these studies, high pH mixes of concrete or simulated pore solutions require high levels of chloride to cause corrosion on reinforcing steel. Within these studies, a high degree of variability and higher chloride concentrations causing corrosion were observed in tests using concrete. These differences between simulated pore solution and concrete tests was attributed to $Ca(OH)_2$ within the concrete providing an alkali reservoir that prolongs pH in regions where corrosion occurs (Hurley and Scully 2002).

Steel surface preparation was also found to greatly influence chloride concentrations needed to initiate corrosion as (Mohammed and Hamada 2001, Novak et al. 2001):

- Sandblasted steel was found to have greater resistance to chlorides than steel which

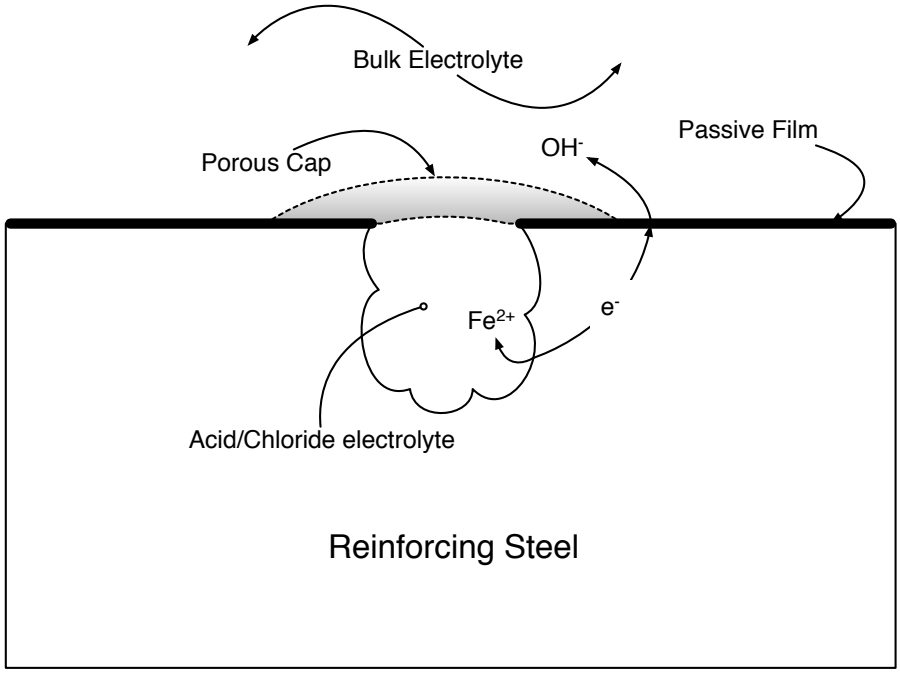

Figure 2.3. Idealized pitting corrosion cell. (Jones 1996)

retained light mill-scale; and

- Uniformly pre-passivated bars were found to have the highest chloride corrosion resistance (Mohammed and Hamada 2006).

These observations are consistent with results reported in pitting or crevice corrosion literature where imperfections in the passivated layer, mill scale, or debris create the necessary conditions for a pit to form (Jones 1996).

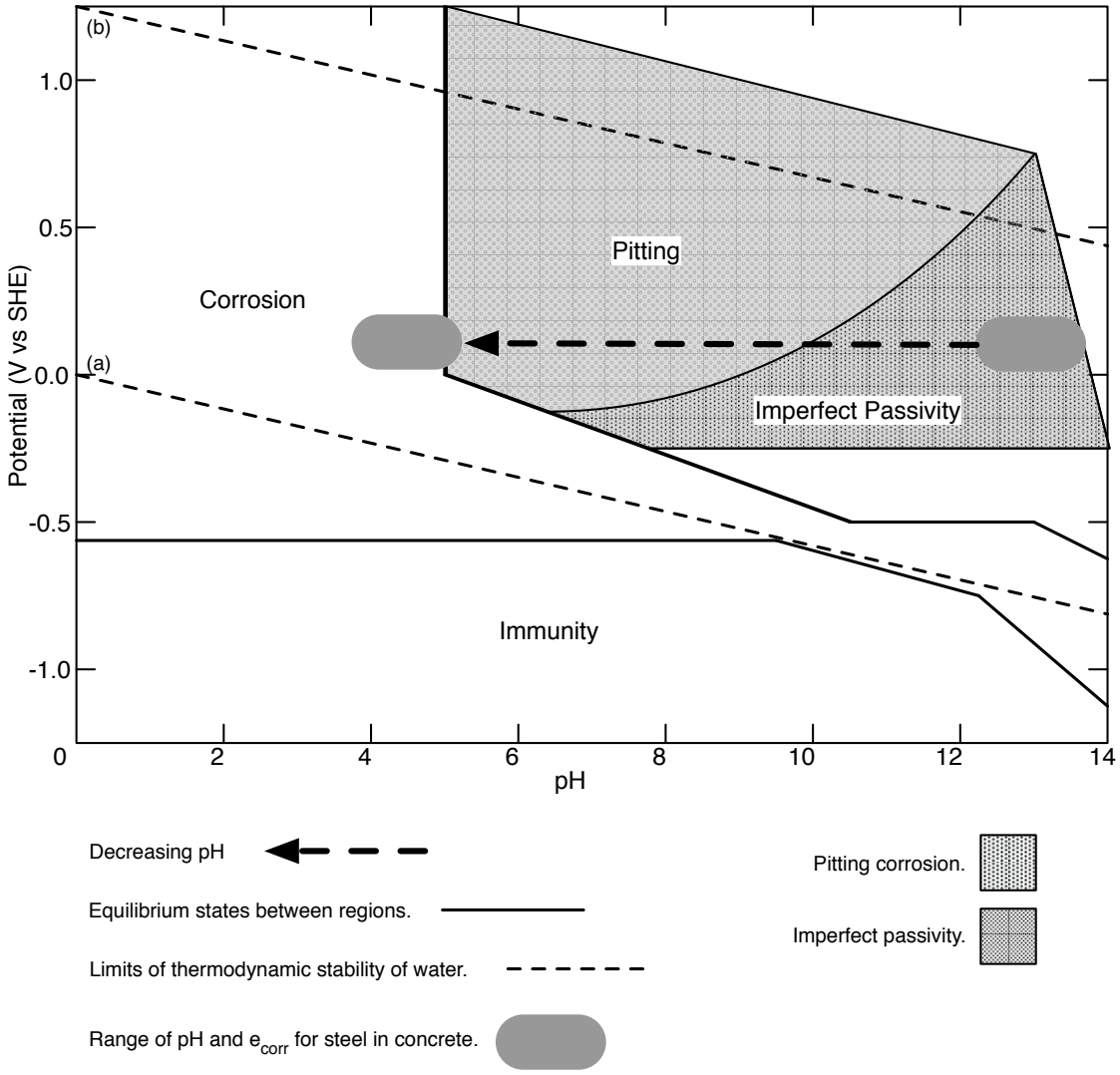

Figure 2.4. Idealized Pourbaix Diagram for Iron in Water with Chlorides (Moreno et al. 2004) with identification of passivated steel potential in concrete and pH range for concrete.

Of note from the preceding discussion is that with both carbonation and chloride induced corrosion, the corrosion potential according to the thermodynamics of the system does not become more negative when corrosion occurs. This observation contradicts current practice employed by Alberta Transportations (AT) and ASTM's corrosion testing interpretations which state that corrosion potentials more negative than -400 mV versus a copper sulfate electrode (CSE) (AT) or -350 mV versus CSE (ASTM) indicate a greater than 90% probability of corrosion is present. This observation is discussed with the use of kinetics of corrosion, which is the subject of the next topic.

2.2.3 Kinetics of Corrosion

Kinetics for each electrochemical reaction described by Equations 2.1, 2.2, and 2.3 control the corrosion cell rate. Figure 2.5 graphically presents the impact of corrosion potential versus corrosion current under changing potentials or current flow. This figure is commonly used in corrosion modeling for reinforced concrete to represent depassivation of reinforcing steel when chlorides are present (Subramaniam and Bi 2010, Soleimani et al. 2010, Kim and Kim 2008, Qian et al. 2006, Isgor and Razaqpur 2006a, Isgor and Razaqpur 2006b). The points labeled e_{rev} and i_{rev} refer to the reversible corrosion potential and exchange current density for each half-cell reaction identified. Two pairs of lines are presented in Figure 2.5 that represent the forward and reverse reaction related to each half-cell reaction described by Equations 2.1 and 2.2. Positive slopes indicate a release of electrons while negative slopes represent consumption of electrons. The slopes of each curve are commonly referred to as Tafel slopes which are normally unique for each anodic or cathodic reaction attributed to each half-cell. The hydrogen cathodic polarization curve represented by Equation 2.3, is not shown in Figure 2.6 as the reversible potential and corrosion current combined with its Tafel slope cause the oxidation branch of the reaction to intercept the anodic branch of the Equation 2.1 at a value so low as to not materially affect the overall corrosion rate (Raupach 1996a, 1996b).

When half-cell reactions are combined on the same surface with no controls related to mass transport or kinetic restrictions, a mixed potential is created as shown in Figure 2.6, represented by the intersection of the cathodic branch of the oxygen half-cell reaction and the anodic branch of the iron half-cell reaction. The reactions presented in Figure 2.6 assume mass transport or reaction limitations do not exist. However, Figure 2.7 (Revie 2006) identifies various kinetic of corrosion diagrams that represent different forms of restrictions that introduce rate-limiting steps

to the overall corrosion process. For reinforcing steel embedded in concrete, the concrete surrounding the bar can produce these restrictions when:

- For Figure 2.7(a), steel is in a passive condition due to the high pH of the local environment and no oxygen restrictions are present (Alonso et al. 2002, Moreno et al. 2004). Under this scenario, higher corrosion rates are prevented from occurring due to the passive layer limiting the corrosion rate;

- For Figure 2.7(b), diffusion barriers in the form of concrete cover or corrosion by-products limit oxygen transport to the corroding surface (Huet et al. 2007). When oxygen is limited on the corroding surface, the local corrosion rate must decrease in order for the oxygen consumption rate to match the oxygen transport rate; and

- For Figure 2.7(c), the system has no diffusion barriers or passivity thereby allowing the

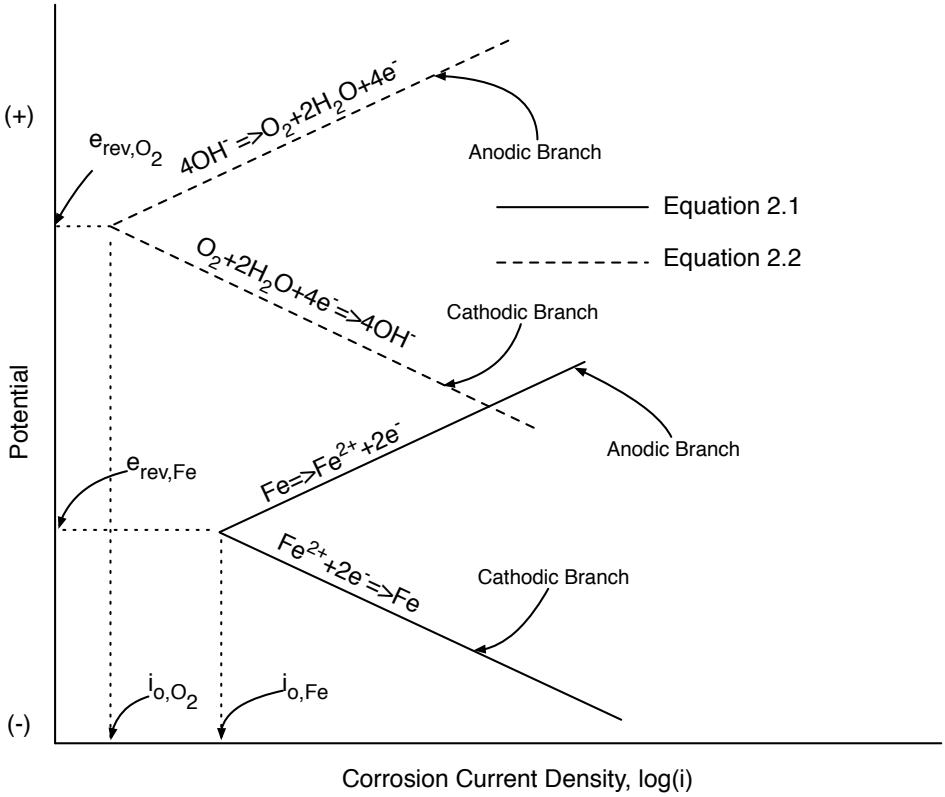

Figure 2.5. Idealized Pourbaix Diagram for Iron in Water with Chlorides (Moreno et al. 2004) with identification of passivated steel potential in concrete and pH range for concrete.

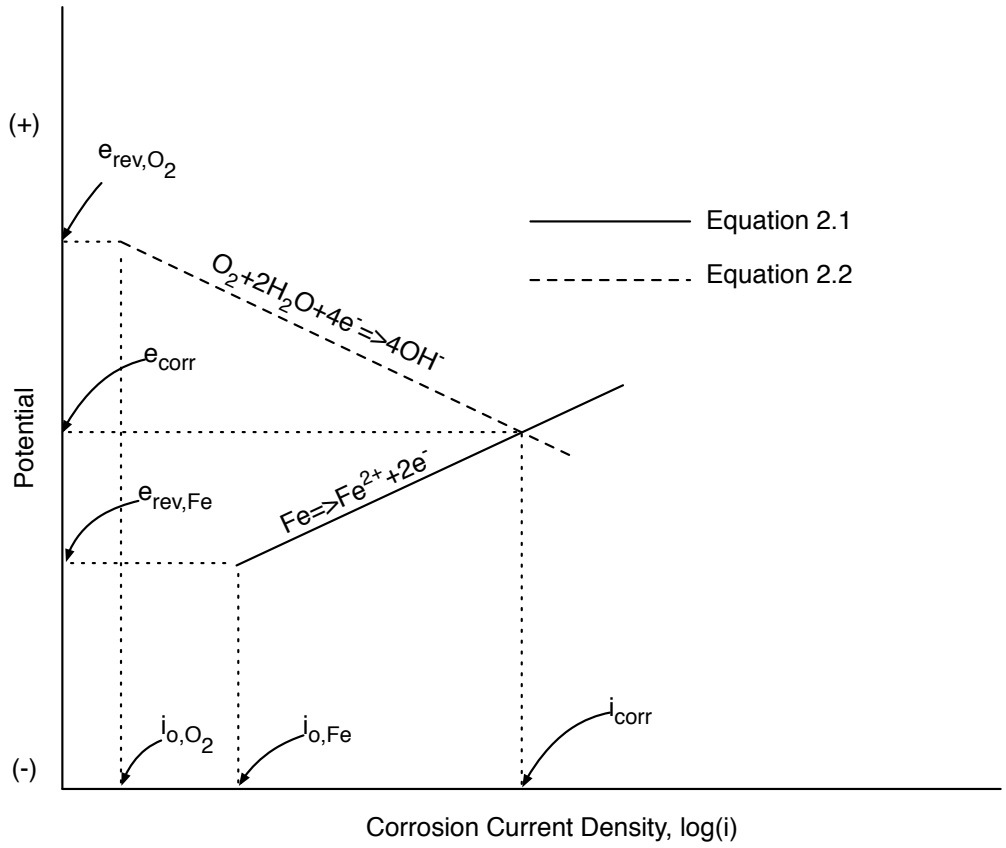

Figure 2.6. Idealized Kinetic Corrosion Diagram Half Cell Reactions of Iron and Oxygen identifying e_{corr} and i_{corr} at a mixed corrosion potential. (Revie (2006), Jones (1996))

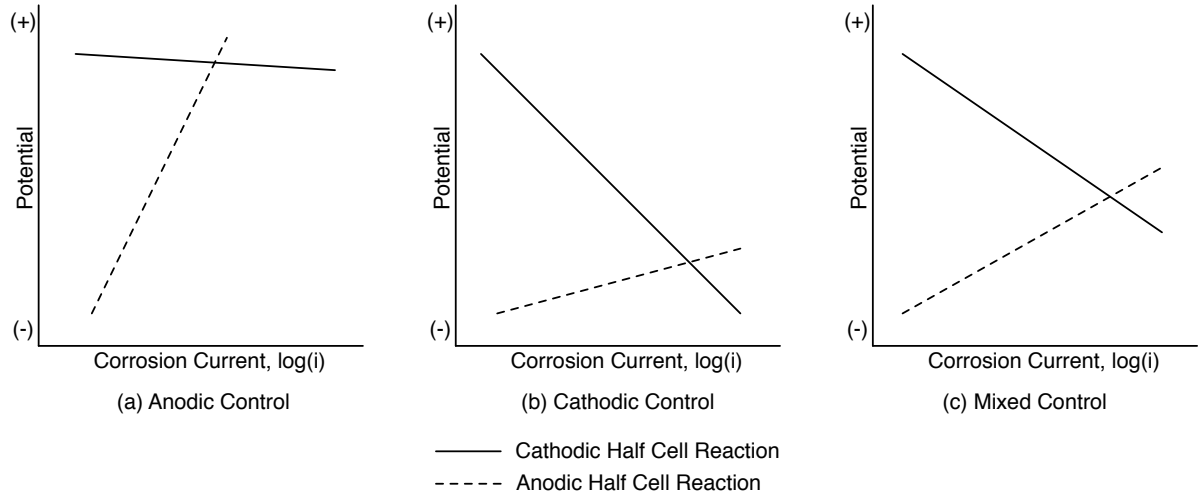

Figure 2.7. Schematic-outlining forms of control in a corroding system (Revie (2006)): (a) Anodic control; (b) Cathodic control; (c) Mixed control.

system to freely corrode.

When these rate-limiting steps occur at different locations within the concrete element, potential differences are formed which create the necessary driving force for the half-cell reactions to occur at separate locations (Soleimani et al. 2010). Under the appropriate circumstances, separation of the half-cell reactions can create the necessary local chemistry to induce other forms of corrosion such as pitting, crevice, or concentration cell corrosion (Jones 1996). Additionally, the movement of ions between the cathode and anode reactions can be restricted by the concrete when reactions occur at different locations on the bar surface (Soleimani et al 2010). This limitation results in potential drops occurring on the bar surface which are connected by the electrolyte. These potential drops have significant implications for the various forms of corrosion that can occur.

Figure 2.8 describes the change in oxygen concentrations from the bulk electrolyte to the corroding surface when diffusion barriers caused by concrete cover or corrosion by-product are present (Huet et al. 2007, Raupach 1996a, 1996b). Figure 2.8(a) presents the condition when the diffusion barrier reduces the oxygen concentrations on the bar/concrete interface without reaching a limiting condition. Figure 2.8(b) identifies the condition created when the diffusion barrier causes oxygen concentrations on the bar/concrete interface to reach a limiting condition. When the corrosion cell is under diffusion control as described by Figure 2.8(b), a maximum current is reached which is referred to as the limiting current density (i_{lim}) which is described for a one-dimensional system by (Jones 1996, Pour-Ghaz et al. 2009):

$$i_{lim} = nF\frac{D_{O_2}C_{O_2}}{d} \qquad [2.11]$$

where n is number of electrons transferred at the cathode and is equal to 4 for reduction of oxygen as per equation 2.2, F is Faraday's constant, D_{O_2} is the diffusion coefficient of oxygen in concrete (m^2/s), C_{O_2} is the amount of dissolved oxygen on the concrete surface ($mole/m^3$), and d is the concrete cover thickness in metres.

Figure 2.9 (Jones 1996) represents the effect diffusion barriers have on a kinetic of corrosion diagram. Three vertical lines are shown representing limiting corrosion current densities that correspond to three diffusion layer thicknesses. The resulting corrosion current densities represented by i_{corr1} through i_{corr3}, indicate that, with increased diffusion control (increased cover

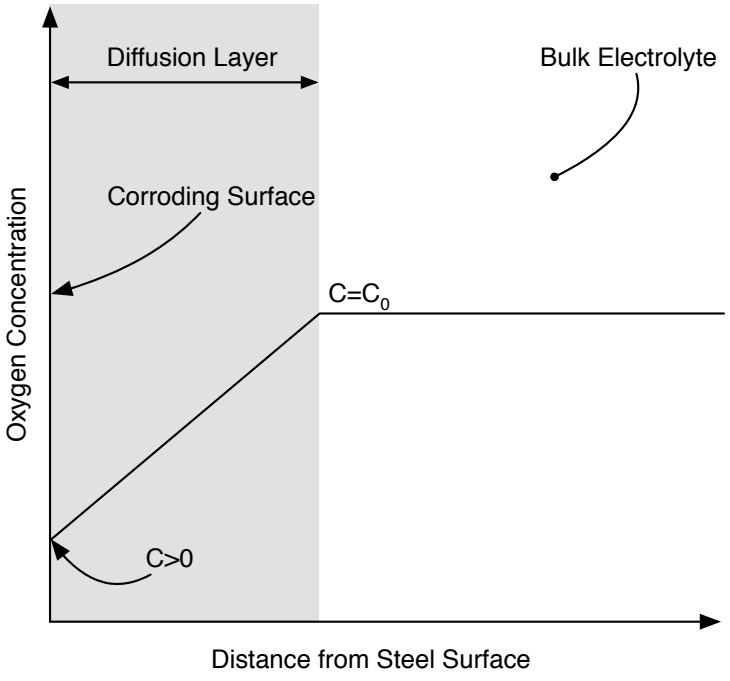

(a)

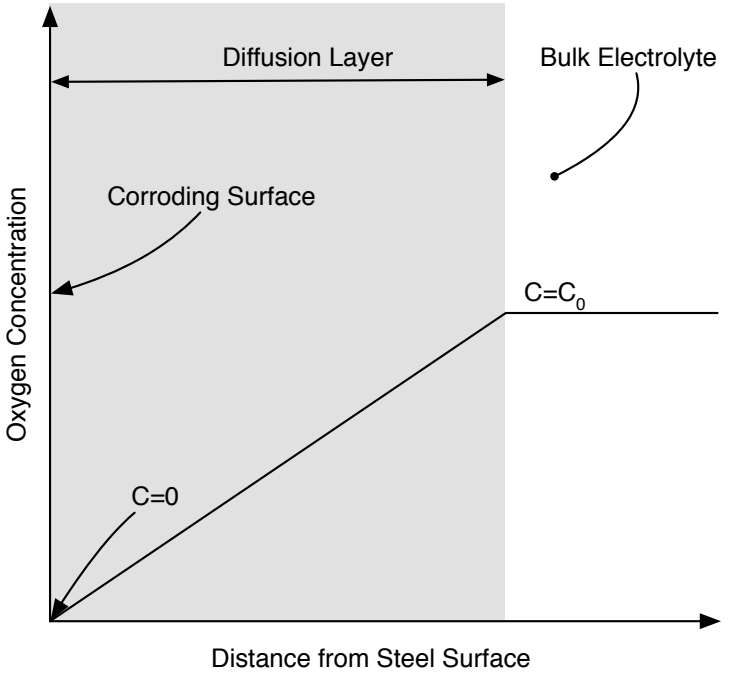

(b)

Figure 2.8. Diffusion layer and oxygen limitations on a corroding surface: (a) Oxygen concentration at corroding surface greater than zero; (b) Oxygen concentration at corroding surface at zero.

or decreased diffusion coefficients), the overall corrosion current density decreases combined with a lowering of the corrosion potential. These different corrosion potentials can occur at different locations within a reinforced concrete element or on two points of the same reinforcing steel bar when variations in electrolyte concentrations occur (Soleimani et al. (2010)), which has implications for current flow through the electrolyte caused by differential cell corrosion, as discussed in later sections.

The second type of corrosion control, anodic control, occurs when steel embedded in concrete forms a passive layer of iron oxides due to the high pH environment afforded by the concrete (Alonso et al. 2002, Moreno et al. 2004). The kinetic of corrosion diagrams represented by Figure 2.5 and 2.6, therefore, are only applicable when the environment surrounding the reinforcing steel is no longer providing sufficient pH to maintain passivity of the iron oxides. In other words, these figures are only applicable for portions of a bar embedded in carbonated

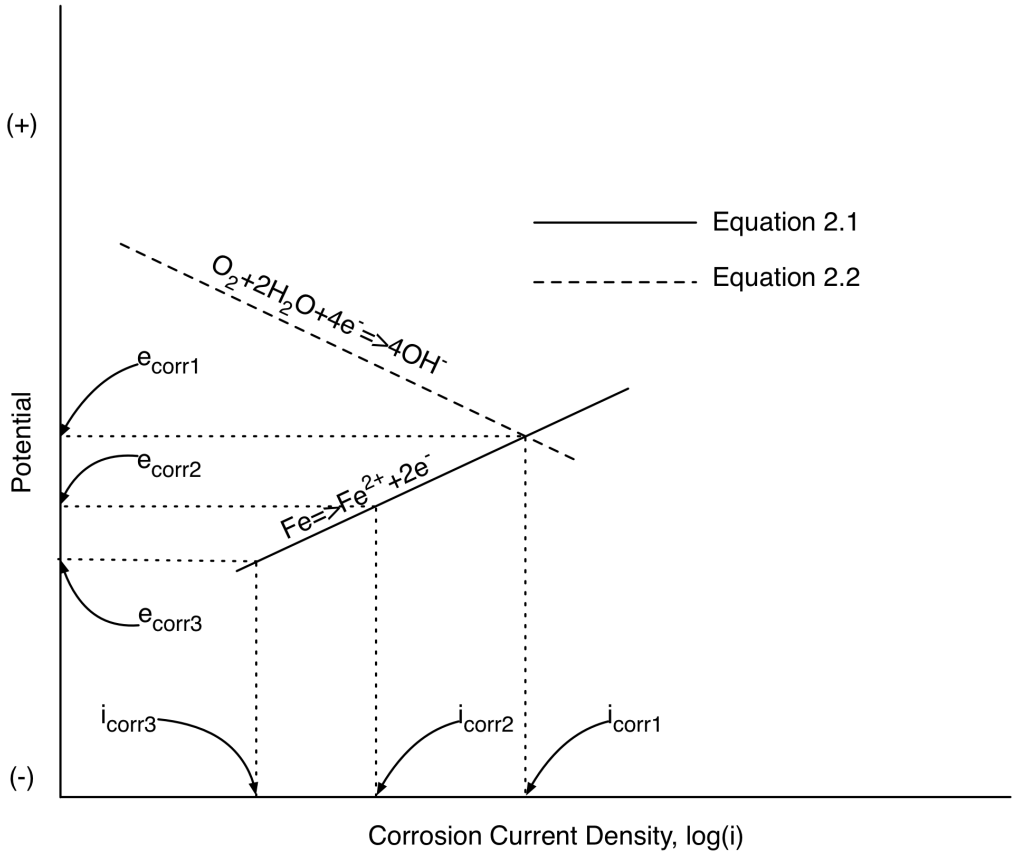

Figure 2.9. Idealized Kinetic Corrosion Diagram – Passivated Metal Increasing Chloride and Increasing Diffusion Control for O_2 (Jones 1996).

concrete where pH of the environment has positioned the steel in the region identified in Figure 2.2 as Corrosion.

Normally, reinforcing steel embedded in concrete is passive due to the formation of a film on the bar/concrete interface, which is stable under the pH and potential afforded by the concrete (Moreno et al. 2004, Poursaee and Hansson 2007). Therefore, the kinetics of corrosion for the anodic branch of Equation 2.1 for an idealized passivated steel change from that shown in Figures 2.5 and 2.6 to that shown in Figure 2.10 (Jones 1996). In this figure three zones are present which are referred to as active, passive, and transpassive.

The portion of the anodic branch labeled as the active zone follows a similar geometry as that shown in Figure 2.5 and 2.6 for the anodic branch of Equation 2.1. As potentials are increased, the primary passive potential is reached, identified as e_{pp}, at which point the maximum corrosion current density is achieved, which is referred to as i_{crit}, following which the corrosion current drops off rapidly until it reaches the passive corrosion current density labeled as i_{pass}. Further increases in system potential do not increase the corrosion current until the transpassive region is reached, at which point the passive layer becomes unstable and pitting corrosion occurs. However, while the transpassive region is shown, it can only be reached when very strong

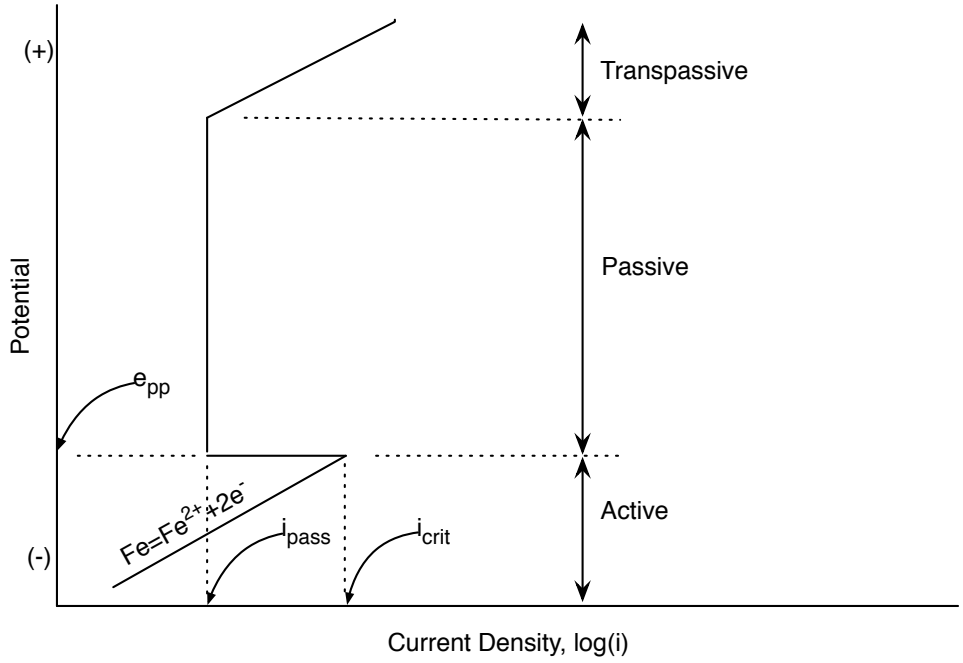

Figure 2.10. Idealized Kinetic Corrosion Diagram – Passivated Metal (Jones 1996).

oxidizers are introduced into the system, which is not a common occurrence (Jones 1996).

Figure 2.11 combines kinetics for oxygen reduction described by equation 2.2 with the kinetics for passivated steel along with the effect increasing chloride has on the system kinetics. When chlorides are not present, kinetics are at a low rate of corrosion with a mixed-potential value tending towards positive, assuming that no diffusion barriers are present. This low corrosion rate maintains the passive characteristics of the oxides present on the surface of the steel/concrete interface. In other words, even without chlorides, corrosion is occurring with steel embedded in concrete, but at such a low rate as to be essentially non-existent (Millard et al. 2001, Moreno et al. 2004). However, if oxygen limitations are present due to diffusion barriers, the local oxygen concentration within the electrolyte can be depleted resulting in an acidification of the local environment. This mechanism is the underlying cause of pitting and crevice corrosion that was presented in the previous section but will be further discussed in Section 2.4.

As chlorides are introduced, the kinetics of the anodic line shift to the right with a corresponding linear reduction in the passive region represented by the dashed lines in Figure 2.11 (Jones 1996) and e_{corr2}/i_{corr2}. This change in kinetics causes the oxygen reduction line to cross at more

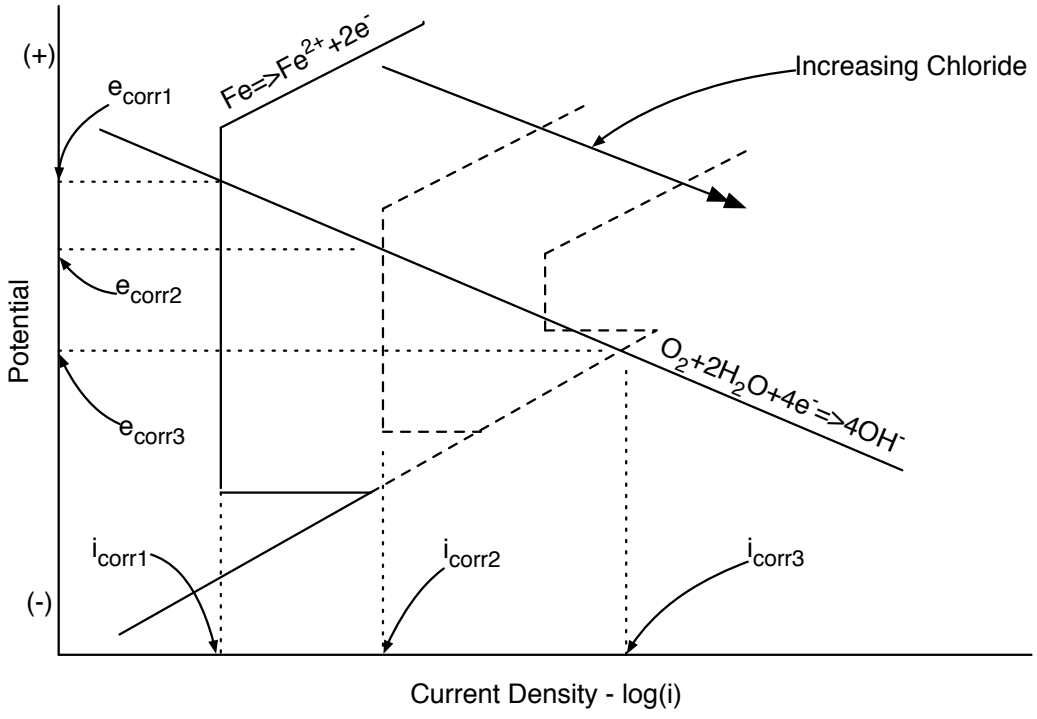

Figure 2.11. Idealized Kinetic Corrosion Diagram – Passivated Metal with Increasing Chloride (Jones 1996).

negative potentials concurrent with an increase in corrosion current density. At the highest chloride concentration represented, the current density jumps significantly as the oxygen line intercepts the anodic line resulting in e_{corr3} and i_{corr3}, which is below the primary passive potential. At this point the corrosion current is at its theoretical maximum for the pH represented by this diagram while the corrosion potential is at the lowest.

Figures 2.10 and 2.11 represent kinetic of corrosion diagrams for idealized passivated steel. Similar diagrams, shown in Figure 2.12 have been adopted for use in modeling corrosion kinetics in reinforced concrete (Maruya et al. 2007, Qian et al. 2006). The major difference between Figures 2.11 and 2.12 is that increasing chlorides are shown to have a different effect on kinetics. Referring to Figure 2.11, increased chlorides shift the entire steel dissolution line to the right with a decrease in the passive portion of the curve. In comparison, Figure 2.12 has the passive region of the curve being reduced with a corresponding downward shifting of the transpassive region until the transpassive region intercepts the cathodic branch of Equation 2.2. The resulting corrosion current density, $i_{microcell}$ is interpreted to represent the corrosion current caused by pitting corrosion. However, these interpretations of the effect chlorides have on the kinetics of corrosion of passivated steel are not consistent with fundamentals of corrosion.

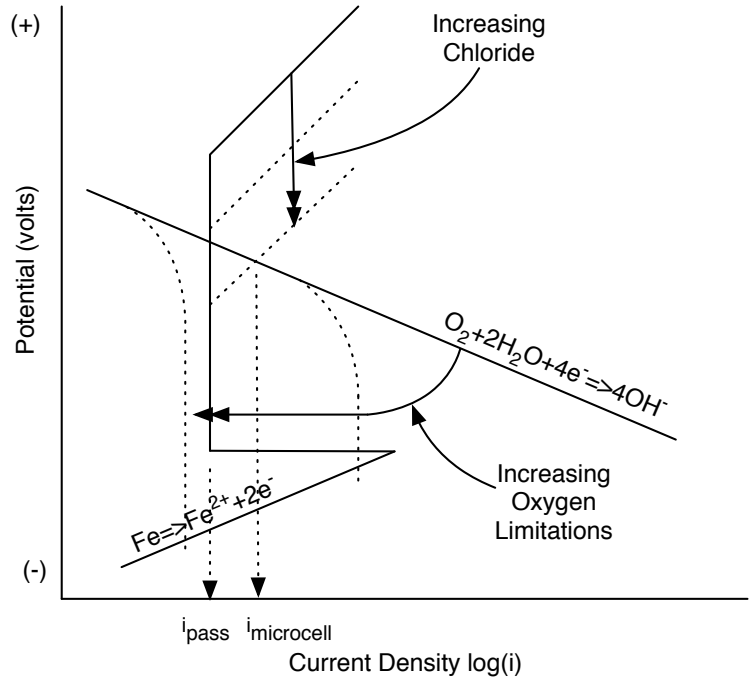

Figure 2.12. Kinetic of corrosion diagram used in corrosion modeling for reinforced concrete (Maruya et al. (2007)).

Polarization experiments on reinforcing steel in simulated pore solutions have been conducted for the purpose of identifying the kinetic of corrosion diagrams for reinforcing steel in concrete (Moreno et al. 2007, Huet et al. 2005, Zhang et al. 2009). Figure 2.13 presents the kinetics of corrosion for reinforcing steel exposed to five different chloride bearing simulated pore solutions. Of note is that while the figure shows three curves, the first two and last two chloride concentrations used in the test did not result in a change in the kinetics of corrosion that effectively caused them to overlap. This result suggests an upper and lower chloride concentration limit is present whereby:

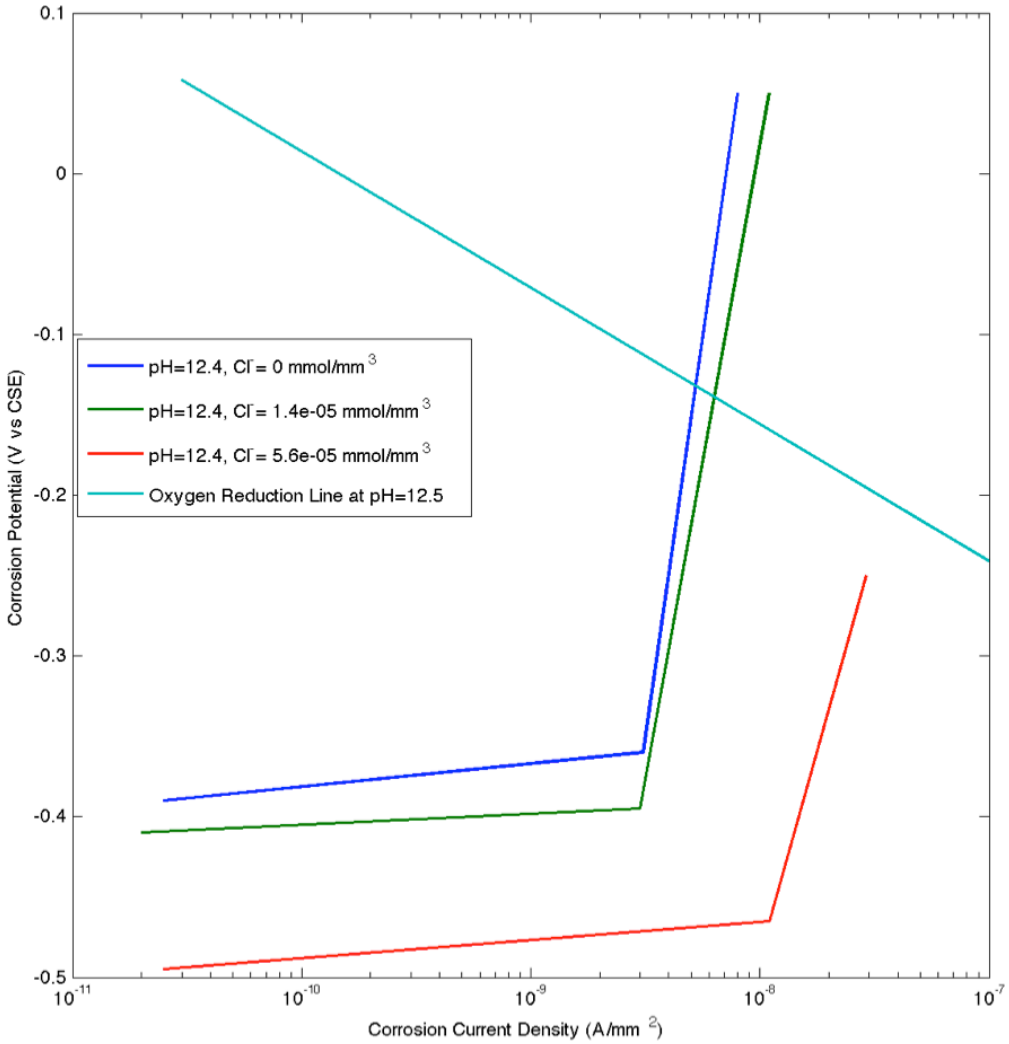

Figure 2.13. Kinetic of corrosion diagram for reinforcing steel in a simulated concrete pore solution at pH = 12.5. (Moreno et al. (2007))

- Corrosion is always present even when chlorides are not; and
- The corrosion rate will reach a maximum after which further additions of chlorides will not produced any increase in corrosion rate.

Figure 2.13 suggest some characteristics of a passivated steel described by Figure 2.11 are not evident such as:

- A well defined passive zone with a sharp reduction in corrosion current density once a certain corrosion potential is reached; and
- A transpassive zone; however, this observation may be a result of the experiment not reaching the levels necessary for pitting corrosion to be produced.

Similar polarization tests have been attempted on reinforcing steel embedded in mortar or concrete; however, results have been highly variable as the effects of mass transport on the kinetics influence the result (Poursaee 2010) and $Ca(OH)_2$ produce a buffering effect for pH that is not present in simulated concrete pore water solutions (Hurley and Scully 2002).

Figure 2.14 outlines how cathodic and anodic controls described by Figures 2.7 and the subsequent figures can occur in practice. As discussed previously, kinetics of corrosion are greatly influenced by concentrations of chloride and oxygen with each species affecting the kinetics in a different way. Therefore, Figure 2.14(a) demonstrates how a single reinforcing bar can be exposed to different concrete when the repaired concrete (patch) is chloride free while the un-repaired (original) concrete contains chloride. Similarly, Figure 2.14(b) demonstrates how variable cover along the bar length will create a condition where chloride concentrations along the bar are variable due to different arrival times for chloride under the same diffusion rate. Additionally, local environmental variations can occur within an element due to the presence of sealers or other forms of membranes, which deteriorate in such a manner as to allow moisture ingress in one location but not in another. These scenarios, therefore, create conditions for either the bar circumference or length to be exposed to different environments, thereby creating different kinetics of corrosion.

Different kinetics of corrosion along or around the same bar creates corrosion potential differences that can result in local increased rates of corrosion (Soleimani et al. 2010). The amount of corrosion rate increase is dependent upon the conductivity of the electrolyte that

exists between the two cells, the distance between the areas that are coupled, and the corrosion potential difference. This type of corrosion process is referred to as macro-cell corrosion within the reinforced concrete literature but, within the corrosion science area, it is referred to as concentration cell corrosion.

Under concentration cell corrosion, localized areas of increased corrosion are possible when two points on the same element are at a different corrosion potential and are electrically connected through an electrolyte. Figure 2.15, demonstrates the kinetics of corrosion that can be created when this condition is present. This is similar to the concrete patch example studied by Soleimani et al. (2010) where corrosion cells were observed to develop near the interface between two materials. Under this scenario, Material 1 limits oxygen transport to the bar surface, thereby producing a limiting corrosion current condition. Conversely, mass transport of oxygen with Material 2 does not result in the same limiting corrosion current condition. Therefore, two potentials develop, e_{corr1} and e_{corr2}, which produce the driving force necessary for

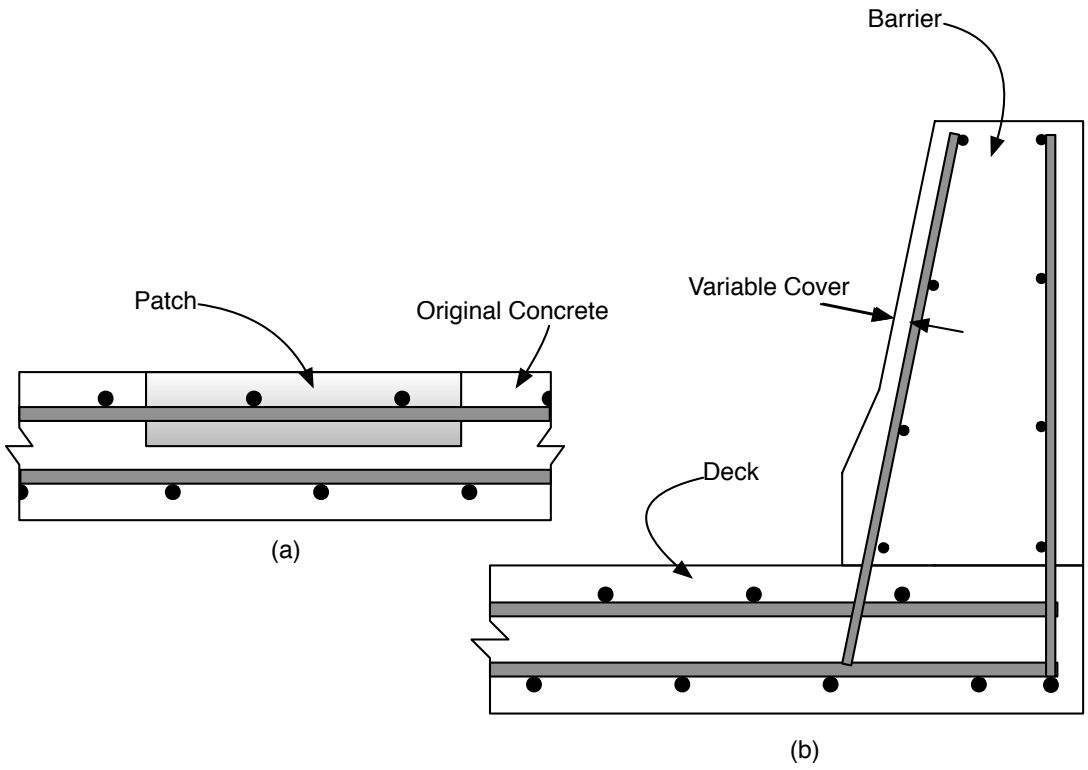

Figure 2.14. Typical locations on a bridge structure where variations in cover and material type create unique kinetics of corrosion: (a) Repaired element, (b) Bridge barrier to bridge deck.

current to flow through the electrolyte.

For corrosion of reinforcing steel in concrete, many researchers have suggested that separation of the cathode and anode is the dominant type of corrosion cell caused by chlorides (Elsener, 2002, Yokota et al. 2008, Zhang et al. 2009). This is supported by research in other fields, where it is commonly understood that metals which form their resistance to corrosion through passivity (rather than immunity) are susceptible to localized breakdown of the passive layer (pitting or crevice corrosion) when chlorides are introduced (Jones 1996). When this localized breakdown occurs, half-cell reactions that normally occur only at the anode and cathode can be supplemented by half-cell reactions occurring at other locations on the same element, resulting in a localized increase in dissolution rates for the material.

In order for half-cell reactions to become separated on the same bar surface, the movement of ions created at the anode and cathode must occur in order for the corrosion cell to be established. Therefore, the following sections describe mass transport processes that affect the kinetics of corrosion on the bar/concrete interface.

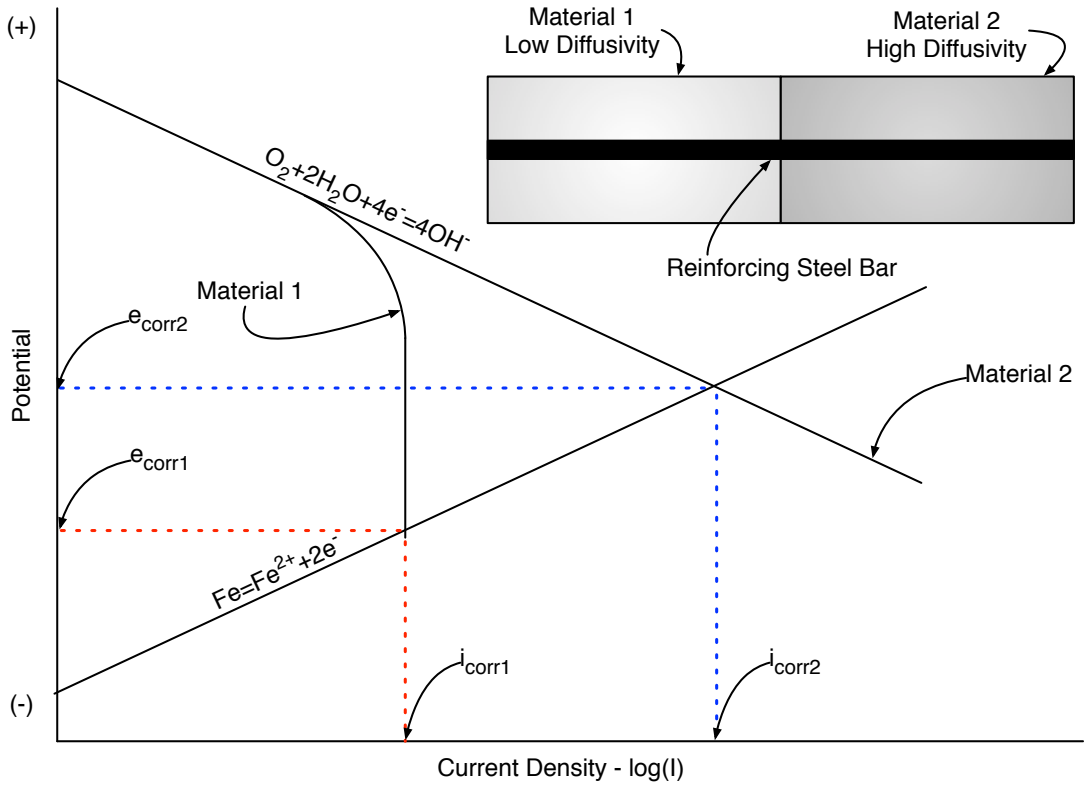

Figure 2.15. Idealized kinetic of corrosion diagram for two materials.

2.3 Mass Transport Processes in Concrete

Concrete, when placed into service, is generally in a chloride free, but fully oxygenated state. These initial conditions change over time due to:

- Kinetics of corrosion for reinforcing steel in a high pH environment discussed in the previous section producing low corrosion currents which deplete oxygen from the electrolyte that is in contact with the steel/concrete interface; and

- Diffusion of chlorides to the steel bar surface caused by de-icing salts or seawater being applied to the concrete surface. When these chlorides reach the steel bar/concrete interface, the local kinetics of corrosion are changed resulting in an increase in the local corrosion and oxygen consumption rate.

Mass transport of oxygen and chloride within the concrete and to the steel bar/concrete interface is, therefore, a crucial aspect to evaluate in understanding the development of corrosion on reinforcing steel in concrete. The movement of different species, such as chloride or dissolved oxygen, within concrete can be influenced by diffusion and advection (Martin-Perez et al. 2001, Huet et al. 2007, Boulfiza et al. 2003), which is described mathematically as:

$$\frac{\partial C}{\partial t} = \nabla(D\nabla C - \mu C) \qquad [2.12]$$

where C is the concentration (mol/mm^3), D is the diffusion coefficient (mm^2/s), and μ_v is Darcy's velocity (mm/s).

Under fully saturated conditions or when internal moisture conditions are constant, Darcy's velocity is effectively 0, which is the case for most above grade reinforced concrete, the second term, related to water movement, can be set to zero resulting in Fick's Second Law of Diffusion:

$$\frac{\partial C}{\partial t} = \nabla D\nabla C \qquad [2.13]$$

The application of Equations 2.12 or 2.13 to a model representing a reinforcing bar embedded in concrete presents a challenge as concrete is a heterogeneous material consisting of solid and pore phases with mass transport being confined to the pore phase (Ye and van Breugel 2009). Additionally, capillary pores, gel pores and air voids are present within the pore phase, which can be filled with different amounts of water depending on the degree of hydration,

quantity of cement, water to cement ratio, and ambient moisture conditions (Papadakis et al., 1991, Huet et al. 2007). Therefore, the degree of saturation, combined with the concrete porosity produces the parameters for transport of species and elements that affect the corrosion process: namely, oxygen and chloride ions (Koretsky et al. 1999).

Oxygen concentrations within the concrete mass are a blend between gaseous and liquid phases while chloride ion concentrations are restricted to the liquid phase alone. Concentrations of these elements must be related to the total volume in order to apply Equation 2.12 or 2.13 to the concrete mass by (Huet et al. 2007):

$$c_{ml} = \phi S_r c_l \qquad [2.14]$$

$$c_{mg,O_2} = \phi(1 - S_r)c_{g,O_2} \qquad [2.15]$$

$$S_r = \frac{\phi_w}{\phi} \qquad [2.16]$$

where c_{ml} represents the concentration of the element (oxygen or chloride) in the liquid phase, converted to the material volume (mol/mm^3), Φ is the porosity of the concrete (%), S_r is the degree of water saturation within the porous structure of the concrete (%), c_l is the concentration of the element (chloride or oxygen) in the liquid phase (mol/mm^3), c_{mg,O_2} represents the oxygen concentration in the gas phase converted to a total material volume concentration, $c_{g,O2}$ represents the gaseous phase oxygen concentration (mol/mm^3), and Φ_w is the water saturated porosity (%). With reasonable approximations of the degree of saturation and porosity of concrete, estimates of the concentration of each species that affects corrosion can be made for the concrete volume that allows the use of Equation 2.13 in a general finite element model. These estimates can be made from:

- Figure 2.16 which presents a relationship reported by Zhitnikov et al. (2002) that relates concrete porosity to water cement ratios (w/c); and
- Figure 2.17, which correlate the degree of water saturation with relative humidity (Papadakis et al. 1991).

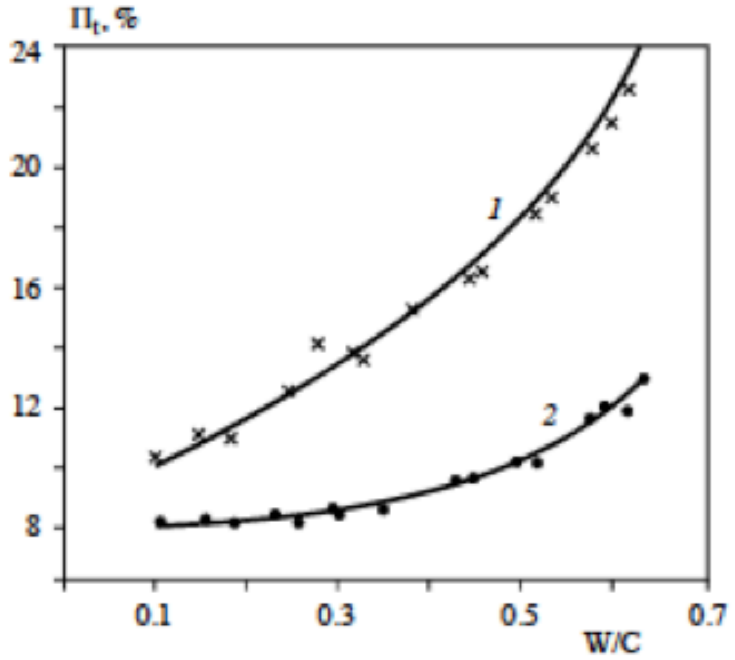

Figure 2.16. Concrete porosity (%) versus water cement ratio (w/c). (Zhitnikov et al. (2002))

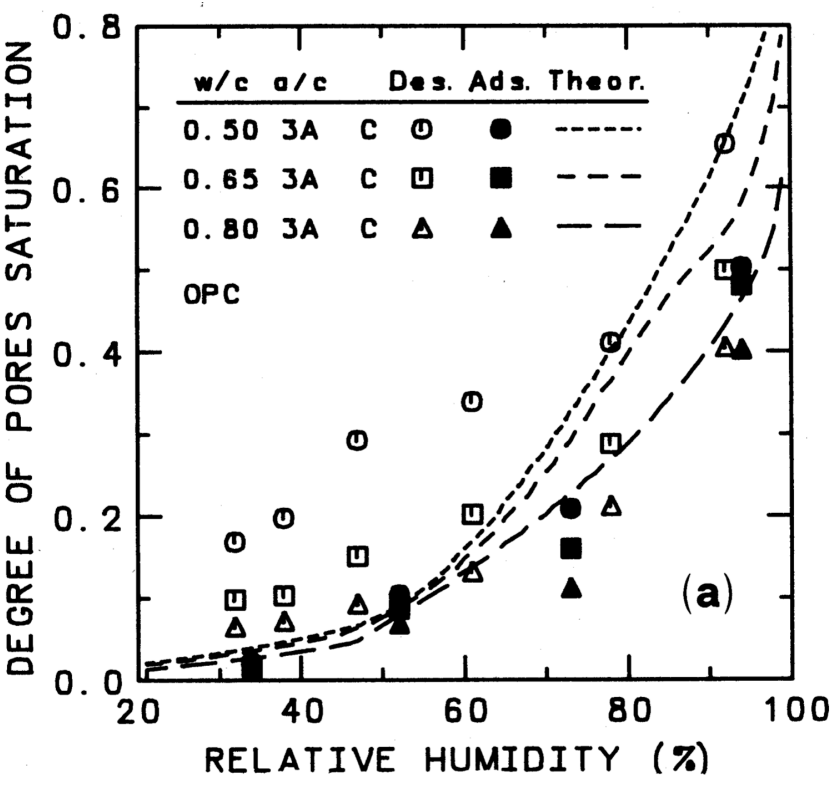

Figure 2.17. Degree of saturation versus relative humidity. (Papadakis et al. (1996))

2.3.1 Oxygen Concentrations and Transport

Oxygen concentrations within the pore water solution contained within the concrete pore structure affect the rate of corrosion on the steel bar surface, as corrosion rates are influence by initial oxygen concentrations. Table 2.1 identifies values reported in the literature for oxygen concentrations used for numerical simulation of concrete pore water. None of the values reported were taken from concrete pore water; rather, they were estimated from other solutions such as fresh or seawater. For corrosion modeling in reinforced concrete, the use of oxygen concentrations in seawater has been adopted, as the total salinity for concrete pore water is similar to seawater (Chin et al. 2001).

The wide variation in oxygen concentrations reported in Table 2.1 is due to water being able to dissolve different levels of oxygen depending on the temperature and salinity of the solution being considered (Debelius et al. 2009, Garcia and Gordon 1991, and Battino et al. 1983). Several methods have been proposed for relating temperature and salinity to dissolved oxygen content by fitting test data to a power series, with the most recent example for seawater proposed by Debelius et al. (2009), as follows:

$$\ln C^{*} = a_0 + a_1\left(\frac{100}{T}\right) + a_2 \ln\left(\frac{T}{100}\right) + a_3\left(\frac{T}{100}\right) + a_4\left(\frac{T}{100}\right)^2 + S\left(b_o + b_1\left(\frac{T}{100}\right) + b_2\left(\frac{T}{100}\right)^2\right) + S^2\left(c_o + c_1\left(\frac{T}{100}\right)\right) \quad [2.17]$$

where C* is the oxygen solubility in μmol/kg at 1 atm of pressure, S is the salinity which represents the total quantity of dissolved solids in g/kg, and a_i, b_i, and c_i are fitting parameters obtained from the regression analysis shown in Table 2.2. Equation 2.17 is appropriate for salinity and temperature ranges between 0 to 133 g/kg and 8 to 35 C respectively. In order to apply Equation 2.17 to the pore water within concrete, the constituents of the concrete pore water must be known examples of which are shown in Table 2.3 for various cementing materials.

Oxygen concentrations within the electrolyte are affected by corrosion kinetics occurring on the bar surface and mass transport of oxygen from the concrete surface to the corroding surface. Mass transport of oxygen within concrete is the result of two processes, namely, diffusion through gas occupying the pore structure phase or diffusion through the liquid present in the

Table 2.1. Concrete Pore Solution Dissolved Oxygen Concentration

Oxygen Concentration ($mmol/mm^3$)	Solution	Reference
1.56×10^{-7}	Seawater	Isgor and Razaqpur (2006)
2.25×10^{-7}	Seawater	Balabanic et al. (1995)
3.00×10^{-13}	Not Stated	Kranc and Sagues (2001)
2.90×10^{-5}	Not Stated	Hussain and Ishida (2010a)

Table 2.2. Parameters required for Equation 2.17 (Debelius et al. 2009)

Parameter	Value	Parameter	Value	Parameter	Value
a_0	-173.9321	b_0	-0.04547	c_0	0.00006644
a_1	256.408	b_1	0.01588	c_1	-0.00001928
a_2	146.3559	b_2	-0.0012		
a_3	-22.2471				
a_4	0.001186				

Table 2.3. Pore solution chemistry resulting from different supplementary cementing materials. (Shi et al. 1998)

Cementing Materials	w/c	Age (days)	pH	Pore Solution Concentrations (mmol/litre)					
				Na^+	K^+	Ca^{2+}	SO_4^{2-}	OH^-	Cl^-
100% Portland cement (PC)	0.6	28	13.69	52	318	2.9	11.1	332	1.9
		91	13.71	54	349	2.4	5.8	346	1.9
		365	13.72	63	351	2.0	18.2	360	1.9
		730	13.66	56	289	2.4	2.3	360	1.8
50% PC + 50% slag	0.6	28	13.67	65	282	5.0	12.4	316	0.7
		91	13.64	61	281	2.2	5.1	300	12.2
		365	13.65	71	264	3.0	11.4	306	2.6
		730	13.55	53	222	1.1	1.5	243	0.7
40% PC + 60% flyash	0.42	28	13.68	116	200	0.6	3.8	325	1.3
		91	13.48	96	208	0.3	7.0	208	3.8
		180	13.54	97	209	4.7	10.5	234	2.6
		730	13.51	91	189	0.2	9.3	223	2.3
75% PC + 25% silica fume	0.6	28	13.06	24	51	4.7	0.1	78	1.2
		91	12.47	16	29	4.0	3.9	20	1.3
		180	12.42	10	13	7.2	0.4	18	1.5
		730	13.05	12	16	9.0	0.2	76	1.6
42.5% PC + 42.5% slag + 15% silica fume	0.6	28	13.05	11	22	2.6	0.8	76	1.8
		91	12.55	19	35	2.2	1.0	24	2.0
		365	12.76	11	14	8.4	0.1	39	1.9
		730	12.79	16	22	7.1	0.5	42	1.1

pore structure (Hussain and Ishida 2010a and 2010b). Under saturated conditions, oxygen diffusion is exclusive to the dissolved phase as the pore void network is effectively blocked by water (Huet et al. 2007). However, as concrete becomes less saturated, the pore void network is no longer fully blocked by moisture, allowing diffusion of oxygen through a combination of gaseous and dissolved oxygen mechanisms.

Papadakis et al. (1996) developed a relationship for establishing a blended oxygen diffusion coefficient that addressed porosity and moisture conditions for a particular concrete. The equation was based on experimental data for concretes with a water to cement ration (w/c) between 0.50 and 0.80 as follows:

$$D_{O_2} = 1.92 \times 10^{-6} \varepsilon_c^{1.8} \left(1 - \frac{RH}{100}\right)^{2.2} \quad [2.18]$$

where D_{O_2} is the diffusion coefficient of oxygen under the specified concrete porosity ε_c and relative humidity RH. The resulting diffusion coefficient represents a combination of oxygen diffusion for both gaseous and dissolved phases.

More complex approaches to oxygen diffusion in concrete have been developed that directly address pore structure and saturation level within concrete (Hussain and Ishida 2010a, 2010b). These models simulate oxygen diffusion through concrete by accounting for porosity, constrictivity, tortuosity, and saturation levels within the concrete. Diffusion coefficients applied within this model were assumed to be fixed and employed values for oxygen in pore water of 1 x 10^{-9} m^2/s and in atmosphere of 1.78 x 10^{-5} m^2/s which were then simulated using the following relationship:

$$\frac{\partial}{\partial t}\left(\varepsilon_c \left(1 - S_r\right)\rho_{gO_2} + S_r \rho_{dO_2}\right) = -\nabla J_{O_2} + Q_{O_2} \quad [2.19]$$

where ε_c is the porosity of the concrete, S_r is the degree of saturation (1 being fully saturated, 0 being completely dry), ρ_{gO_2} and $\rho_{dO_2}$is the density of gaseous and dissolved O_2 (g/m^2) J_{O_2} is the flux of dissolved oxygen within the concrete ($g/m^2/s$), and Q_{O_2} is a sink term representing the consumption of oxygen on the bar surface due to corrosion (g/m^2).

The first term of the right hand side of Equation 2.19 represents the flux term which evaluates the porosity and saturation of the concrete by integrating the diffusion contribution of dissolved and gaseous phases of oxygen over the entire porosity distribution as follows:

$$J = -\left(\frac{\phi D_{d,O_2}}{\Omega_1} \int_0^{r_c} dP_v \frac{\partial \left[O_{2_d} \right]}{\partial x} + \frac{\phi D_{g,O_2}}{\Omega_1} \int_0^{\infty} \frac{dP_v}{1+N_k} \frac{\partial \left[O_{2_g} \right]}{\partial x} \right) \quad [2.20]$$

where D_{d,O_2} and D_{g,O_2} are the diffusion coefficient for dissolved and gaseous oxygen (m^2/s), Ω_1 is equal to $(\pi/2)^2$ which accounts for the average tortuosity of a single pore, P_v is the pore volume per m^3 of concrete, $[O_{2_d}]$ and $[O_{2_g}]$ is the concentration of dissolved and gaseous oxygen within the pore solution and atmosphere respectively (kg/m^3), N_k is the Knudsen number which is established by:

$$N_k = \frac{l_m}{2r_e} > 1.0 \quad [2.21]$$

where l_m is the free path length of a molecule of gas (m), and r_e is the actual pore radius minus the thickness of the adsorbed layer of water (m).

The second term of the right hand side of Equation 2.19 represents the sink term and is related to the corrosion current generated on the bar surface by:

$$Q_{O_2} = -\phi S_r M_{O_2} \frac{i_{corr}}{n_{O_2} F} \frac{A_{bar}}{V_{elem}} \quad [2.22]$$

where M_{O_2} is the molecular density of oxygen (32 g/mol), i_{corr} is the corrosion current density occurring on the bar surface (A/mm^2), n_{O_2} is the number of electrons transferred in the corrosion process which is equal to 4 as outlined in Equation 2.2, F is Faraday's constant (C/mol), A_{bar} is the area of the bar surface (m^2), and V_{elem} (mm^3) is the referential finite volume.

The sink term described by Equation 2.22 represents the oxygen consumed by the corrosion process occurring on the bar surface in contact with the concrete pore water. Therefore, only oxygen dissolved within the pore water can be affected by this reaction. However, the quantity of dissolved oxygen in the pore water is a function of the oxygen concentration in the gaseous state so removal of oxygen from one is replenished from the other. The relationship between

dissolved and gaseous oxygen described by Henry's law that relates the quantity of dissolved oxygen to the partial pressure of the oxygen within the gas that is in contact with the pore water. This relationship is described by (Hussain and Ishida 2010a, 2010b):

$$P_{O_2} = \frac{\left[O_{2_d}\right]}{H_{O_2}} \qquad [2.23]$$

Where H_{O_2} is Henry's constant (mol/mm^3/Pa, $[O_{2_d}]$ is the concentration of dissolved oxygen in the electrolyte (mol/mm^3), and P_{O_2} is the partial pressure of O_2 in the gaseous phase (Pa).

Henry's constant is unique for each temperature and type of liquid and gas being considered. However, the constant can be established by relating dissolved oxygen concentrations derived from Equation 2.17 to the partial pressure of oxygen in the atmosphere of 21,227 Pa at sea level.

2.3.2 Chloride Transport

Chloride transport through concrete is restricted to the pore water contained within the pore structure of the concrete. Therefore, in a similar fashion to diffusion of oxygen through concrete, the relative humidity (or degree of saturation) combined with the actual porosity of the concrete influences the final chloride diffusion coefficient.

Relationships for establishing the diffusion coefficient of chloride in concrete have ranged from empirical relationships developed from test data (Boulfiza et al. 2003, Papadakis et al. 1996) to multi-scale modeling where the pore structure of concrete and chloride transport is simulated (Sun et al. 2011). The empirical relationships from test data represent a simpler approach to chloride diffusion modeling, as fewer parameters are required to fully describe the concrete being considered.

Papadakis et al. (1996) proposed the following relationship for estimating the diffusion coefficient of chloride in concrete under various moisture conditions, water to cement (w/c) ratios, and aggregate combinations:

$$D_{c,ref,\infty} = 0.15 D_{H_2O} \frac{1 + S_{g,c}\frac{w}{c}}{1 + S_{g,c}\frac{w}{c} + \frac{S_{g,c}}{S_{g,a}}\frac{a}{c}} \left(\frac{S_{g,c}\frac{w}{c} - 0.85}{1 + S_{g,c}\frac{w}{c}} \right)^3 \quad [2.24]$$

where D_{H_2O} is the diffusion coefficient of chloride in an infinite solution (1.6×10^{-9} m^2/s for NaCl), $S_{g,c}$ is the specific gravity of cement, $S_{g,a}$ is the specific gravity of the aggregate, w/c is the water to cement ratio, a is the aggregate content (kg/m^3), and c is the cement content (kg/m^3). Additional modifications were proposed to Equation 2.24 to account for variations in humidity levels, curing time, and aging as follows (Han 2007):

$$D_c = D_{c,ref,\infty} F_1(h) F_2(T) F_3(t) \quad [2.25]$$

where $F_1(h)$ adjusts for relative humidity:

$$F_1(h) = \gamma + (1-\gamma)\frac{1}{1 + \left(\frac{1-h}{1-h_c}\right)^{n_h}} \quad [2.26]$$

and h is the relative humidity as a value between 0 and 1, γ, h_c and n_h are factors that are dependent on concrete mix proportions and curing conditions. $F_2(T)$ accounts for temperature:

$$F_2(T) = e^{\left(\frac{E}{R}\left(\frac{1}{T_{ref}} - \frac{1}{T}\right)\right)} \quad [2.27]$$

where E is the apparent activation energy (KJ/mol) with representative values shown in Table 2.4, R is the universal gas constant which is equal to 8.314 J/K/mol, T_{ref} is the reference curing temperature (Kelvin) equal to 296 K, and T is the actual temperature (Kelvin). $F_3(t)$ accounts for the age of the concrete at the time when diffusion is being assessed:

$$F_3(t) = 1 + \left(\frac{1}{\beta_3} - 1\right)\left(\frac{28}{t}\right)^{0.5} \quad [2.28]$$

where t is the age (days), and β_3 is a correction factor applied to offset errors introduced with of Equation 2.24 assuming concrete has reached its ultimate age.

In addition to the factors presented previously, chloride diffusion is affected by the local chemistry of the pore water solution as free chloride ions bind with C_3A, C_4AF, and their hydration products to produce Friedel's salt (Han 2007). Chloride binding models are typically based on binding isotherms that relate bound to free chlorides at a given temperature (Martin-Perez et al. 2000, Isgor and Razaqpur 2006a, 2006b). Using the Freundlich isotherm, a relationship between bound and free chlorides was developed by Han (2007) as follows:

$$C_{bc} = gC_f^h \quad [2.29]$$

$$g = 0.056 + 0.02C_3A \quad [2.30]$$

$$h = \frac{1}{0.076C_3A + 1.91} \quad [2.31]$$

where C_{bc} is the bound chloride concentration (%, bound chloride weight/cement weight), C_f is the free chloride concentration within the pore electrolyte (kg/m^3), and C_3A is the composition of cement (%).

2.4 Corrosion Initiation Levels

The electrochemistry presented previously identified chloride as a critical component in whether corrosion would occur on passivated steel. Table 2.5 outlines the range of values reported in the literature that have been observed to cause corrosion for reinforcing steel embedded in concrete (Hurley and Scully 2002). This table identifies multiple values with no clear indication of a single chloride concentration above which corrosion will occur. This observation combined with the range of tests and methods of reporting threshold values creates significant confusion in determining when chlorides will reach a sufficient concentration to cause corrosion to increase for reinforcing steel in concrete.

Izquierdo et al. (2004) suggested this single chloride concentration for corrosion initiation likely

Table 2.4. Diffusion activation energies E in various cement pastes (Saetta et al. 1993))

w/c	E, KJ/mol	
	Ordinary Portland Cement	Pozzolan Cement
0.4	41.8 ± 4.0	-
0.5	44.6 ± 4.3	4.18
0.6	32.0 ± 2.4	-

Table 2.5. Survey of existing data identifying the chloride threshold concentrations that initiated active corrosion on carbon steel reinforcement. (Hurley and Scully 2002)

Test Conditions	Reference	Env.	Threshold Values or Ranges % by weight of cement Free Cl^-	Total Cl^-	Cl/OH	Depassivation Detection Method
Solutions simulating concrete	Hausmann (1967)	Solution			0.60	Shift in Ecorr
Solutions simulating concrete	Gouda (1978)	Solution			0.35	Anodic polarization, shift in Ecorr, visual inspection
Steel in alkaline solutions with chlorides	Goni and Andrade (1990)	Solutions			0.25-0.8	Avg. corrosion rate
Mortar suspensions	Gouda and Halaka (1970)	OPC BFSC		2.42 1.21		Anodic polarization
Cements with high or low alkali content	Petterson (1992, 1994, 1996)	80% RH 100% RH		0.6-1.8 0.5-1.7	2.5-6.0 1.7-2.6 1.7-2.6	Corrosion rate
OPC and BFSC	Andrade and Page (1986)	OPC BFSC			0.15-0.69 0.12-0.44	Corrosion rate
Three OPC Mortar (external Chloride)	Hansson and Sorenson (1990)	100% RH 50% RH		0.6-1.4		Corrosion rate, potentiostatic
Concrete slabs stored in 10% seawater	Petterson (1992, 1994, 1996)	Concrete			1.8-2.9	Corrosion rate
Concrete (external chloride)	Lambert et al. (1991)	Concrete			3.0	Corrosion rate
Concrete with added Cl^-	Gouda and Halaka (1970)	OPC BFSC		3.04 1.01		Anodic polarization
No pre-cleaning bars	Gouda and Halaka (1970)	OPC		0.6		Anodic polarization
Cl- added to admixture MSC HSC HSC + supplement HSC + supplement + fly ash	Kayyali and Haque (1995)	Concrete	 1.15 0.85 0.80 0.45			Assumed threshold Cl^- /OH^- = 0.6
Cement with different C3A content C_3A = 2.43% C_3A = 7.59% C_3A = 14.00%	Hussain et al. (1995)	Concrete	 0.14 0.17 0.22	 0.35 0.62 1.0		Assumed threshold Cl^- /OH^- = 0.3
Concrete with admixed and externally exposed to Cl^-	Schiessl and Breit (1996)			0.5-1 1-1.5		Macrocell currents
Concrete prisms	Thomas et al. (1990)	Concrete /Marine		0.5		Visual observation, mass loss
Concrete prisms Fly ash = 0% Fly ash = 15% Fly ash = 30% Fly ash = 50%	Thomas (1996)	Concrete /Marine		 0.70 0.65 0.50 0.20		Mass loss
Cl- admixed concrete slabs various exposure conditions	Hope and Ip (1987)	OPC		0.1-0.19		Corrosion rate, visual inspection, mass loss
Simulated pore solution	Li and Sagues (2001)	pH = 2.6 pH = 3.5			0.25-0.7 1.05-.25	Shift in Ecorr, polarization resistance
Simulated solution and mortars	Alonso et al. (2000)	Solution Mortar	1.24-.08	0.39-.16	0.25-0.8 1.17-.98	Various

Legend:
OPC – Ordinary Portland Cement. MSC – Medium Strength Concrete.
BSFC – Blast Furnace Slag Cement HSC – High Strength Concrete.

does not exist as methods used for comparing chloride concentration to cement content or OH^- do not address the range of factors that contribute to the corrosion process such as: cement type and presence of supplementing cementitious materials; moisture, oxygen and OH^- levels in the pore water; temperature; concrete porosity; and type and surface roughness of steel.

Alternate approaches for identifying relationships between chloride and corrosion in concrete were developed by Alonso et al. (2002). The original application for this approach was to assess the level of impressed current cathodic protection required to protect reinforcing steel embedded in concrete under a range of chloride concentrations. Results of this research, shown in Figure 2.18, identified a bi-linear relationship between chloride concentrations and the required corrosion potential necessary to protect the reinforcement. This observation is

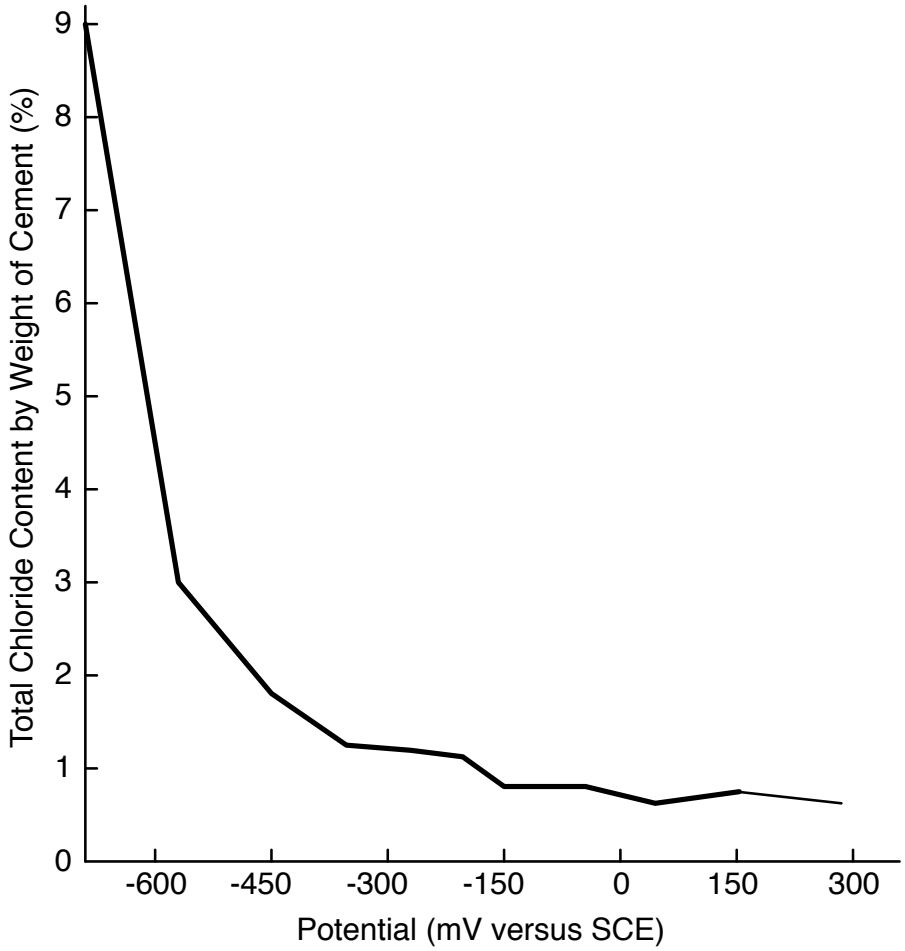

Figure 2.18. Total chloride concentration by weight of cement (%) versus the potential. (Alonso et al. 2002)

consistent with the corrosion thermodynamics shown in Figure 2.4 that identify more negative potentials are required to prevent steel from corroding when chlorides are introduced.

Li (2001, 2002) produced a probabilistic relationship between chloride concentrations and the presence of corrosion by-product on the bar/concrete interface for reinforcing steel embedded in concrete under a wide range of environmental conditions. Several hundred concrete specimens were placed in a chloride-contaminated environment and subjected to load. Parameters varied included the type of cement, cover, and moisture conditions within the concrete in order to capture the effect these variables had whether corrosion would be present. Results from this research are presented in Figure 2.19 as a probability of corrosion versus chloride content. The range of chlorides covered in this research effectively covered the chloride ranges reported in the literature but did not consider the effect cover or concrete pH

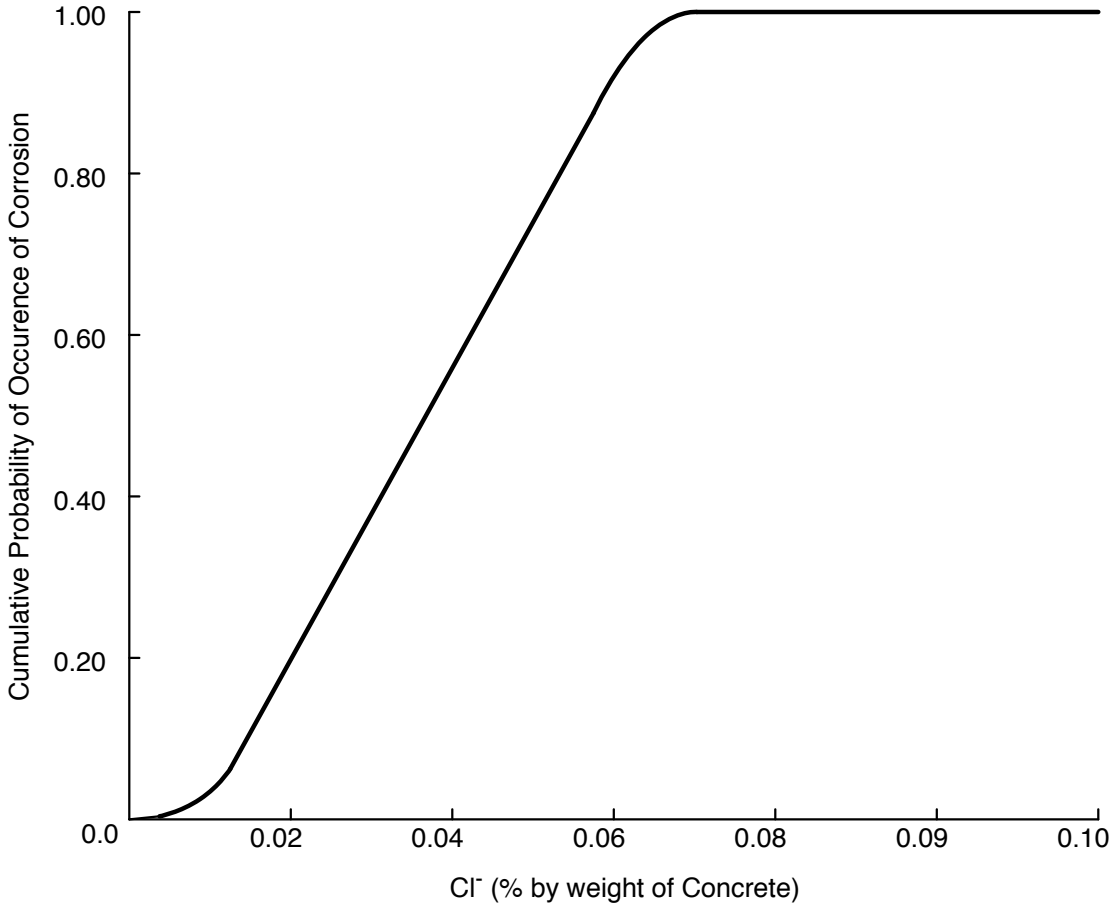

Figure 2.19. Probability of corrosion versus chloride concentration as a % by weight of concrete (Li 2001,2002)

would have on the electrochemistry occurring on the reinforcing steel/concrete interface.

Electrochemical studies on steel in chloride-contaminated environments have been completed in simulated concrete pore solutions and concrete/mortar (Moreno et al. 2004, Garćes et al., 2005, Yu et al. 2012) with the intent of identifying corrosion rates, extent of corrosion, and critical chloride contents required to initiate corrosion. Observations from these tests revealed that simulated pore solution tests were generally consistent while tests conducted on reinforcing steel embedded in mortar or concrete produced a wide range of results that were on average higher (Poursaee 2010, Yu et al. 2012). This variability and high chloride concentration have been attributed to:

- The use of admixed chlorides that become bound to the concrete therefore lowering the concentration of chloride contained in the pore solution in contact with the embedded reinforcing steel; and

- The buffering effect afforded by the concrete providing additional protection over simulated concrete pore solutions.

However, Garćes et al. (2005) suggested the buffering effect provided by concrete to the pore solution at the bar/concrete interface may be overcome as the corrosion process hydrolyzes water molecules to produce $Fe(OH)_2$. This process of hydrolyzing effectively acidifies the pore solution in a local area thereby changing the kinetics of corrosion provided by the original high pH environment. Figure 2.20 describes the change in kinetics for this scenario for a range of chloride concentrations at pH of 9 and 12.5 (Moreno et al. 2004). Included in this figure are lines representing the cathodic reaction described by Equation 2.2 for the pH values considered. As the pH is reduced, anodic reaction lines representing Equation 2.1 shift to more negative potentials with a corresponding increase in corrosion current density. Similarly, as the pH is reduced, the cathodic reaction lines represented by Equation 2.2 shift to more positive potentials due to the relationship described by the Nernst Equations. Therefore, as the pH becomes reduced, the corrosion rate will increase, which may result in high negative corrosion potentials being produced if diffusion barriers are present that restrict the flow of oxygen to the corroding surface.

However, the presence of this acidification will only occur when there is an imbalance between Fe^{2+} created by the anodic reaction described by Equation 2.1 and OH^- created by the cathodic reaction described by Equation 2.2. For uniform corrosion, anodic and cathodic reactions occur

immediately adjacent resulting in a complete balance between the two reactions, thereby maintaining the pore water solution chemistry and pH. However, when anodic and cathodic processes are separated, such as when concentration cell corrosion like pitting or crevice corrosion is present, then Fe^{2+} is created at the anodic site while OH^- is created at the cathodic site. Initially, Fe^{2+} combines with OH^- present in the local electrolyte causing a local reduction in pH. This local reduction is immediately offset by two processes, the first being mass transport of OH^- from the surrounding bulk pore water solution, the second being dissolution of hardened cement paste restoring the chemical equilibrium within the pore solution. If diffusion barriers are present for either of these processes, localized acidification can occur, as has been reported in the literature from studies in crevice corrosion (Heppner 2006, Evitts 1997, Kennell 2012).

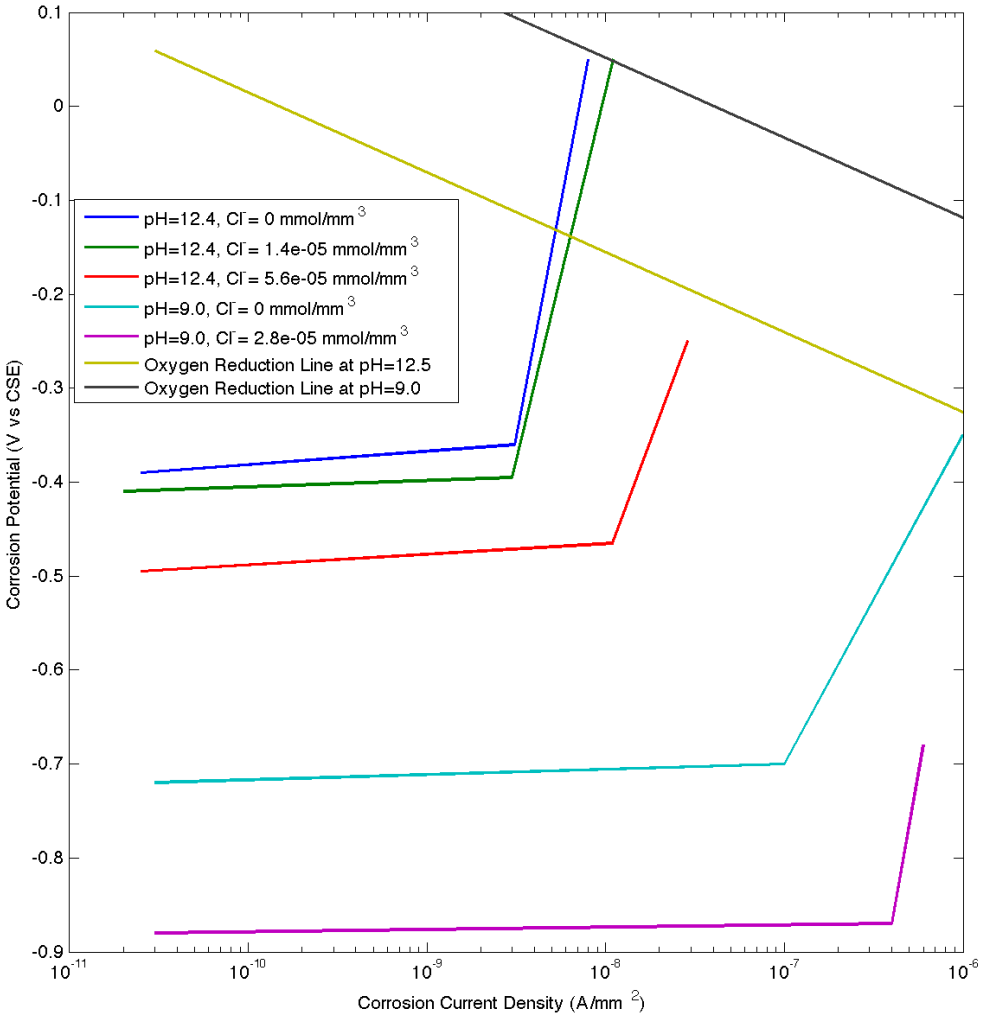

Figure 2.20. Kinetics of corrosion for pH 12.5 and pH 9.0, modified to include cathodic reaction line for oxygen. Moreno et al. (2004).

2.5 Corrosion Models

In previous sections, the corrosion process, mass transport of species that affect the corrosion process, and chloride concentrations for corrosion initiation were reviewed. Using the principles of electrochemistry, many attempts have been made to incorporate this information into numerical models for simulating the corrosion process in order to better understand the mechanisms by which corrosion develops on a bar embedded in concrete. The models developed have several similarities that allow them to be grouped as follows:

- Micro-cell models where corrosion sites on the bar are assumed to be either anodes or cathodes with the area of each being balanced;
- Macro-cell models where one bar is assumed to be the anode with another bar at a distance being the corresponding cathode; or
- Combined micro and macro cell models where electrolyte conductivity and potential differences created result in coupling of cathodic and anodic processes along the linear axis of a single bar.

A micro-cell model developed by Hussain and Ishida (2010a and 2010b) and shown in Figure 2.21 was created to evaluate the effect different geometrical configurations combined with

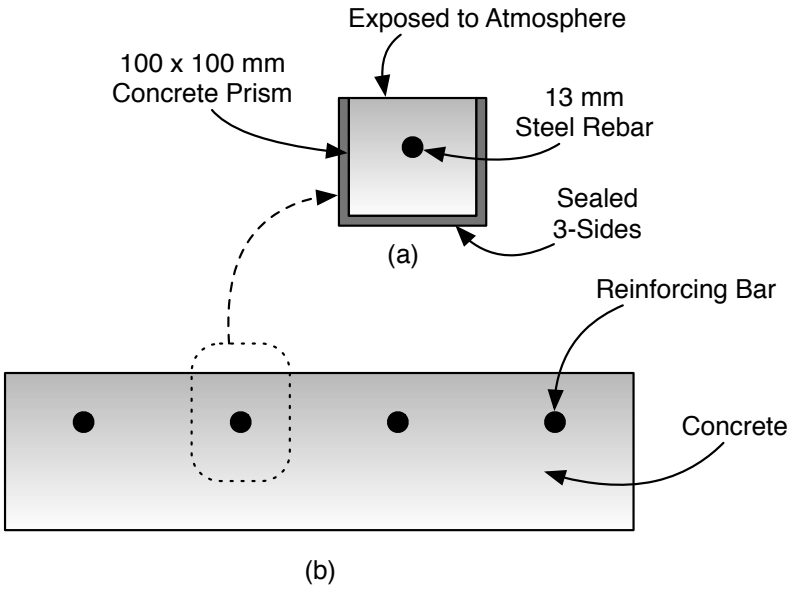

Figure 2.21. Micro-cell corrosion model: (a) Test setup used to validate numerical model, (b) Simulated concrete deck slab. (Hussain and Ishida (2010a).

chloride concentrations would have on the overall corrosion rate for a bar exposed to the environment on one side. The kinetics of corrosion were assumed to follow a fully-depassivated kinetic diagram similar to Figure 2.6, combined with potential oxygen limitations induced by the concrete cover. Field test models used concrete that contained admixed chlorides, thereby providing a uniform chloride environment around the bar circumference. The simulations and test program indicated that diffusion of oxygen is a limiting factor for corrosion, but only when high covers, high relative humidity or low permeability concrete are present.

Isgor and Razaqpur (2006a, 2006b) developed a model, shown in Figure 2.22, for evaluating the effect concrete resistivity, cover thickness, oxygen availability, and the anode to cathode ratio would have on the half-cell corrosion potentials measured on the concrete surface measurement. The model identified represents the surface of a length of bar with constant cover, with the length assigned to the cathode and anode being a user defined input to the model. Corrosion was assumed to occur when chlorides reached a pre-set value identified by the user. Once corrosion was initiated, kinetics was based on a fully depassivated kinetic diagram similar to Figure 2.6. Numerical corrosion rates were compared to experimental measurements of corrosion rates obtained from a parallel study using a galvanostatic pulse technique. For all cases, the numerical simulation appeared to over predict the corrosion rate obtained from the experimental study. This discrepancy was deemed a result of corrosion being highly localized, which the galvanostatic pulse technique could not accurately identify or

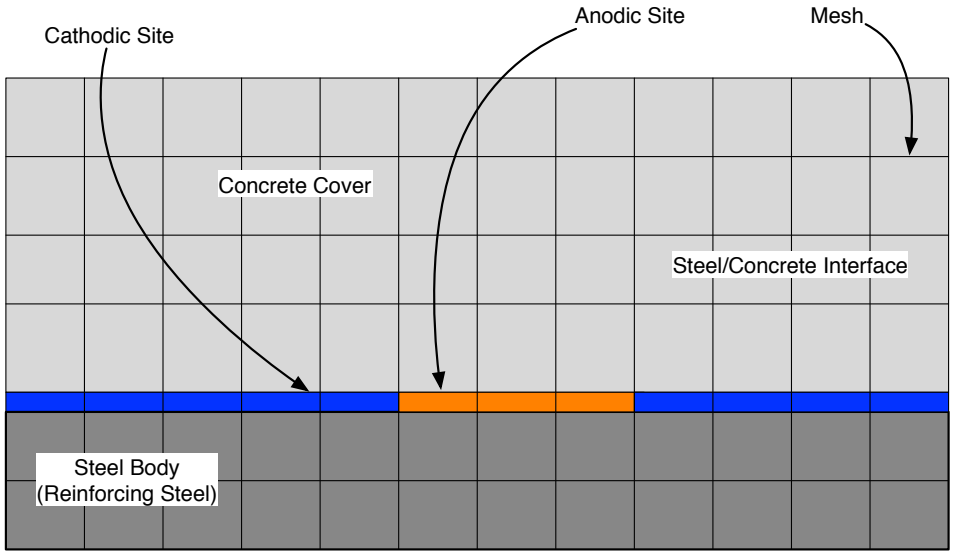

Figure 2.22. Macro-cell Numerical Model (Isgor and Razaqpur 2006a, 2006b).

quantify.

Maruya et al. (2007) developed a combined micro/macro-cell model and performed field tests on concrete beams of similar geometry for evaluating corrosion processes in a reinforced concrete element. The model shown in Figure 2.23 contained a single bar embedded in concrete exposed to the atmosphere on two sides, one of which contained chloride. The finite element mesh employed for the numerical simulation, while in two dimensions, resulted in transport processes from the concrete surface to the bar surface being one-dimensional. The micro-cell corrosion model adopted was identical to that shown in Figure 2.12, which contradicts the impact chlorides produce on passivated metals reported in most corrosion textbooks and results obtained from polarization experiments on simulated pore solutions shown in Figure 2.20.

The micro cell corrosion phase developed corrosion potentials along the bar axis that were then

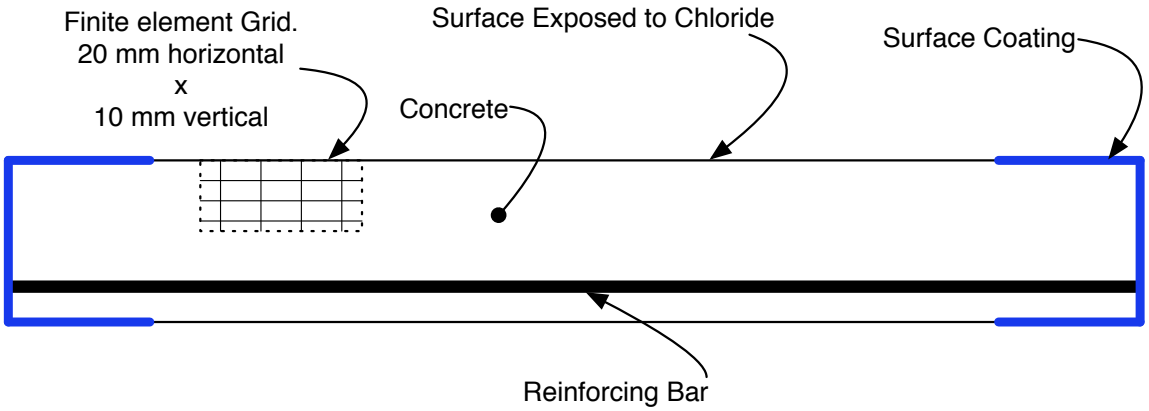

Figure 2.23. Micro and Macro cell model arrangement. (Maruya et al. 2007)

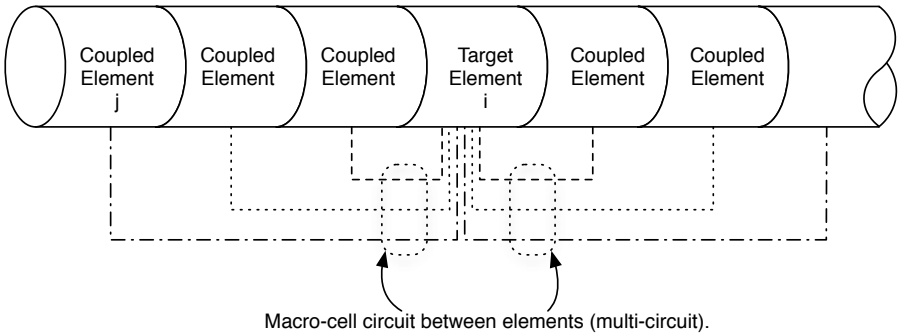

Figure 2.24. Multi-circuit model. (Maruya et al. 2007)

used to evaluate the magnitude of coupling between adjacent bar sections due to differences in micro-cell potential. The model employed is represented in Figure 2.23, which identifies the electrical circuit that connects each segment along the bar. Current flow was estimated between each segment using:

$$i_i = \frac{1}{B_L \Delta L_i} \sum_{j=1}^{n_e} \frac{\Delta e_{i,j}}{w \Delta L_{i,j}} B_L \Delta L_j \qquad [2.32]$$

where i_i is the current density (A/mm^2) for element i, $\Delta e_{i,j}$ is the potential difference between elements i and j (Volts), $\Delta L_{i,j}$ is the distance between element i and j (mm), w is the specific resistance of concrete (Ω), B is the width of the element (mm), ΔL_i is the length of element i and ΔL_j is the length of element j (mm). This coupling model assumed each coupled segment was directly connected to the target element thereby eliminating the effect on $\Delta e_{i,j}$ that current flow from one element has on the adjacent element.

The models presented previously have assumed corrosion around the bar circumference is uniform. Kim and Kim (2008) developed a model to evaluate the circumferential variation in corrosion behavior of a bar embedded in concrete for the purpose of assessing the time to cracking caused by localized corrosion. Figure 2.25 outlines the model employed for this research that describes a single bar positioned within a block of concrete. Boundary conditions assumed that oxygen and chloride would be available on the top surface with the remaining surfaces preventing transfer of oxygen or chloride. Kinetic behavior for the reinforcing steel assumed full depassivation when a preset chloride concentration was reached. Once initiated, corrosion behavior was assumed to be similar to uniform corrosion so the effects of coupling between different portions of the bar circumference were not considered. Results identified that corrosion by-product would build up on the bar/concrete surface closest to the concrete surface, an observation that is consistent with observations from in-service structures.

The numerical models presented above have employed simplifications for addressing kinetics of corrosion, mass transport of chlorides and oxygen to the bar/concrete interface, and macro-cell formation, which introduces significant uncertainty to the results obtained. However, improvements to current modeling practices for reinforced concrete corrosion are possible by considering techniques developed for modeling similar corrosion processes in different environments and configurations.

Pitting corrosion has been identified as the main type of corrosion observed in reinforced corrosion (Liu and Weyers 1998, Kim and Kim 2008). Pitting corrosion is a form of concentration cell corrosion that has many similar characteristics to crevice corrosion that has been extensively modeled by Kennell and Evitts (2009) and Kennell et al. (2008). This model, shown in Figure 2.24, addresses many of the simplifications adopted for reinforced concrete by accounting for:

- Diffusion of species along the surface outside of the crevice (bold surface) and crevice thereby creating variations in electrolyte chemistry along the two surfaces;
- Consumption of oxygen on the bold surface and within the crevice due to electrochemical reactions creating different electrochemical environments in each location; and
- Changes to the kinetics of corrosion caused by changes in the local electrolyte are matched to experimental results obtained for kinetics of corrosion for different pH and Cl^- concentrations.

The model, used by Kennel and Evitts (2009), was based on an earlier model developed by

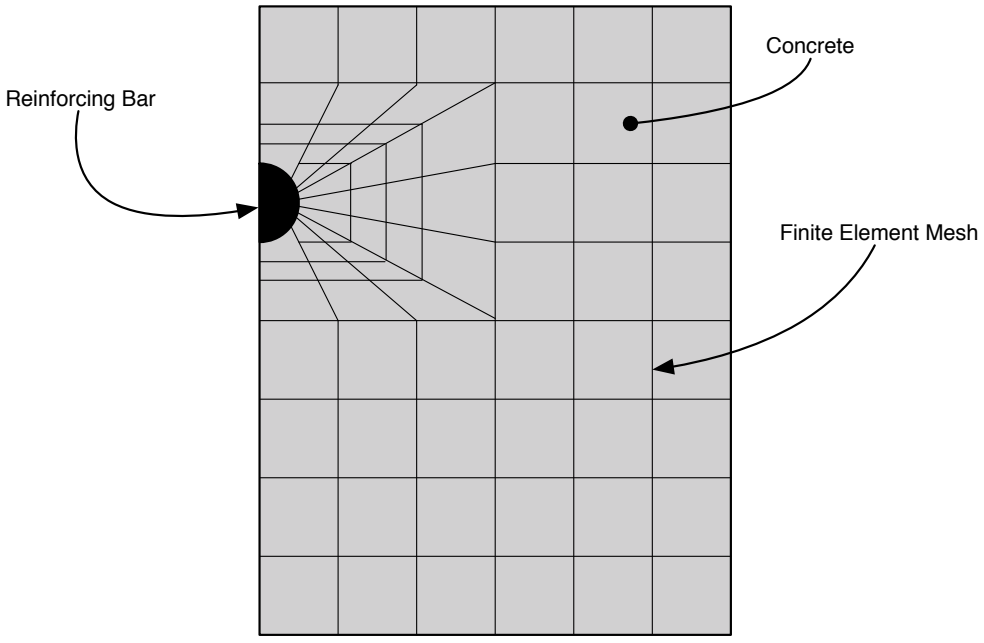

Figure 2.25. Macro-cell model for evaluating circumferential variation in chloride and oxygen concentrations. (Kim and Kim 2008).

Watson (1989), Watson and Postlethwaite (1990a, 1990b, 1991), Evitts (1997), and Heppner (2006) that employed a one-dimensional lumped parameter model to describe the electrochemistry occurring in a stainless steel pipe flange connection. While this model was based on simulating corrosion for stainless steel, the principles employed are portable to any material if information is available for describing the kinetics of corrosion and electrolyte chemistry under a wide range of environmental conditions.

Mass transport within the Kennell and Evitts (2009) model between the bold surface and crevice was described using a mass transport model developed by Watson and Postlethwaite (1990a, 1990b, and 1991), which is reproduced as follows:

$$\frac{\partial C_i}{\partial t} = n_i \mu_i \frac{F^2}{\varepsilon} C_i \sum_{j=1}^{m} n_j C_j$$

Poisson Term: Minimizes charge imbalances in the solution. [2.33a]

$$- \frac{n_i \mu_i \nabla C_i}{F \sum_{j=1}^{m} n_j^2 \mu_j C_j} i_{corr}$$

Migration Term: Calculates concentration changes due to current flowing through the electrolyte. [2.33b]

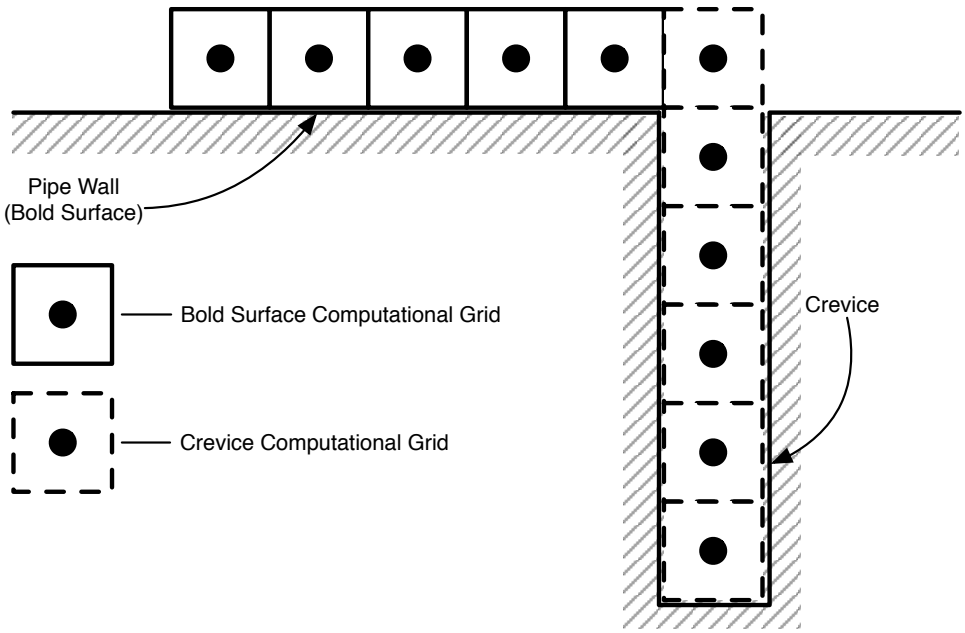

Figure 2.26. Crevice corrosion model as proposed by Kennell and Evitts (2009)

$-\frac{n_i\mu_i\nabla C_i}{\sum_{j=1}^{m} n_j^2\mu_j C_j}\sum_{j=1}^{m} n_j D_j \nabla C_j$	Diffusion Potential Term: Determines concentration changes due to electrostatic potential gradients caused by variations in electrolyte composition.	[2.33c]
$+D_l\nabla^2 C_l$	Diffusion Term: Calculates changes in solution composition due to concentration gradients in the electrolyte.	[2.33d]
$+R$	Reaction Term: Calculates production or loss of species due to homogeneous chemical reactions.	[2.33e]

where i represents the species under consideration; n is the species charge (one for OH^-, two for Fe^{2+}); μ is the ionic mobility of each species which is described by Equation 2.34 below; C is the concentration of the species under consideration (mol/mm^3); i_{corr} is the corrosion current density (A/mm^2); D is the diffusion coefficient of the species under consideration (mm^2/s); ε is the permittivity in Farad/m; and F is Faraday's constant.

$$\mu_j = \frac{D_j}{RT} \qquad [2.34]$$

where R is the universal gas constant, T is the temperature in Kelvin, and D_j is the diffusion coefficient of species j.

The Poisson Term, Migration Term, and Diffusion Potential Term were all included as the environment considered in the simulation created significant potential drops through the electrolyte that were attributed to these parameters. For other types of electrolytes, such as a supporting electrolyte, these parameters can be ignored as the conductivity of the solution effectively negates the effects induced by the Poisson's Term, Migration Term, and the Diffusion Potential Term (Newman and Thomas-Alyea (2004)).

Potential drops and corresponding current flow through the electrolyte were related using fundamental principles described by (Newman and Thomas-Alyea 2004):

$$\nabla\phi = -\frac{i}{\kappa} - \frac{F}{\kappa}\sum_{j=1}^{m} n_j D_j \nabla C_j \qquad [2.34]$$

where Φ is the potential difference between the two locations (volts), i is the current flow (A/mm^2), κ is the conductivity of the electrolyte (1/ohm/mm) described by Equation 2.36, z_j, D_j, and C_j are the number of electrons transferred in the reaction, diffusion coefficient (mm^2/s), and concentration of each species j being transferred (mol/mm^3).

Solution conductivity was related to concentration and mobility of each species present in the electrolyte by:

$$\kappa = F^2 \sum_{j=1}^{m} n_j^2 \mu_j C_j \qquad [2.36]$$

At initial conditions, oxygen concentrations within the crevice and bold surface were set to the same value. A low corrosion current is generated by these conditions which causes the crevice to become deoxygenated resulting in the corrosion potential within the crevice to become more negative. The lower corrosion potential relative to the bold surface created a corrosion couple between these two sites resulting in an increase in the metal dissolution rate in the crevice, increased oxygen reduction on the bold surface and ionic current flow through the electrolyte that completed the corrosion cell circuit.

Corrosion currents through the electrolyte were calculated by isolating each half-cell, solving the resulting non-linear equations sequentially, and then balancing current generated from each cell to ensure equal currents were produced. The sequential solution was necessary, as the number of segments contributing cathodic or anodic current was not set as part of the analysis. Rather the size of each half-cell was calculated from the corrosion potential differences present, conductivity of the solution, and species concentrations separating the two regions. This approach allowed segments to be de-coupled from the corrosion cell if insufficient potential differences existed between segments or if potential drops induced by current flow from adjacent segments were sufficient to eliminate a contributing segment from the current flow. Results of this model accurately predicted experimental data from similar test geometries that recorded corrosion potential, corrosion current, pH, and the location of anodic and cathodic zones along the bold and crevice surfaces for stainless steel exposed to chlorides.

2.6 Summary of Literature Review

Extensive research has been completed on electrochemical processes that occur on reinforcing steel embedded in concrete. However, the literature search identified that implementation of electrochemical principles were not consistent between models or with the fundamentals of electrochemistry such as:

- Electrolyte chemistry at the bar/concrete interface is assumed to be constant around the bar circumference for most models except for the model proposed by Kim and Kim (2008);

- Corrosion occurs when a pre-set chloride concentration is reached (Isgor and Razaqpur 2004, Kim and Kim 2008, Hussain and Ishida 2010a, 2010b). When this value is attained, a kinetic of corrosion diagram similar to Figure 2.6 that is based on steel in a neutral pH environment. This assumption is inconsistent with results from electrochemical studies such as those reported in Figure 2.12 which indicate a low rate of corrosion is occurring when chlorides are not present and that corrosion rates slowly increase with increasing chloride until a maximum rate is reached;

- Under macro-cell corrosion, acidification at the regions where the anode is formed is ignored or assumed to occur when a pre-set chloride level is reached. In other words, the change in local electrochemistry as corrosion develops is not considered as part of the models reviewed;

- Passivated kinetic of corrosion diagrams have adopted an idealized shape (Maruya et al. 2007); however, the effect of chloride on this diagram does not follow observations recorded in other fields of corrosion engineering; and

- When macro-cell corrosion is modeled, adjacent segments which cover the entire bar circumference are electrically connected to a target element thereby forcing all corrosion current generated at each segment to by-pass adjacent segments (Maruya et al. 2007). This simplification does not address field observations of corrosion by-product present on the side of the bar closest to the chloride-contaminated surface.

Therefore, including features from models developed from other forms of corrosion can address many of the simplifications adopted in models for corrosion in reinforced concrete. The

methods by which these features are adapted to reinforced concrete, along with the methodology employed for calibration, are covered in the next section.

3 RESEARCH METHODOLOGY

3.1 Overview

Several models for describing the corrosion process occurring on the surface of a reinforcing steel bar imbedded in concrete have been described in the previous section. However, each of these models and experimental test setups used to validate the models has included simplifications in their development that were identified in Section 2.6. These simplifications produce results that are inconsistent with corrosion patterns obtained from field observations such as those presented in Figure 1.1. Therefore, developing models that accurately reflect field observed corrosion patterns would enable practicing engineers to improve predictions related to existing structures so that effective repairs are implemented that reduce the overall life cycle cost.

The model proposed by Kim and Kim (2008) recognized the circumferential variation of the pore solution chemistry caused by chloride reaching the side of the bar closest to the concrete surface. However, this model was developed to describe corrosion buildup that would occur on the bar surface closest to the concrete surface; as a result a simplified kinetic of corrosion curve was employed and coupling due to differences in corrosion potential around the bar surface were ignored. Therefore, this model represents a suitable starting point that can be modified to include:

- Kinetic of corrosion curves that account for chloride, oxygen, and hydroxide ion concentrations that change during the simulation;
- Corrosion current models that account for:
    - Ohmic potential drops through the electrolyte;
    - Variation in pore solution conductivity as ionic concentrations change with the arrival of chloride; and
    - Electrical connectivity at the bar/concrete interface influencing the corrosion current contribution from each segment around the bar.
- Development of acidified zones on the bar/concrete interface where chlorides have produced sufficient corrosion by-product to isolate the bar from the concrete; and

- Accommodation of uniform and concentration cell corrosion on the same surface.

The proposed numerical model simulates corrosion processes present in reinforced concrete by allowing development of micro and macro cell corrosion on the same surface due to local chemistry changes induced by chloride and oxygen. The model is also able to simulate corrosion on any uncoated reinforcing bar type such as stainless steel or low carbon chromium steel (trade name MMFX), if sufficient kinetic of corrosion data is available for the steel used.

The development of local chemistry changes are described in Figure 3.1, which represent a single idealized reinforcing steel bar embedded in concrete with a uniform chloride front reaching the bar. While the assumption of a uniform chloride front is not realistic in practice it

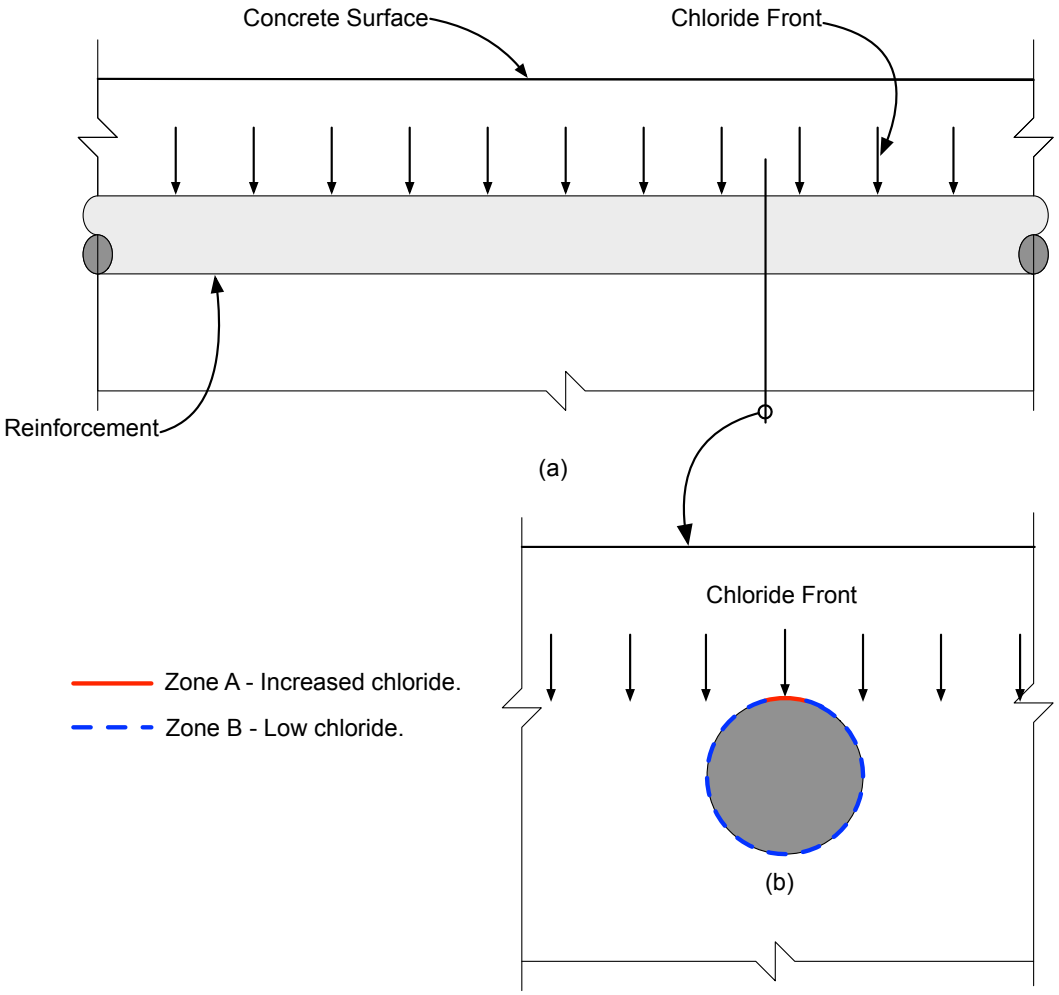

Figure 3.1. Rebar depassivation with variable chloride front. (a) Elevation of idealized reinforcing steel embedded in concrete. (b) Section through reinforcing steel bar showing chloride contacting the bar.

serves to illustrate the circumferential variation of chloride that occurs on a reinforcing steel bar embedded in concrete. Figure 3.2 presents the effect this circumferential variation has on the local kinetics of corrosion. This figure contains experimentally derived kinetic of corrosion data for reinforcing steel in a high pH environment published by Moreno et al. (2007) modified to include the cathodic reactions represented by oxygen reduction (Equation 2.2). Kinetics for the oxygen reduction line was selected to provide corrosion potentials under chloride free conditions that were consistent with field observations of -0.100 to -0.200 V versus CSE (Skeet and Kriviak 1994). On this basis, the following values were selected:

- Reversible potential = 0.083 V relative to the copper sulfate electrode (CSE) (Ge and Isgor 2007);
- Reversible corrosion current = $6x10^{-12}$ A/mm^2 (Ge and Isgor 2007); and
- Tafel Slope = -0.085 V/decade (Gojkovic et al., 1994).

The remaining lines represent the kinetics of corrosion for a reinforcing steel bar in a simulated concrete pore solution at different chloride concentrations. The terms $e_{uncoupled}$ and $i_{uncoupled}$ refer to corrosion potentials and current densities for the two zones identified which are shown as Zone A – Increased Chloride, and Zone B – Chloride Free.

The electrochemical processes and the effect of mass transport on a bar embedded in concrete can be understood by combining Figures 3.1 with the kinetic of corrosion diagram presented in Figure 3.2. When these figures are combined, the following observations can be made:

- Zone A - When chlorides reach the reinforcing steel surface in sufficient amounts, a small area is created where kinetics are changed as the line representing Equation 2.1 is shifted to the right. With this shift, the intersection of the oxygen reduction line with the steel dissolution line (Equation 2.2) is shown as two points in Figure 3.2, which identify oxygen conditions that may be present within Zone A that will affect the local corrosion current density and corrosion potential. These points are labeled as Zone A – No Oxygen Limit and Zone A – Limiting Current Reached. The selection of one point over the other is dependent on the mass transport properties of the surrounding concrete and

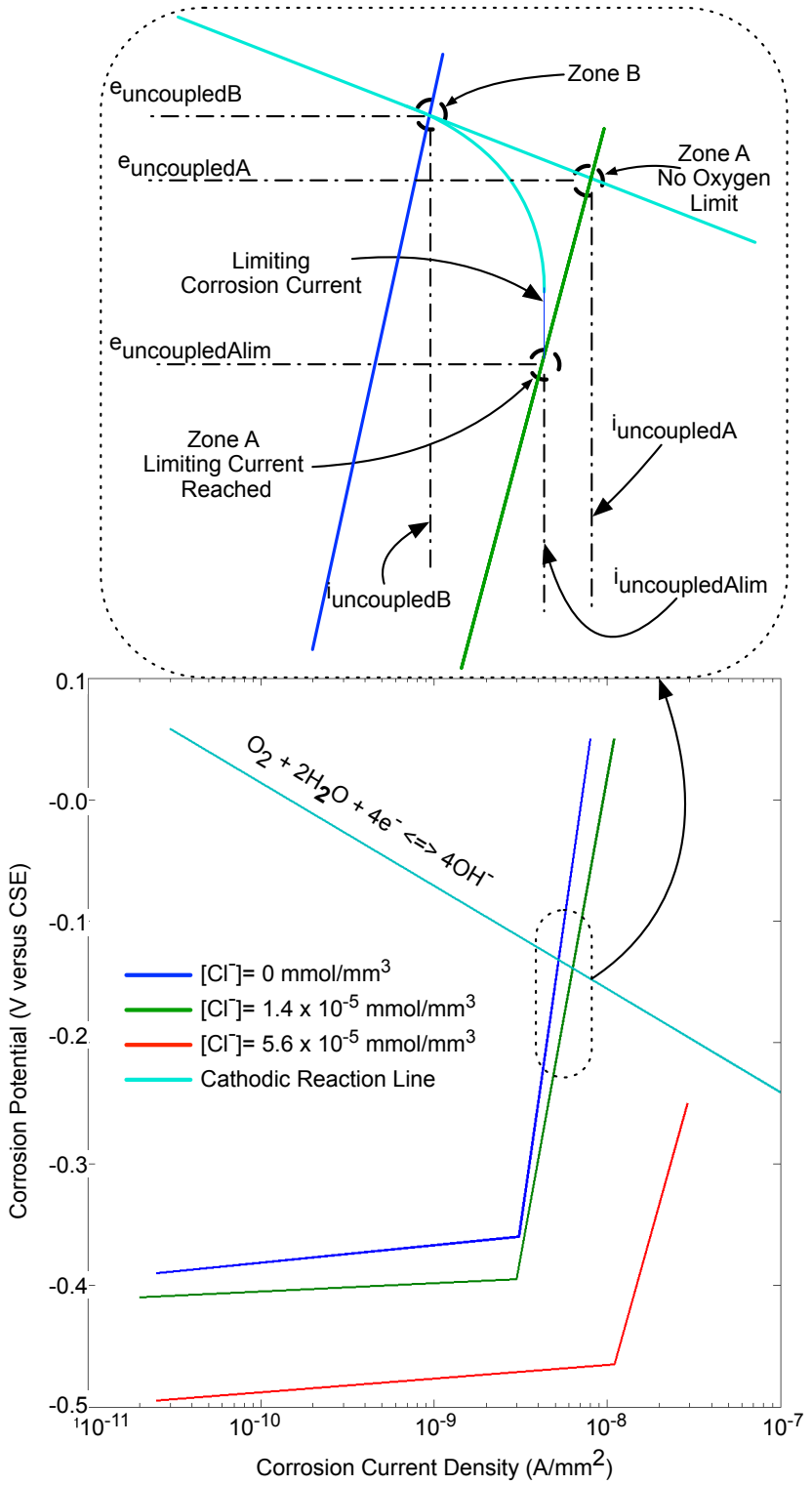

Figure 3.2. Kinetic of corrosion diagram for reinforcing steel shown in Figure 3.1 modified to include the Cathodic Reaction Line and the two zones identified as Zone A – Increased Chloride and Zone B – Chloride Free.

the rate at which oxygen is consumed on the bar/concrete interface. If sufficient oxygen is present to sustain local corrosion rates, the effect of increased chloride results in $e_{uncoupledA}$ and $i_{uncoupledA}$. If oxygen limitations are present, then corrosion potentials and corrosion current densities change to $e_{uncoupledAlim}$ and $i_{uncoupledAlim}$; and

- Zone B – On the remainder of the bar, chlorides have not affected the kinetics so the intersection of the oxygen reduction line with the steel dissolution line occurs at $e_{uncoupledB}$ and $i_{uncoupledB}$.

From the preceding discussion it is apparent that Zone A and B will be at different corrosion potentials and current densities on the same surface. If there is no pore solution on the bar/concrete interface to electrically connect these points through the concrete then the local corrosion rates will be as predicted by Figure 3.2. However, pore solutions are normally present which result in the bar/concrete interface being electrically connected which allows corrosion process on the bar surface to become coupled which is discussed in more detail in Section 3.3.

Kim and Kim (2008) and others have demonstrated that chloride transport through concrete produces different environmental conditions around the bar. Combining these different environmental conditions with kinetics of corrosion results in areas of the bar circumference corroding at different rates and potentials. Similar examples of spatial separations of the anodic and cathodic reactions on a reinforcing bar have been found to occur at (Raupach 2006, Qian et al. 2006, Soleimani et al. 2010):

- Interfaces between two types of concrete such as repaired to unrepaired or barrier to bridge decks;
- Cracks which intercept embedded reinforcement; or
- Locations where different moisture conditions exist such as the transition between a barrier to bridge deck.

Spatial separation of the cathode and anode around the bar circumference has not been documented in the literature, which is counter intuitive given that mass transport of chloride requires time to fully encapsulate the reinforcing steel. Therefore, the proposed model is structured to simulate the arrival of chloride and oxygen to the bar/concrete interface at different times. As well, the proposed model simulates mass transport of oxygen and chloride to the bar

surface in conjunction with the corrosion processes that result from the chemistry imposed. Therefore, the final model is a hybrid that incorporates principles of:

- Differential corrosion cells developed by Kennell and Evitts (2009) that describe the corrosion process resulting from separation of the cathodic and anodic processes on a common steel surface; and

- Mass transport using Fickian processes that account for the delay in transport of chloride and oxygen to the corroding surface caused by the concrete cover.

At this time, the proposed model does not account for the presence of an asphalt wearing surface or membrane. However, these features could be added at a later date without affecting the underlying corrosion principles developed to simulate corrosion on the bar/concrete interface.

Modifications to Kennell and Evitts (2009) model have been proposed as several features required for their study are not necessary for applications involving reinforced concrete as the concrete cover simplifies some of the mass-transport and chemical reaction processes. The modifications proposed for this research include:

- Mass transport effects caused by Poisson's term (Equation 2.33a), migration (Equation 2.33b), and diffusion potential (Equation 2.33c) can be neglected as the pore solution is considered a supporting electrolyte (Newman and Thomas-Alyea 2004); and

- Interactions between the species liberated at each half-cell site and the electrolyte will not result in significant changes to the local electrolyte chemistry as the pore solution and hardened cement are assumed to act as buffers. While this modification was employed to simplify the overall model, discussions are presented in Chapter 5 which outline how this buffer can be eliminated, resulting in acidification of the corroding area on the bar/concrete interface.

Therefore, the final model used to simulate mass transport and corrosion processes on the bar surface includes:

- A two-dimensional finite element model for describing chloride and oxygen transport to the bar surface. Results from this analysis will be used to establish uncoupled corrosion

potentials around the bar circumference from the kinetics of corrosion shown in Figure 3.2, using local chemistry and oxygen limitations induced by the concrete; and

- From the starting uncoupled corrosion potentials derived from the two-dimensional finite element model, a one-dimensional current flow model will be implemented to determine if current flow is possible and, if so, to what magnitude between portions of the bar circumference.

The two-dimensional model was developed using the MATLAB™ Partial Differential Equation Toolbox, while the one-dimensional model has been programmed using the MATLAB™ language (MATLAB™ 2009, Mathworks 2009).

3.2 Two-Dimensional Model

The proposed two-dimensional model is based on a typical bridge deck geometry outlined in Figure 3.3, combined with the boundary conditions identified in Table 3.1. While the model is based on simulating mass transport and electrochemical processes for reinforcing bar embedded in a bridge deck, the principles and results are applicable to a reinforcing bar embedded in other elements such as a barrier, abutment, or pier.

Variables introduced into the model include:

- Geometry – cover to the embedded bar, bar diameter, and bar spacing; and
- Materials – concrete diffusivity parameters for chloride and oxygen.

Principles used to model the transport of chloride and oxygen to the bar surface have been assumed to follow Fick's Second Law of Diffusion as presented in Section 2.3. Initial conditions within the model space are set to be chloride free and oxygenated to the levels sustainable by the relative humidity adopted for each simulation. Values for oxygen concentrations within the

Table 3.1. Two-Dimensional Model Boundary Conditions

Species or Element	Top	Bottom	Sides	Bar Surface
O_2	Constant	Constant	Zero Flux	Flux set by Kinetics
Cl^-	Constant set at the beginning of each run.	Zero Flux	Zero Flux	Zero Flux
Fe^{2+}, OH^-	Zero Flux	Zero Flux	Zero Flux	Flux set after O_2 flux is known

model space, concrete porosity, and pore saturation assumed for this analysis are shown in Table 3.2.

Diffusion coefficients for chlorides and oxygen are calculated using the relationships reported by Papadakis et al. (1996), expressed in Equation 2.24 for chloride, and Papadakis et al. (1991) for oxygen, as given in Equation 2.18. To account for humidity, temperature and curing conditions, Equation 2.24 is modified in accordance with Equations 2.25 to 2.28.

Using the above relationships, chloride and oxygen transport to the reinforcing steel can be simulated under a variety of moisture and boundary conditions. Corrosion potential differences on the bar surface created by either the presence of chloride or a depletion of oxygen are evaluated to determine the extent of current flow occurring through the electrolyte using the current flow model described in the next section.

3.3 One-Dimensional Current Flow Model

Corrosion current and potentials around the bar circumference generated from the two-dimensional model are used to determine if current flow is possible through the connecting electrolyte. If current flow is possible, the resulting corrosion potentials and current are considered coupled as the two half-cell processes are occurring at different points on the same bar. Referring to Figure 3.2, it is apparent that a drop in corrosion potential occurs between Zone B that is chloride free to Zone A – No Oxygen Limit where chlorides are present. A greater drop in potential occurs between Zone B and Zone A – Limiting Current Reached where transport of oxygen to the corroding surface cannot sustain the higher corrosion rate. This limiting corrosion current is possible when high covers, low diffusivity materials, or membranes are present which can result in the portion of bar furthest from the concrete surface reaching a limiting corrosion current condition resulting in a sharp lowering of the corrosion potential.

Either scenario produces the conditions for ionic flow to occur through the pore solution that connects the two areas (Soleimani et al. 2010). When this ionic flow occurs, anodic processes

Table 3.2. Constants Assumed for Oxygen Concentration Calculations

Variable	Value	Reference
PS	Variable as per Figure 2.17	Papadakis et al. 1991
ε_p	8% (w/c 0.4)	Papadakis et al. 1991
$[O_2]_g$	8.56×10^{-7} mol/mm^3	
$[O_2]_d$	Variable, based on salinity, porosity, and humidity	Debelius et al. 2009

in zones with more negative corrosion potentials are increased while zones of higher corrosion potential affect the cathodic process by either increasing the rate of oxygen consumption or by suppressing the local dissolution rate. This phenomenon is discussed in more detail in Section 4.

The model proposed to simulate flow of charged ions between the cathode and anode on the bar perimeter is based on corrosion fundamentals outlined by Newman and Thomas-Alyea (2004). Figure 3.4 outlines the electrical circuit proposed to model the current flow between half-cells as a series of potential drops that represent:

- Overpotentials at the anode (Φ_{Anode}) and cathode ($\Phi_{Cathode}$) which occur when current flows through the electrolyte;
- Ohmic potential drops through the electrolyte ($\Phi_{\Omega,Cathode}$ and $\Phi_{\Omega,Anode}$) caused by

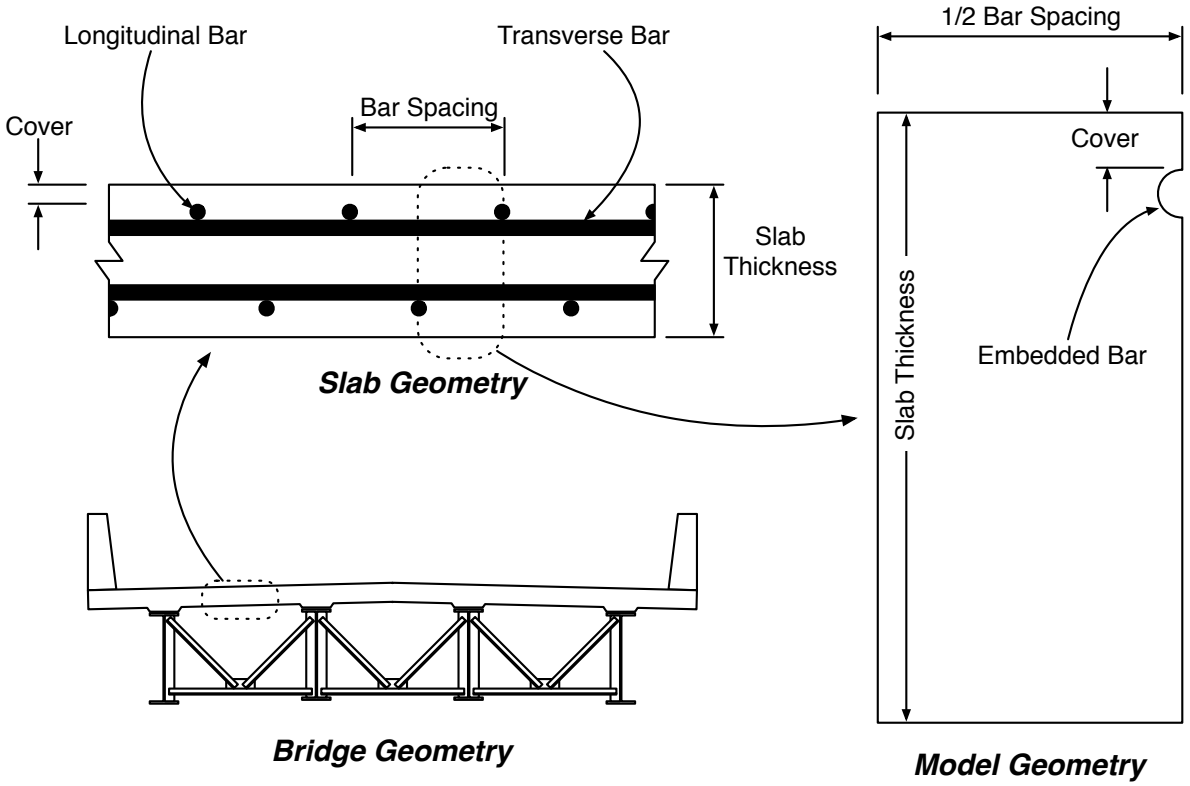

Figure 3.3. Proposed model geometry and its relation to a typical bridge deck.

resistivity of the pore solution connecting the two sites; and

- Concentration potential drops through the electrolyte ($\Phi_{conc,Cathode}$ and $\Phi_{conc,Anode}$) caused by concentration differences within the electrolyte separating the half-cells.

Corrosion potentials $e_{uncoupled,Cathode}$ and $e_{uncoupled,Anode}$ represent the uncoupled corrosion potentials identified in Figure 3.2 as Zone A and Zone B respectively. The coupled corrosion potentials represented by $e_{coupled,Cathode}$ and $e_{coupled,Anode}$ are created when current flows between the half-cells. This current flow only occurs when sufficient corrosion potential differences are present in the uncoupled condition to overcome the potential drops identified.

For this research, potential drops caused by concentration changes in the pore solution have been neglected as the electrolyte is expected to act as a buffer and absorb or release the appropriately charged species as necessary. However, ohmic potential drops will be evaluated using (Newman and Thomas-Alyea 2004) where:

$$\phi_{\Omega} = \frac{i}{\kappa} \qquad \text{Eq 3.1}$$

where i is the current density through the electrolyte (A/mm^2) and κ is the conductivity of the electrolyte defined in Equation 2.36. The use of Equation 2.36 for establishing the solution

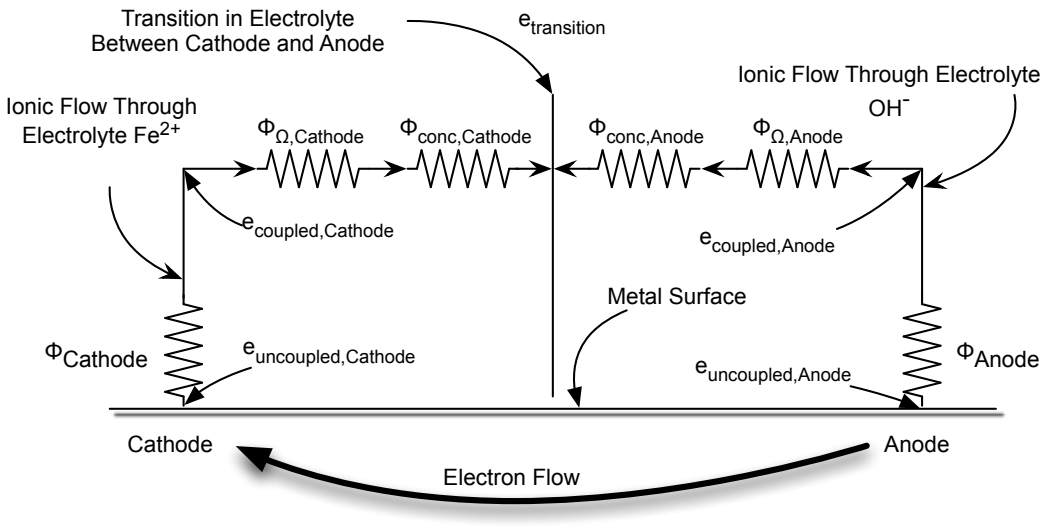

Figure 3.4. Schematic of the electrical circuit used to model current flow through the pore solution of a corrosion cell on the bar/concrete interface (Newman and Thomas-Alyea (2004)).

conductivity represents a significant improvement over other models, which assume a constant conductivity based on either dry or wet concrete. Additionally, the selected conductivity relationship will account for the changes induced in the pore solution when chlorides are present, as chlorides will increase the conductivity over adjacent locations where chlorides have not arrived.

Anodic and cathodic surface overpotentials are established by assuming Tafel behavior on the appropriate anodic or cathodic branch of the kinetics of corrosion shown in Figure 3.2. Further discussion on overpotentials is provided in Section 4 where the effect of different environmental conditions on kinetics is presented.

The model presented in Figure 3.4 represents a simplified corrosion cell where the electrolyte chemistry within each half-cell is assumed to be constant. For reinforcing steel embedded in concrete, this assumption is inaccurate as local pore solution chemistry is affected by mass transport of chloride and oxygen and the corrosion rate present on the bar/concrete interface. Therefore, this simplified model must be modified to account for variation in pore solution chemistry that will occur around the bar circumference. Figure 3.5(a) presents the first step of modifying Figure 3.4 by discretizing one half of the bar circumference into elements with the first segment located at the top and segment n at the bottom. These segments are used to identify uncoupled corrosion potentials and currents from Figure 3.2 based on the local chemistry established by the two-dimensional model. Figure 3.5(b) identifies how corrosion current from each half-cell flows through the adjacent segment to match up with the current being generated from the opposite half-cell. The control segment height (dz) is set to approximate the height of the interfacial zone (Basheer et al. 2005) as this zone is known to have a higher w/c ratio than the bulk concrete due to the bar causing a non-uniform distribution of aggregates at this interface (Garboczi and Bentz (1998), Scrivener et al. (2004), Basheer et al. (2005)). This higher w/c ratio layer will effectively focus the coupled current flow to the bar/concrete interface while limiting the current flow through the bulk concrete. Several different control volume lengths (dx) were explored to determine the best fit between computational efficiency and precision, which is further discussed in Chapter 4. The control volume width (dy) was set to unity as no variations in pore solution were allowed in this direction.

Figure 3.6 presents one-half of the final electrical circuit created by expanding the simplified corrosion circuit from Figure 3.4 to the discretized bar surface in Figure 3.5. The total number of segments (n) for each simulation is calculated for each half-cell based on the magnitude of the

corrosion potential difference from $e_{transition}$ to the last segment $e_{n,uncoupled}$ and the potential drops through the pore solution. Concentration potential drops have been eliminated in Figure 3.6; so only potential drops within the electrolyte related to ohmic resistance (Φ_{Ω}) are evaluated.

Corrosion current from each segment is identified by Δi_1 to Δi_n, which represent the corrosion current contribution from each segment. The Δ symbol is used to represent this current density as the process of coupling increases the corrosion current density at the affected segments but only the difference between the corrosion current under mixed corrosion potentials and

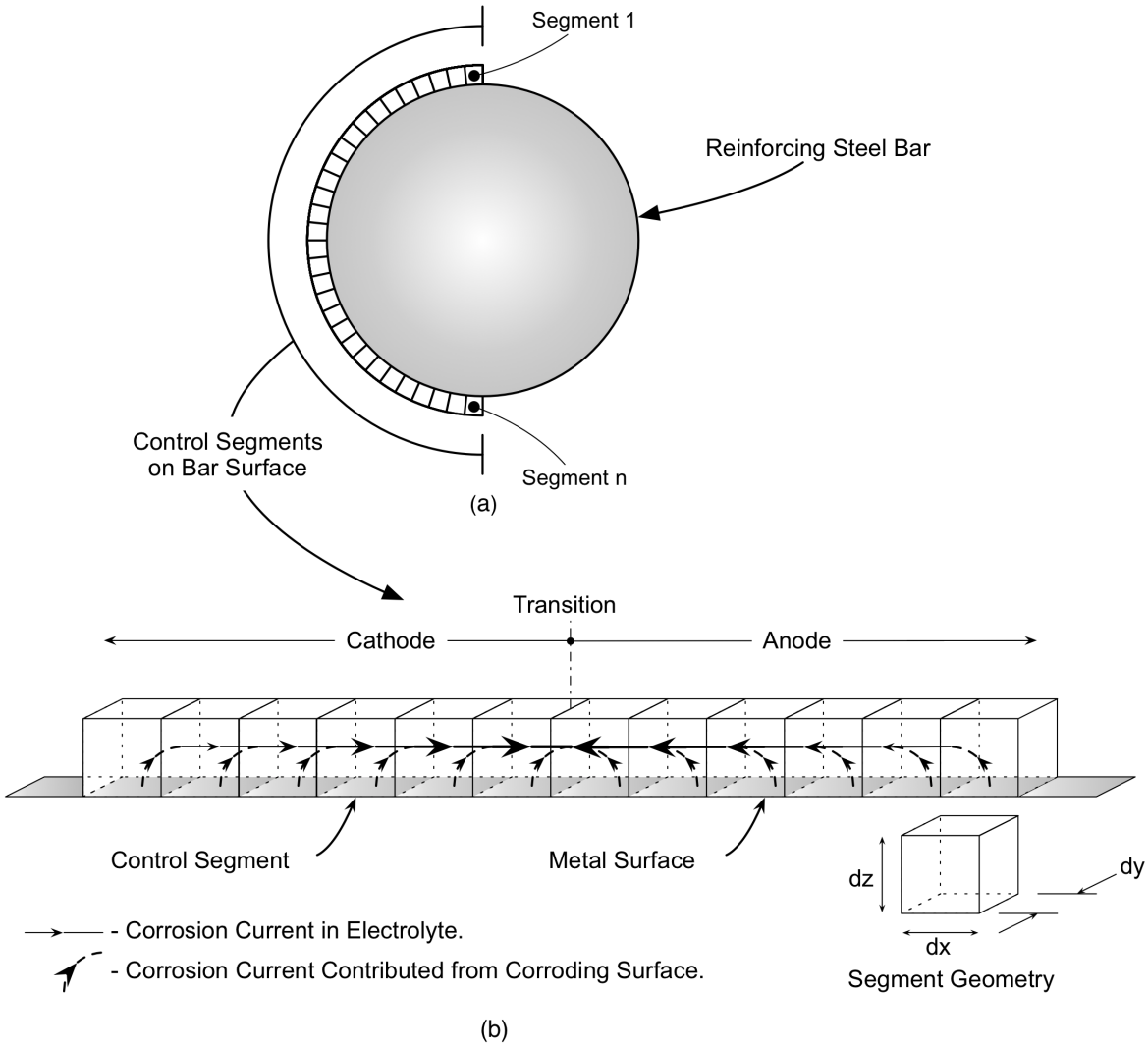

Figure 3.5. Schematic of the control volumes used in the proposed model for evaluating coupling effects on the bar surface between the cathode and anode: (a) Reinforcing steel bar with control segments identified on surface; and (b) Control segments identifying corrosion current contribution from the cathode and anode.

uncoupled corrosion potentials is available to pass into the pore solution. The corrosion circuit represented in Figure 3.6 is an improvement over the model employed by Maruya et al. (2007) which connected each contributing segment directly to the target segment without accounting for the effect current from each segment would have on adjacent segments. Ignoring the effect each segment has on the adjacent segments prevents decoupling of segments when current flow causes local ohmic potential drops to exceed the available corrosion potential difference between the transition point and the uncoupled bar surface.

With the expansion of Figure 3.4 into Figure 3.6, a system of non-linear equations is generated the solution of which is discussed in Section 4.

3.4 Summary

In this chapter an outline of the model that has been developed to simulate the corrosion process on a reinforcing steel bar embedded in concrete has been demonstrated. In subsequent chapters, this model is used to simulate a range of cover, diameter, spacing, and relative humidity for comparison to current standards used for the interpretation of corrosion potentials.

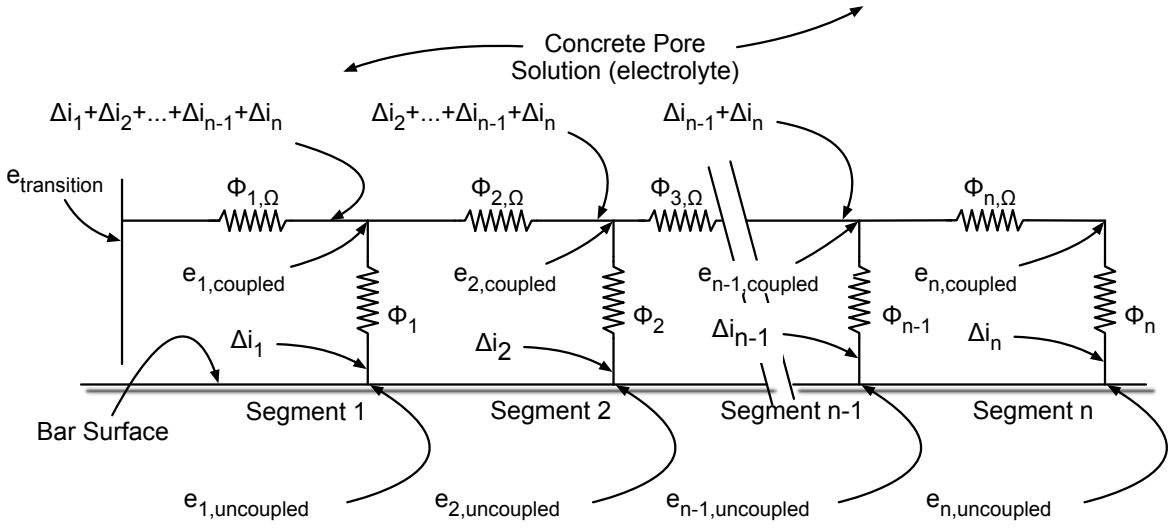

Figure 3.6. Expanded electrical circuit for one half-cell identifying overpotential drops, and ohmic resistances within half-cell for each control segment.

4 MODEL DEVELOPMENT

4.1 Overview

Appendix C contains the complete algorithm developed to simulate circumferential corrosion processes with coupling for a reinforcing steel bar embedded in concrete. Within this section the implementation of the fundamental corrosion principles outlined in Sections 2 and 3 are presented for each stage required to model the corrosion process.

Figure 4.1 presents the flowchart outlining the overall model for simulating mass transport and corrosion processes occurring around and on a bar embedded in concrete, with the main

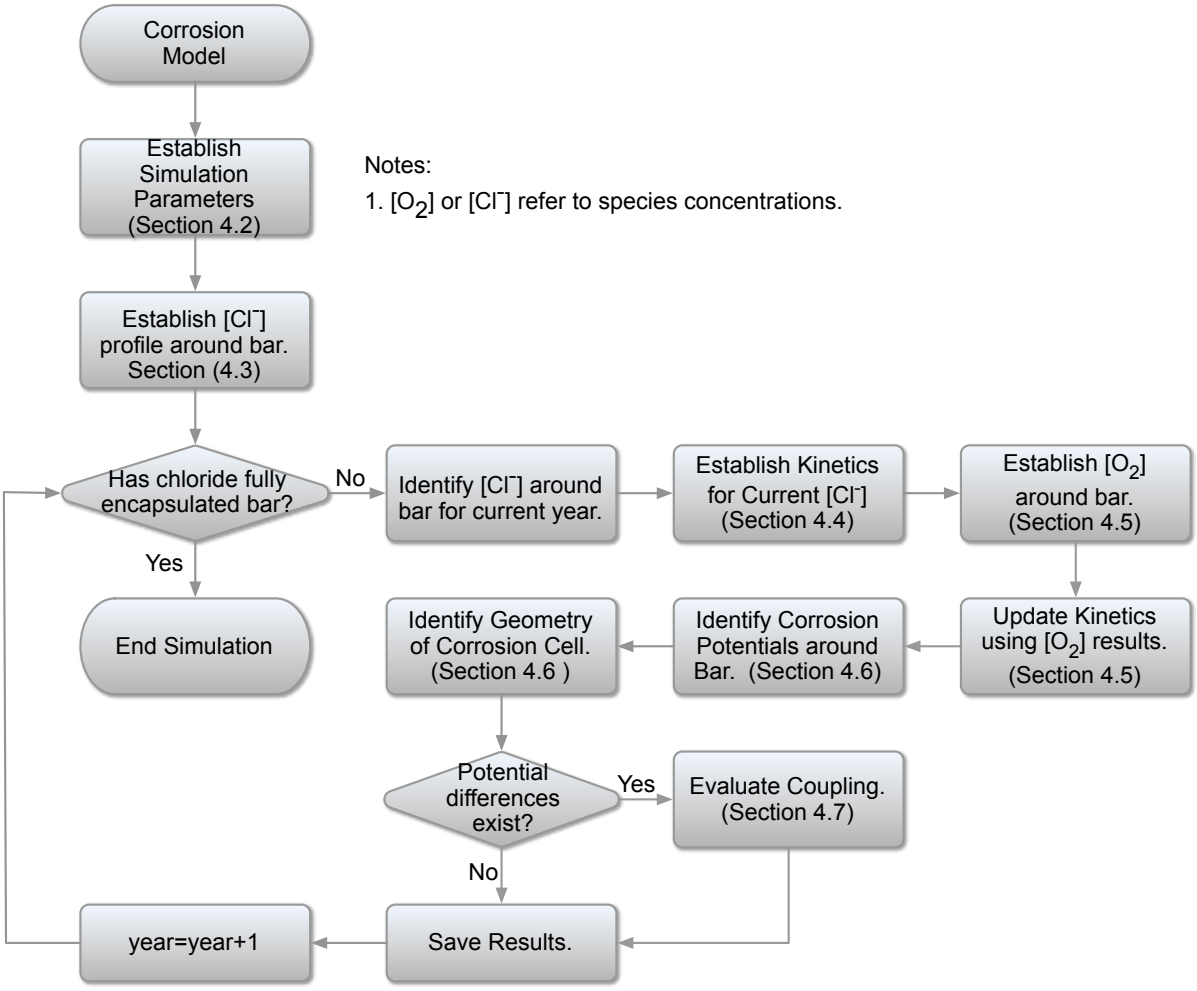

Figure 4.1. Two dimensional model flowchart for simulating chloride and oxygen mass transport and corrosion on the bar/concrete interface.

features of the program detailed in subsequent sections. Upon initialization, simulation parameters are created which include model geometry and relative humidity conditions, along with all required constants. Chloride and oxygen transport processes are solved independently as:

- The movement of chloride is significantly slower than oxygen due to the different transport mechanisms present for these two species; and
- The corrosion process directly influences oxygen concentrations on the bar/concrete interface, which require an iterative approach to achieve a solution.

Therefore, solving the chloride and oxygen concentrations independently improved the overall simulation speed.

Immediately following initialization, chloride profiles at the bar/concrete interface for the entire simulation duration were created which were then used to establish the kinetics of corrosion that dictate oxygen consumption rates. These oxygen consumption rates are then used as boundary conditions in the two-dimensional model employed for simulating oxygen transport within the model space.

Since an estimate of the final oxygen concentration is required to establish the kinetics of corrosion, results from the two-dimensional oxygen model are compared to initial oxygen concentrations. If oxygen concentrations have changed sufficiently to affect kinetics, a separate algorithm is called to adjust kinetics so that oxygen concentrations before and after the simulation are within the specified tolerances.

Once oxygen concentrations and corrosion kinetics are consistent, corrosion potentials around the bar circumference are identified along with the corrosion cell geometry. If corrosion potential differences are present, coupling on the bar/concrete interface and the resulting current flow through the pore solution are determined for the current time step.

Once coupling is assessed, the time period is incremented to the next time step, following which the processes described above are repeated. This loop is continued until chloride concentrations around the bar reach the point at which no further changes in kinetics occur, which terminates the current simulation.

The following sections outline the logic used in the development of each algorithm to address the fundamental corrosion processes and the unique challenges created with modeling corrosion on a reinforcing steel bar embedded in concrete.

4.2 Establish System Parameters

Figure 4.2 presents the flowchart for creating the system parameters used in later portions of the algorithm. Table 4.1 identifies system constants used for each simulation while Table 4.2 identifies the system geometry considered. Parameters related to cover, bar spacing, and bar diameter were varied to capture the range of values commonly found with in service structures. These variations allowed the simulation to determine the effect each variable would have on the formation of circumferential coupling on the bar/concrete interface and the final mixed corrosion potential and corrosion current densities. Once system constants and geometry are established, material properties are developed based on the relative humidity assumed for the simulation being considered. Table 4.3 identifies material properties set by the user along with the relationships between these properties and physical parameters such as chloride and oxygen diffusion coefficients.

Circumferential corrosion coupling and the resulting mixed corrosion potentials and corrosion current densities created on the bar/concrete interface are the focus of this research. Therefore, a tight segment spacing was expected on the bar/concrete interface to ensure changes in pore solution chemistry related to oxygen and chloride, which set the kinetics of corrosion, were identified. Segment sizes of 0.1, 0.5, and 1 mm in length (dx in Figure 3.5) were evaluated to determine the best balance between precision and computational efficiency.

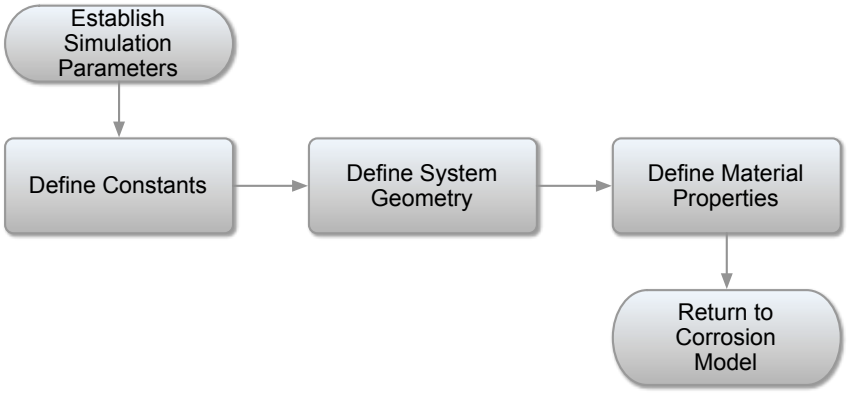

Figure 4.2. Simulation parameter flowchart.

Segment lengths below 0.5 mm were found to produce excessive solution times, while lengths greater than 0.5 produced a coarse result. Therefore a 0.5 mm segment length was selected as it produced a reasonable compromise between accuracy for identifying changes in chemistry around the bar/concrete interface and computational speed. Once the geometry and segment length on the bar/concrete interface were established, the model was then discretized using the Partial Differential Equation (PDE) Toolbox for MATLAB^{TM} to create a two-dimensional model for evaluating mass transport of chlorides and oxygen to the bar surface.

Initial conditions for chloride and oxygen concentrations within the model space were set to chloride free and fully oxygenated. As outlined in Section 2.3, the mass transport of these species is assumed to follow a Fickian process even though all of the movement is confined to

Table 4.1. System constants.

Constant or Reaction	Value	Reference
Temperature	298.15 K	-
Ideal Gas Constant	8.31 J/K/mol	-
Faraday's Constant	96485 C/mol	
SHE to CSE Conversion	-0.318 V	Jones (1994)
SCE to CSE Conversion	-0.077 V	Jones (1994)
Reversible Potential - e_{oO_2}	0.401 V	Jones (1994)
Reversible Current Density - i_{revO_2}	6.0×10^{-6} A/m^2	Ge and Isgor (2007)
Tafel Slope O_2 - β_c	0.085	Gojkovic et al. (1994)
$[O_2]_d$	Based on local salinity	Equation 2.17
$[O_2]_g$	8.56×10^{-7} mol/mm^3	-
$[Cl^-]_{bulk}$	8 kg/m^3	-

Table 4.2. System geometry.

Geometry Parameter	Value
Slab Thickness	215 mm
Cover	Varies from 10 to 90 mm
Bar Spacing	Varies from 50 to 150 mm

Table 4.3. Material parameters geometry.

Material Parameter	Value
Relative Humidity	Varies from 50 %to 100%
Concrete Porosity - ϕ	11%
Concrete w/c	0.42
Concrete cement content	335 kg/m^3
Chloride diffusion coefficient	Equation 2.24, 2.25, 2.26, and 2.27
Oxygen diffusion coefficient	Equation 2.18

the pore structure. Therefore, concentrations produced by the two-dimensional model must be related to concentrations within the pore solution as the chemistry of the pore solution establishes the kinetics of corrosion for the bar/concrete interface.

Using data published by Haque and Kayyali (1995), a relationship between chloride concentrations in bulk concrete (decanted) and pore solution (expressed) were developed for this research. Figure 4.3 and Equation 4.1 and 4.2 present the relationships implemented within the algorithm to allow easy conversion between these two methods for measuring chloride:

$$Cl_{decanted} = 0.4809 \log Cl_{expressed} - 0.3968 \quad \text{for } \log Cl_{expressed} < 1.67 \qquad [4.1]$$

$$Cl_{decanted} = 1.1625 \log Cl_{expressed} - 1.5286 \quad \text{for } 1.67 < \log Cl_{expressed} \qquad [4.2]$$

where $Cl_{expressed}$ is the chloride concentration in the pore solution in mmol/mm^3 and $Cl_{decanted}$ is

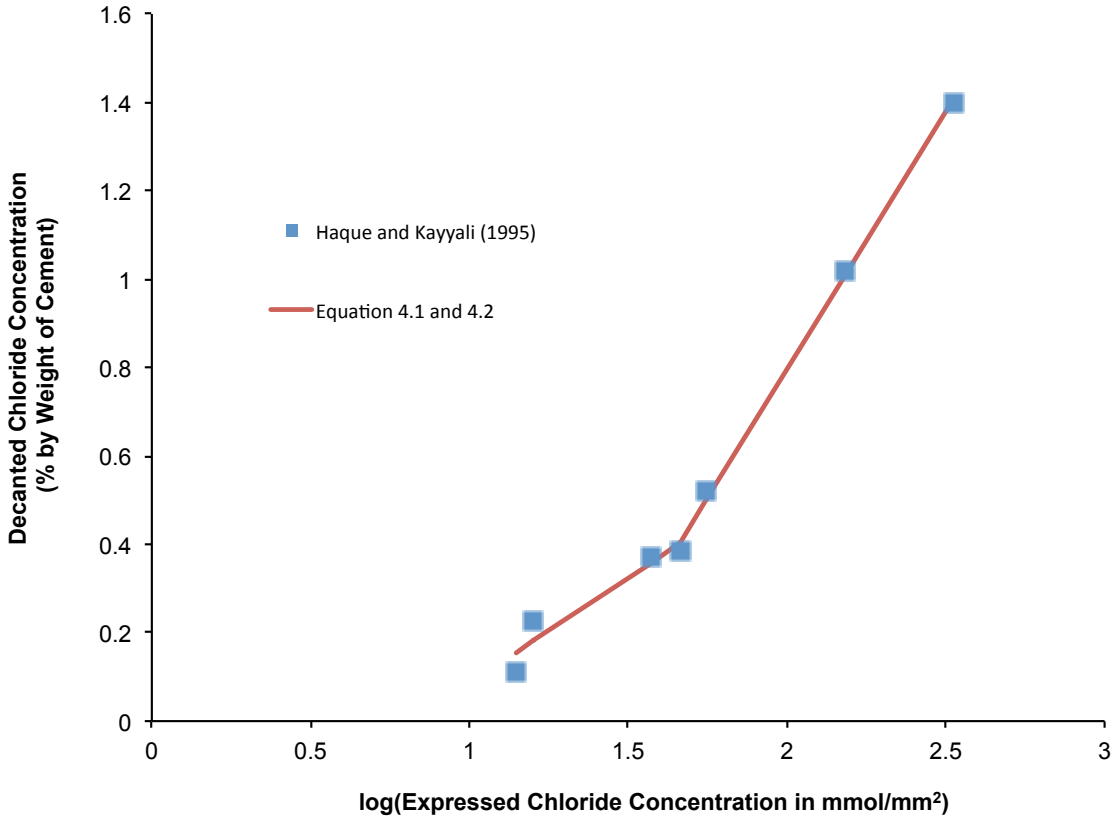

Figure 4.3. Chloride concentration relationship between decanted and expressed chlorides (after Haque and Kayyali (1995))

the chloride concentration in bulk concrete in percent by weight of cement. The correlation coefficient produced from these equations to the test data was 0.996. This relationship was applied to concentrations produced from the two dimensional model which represented the bulk concrete in order to produce chloride concentrations in the pore solution on the bar/concrete interface. Chloride concentrations in the pore solution were then related to kinetics of corrosion for various concentrations of chlorides in simulated pore solutions represented by Figure 3.2 in order to establish the kinetics for Equation 2.1 for the chloride concentration at a particular segment on the bar/concrete interface.

In a similar manner, oxygen concentrations within the model space were related to porosity and moisture conditions within the pore space. While chloride transport is exclusively confined to the pore solution, oxygen is transported through a combination of gaseous and dissolved phases. Therefore a relationship between pore water oxygen concentration, atmospheric oxygen concentration, and bulk concrete oxygen was developed the full derivation of which is included in Appendix B and displayed as follows:

$$[O_2]_{bulk} = \phi\left(PS[O_2]_d + (1-PS)[O_2]_g\right) \qquad [4.3]$$

where $[O_2]_{bulk}$ is the concentration of oxygen within the concrete including the solid and pore phases (mol/mm^3), $[O_2]_d$ is the dissolved oxygen within the pore solution (mol/mm^3), $[O_2]_g$ is the oxygen concentration within the gaseous phase (mol/mm^3), and ϕ is the porosity of the concrete (%) being considered, each of which are defined in Table 4.1, while PS is the pore saturation (%) representing the amount of moisture contained within the pore structure estimated from Figure 2.17 for varying degrees of relative humidity. The final conversion from bulk to dissolved oxygen concentrations incorporates porosity, pore saturation and Henry's constant as follows:

$$[O_2]_d = \frac{[O_2]_{bulk}}{\phi\left(PS - \frac{(1-PS)}{RTH}\right)} \qquad [4.4]$$

where R is the universal gas constant, T is the temperature in Kelvin, and H is Henry's constant which is described by Equation 2.23.

4.3 Chloride Profile Around Bar

Figure 4.4 presents the flowchart employed for determining chloride concentrations within the model space, which are then used to establish kinetics of corrosion for setting oxygen consumption rates at the bar/concrete interface. Chloride diffusion coefficients are set in Section 4.2 for the w/c, cement content, aggregate content, and moisture conditions selected for the material being evaluated. Boundary conditions, presented in Table 4.4, for the chloride diffusion model are set to zero flux across the boundary except for the top concrete surface, which is exposed to chlorides at a surface concentration of 8kg/m^3. This value for surface chloride concentrations was chosen to match design values commonly employed in Western Canada for new infrastructure.

4.4 Kinetics Algorithm

Once chloride profiles for the time period being considered are identified, the kinetics of corrosion on the bar/concrete interface are developed using chloride concentrations at each segment with the kinetics of corrosion from Figure 3.2. The first step in the algorithm is to convert bulk oxygen concentrations to oxygen concentrations in the pore solution (Equation 4.4) as dissolved oxygen concentrations affect the reversible corrosion potential according to Equation 2.6. An iterative procedure is executed at this stage where chloride and oxygen

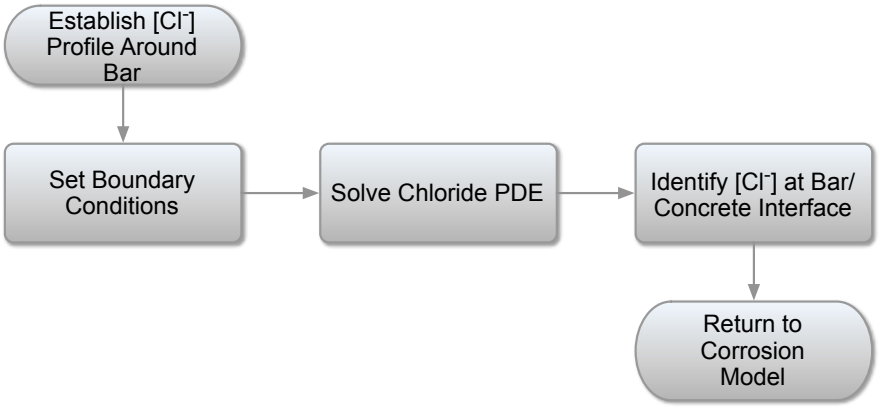

Figure 4.4. Flowchart outlining the algorithm employed for determining the chloride concentrations on the bar/concrete interface.

Table 4.4. Boundary conditions.

Species or Element	Top	Bottom	Sides	Bar Surface
O_2	Constant	Constant	Zero Flux	Flux set by Kinetics
Cl^-	Constant	Zero Flux	Zero Flux	Zero Flux

concentrations at each segment are identified, following which reversible corrosion potentials for the oxygen reduction line and the reinforcing steel dissolution line at the chloride concentration present are developed. For the oxygen reduction line described by Equation 2.2, the reversible corrosion potential is the only value that is adjusted as the reversible corrosion current density and the Tafel slope are independent of the local oxygen concentrations. However, the kinetics of corrosion for reinforcing steel is affected by chloride concentrations on the bar/concrete interface, which could fall between the curves identified in Figure 3.2. Therefore, for each segment, a unique kinetic of corrosion curve was constructed by linear interpolation of the actual chloride concentration produced by the two-dimensional model to the chloride concentrations identified in Figure 3.2.

Once developed, the corrosion potential, e_{corr} and corrosion current density i_{corr} for the unique chloride and oxygen concentrations on the bar surface were passed back to the main program shown in Figure 4.1.

4.5 Establish Oxygen Concentrations around Bar and Update Kinetics

After e_{corr} and i_{corr} were established in the previous algorithm, the effect these corrosion parameters have on oxygen concentrations within the model space are evaluated. Figure 4.6 presents the flowchart that describes the steps for determining oxygen concentrations around the bar given i_{corr} at the bar/concrete interface and the initial oxygen concentrations within the pore solution. Corrosion current densities (i_{corr}) established in the previous step are converted into an oxygen consumption rate using the relationship between corrosion current and oxygen consumption identified by Newman and Thomas-Alyea (2004):

$$g = -\frac{i_{corr}}{nF} \qquad [4.5]$$

where g is the rate of oxygen consumption on the bar surface in mol/m^2/s, i_{corr} is the corrosion current density in A/m^2, n is the number of electrons transferred in the reaction, which is 4 for the oxygen reduction reaction represented by Equation 2.2, and F is Faraday's constant which has units of Coulombs/mol.

Once oxygen consumption rates on the bar surface are identified, boundary conditions for the oxygen transport model identified in Table 4.2 are updated on the bar/concrete interface which are then used in the two dimensional model to generate an oxygen profile throughout the model

space. This new oxygen profile at the bar/concrete interface is generally different than the values used to prepare the initial kinetics. Therefore, these new concentrations are used to update the kinetics of corrosion for the oxygen reaction, which changes the kinetics for the reinforcing steel/oxygen corrosion system. This loop continues until the old and new values of e_{rev} for the oxygen reduction line reach the error limit identified by the user, which for this research, was set to 0.0001 V. This value was selected for two reasons, the first being related to the precision of the test data obtained from Alberta Transportation for comparison, which was recorded to a precision of 0.01 V. The second is presented in Table 4.5, which identifies the error introduced into the predicted local corrosion rate due to the error tolerance used in establishing the final corrosion potential. Curve 1 and 2 identified in Table 4.5 represent the slopes of the bi-linear curve shown in Figure 3.2. Curve 1 represents the flatter of the two curves while Curve 2 represents the steeper of the two curves. Initially, the lowest error tolerance was originally selected, however, computational effort was greatly expanded and in some instances the solution would fail to converge. Therefore, the error limit of 0.0001 V was selected as it produced reasonable accuracy for corrosion potentials and current densities while minimizing the computational effort.

The kinetics developed for the system would, in some situations; result in negative dissolved

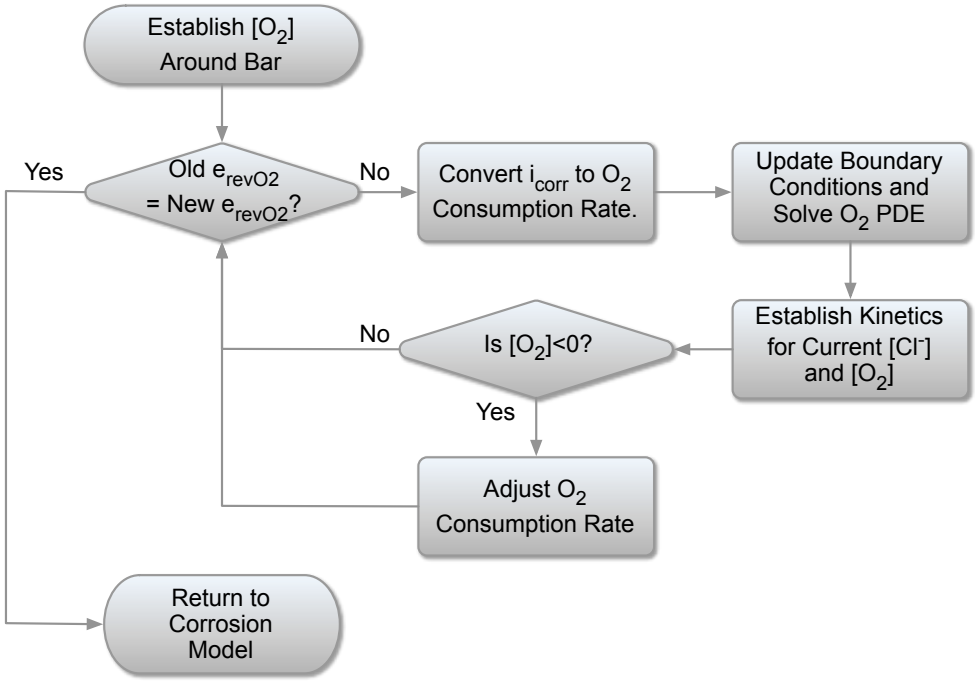

Figure 4.5. Flowchart of logic describing how $[O_2]$ is established within the model space.

oxygen concentrations at the bar/concrete interface. While zero or negative dissolved oxygen concentrations are possible within the numerical model, they are not possible in real systems, as the corrosion process would slow as oxygen is depleted from the surrounding pore solution. Therefore, in practice, oxygen consumption rates decrease if oxygen transport limitations are present until transport of oxygen to the corroding surface matches the consumption rate on the corroding surface.

Within the model, when boundary conditions create negative oxygen concentrations, the oxygen consumption rate on the bar/concrete interface is reduced until the transport of oxygen can sustain the consumption rate. Figure 4.7, outlines the logic used to obtain this result, which is based on the following:

- If $[O_2]>0$ and the maximum rate of oxygen consumption based on the kinetics of corrosion are present then no change to the oxygen consumption rate occurs;
- If $[O_2]>0$ and the adjusted oxygen consumption rate is less than the maximum rate of oxygen consumption based on the kinetics of corrosion, then the oxygen consumption rate is increased; and
- If $[O_2]<0$ then the oxygen consumption rate is lowered.

Initially, segments on the bar surface which have negative oxygen concentration are identified as Area 1. Segments, which have positive oxygen concentrations with oxygen consumption rates less than the maximum predicted by the system kinetics, are identified as Area 2.

Table 4.5. Comparison of corrosion potential error limits versus corrosion current.

Error Tolerance (V)	Curve	Error in Corrosion Current (%) for each Kinetic Curve		
		Cl^- at 0% and 0.2%	Cl^- at 0.05%	Cl^- at 0.10% and 0.20%
0.01	1	399%	2723%	661%
	2	2.34%	2.96%	4.61%
0.001	1	17.4%	39.7%	22.5%
	2	0.23%	0.29%	0.45%
0.0001	1	1.62%	3.40%	2.05%
	2	0.02%	0.03%	0.05%
0.00001	1	0.16%	0.33%	0.20%
	2	0.00%	0.00%	0.00%

Adjustments to oxygen consumption rates are made to Area 1 and 2 according to the logic outlined above, after which boundary conditions are updated, following which the two-dimensional model updates the oxygen concentrations within the model space. This iterative process continues until the difference between initial and adjusted oxygen concentrations fall within the selected error limit.

Table 4.6 presents a summary of the sensitivity analysis performed for selecting the error limit for this aspect of the simulation. The final value selected was 1×10^{-11}, which represented the best value for attaining reasonable convergence and high accuracy.

Significant challenges were experienced with achieving oxygen concentrations on the bar/concrete interface that met with the logic identified previously, as the bar curvature created unique covers and volumes for each segment through which oxygen was transported. Therefore, small changes in consumption rate on one part of the bar circumference resulted in changes to oxygen concentrations in adjacent areas even if consumption rates in these adjacent areas were not adjusted. This sensitivity made it difficult to arrive at a computationally efficient methodology that would produce a solution that met with the logic previously presented. Multiple approaches were attempted with the following methodology found to produce the best balance of accuracy and speed.

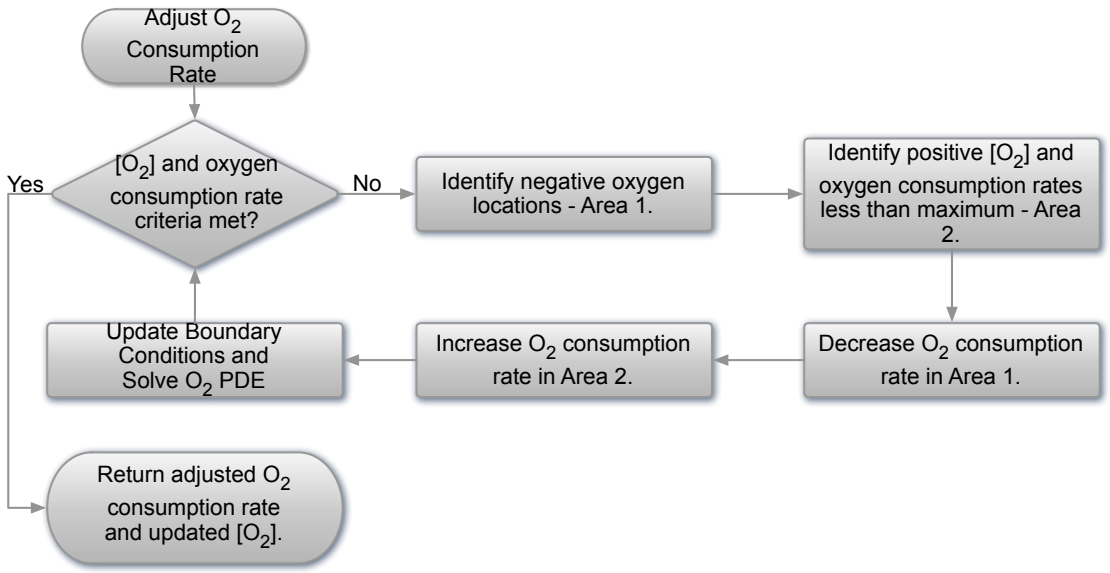

Figure 4.6. Algorithm flowchart for adjusting the corrosion current around the bar when oxygen transport limitations are present.

When adjustments were required, an adjustment factor k_{adj} was created which reduced the original oxygen consumption rate according to:

$$g_{new} = g_{original}\left(k_{adj}\right) \quad [4.6]$$

where g_{new} is the adjusted oxygen consumption rate, $g_{original}$ is the value obtained from Equation 4.5, and k_{adj} is value that is initially set to 1 but is modified by Equation 4.7 until the criteria for oxygen concentration and oxygen consumption rates are met:

$$k_{adj} = k_{adj} - 0.1^{N} \quad [4.7]$$

N is a counter that increments after a segment's $[O_2]$ changes from negative to positive.

Initial implementation of this adjustment algorithm produced highly irregular results, as the system would get caught in a local minimum at one segment, which then caused adjacent segments to overcompensate by either increasing or decreasing the oxygen consumption rate to extreme values. Therefore, controls to N were implemented to prevent segments from becoming trapped in a local minimum. These controls were essentially created from a trial and error approach whereby different constraints were implemented, the best of which was selected for use in the final simulation.

Once oxygen concentrations on the bar/concrete interface were established and consistent with the reversible corrosion potentials related to the oxygen reduction reaction represented by Equation 2.2, the corrosion potentials and currents were returned to the main algorithm. The values at this point represented uncoupled conditions whereby current flow through the pore

Table 4.6. Comparison of corrosion current error limits versus corrosion potential.

Error Tolerance (A/mm^2)	Curve	Error in Corrosion Potential for Each Kinetic Curve		
		Cl^- at 0% and 0.2%	Cl^- at 0.05%	Cl^- at 0.10% and 0.20%
1.0×10^{-8}	1	22%	7%	2%
	2	877%	369%	45%
1.0×10^{-9}	1	4%	1%	0%
	2	127%	50%	5%
1.0×10^{-10}	1	0%	0%	0%
	2	13%	5%	1%
1.0×10^{-11}	1	0%	0%	0%
	2	1%	1%	0%

solution and the effect of this current flow on the overall corrosion potentials and corrosion current had not been considered.

4.6 Identify Corrosion Potentials Around the Bar and the Corrosion Cell Configuration.

Prior to evaluating current flow through the pore solution, corrosion potentials on the bar/concrete interface are evaluated to identify the frequency and type of corrosion cell that had been created. This step is necessary as initial modeling attempts assumed the corrosion cell would only form on the bar/concrete interface when chlorides were present. Since chlorides would arrive on the bar surface closest to the concrete surface, this corrosion cell configuration would have the anode on the surface with chlorides, with the remaining surface forming the cathode. However, when implemented, simulations revealed multiple corrosion cells could form with different arrangements of anodic and cathodic zones depending on the chloride and oxygen concentrations present at a particular time step. Therefore, this step in the simulation became necessary to identify the number of cells and configuration in order to establish the key parameters used in later algorithms that evaluate corrosion current through the pore solution caused by coupling.

Figure 4.8 describes the process for converting oxygen consumption rates obtained in the

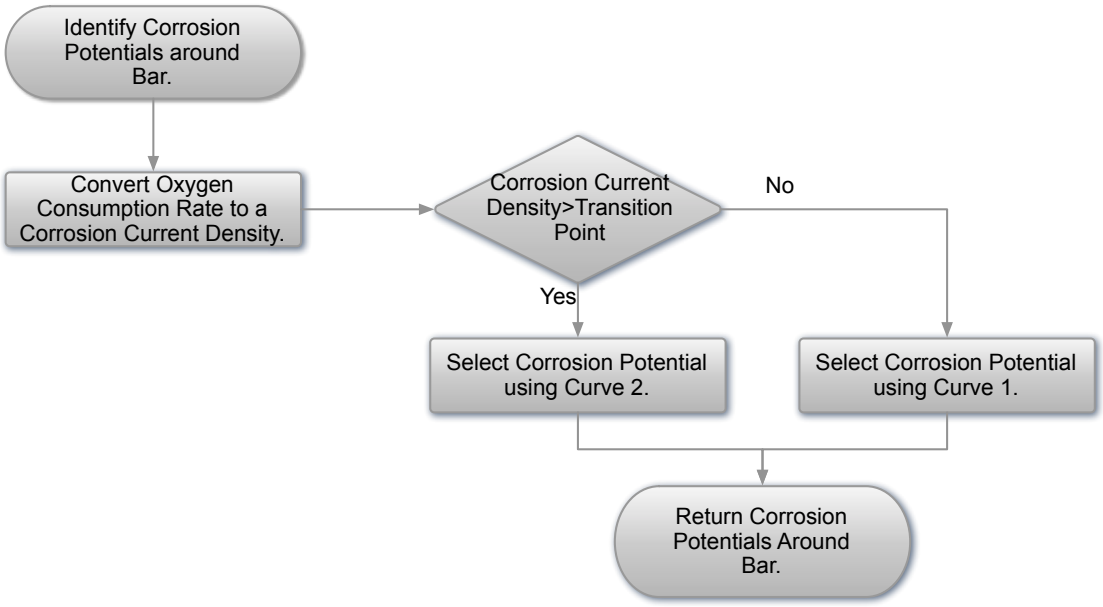

Figure 4.7. Algorithm flowchart for converting the oxygen consumption rates on the bar/concrete interface to corrosion current density and potential.

previous steps to a corrosion current density (Equation 4.4) and corrosion potential. Once the corrosion current density is known for each segment, the corresponding corrosion potential is established by using the bilinear curve representing the kinetics of corrosion of Figure 3.2 for the chloride concentration at each segment. Once the corrosion potentials are established around the bar/concrete interface, the frequency and type of corrosion cell can be determined.

Identification of the corrosion cell configurations begins with Figure 4.9 which presents the kinetic of corrosion diagram from Figure 3.2 further expanded to show the effect different chloride and oxygen concentrations around the bar circumference have on the corrosion potentials and corrosion current densities. Two points are identified in Figure 4.9 on the bar circumference which are labeled as Point A and Point B. At each of these points, concentrations of chlorides and oxygen will change as chlorides diffuse and oxygen is consumed by corrosion occurring on the bar/concrete interface. From Figure 4.9 it is apparent the geometrical characteristics of the system, such as bar diameter, cover, and bar spacing, combined with the diffusivity of concrete, will create different corrosion potentials around the bar circumference. Therefore, several corrosion potential configurations around the bar surface are possible depending on the progression of chlorides around the bar combined with oxygen concentrations on the corroding surface.

The possible corrosion potential configurations on the bar/concrete interface are shown in Figure 4.10 and 4.11, which are based on the kinetics of corrosion presented in Figure 4.9. The development of these figures can be understood by considering the movement of chlorides to the bar surface combined with the availability of oxygen at each location around the bar as follows:

- Condition 1 – Figure 4.9, Point A and Point B with no [O_2] restriction or Cl^- present. Figure 4.10(a)(i) represents [O_2] with depth when this scenario of Cl^- and O_2 is present while Figure 4.10(a)(ii), represents the resulting corrosion potentials. Both [O_2] and corrosion potentials are constant with depth which prevent coupling around the bar perimeter from occurring as there is no potential difference available to cause current flow through the pore solution. However, coupling along the length of the bar is possible if different corrosion potentials along this axis are present;

- Condition 2 – Figure 4.9, Point A with no [O_2] restriction or Cl^- present and Point B with O_2 restrictions. Figure 4.10(b)(i) represents [O_2] with depth when chloride has not

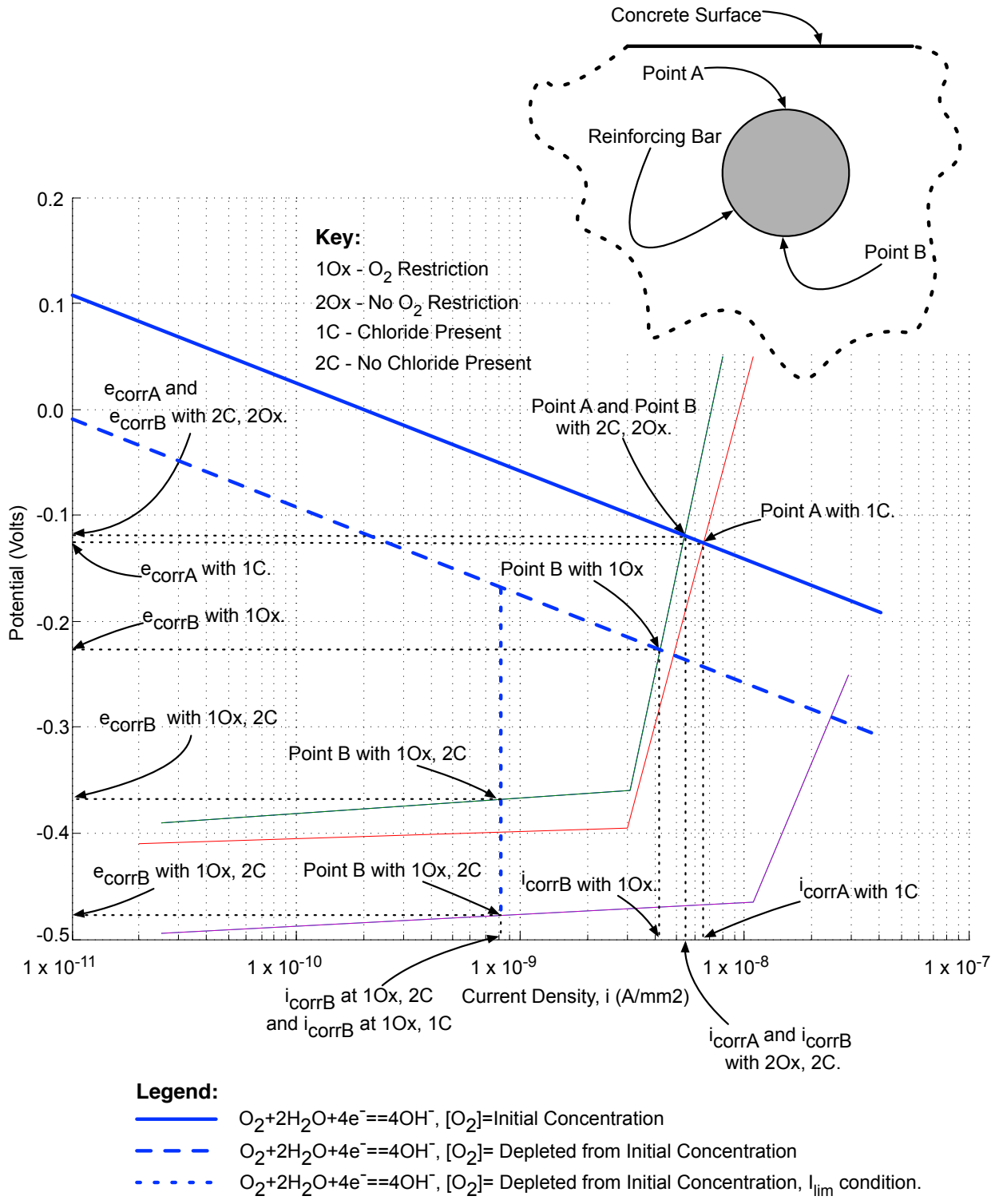

Figure 4.8. Kinetics of corrosion diagram demonstrating uncoupled corrosion current and corrosion potentials.

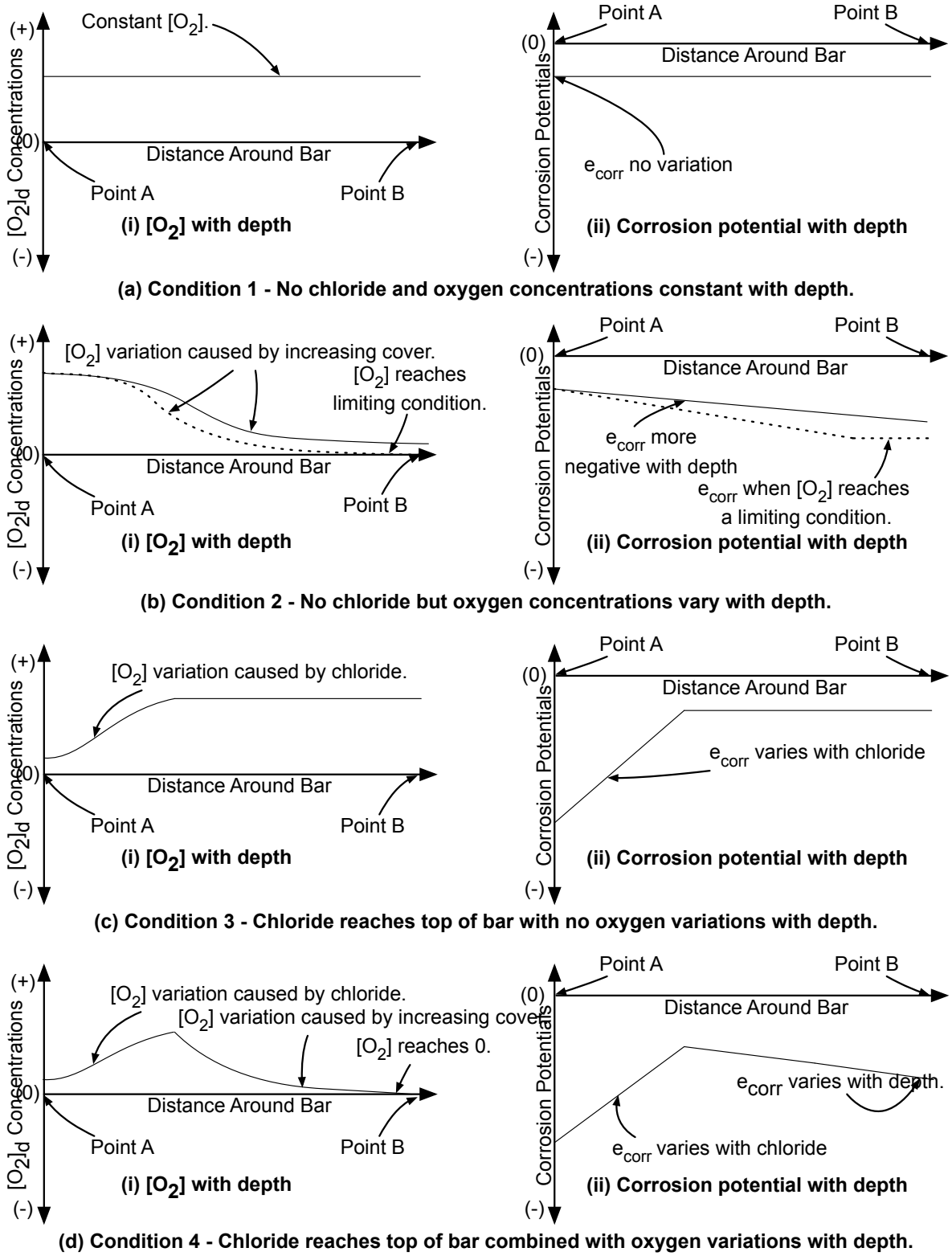

Figure 4.9. $[O_2]$ and corrosion potentials created as chlorides are introduced.

reached either Point A or B but oxygen concentrations around the bar decrease with depth. This condition is likely the most common condition created, as concrete cover will always cause a reduction in $[O_2]$ with depth due to the increased distance oxygen must travel to replace the oxygen consumed on the bar/concrete interface. Two sub-conditions are represented in this figure as $[O_2]$ variation caused by increasing cover and $[O_2]$ reaches a limiting condition. The development of the second sub-condition occurs under large concrete covers or when high humidity's are present which reduce the O_2 diffusion coefficient. Figure 4.10(b)(ii) represent corresponding corrosion potentials generated from $[O_2]$ presented in Figure 4.10(b)(i). A linear decrease in corrosion potential with depth is created unless the limiting oxygen condition is reached which causes a lower limit in corrosion potential to be reached. Under these conditions, the more negative corrosion potentials near Point B cause the corrosion cell geometry to have the cathode near Point A while the anode is near Point B;

- Condition 3 – Figure 4,9, Point A with Cl^- present but no oxygen restriction and Point B with no Cl^- or oxygen restrictions. Figure 4.10(c)(i) represents Condition 1 with the addition of chloride near Point A, which produces an increase in the corrosion rate which lowers the local $[O_2]$, while Figure 4.10(c)(ii) represents the corresponding corrosion potentials. With decreased $[O_2]$ near Point A, corrosion potentials also decrease in this region, resulting in more negative corrosion potentials near the top of the bar which increase as the depth increases. Under this scenario, the more negative corrosion potential region will experience an increase in the anodic reactions, thereby creating a corrosion cell geometry where the anode is positioned above the cathode on the bar circumference; and

- Condition 4 – Figure 4.9, Point A with Cl^- and no oxygen restriction and Point B with oxygen restrictions and no Cl^-. Figure 4.10(d)(i) represents a combination of Condition 2 and Condition 3 where $[O_2]$ changes with depth and chloride is present near Point A. Under this scenario, oxygen concentrations increase with depth until a maximum value is reached after which oxygen concentrations decrease with depth. Figure 4.10(d)(ii) represents the corresponding corrosion potentials, which follow a similar pattern. Under this condition, two corrosion cells are produced which have the anode near Point A and B and a cathode near the point where the maximum corrosion potential occurs.

Two additional corrosion potential geometries can potentially form as the chloride front moves deeper into the concrete. These conditions are effectively an extension of Condition 4 where chloride concentrations gradually increase to the maximum point beyond which kinetics of corrosion no longer change with increasing chloride. At this point, and depending on the system geometry, the following two conditions can develop:

- Condition 5 – Figure 4.11(a)(i) $[O_2]$ with depth is very similar to Condition 4; however, the effect of chloride on the kinetics has reached a maximum so $[O_2]$ with depth near Point A are affecting corrosion potentials as small variations in $[O_2]$ are induced by mass transport. The resulting corrosion potentials shown in Figure 4.11(a)(ii) reveal that corrosion potentials with depth decrease until a minimum value is reached after which corrosion potentials increase until a maximum is reached. The maximum corrosion potential location is related to where chlorides have not affected the kinetics of corrosion. After this maximum corrosion potential is reached, corrosion potentials decrease with depth due to lower $[O_2]$ affecting the oxygen reduction reaction. Under this scenario,

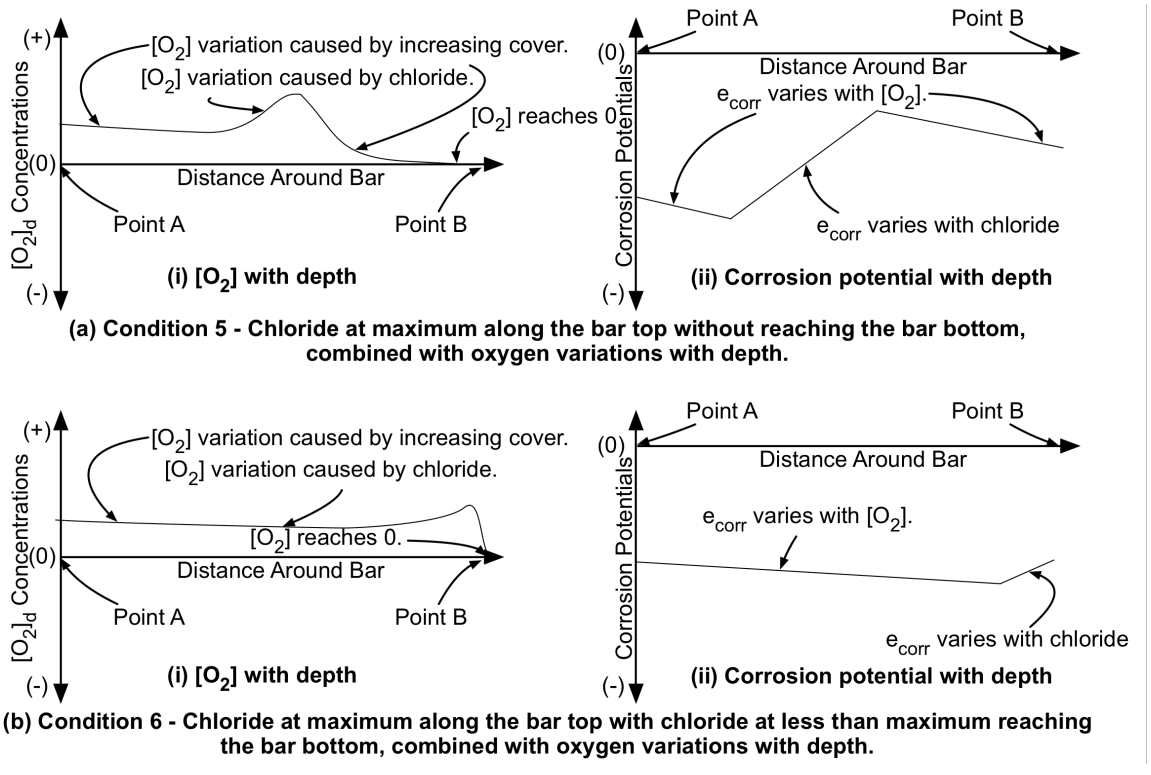

Figure 4.10. $[O_2]$ and corrosion potentials created as chlorides reach a maximum concentration.

three corrosion cells can be present with the following configurations:

  - Cell 1 – Starting at Point A and continuing to the minimum corrosion potential between Points A and B. The cathode would be located near Point A while the anode would be located towards the minimum corrosion potential location;
  - Cell 2 – Starting at the minimum corrosion potential and continuing to the maximum corrosion potential. The anode would be located near the minimum corrosion potential with the cathode near the maximum corrosion potential; and
  - Cell 3 – Starting at the maximum corrosion potential and continuing to Point B. The cathode would be located near the maximum potential region while the anode would be near Point B.

- Condition 6 – Figure 4.10(b)(i) presents the $[O_2]$ with depth when chloride has reached Point B on the bar. Under this scenario, chloride concentrations have reached a maximum from the top of the bar to some point around the perimeter, so any changes to corrosion potential are from variations in oxygen concentrations. Since oxygen concentrations are generally decreasing with increasing depth, the resultant corrosion potential curve represents decreasing corrosion potentials with depth. Near the bottom of the bar, corrosion kinetics vary with chloride concentrations so corrosion potentials increase at deeper locations as chloride concentrations are lower at this point.

A third configuration is possible whereby the maximum chloride concentration passes the bottom of the bar. Under this scenario, the corrosion potential configuration becomes similar to Condition 2. Conditions 5 and 6 were not evaluated as part of this study as the corrosion potential differences produced under these scenarios were negligible.

Figure 4.12 presents the flowchart that describes the algorithm employed to identify the different corrosion potential geometries outlined previously. This flowchart is essentially a series of logic statements that select one of the four conditions presented in Figure 4.10 and identifies the number of corrosion cells and the relative position of the anode and cathode. This step establishes the orientation of each corrosion cell, which dictates the order by which calculations for establishing the anode and cathode can occur.

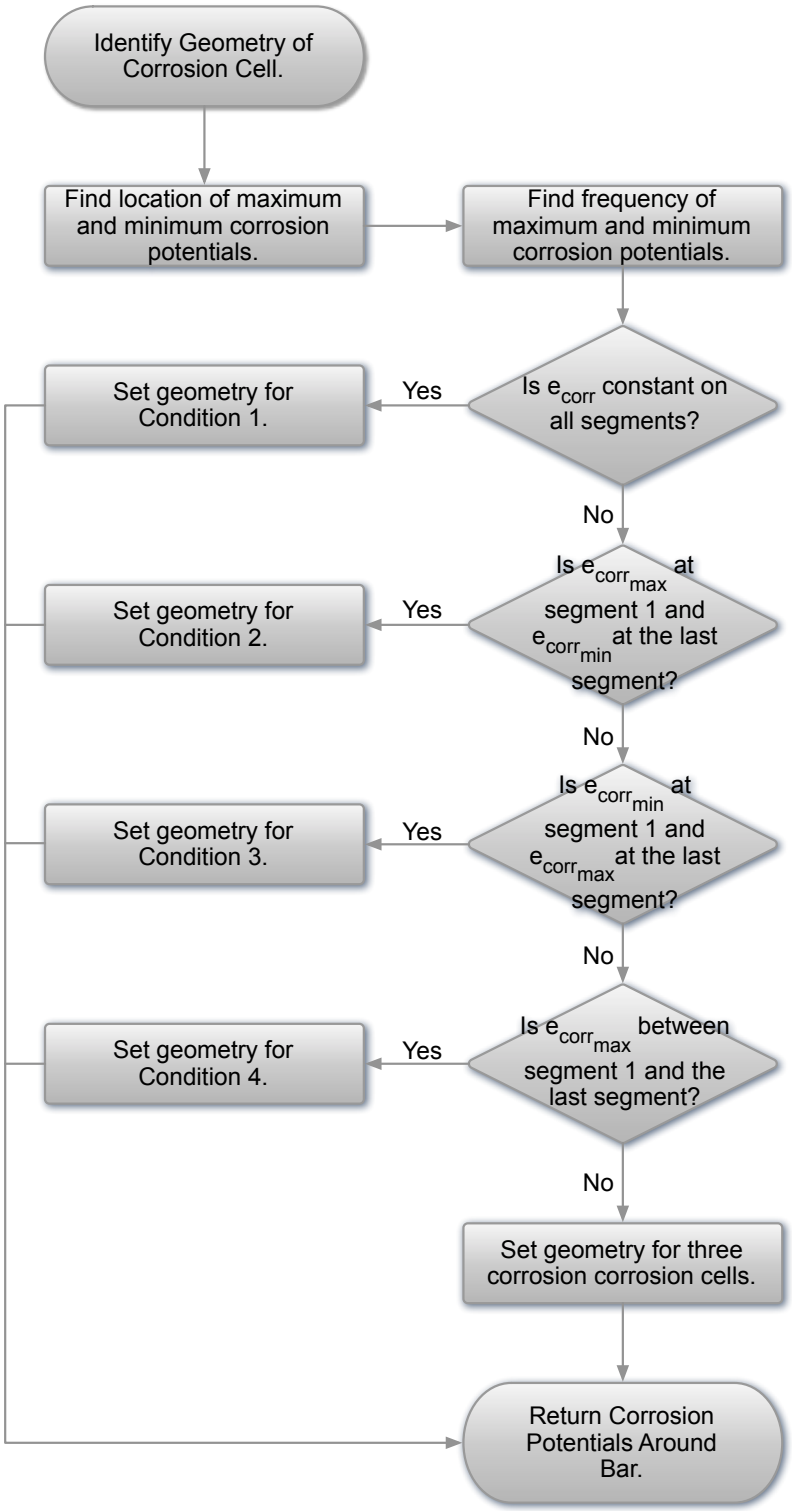

Figure 4.11. Algorithm flowchart for identifying the corrosion cell configuration used in later algorithms to establish the location of the anodic and cathodic zones.

4.7 Coupling Algorithms

If one of the corrosion cell geometries for Condition 2 through 4 is identified in the previous algorithm, coupling on the bar/concrete interface can occur as a corrosion potential difference is present which can permit current flow through the pore solution if the difference is sufficient to overcome ohmic resistances. Figure 4.13 presents the flowchart of the process used to assess whether coupling is possible and the magnitude of corrosion current produced by this coupling.

In earlier algorithms, the effect of oxygen concentrations on corrosion potentials were identified and iterative methods were presented to ensure consistency between oxygen concentrations and kinetics of corrosion. When coupling occurs, a similar iterative method is required as

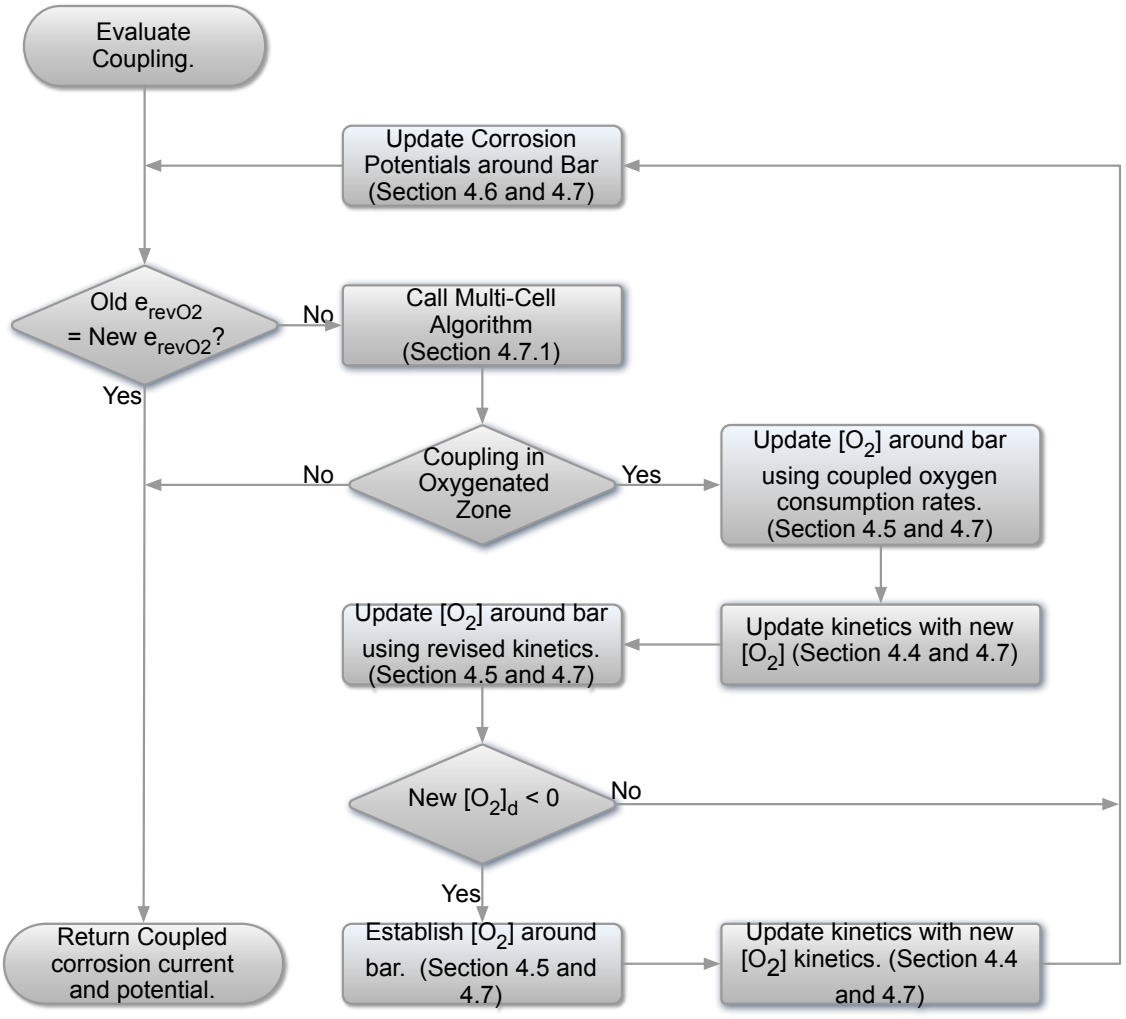

Figure 4.12. Algorithm flowchart for establishing location of coupling on the bar circumference and the resulting corrosion current.

coupling between zones on the bar circumference cause increased oxygen consumption rates in cathodic zones that reduce oxygen concentrations from the uncoupled condition.

Initially, the evaluation of new e_{revO2} and old e_{revO2} is by-passed and the Multi-Cell Coupling Algorithm (Section 4.7.1) is executed. Values returned from this algorithm identify the magnitude of coupling, location of the anode and cathode, and oxygen consumption rates on the bar circumference. Since coupling in the cathodic zone can either increase the oxygen consumption rate or depress the local metal dissolution rate, a check is performed to determine which condition has occurred. If oxygen consumption rates have increased over the uncoupled condition, then kinetics are updated using the same principles outlined in Section 4.4 with the resulting oxygen consumption rate (g_{new}) blended with the old oxygen consumption rate (g_{old}) according to Equation 4.7:

$$g_{blend} = 0.2 \times g_{new} + 0.8 \times g_{old} \qquad [4.8]$$

The blended rate was used as initial simulations that implemented g_{new} without blending generally failed to converge to the error limits identified. This blended value (g_{blend}) is passed to the same algorithm outlined in Section 4.5 to update the model space [O_2].

After this step, [O_2] is checked around the bar circumference and, if negative values are present, the blended oxygen consumption rates (g_{blend}) are passed to the Adjust O_2 Consumption Rate algorithm outlined in Figure 4.7, which reduces g_{blend} until negative oxygen concentrations are no longer present. Results for [O_2] obtained from this step are then used to update the kinetics of corrosion for the oxygen reduction reaction, the results of which are used to update the corrosion potentials around the bar. Segments where g_{blend} are reduced are flagged within the simulation as segments where cathodic coupling can only increase the local corrosion rate to g_{blend}, with increases beyond this value produced by reducing the local metal dissolution rate.

Once updated, corrosion potentials around the bar are set as the uncoupled corrosion potentials that will be present when coupling occurs and cause an increase in oxygen consumption rates. A comparison between old and new e_{revO2} is performed at this point and, if the difference is within the tolerance of 0.0001 V, the algorithm returns the coupled corrosion potentials and current densities to the main program. If the tolerance is not met, then the loop is continued until old and new e_{revO2} tolerances are met.

Early versions of the model included a step at the completion of this algorithm to adjust local chemistry for imbalances in Fe^{2+} and OH^- when coupling caused these processes to be accelerated at different locations on the bar circumference. The initial methodology assumed that simple diffusion from the surrounding concrete would be sufficient to replenish OH^- within the pore solution in the affected area. However, preliminary simulations produced highly acidic zones at anodic portions of the bar circumference when chloride was not present. This result suggested that alternative processes were present which sustained the local pH even when OH^- was depleted due to coupling of corrosion processes.

Due to time constraints, these alternative processes were not investigated; therefore, a decision was made to ignore local depletion of OH^- in order to complete the work related to circumferential corrosion coupling on the bar/concrete interface. However, the implication of this acidification is discussed in detail in Section 5 as simulations conducted as part of this research indicated that acidification is a necessary step for kinetics of corrosion to transition from a passivated to non-passivated state.

In the following sections, details for the Multi-Cell Algorithm and algorithms required for the simulation are discussed.

4.7.1 Multi-Cell Algorithm

The flowchart in Figure 4.14 outlines the process for establishing the number of corrosion cells and the position of the anode relative to the cathode. Conductivities of the pore solution are established, as these values are used in later algorithms to establish potential drops through the pore solution. Following the conductivity calculation, the position of the anode and cathode within the cell is identified along with the number of corrosion cells. For each cell configuration, the start and stop segment for the cell is identified along with a step parameter for adding segments to the anode and cathode in order to achieve a balance of corrosion current between each half-cell reaction.

Once identified, parameters for each corrosion cell are passed to the Maximum Coupled Current Algorithm, which establishes the relative size of the anode and cathode within the corrosion cell.

4.7.2 Maximum Coupled Current Algorithm

The maximum-coupled current algorithm accepts uncoupled corrosion potentials and electrolyte conductivities and determines the maximum amount of current flow through the pore solution that can be generated. Figure 4.15 presents the algorithm used for assessing the relative size of the anode and cathode and how corrosion currents are maximized. This algorithm employs a transition point to separate the cathode from the anode, as shown in Figure 3.6. This transition point is initially positioned at the end of the corrosion cell closest to the maximum corrosion potential and then incremented across the length of the cell until the point of minimum corrosion potential is reached. After each increment, anodic and cathodic currents are evaluated using algorithms outlined in Section 4.7.3 and 4.7.4.

Unlike the models presented in Section 2.0, the user does not set the size of the anode and cathode within the corrosion cell. For this research, the relative size of the anode and cathode is set by identifying the transition point that produces the largest current flow through the pore solution which also maximizes the change in corrosion potential from uncoupled to mixed. This approach produces mixed corrosion potentials along the bar/concrete interface that have minimal corrosion potential differences between segments.

Once the transition point is identified, the resulting anodic and cathodic currents are balanced. The balancing approach used for this algorithm sets the lesser of the anodic or cathodic current to be the maximum corrosion current flowing between the anode and cathode.

4.7.3 Anodic Coupling Algorithm

The algorithm developed for determining the coupled anodic current is based on the corrosion circuit created through the electrolyte represented by Figure 3.6. A system of equations is produced from this figure, the full derivation of which is provided in Appendix A.

Figure 4.16 outlines the process by which anodic current is calculated along with the number of segments that contribute. Initially, the segment closest to the transition point is assumed to be the sole contributor of coupled corrosion current, which allows for a direct solution. Once this initial step is completed, a second segment is added and the following process is implemented for this second and all subsequent segments:

- Using current flow from the previous segments, corrosion potential drops through the electrolyte to the next segment are estimated;

- If the difference between the transition potential and uncoupled corrosion potential at the new segment is greater than the estimated potential drop through the pore solution, the segment is assumed coupled and evaluated for coupling. If insufficient corrosion potential differences are present, the new segment is considered to be uncoupled and unable to contribute current flow through the pore solution;

- Anodic current contribution for the new segment is established using the appropriate equation from Table A.1;

- Once current from the new segment is identified, potential drops at each node labeled

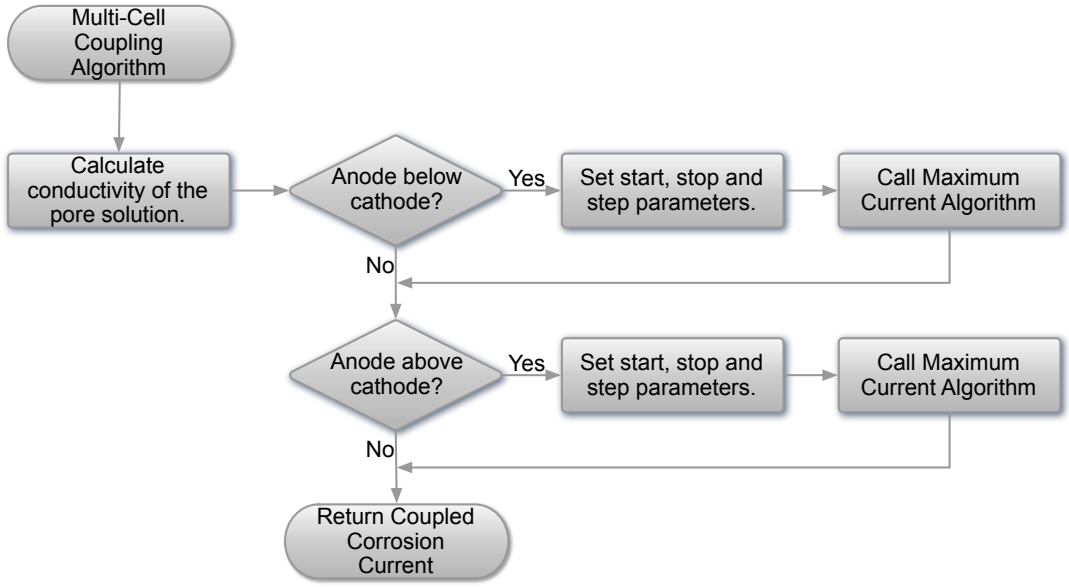

Figure 4.13. Multi-Cell algorithm flowchart.

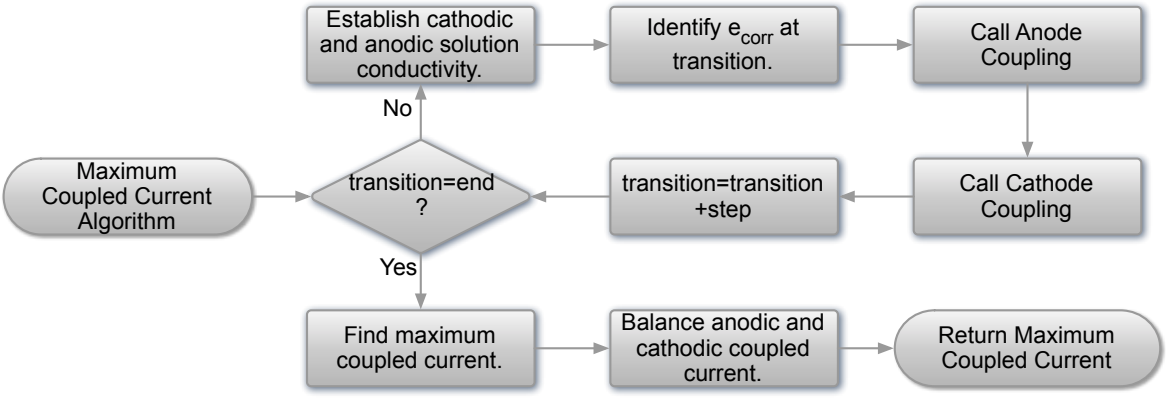

Figure 4.14. Maximum coupled current algorithm flowchart.

as $e_{n,coupled}$ in Figure 3.6 are evaluated using Equation 4.9 and 4.10:

$$e_{n,coupled,solution} = e_{transition} - \sum_{j=1}^{n} \phi_{\Omega,j} \quad [4.9]$$

$$e_{n,coupled,overpotential} = e_{n,uncoupled} + \phi_n \quad [4.10]$$

where $e_{n,coupled,solution}$ and $e_{n,coupled,overpotential}$ are mixed corrosion potentials after coupling established through the solution and overpotential, respectively, $e_{transition}$ is the corrosion potential at the transition point between the anode and cathode, $\phi_{\Omega,j}$ is the potential drop through the pore solution, $e_{n,uncoupled}$ is the uncoupled corrosion potential on the bar/concrete interface and ϕ_n is the overpotential drop caused by coupling. The differences in corrosion potentials calculated by Equation 4.8 and 4.9 represent the error introduced as new segments are added. If the error is within the tolerance of

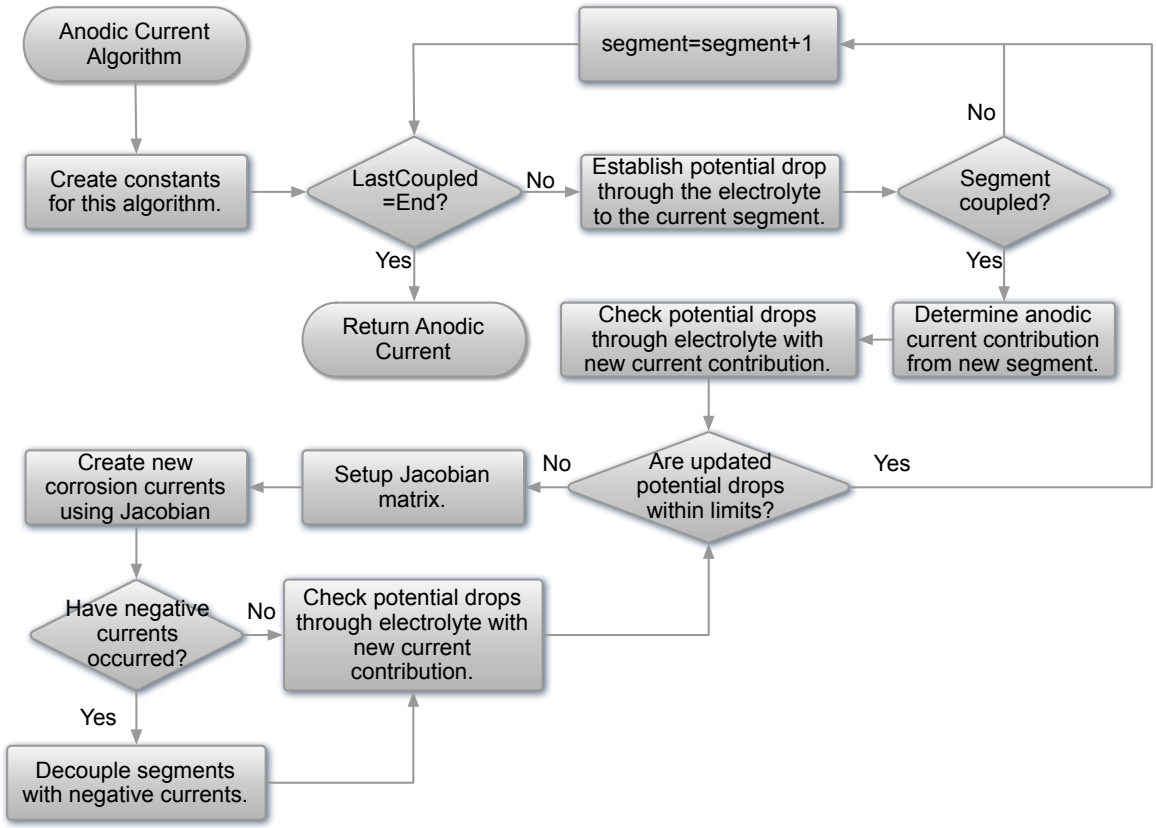

Figure 4.15. Anodic zone flowchart for algorithm to establish current contribution through coupling.

0.0001 V, the next segment is added; otherwise

- Current contributions from each segment are adjusted using Newton-Raphson's Method for solving non-linear equations, as outlined in Appendix A, until the difference in corrosion potentials calculated from Equations 4.9 and 4.10 fall within the specified tolerance. Adjustments in some situations produce segments with negative current, which is allowed to occur until the difference in corrosion potential tolerance is achieved. If final current values are negative, the affected segments are assumed decoupled and calculations repeated using the same total number of segments less the segments that produced negative currents.

These steps are repeated for each segment that is present from the transition point to the end of the anodic zone. Once the end is reached, the total current produced, along with the segments that produced this current, is returned to the Maximum Coupled Current Algorithm.

4.7.4 Cathodic Coupling Algorithm

The rate of oxidation from the anodic side of the corrosion cell must be balanced by the rate of reduction of oxygen on the cathodic side to avoid accumulating charge in the corrosion cell. Therefore, the total current from the anodic zone must be balanced by current flow from the cathodic zone. Figure 4.17 represents the flowchart that describes the algorithm used to establish the cathodic current that balances current flow from the anodic zone. Similar to the anodic coupling algorithm, an iterative process is employed to determine the current contribution from each segment caused by coupling. Since the total coupled corrosion current from the anodic side is known, ohmic potential drops through the pore solution are known, which allows a direct solution of the current contribution from a particular segment. However, this direct solution is dependent on whether excess oxygen is available or limited at the segment being evaluated. If excess oxygen is present, the cathodic reaction results in an increase in OH^- production without a corresponding increase in Fe^{2+}. However, if oxygen is limited, then the total OH^- production remains unchanged but Fe^{2+} production is depressed. This phenomenon is similar to galvanic corrosion whereby the more active metal reduces the corrosion rate on the noble metal. Equations developed for representing these two oxygen conditions are presented in Appendix A.

4.8 Summary

A detailed overview of the implementation of fundamental principles of corrosion for simulating circumferential corrosion process occurring on a reinforcing steel bar embedded in concrete were presented. Limitations of the model were identified along with how errors at various stages of the simulation were minimized due to the iterative processes used to arrive at a solution. The unique aspects of the model developed were also identified which included:

- Multiple corrosion cells can form on the circumferential surface formed at the bar/concrete interface as chlorides diffuse to, and around, the bar. The formation of these cells has not been reported in the literature; and

- The ratio of anodic to cathodic areas is set by the difference in corrosion potentials and the conductivity of the solution between these two half-cells. This methodology is a

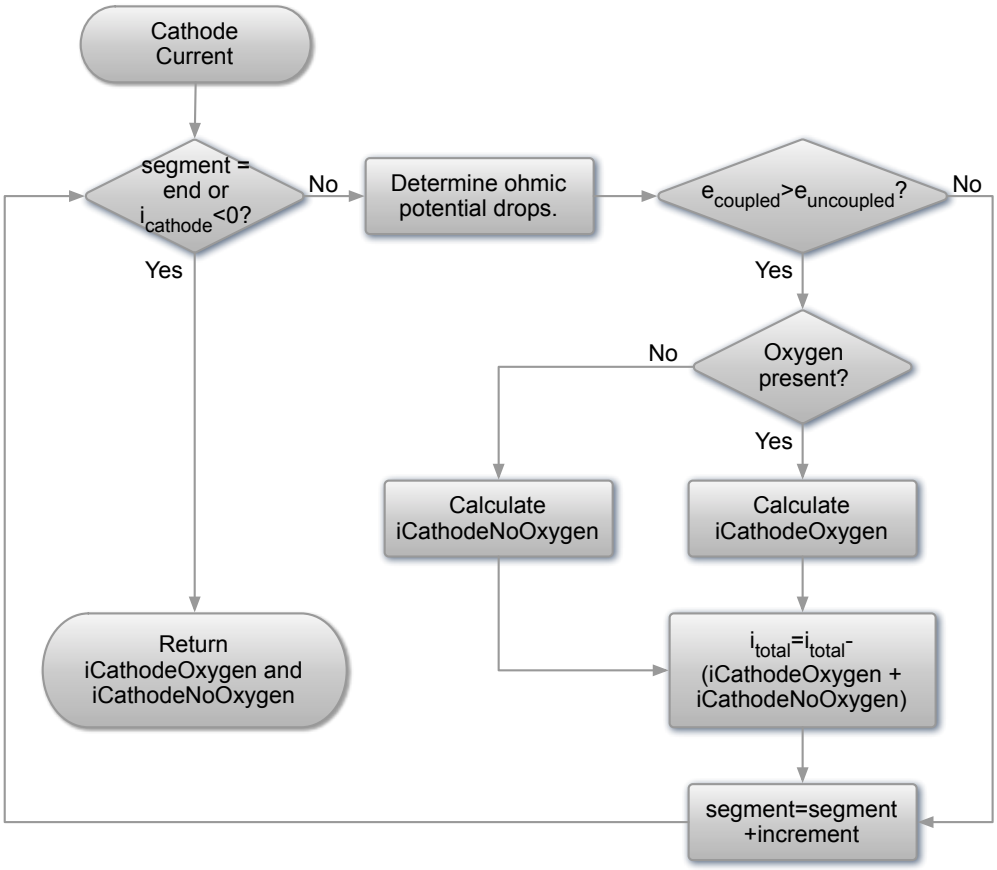

Figure 4.16. Cathodic zone flowchart of algorithm to calculate current contribution through coupling.

new approach to establishing current flow in a coupled corrosion cell as existing models force the user to assign an area to the anode and cathode.

5 NUMERICAL MODEL RESULTS AND DISCUSSION

5.1 Introduction

Section 4.0 presented algorithms used for simulating corrosion present on the bar/concrete interface for a bar embedded in concrete. The simulation considered chloride concentrations that varied between a chloride free condition to a maximum value defined by the kinetics of corrosion obtained from polarization tests conducted on reinforcing steel in a simulated concrete pore solution. Within this section, results of the simulation under selected geometrical configurations describing specific bar sizes, covers, and spacing are presented and discussed to highlight:

- How concrete cover, spacing, and bar diameter affect oxygen levels within the concrete pore water electrolyte which, in turn, influence the corrosion current and corrosion potentials on the bar surface;

- How the creation of varying corrosion potentials around the bar circumference due to circumferential variation in chloride and oxygen concentrations cause current flow through the connecting electrolyte which increases dissolution rates at anodic sites;

- How transition from a passivated to a fully corroding condition requires coupling between high and low corrosion potentials on the bar circumference or along the longitudinal axis of the bar; and

- How the current model can be used to determine when damaging levels of corrosion are possible without having to specify a cathodic and anodic area or a fixed value for chloride concentrations that initiate corrosion.

Results of the numerical simulations are presented by relating corrosion processes occurring on the bar/concrete interface with corrosion potentials that would be measured on the concrete surface with the use of a reference half-cell. The effects of concrete cover, bar diameter, bar spacing and moisture conditions are all evaluated. A brief discussion of the impact of these variables on the corrosion processes is also included.

5.2 Simulation Overview

The numerical model simulated corrosion processes over a range of bar diameter, concrete cover, bar spacing and relative humidities with the intent of identifying whether geometrical or moisture conditions had the greatest impact on the corrosion current generated on the bar/concrete interface. The model could also be used to simulate corrosion processes under a range of temperatures; however, for the purposes of this study, temperatures were held constant.

Within the simulation, corrosion potentials on the bar/concrete interface were projected to the concrete surface to produce potentials that could be measured with a reference half-cell, thereby correlating the corrosion processes with measurements that can be made using readily available non-destructive testing equipment. In order to reduce the number of simulations, diffusion parameters related to the water-to-cement ratio, and aggregate type and quantity, were kept constant for each simulation. However, the effect of moisture conditions was addressed. In a similar fashion, surface chloride loading was held constant for each simulation, as the net effect of varying this parameter would result in a proportional lengthening or shortening of the time for chloride to reach the bar/concrete interface consideration.

As presented in Section 4.6, concrete cover affects the mass transport of oxygen and chloride to the bar/concrete interface, producing chemistry within the electrolyte present on the bar/concrete interface that changes with depth. This variation in chemistry, combined with the kinetics of corrosion, produce unique corrosion potentials and current at each point around the bar. These different corrosion potentials produce current flow through the electrolyte, which connects high and low corrosion potential zones. Since these zones are at different corrosion potentials and are electrically connected, a mixed corrosion potential is created resulting in an increase in metal dissolution in zones at more negative potentials. Cathodic reduction processes within the zones of more positive potentials, on the other hand, will be affected differently depending on the local oxygen concentrations such as:

- Excess oxygen is present - Cathodic reduction processes are increased without a corresponding increase in the local metal dissolution rate; or
- Oxygen limitations are present - Local cathodic reduction processes are maintained at the rate dictated by the oxygen supply; however, local metal dissolution rates decrease in order for excess electrons produced by the adjacent coupled surface to be consumed.

This process is similar to the condition created under impressed current or galvanic cathodic protection.

Figure 5.1 presents a typical example of simulated corrosion potentials around the bar circumference as chlorides diffuse to the bar/concrete interface. The system geometry used for this example is based on a typical bridge deck constructed with 20 mm nominal diameter bar, spaced at 200 mm, with a cover of 50 mm. The relative humidity was set at 90% to simulate moisture conditions that could be present at locations on a bridge deck where ponding regularly occurs. Corrosion potentials around the bar circumference are shown as a function of time for each control segment used in the simulation and following the numbering scheme identified in Figure 3.5. Numbering for each segment begins with the first segment positioned at the top of the bar and incremented counterclockwise until the last segment is reached at the bottom of the bar. Only one-half of the bar is presented as results for the other half would be effectively a

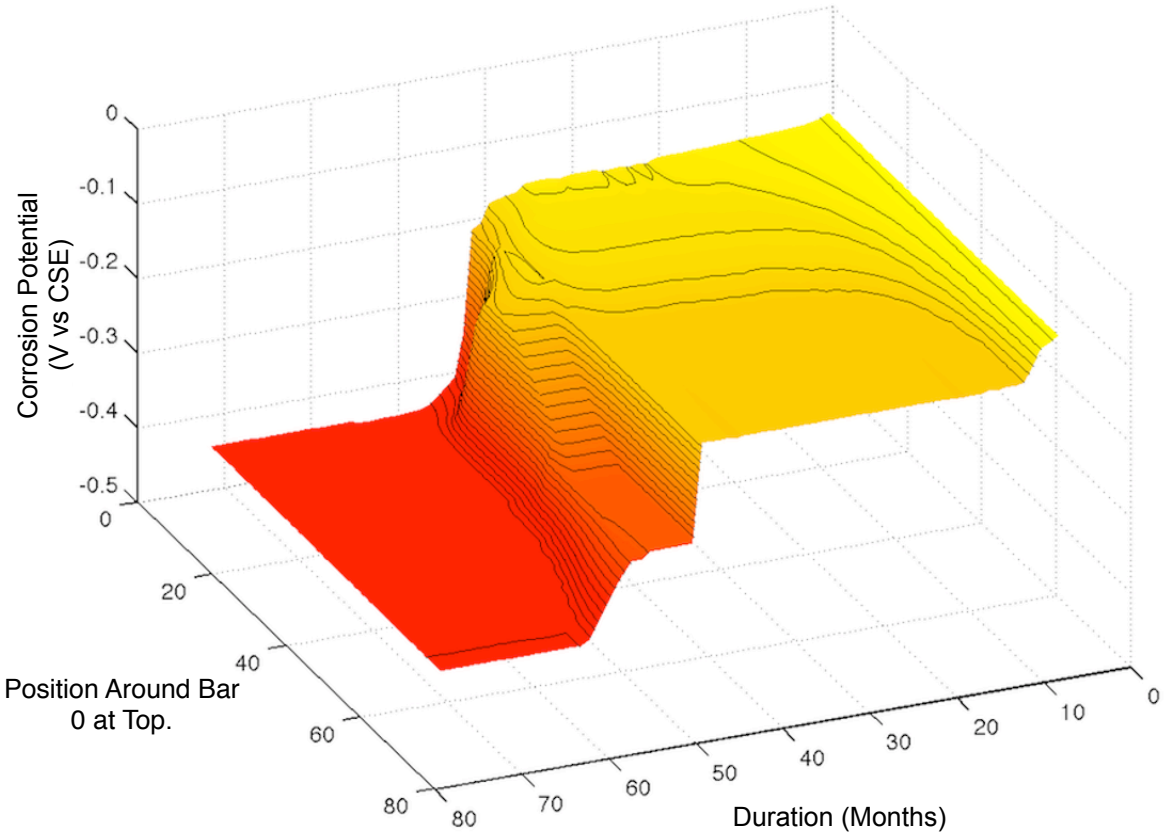

Figure 5.1. Uncoupled corrosion potential around the bar circumference through time for constant pH with contours set at 0.01 V increments. Bar diameter = 20 mm, Bar spacing = 200 mm, Cover = 50 mm, Relative Humidity = 90%.

mirror image.

The starting time period of 0 represents initial conditions when chlorides are first placed on the concrete surface and oxygen concentrations within the model space are at a fully saturated condition. From this initial condition, the simulation proceeds until chloride concentrations around the bar perimeter reach the point where no further changes in kinetics occur.

Figure 5.1 shows that local corrosion potentials around the bar perimeter vary with depth and time depending on the presence of oxygen and chloride. For discussion purposes, four time periods have been selected to outline how variations in corrosion potential around the bar circumference change with time, and how these corrosion potentials affect the corrosion current density. The time periods identified were selected to capture the unique corrosion potentials generated around the bar circumference at: Stage 1 – Initial Conditions; Stage 2 – Steady State Without Chloride; Stage 3 – Maximum Current Flow through the Electrolyte; and Stage 4 – End of Simulation. Stage 4 – End of Simulation is defined as the point at which chloride concentrations at all points around the bar exceed the chloride concentration after which no further change in kinetics is possible.

5.2.1 Stage 1 – Initial Conditions.

Each simulation was initiated assuming uniform oxygen concentrations for the humidity conditions identified for the particular simulation as well as an absence of chlorides throughout the model space. Under this scenario, a uniform corrosion potential is produced around the bar circumference. However, once the local kinetics of corrosion are adjusted to match initial concentrations, a drop in oxygen concentration within the pore solution with depth occurs which causes corrosion potentials to become more negative, as predicted by the Nernst Equations (Equation 2.6). Figure 5.2 presents the chloride concentrations (Figure 5.2(a)), oxygen concentrations (Figure 5.2(b)), mixed and uncoupled corrosion potentials (Figure 5.2(c)), and the mixed and uncoupled corrosion current density (Figure 5.2(d)) for each segment around the bar circumference.

The terms uncoupled and mixed describe whether current flow through the electrolyte has been included. For the case of uncoupled corrosion potentials and current densities, these are the values obtained directly from the kinetic of corrosion diagrams assuming no current flow through the electrolyte. Effectively, the uncoupled values represent the driving force that is present to cause current flow through the electrolyte. Conversely, mixed corrosion potentials are the

values that would be recorded when the bar surface is electrically connected through the electrolyte. Similarly, mixed current densities are the total corrosion currents produced which include the uncoupled corrosion current and the corrosion current flowing through the electrolyte.

Table 5.1 provides supplementary information obtained from Figure 5.2, which includes:

- Maximum corrosion potential differences between different points on the bar circumference in the uncoupled condition (Δe_{corr}, (volts));
- Maximum, minimum, and average corrosion currents created by coupling around the bar circumference (i_{anode} (A/mm^2);
- Uncoupled corrosion currents ($i_{uncoupled}$, (A/mm^2)) corresponding to the maximum, minimum and average corrosion currents occurring in zones with increased metal dissolution rates;
- Total corrosion current generated at zones of increased metal dissolution rates at the mixed corrosion potential condition ($i_{coupled}$, (A/mm^2)) for each of the maximum, minimum and average corrosion currents reported previously; and
- The percentage of the bar circumference with increased metal dissolution rates (anode) as well as that with increased oxygen consumption rates or depressed metal dissolution rates (cathode).

At initial conditions, chlorides are not present, as shown in Figure 5.2(a), and oxygen concentrations are near the maximum for this simulation. However, once the corrosion rate predicted by the kinetics of corrosion for the electrolyte concentration is applied to the bar/concrete interface, oxygen is depleted within the electrolyte on this surface, and must be

Table 5.1. Stage 1 - Corrosion potential differences, corrosion current density, supplementary anodic current, anodic and cathodic area. Bar Diameter = 20 mm, Bar Spacing = 200 mm, Cover = 50 mm, Relative Humidity = 90%.

	i_{anode} 10^{-9} (A/mm^2)	$i_{uncoupled}$ 10^{-9} (A/mm^2)	$i_{coupled}$ 10^{-9} (A/mm^2)	Δe_{corr} (volts)	Anode %	Cathode %
Maximum	0.0004	4.8510	4.8510			
Minimum	0.0000	4.8514	4.8514	0.0003	49%	22%
Average	0.0002	4.8510	4.8484			

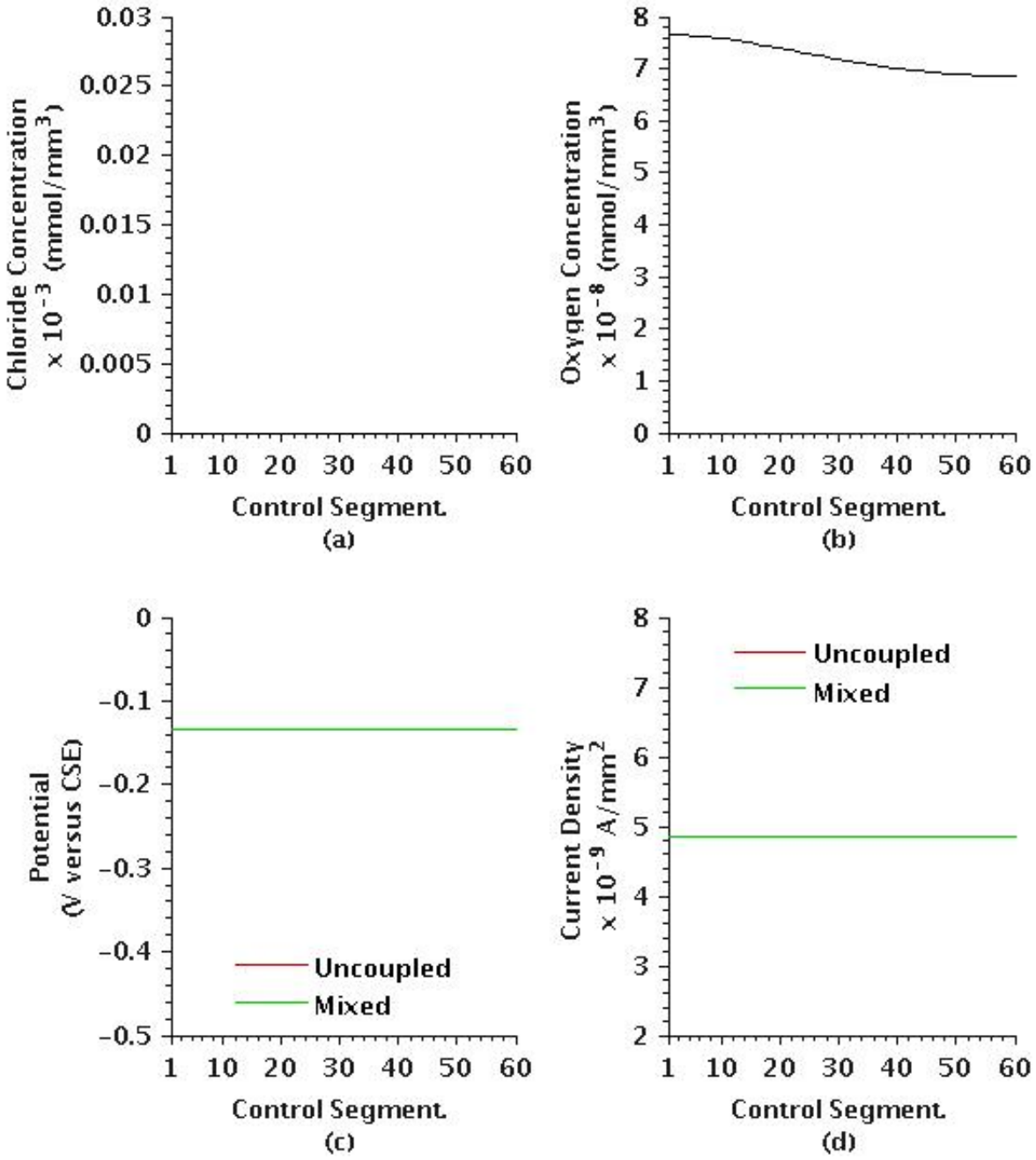

Figure 5.2. Stage 1 chloride concentration, oxygen concentration, corrosion potential and corrosion current density around the bar perimeter: (a) Chloride concentration. (b) Oxygen concentration. (c) Uncoupled and mixed corrosion potential; (d) Uncoupled and mixed corrosion current density. Month=1, Bar diameter = 20 mm, Bar spacing = 200 mm, Cover = 50 mm, Relative Humidity = 90%.

replenished by mass transport through the concrete. This depletion is represented in Figure 5.2(b) by a decrease in oxygen concentration with depth around the bar circumference.

Since oxygen concentrations have moved away from initial conditions, corrosion potentials must also change to be consistent with the Nernst Equations with depth, which is not readily apparent in Figure 5.2(c). However, Table 5.1 identifies a corrosion potential difference of 0.0003 V that is created under these conditions. This corrosion potential difference increases the average anodic rate around 49% of the bar circumference by 0.0002×10^{-9} A/mm^2, which is negligible, as shown in Figure 5.2(d) and Table 5.1, when compared to the uncoupled corrosion current density of 4.851×10^{-9} A/mm^2. This increased anodic rate is located toward the underside of the bar where oxygen concentrations are lower. The corresponding cathodic reactions which counter the increased anodic reaction require only 22% of the bar circumference, suggesting that, under these conditions, less cathodic area is required to offset the increase in anodic current.

Corrosion potentials around the bar circumference do not remain at these values as the corrosion current generated on the bar/concrete interface consumes oxygen which must be replenished through oxygen mass transport. Therefore, as represented in Figure 5.1, the initial corrosion potentials around the bar decrease with depth as oxygen is extracted from the pore solution due to the corrosion current generated. These changes continue until Stage 2 is reached.

These initial simulation results demonstrate that current flow within the electrolyte that encapsulates the bar is likely to occur when longitudinal variations in electrolyte chemistry are not present. Therefore, when longitudinal variations occur, the amount of current flow through the electrolyte will be increased, as coupling will be occurring circumferentially and longitudinally a process which is not addressed in any current corrosion models.

5.2.2 Stage 2 – Steady State Without Chloride

Immediately following Stage 1, oxygen concentrations on the bar surface will be lowered as oxygen is consumed by the passivated corrosion process while oxygen transport from the concrete surface is not sufficient to maintain the initial concentrations. Corresponding with the reduction in local oxygen concentrations is a lowering of the corrosion potential due to one or both of the following processes:

- Reversible corrosion potentials are a function of local oxygen concentrations by the Nernst Equations (Equation 2.6). As oxygen concentrations are reduced, the reversible corrosion potential becomes more negative, resulting in a lowering of the corrosion potential, and a reduced corrosion current density. This phenomenon is present under Stage 1; and

- Increased corrosion rates exceed the ability of the system to deliver oxygen to the corroding surface through mass transport. Under this situation, the corroding surface reaches a limiting corrosion current condition resulting in the corrosion current density being reduced, with a corresponding reduction in the corrosion potential.

After the model is initiated, the system approaches a steady-state condition of oxygen concentration and corrosion potentials around the bar circumference. This steady-state condition is maintained until sufficient concentrations of chlorides arrive at the bar/concrete interface to affect the kinetics of corrosion. When this occurs, the system transitions into Stage 3.

Figure 5.3 outlines chloride concentrations, oxygen concentrations, corrosion potentials and corrosion currents present once steady-state conditions are reached. The results corresponding to this figure are presented in Table 5.2.

Figure 5.3(a) indicate chlorides have arrived at the bar/concrete interface but not of sufficient concentration to affect the kinetics of corrosion. However, Figure 5.4(b) indicates oxygen concentrations have been reduced due to the corrosion current density predicted by the kinetics of corrosion, resulting in a limiting corrosion current condition produced near segment 30 and continuing to the underside of the bar. This limiting corrosion current causes corrosion potentials shown in Figure 5.4(c) to become more negative with depth, produces a maximum corrosion potential difference of 0.0377 V, which is significantly higher than that under Stage 1.

Table 5.2. Stage 2 - Corrosion potential differences, corrosion current density, supplementary anodic current, anodic and cathodic area. Bar Diameter = 20 mm, Bar Spacing = 200 mm, Cover = 50 mm, Relative Humidity = 90%.

	i_{anode} 10^{-9} (A/mm^2)	$i_{uncoupled}$ 10^{-9} (A/mm^2)	$i_{coupled}$ 10^{-9} (A/mm^2)	Δe_{corr} (volts)	Anode %	Cathode %
Maximum	0.0761	4.2540	4.3265			
Minimum	0.0160	4.2088	4.2248	0.0377	57%	11%
Average	0.0374	4.2292	4.2666			

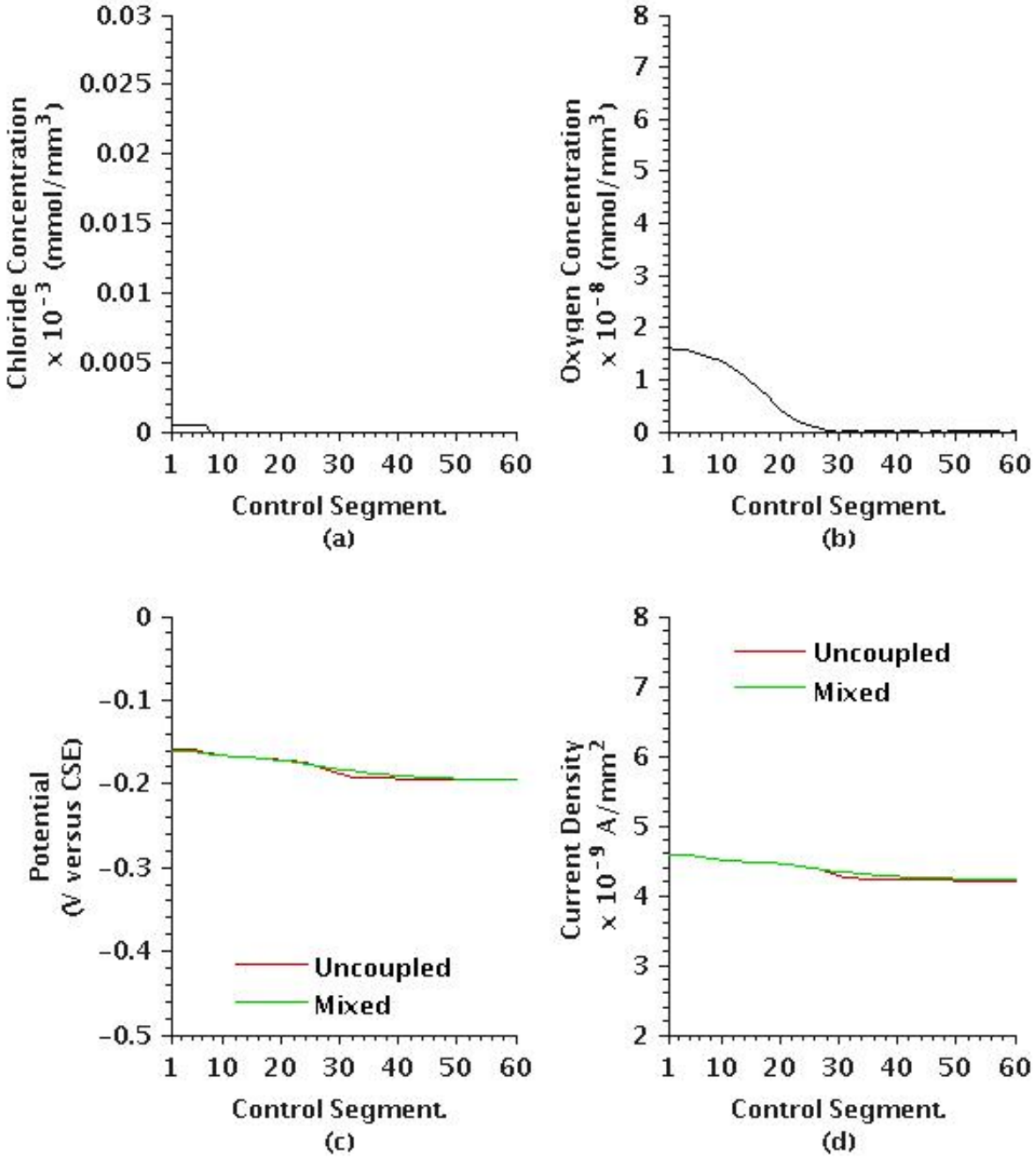

Figure 5.3. Stage 2 chloride concentration, oxygen concentration, corrosion potential and corrosion current density around the bar perimeter: (a) Chloride concentration. (b) Oxygen concentration. (c) Uncoupled and mixed corrosion potential; (d) Uncoupled and mixed corrosion current density. Month=1, Bar diameter = 20 mm, Bar spacing = 200 mm, Cover = 50 mm, Relative Humidity = 90%.

With this corrosion potential difference present, current flow through the pore solution is produced and results in an average increase in corrosion current density along 57% of the portion of bar modeled of 3.74×10^{-11} A/mm^2. Figure 5.3(d) shows this slight increase as a separation between the corrosion current density at uncoupled and mixed levels near segment 30. This increased corrosion current density increases the local corrosion current rate by 0.9% over the uncoupled corrosion current density of 4.23×10^{-9} A/mm^2. In a manner similar to Stage 1, increased anodic reactions are positioned on the underside of the bar where an oxygen-limited condition has been reached. Corresponding cathodic reactions are sustained on 11% of the modeled circumference located closer to the concrete surface. Of note is that, while anodic corrosion current created under mixed corrosion potentials are significantly higher than Stage 1 (3.74×10^{-11} versus 2.0×10^{-13}), the overall corrosion current under Stage 2 is 12% lower, as the uncoupled corrosion current rate is limited to the amount of oxygen available on the corroding surface.

This reduced corrosion rate under Stage 2 would appear to be a benefit to the life of the reinforcing steel; however, the increased current flow caused by coupling on the bar circumference has implications to the local electrochemistry, which is not presently addressed by the model developed for this research or any other model reported in the literature. For simplicity, the current model assumes changes to the local OH^- concentrations in the electrolyte due to creation of $Fe(OH)_2$ is offset by dissolution of OH^- from hardened portions of the cement paste. In other words, the local pH remains constant. However, this assumption does not address the effect that formation of $Fe(OH)_2$ has on the continuity of the surrounding environment. As $Fe(OH)_2$ forms, it precipitates into the pore structure, effectively decreasing the diffusion coefficient immediately surrounding the area experiencing metal dissolution. This decreased diffusion coefficient has the two-fold effect of:

- Reducing transport of oxygen to the corroding surface, results in a further decrease in corrosion potentials which increases the corrosion potential difference, causing further coupling to occur; and

- Reducing the transport of OH- from the hardened cement paste into the electrolyte, resulting in the acidification of the local environment. When this acidification occurs, the local thermodynamics are changed, resulting in an increase in the local corrosion rate without changing any of the other parameters such as oxygen or chloride concentrations.

This effect of $Fe(OH)_2$ diffusing into the pore structure immediately around the corroding areas is well documented in the literature (Balafas and Burgoyne 2010) and is supported by observations from the field, as shown in Figure 5.4. Future models must incorporate this physical result of $Fe(OH)_2$ generation in order that changes to the localized rate of transport of oxygen and OH^- to the bar/concrete interface be identified, combined with the effect this change incurs on the local pH and kinetics of corrosion.

Stage 2 demonstrates coupling between adjacent sites on the bar circumference is possible under non-chloride contaminated conditions. However, the rate of corrosion predicted by this

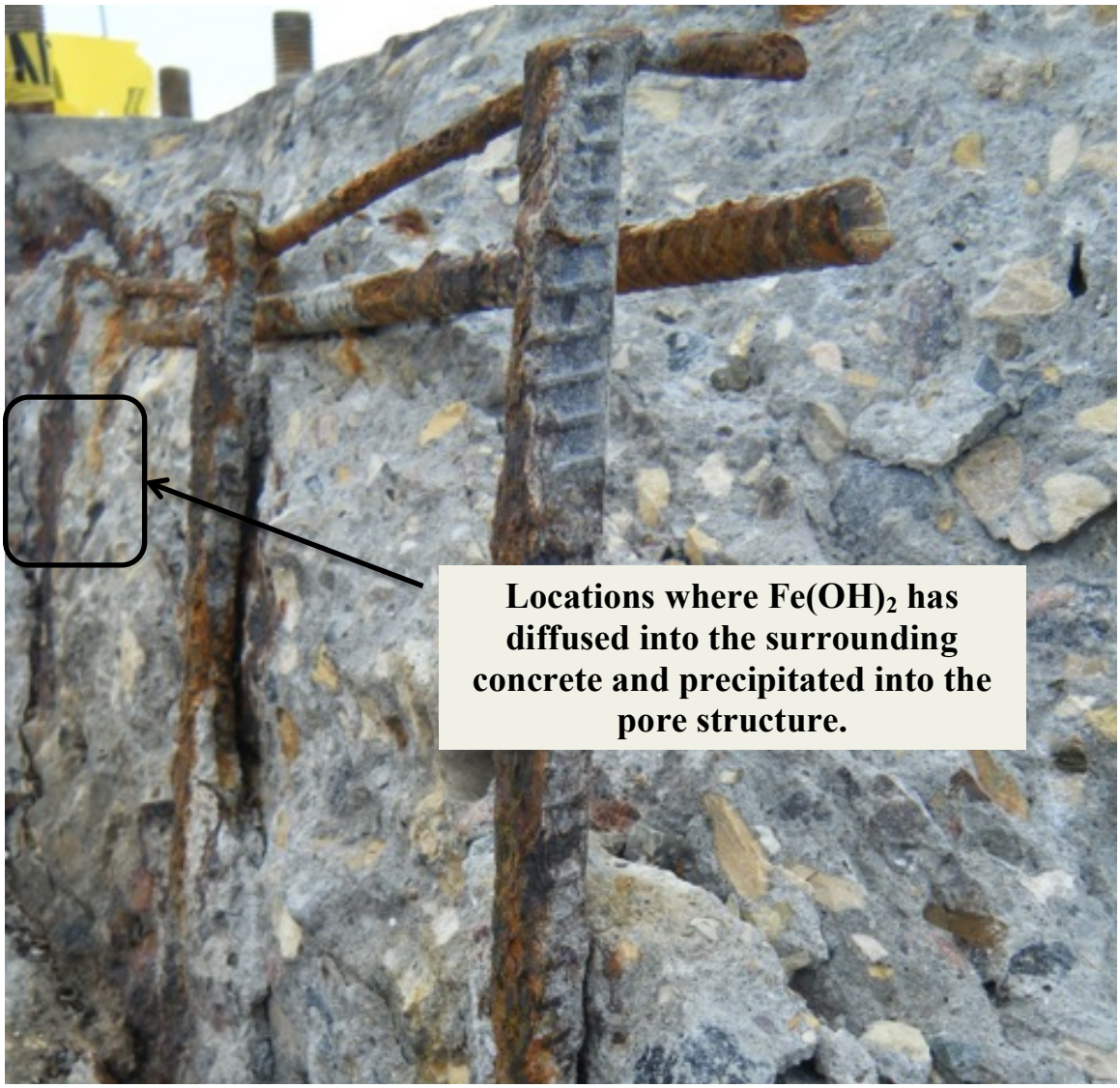

Figure 5.4. Visual evidence of corrosion byproduct diffusing into surrounding concrete and precipitating.

simulation is very low so the resulting production of corrosion by-product will also be minimal. However, any production of $Fe(OH)_2$ will cause further restrictions in oxygen transport which results in a lowering of the corrosion potential with a corresponding decrease in corrosion rate. Therefore the secondary effect caused by $Fe(OH)_2$ creates zones where oxygen is further restricted, potentially creating acidified areas. Under this scenario, localized dissolution of the reinforcing bar can be estimated from Figure 2.20, which shows the kinetics of corrosion for reinforcing steel embedded in either non-carbonated or carbonated concrete. From this figure, assuming that the final localized pH is equal to 9 and the chloride concentration within the electrolyte has exceeded the maximum value of 2.8×10^{-5} mmol/mm^3 shown in the figure, the corrosion rate would increase to between 1×10^{-7} to 1×10^{-5} A/mm^2, which represents an increase of between 20 and 2000 times the non-carbonated average uncoupled corrosion rate identified for this stage. Under this corrosion scenario, the local oxygen consumption rate would increase significantly as this value is directly related to the corrosion current density which would further deplete the oxygen concentrations within the electrolyte. This further depletion would likely cause an oxygen limiting corrosion current being reached resulting in further lowering of the corrosion potential. Currently, this scenario was not modeled, as the existing model does not permit this type of phenomenon to occur. However, the current model can be modified to include this effect.

The conditions that create Stage 2 remain in effect until chlorides reach the bar surface. Once chlorides are present and in sufficient concentrations to affect the local kinetics of corrosion then Stage 3 develops.

5.2.3 Stage 3 – Chloride Arrives

The arrival of chloride to the upper portion of the reinforcing bar causes an increase in the corrosion current density due to the kinetics of corrosion curves being shifted to the right as presented in Figure 3.2. Figure 5.5 shows the effect this change in chloride concentration has on the system as chloride concentrations, oxygen concentrations, corrosion potential, and corrosion current density around the bar circumference at month 45 are quantified. Tables 5.3 and 5.4 present the corresponding corrosion data.

Figure 5.5(a) identifies chloride concentrations are present on the upper one-half of the bar circumference nearest the concrete surface. These chlorides have increased the corrosion current density in this area, which results in oxygen concentrations around the bar perimeter

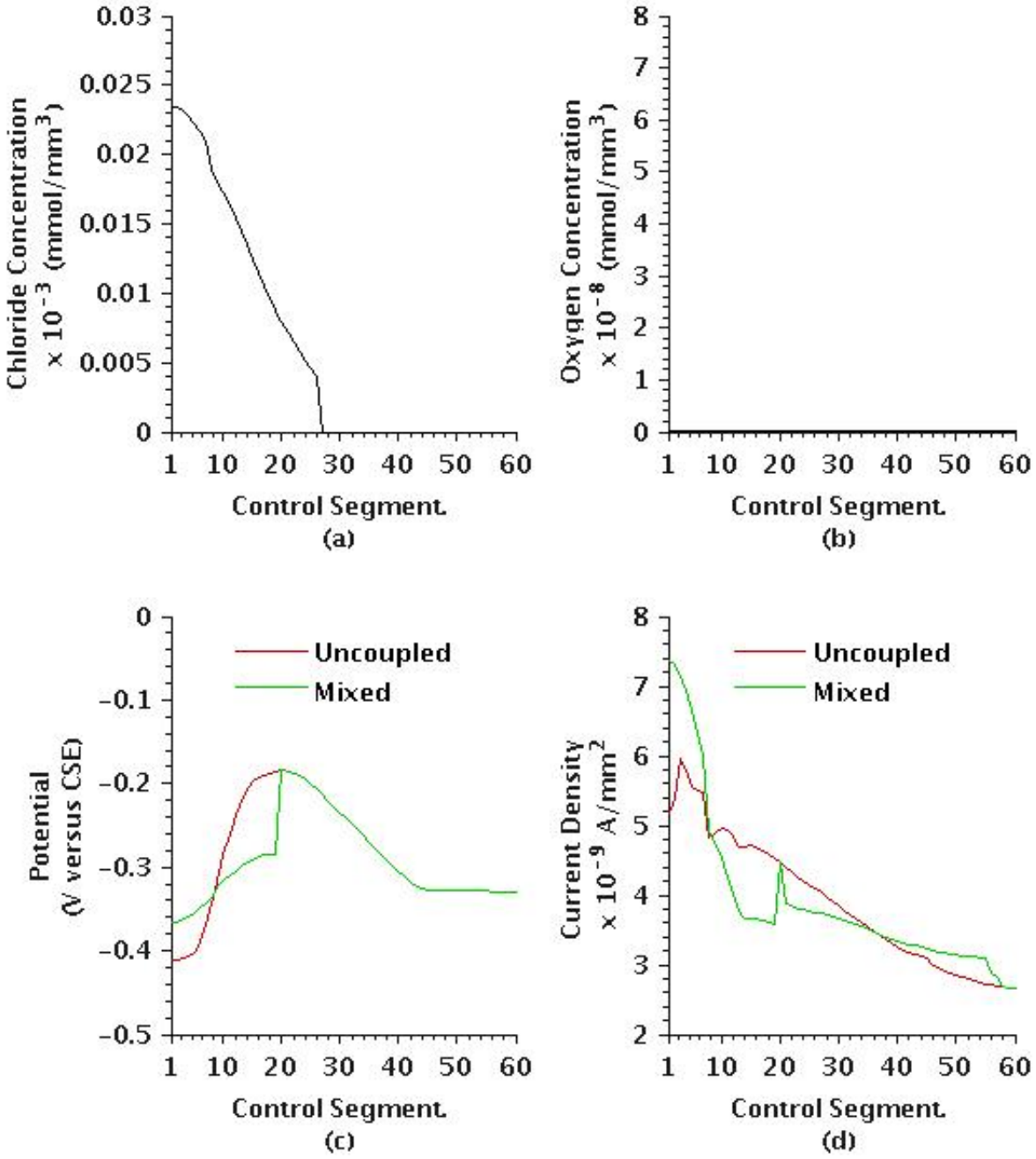

Figure 5.5. Stage 3 chloride concentration, oxygen concentration, corrosion potential and corrosion current density around the bar perimeter: (a) Chloride concentration. (b) Oxygen concentration. (c) Uncoupled and mixed corrosion potential; (d) Uncoupled and mixed corrosion current density. Month=1, Bar diameter = 20 mm, Bar spacing = 200 mm, Cover = 50 mm, Relative Humidity = 90%.

reaching a limiting oxygen condition. Figure 5.5(b) demonstrates this limiting condition as oxygen concentrations are near zero.

Figure 5.5(c) presents the corresponding corrosion potentials induced by chloride and oxygen concentrations at each point around the bar. Under this scenario, uncoupled corrosion potentials around the bar produce a unique shape. This shape has corrosion potentials more negative at the top of the bar, which increases with depth due to decreasing chloride concentrations until a maximum corrosion potential is reached near segment 20. Below Segment 20, corrosion potentials decrease with depth due to oxygen limitations induced by the increasing cover. This unique corrosion potential configuration cause the formation of two corrosion cells with the first cell (Cell 1) occupying the bar circumference from segment 1 to 20 and the second cell (Cell 2) occupying the remainder of the bar circumference.

The second cell is in the same general location as the anodic zone created in Stages 1 and 2. Mixed corrosion potentials in Cell 1 are significantly modified from the uncoupled corrosion potentials while Cell 2 mixed corrosion potentials are similar to the uncoupled values. The different effect on the mixed corrosion potential between the two cells is related to the presence of chloride in Cell 1 while Cell 2 is chloride free. The presence of chloride in Cell 1 increases the pore solution conductivity thereby reducing ohmic potential drops. With a decreased ohmic potential drop, more current flow can occur under the same corrosion potential differential,

Table 5.3. Stage 3, Cell 1 - Corrosion potential differences, corrosion current density, supplementary anodic current, anodic and cathodic area. Bar Diameter = 20 mm, Bar Spacing = 200 mm, Cover = 50 mm, Relative Humidity = 90%.

	i_{anode} 10^{-9} (A/mm^2)	$i_{uncoupled}$ 10^{-9} (A/mm^2)	$i_{coupled}$ 10^{-9} (A/mm^2)	Δe_{corr} (volts)	Anode %	Cathode %
Maximum	2.2431	5.1361	7.3792			
Minimum	0.1213	4.8235	4.9447	0.2276	13%	17%
Average	1.1296	5.1361	6.5836			

Table 5.4. Stage 3, Cell 2 - Corrosion potential differences, corrosion current density, supplementary anodic current, anodic and cathodic area. Bar Diameter = 20 mm, Bar Spacing = 200 mm, Cover = 50 mm, Relative Humidity = 90%.

	i_{anode} 10^{-9} (A/mm^2)	$i_{uncoupled}$ 10^{-9} (A/mm^2)	$i_{coupled}$ 10^{-9} (A/mm^2)	Δe_{corr} (volts)	Anode %	Cathode %
Maximum	0.3722	2.7262	3.0984			
Minimum	0.0004	2.6466	2.6470	0.1448	43%	25%
Average	0.1497	2.9236	3.0733			

producing a large potential shift from uncoupled to mixed corrosion potentials.

For Cell 1, the corrosion potential difference within this region is 0.2276 V, which is a significant increase in corrosion potential difference over the previous two stages. This corrosion potential difference increases the average uncoupled corrosion current density by 17% with localized areas exhibiting 30% increases. From Figure 5.5(d), in contrast to Stages 1 and 2, the orientation of the corrosion cell has the anodic zone located overtop of the cathodic zone with the anode and cathode consuming 13% and 17% of the modelled circumference, respectively. This increased localized rate of corrosion will result in additional formation of $Fe(OH)_2$, which will lower the local diffusion coefficient of the concrete, creating further restrictions on oxygen transport to the areas where the anodic processes are increased. This process produces a similar environment to that found in a pitting corrosion cell where a pit is isolated from the surrounding electrolyte by a gel. Figure 2.3 shows this phenomenon, which allows ionic transfer but restricts the transfer of oxygen. Under this corrosion scenario, the electrolyte within the pit is isolated from the bulk electrolyte, which becomes more acidic, resulting in the corrosion process on a potential versus pH diagram moving into the corrosion zone, as shown in Figure 2.2.

This pitting corrosion phenomenon has been observed in the field on many reinforced concrete structures exposed to chloride, a typical example of which is shown in Figure 5.6, which is a photograph of a reinforcing bar positioned on the traffic side (ie: splash) of a reinforced concrete barrier. This photograph supports the results of this model whereby section loss is focused in areas that are initially exposed to chlorides, producing equivalent section loss patterns similar to that resulting from pitting corrosion.

Cell 2 has a corrosion potential difference of 0.1448 V, which is smaller than the value produced by Cell 1, but larger than the values produced in Stages 1 or 2. Within Cell 2, the average corrosion current density is increased by 4%, with localized areas reaching 12%. The orientation of this cell is similar to that produced under Stage 1 and 2, which has the cathodic zone overtop of the anodic zone. As discussed previously, the lack of chlorides within Cell 2 increases the ohmic resistance, which limits current flow through the pore solution, and the corresponding change in corrosion potential from uncoupled to mixed. Figure 5.5 (c) illustrates these differences in corrosion potential between the uncoupled to mixed values which is evident in Cell 1. However the same change in uncoupled to mixed corrosion potential is not present in Cell 2.

The conditions evident in Stage 3 remain in place until chlorides reach the bottom of the bar, at which time the system transitions into Stage 4.

5.2.4 Stage 4 – Chloride Fully Encapsulates the Reinforcing Steel Bar

This stage represents the point at which chlorides have reached sufficient concentrations to affect the kinetics of corrosion around the entire bar circumference. Figure 5.7 shows the chloride concentrations, oxygen concentrations, corrosion potentials, and corrosion current densities produced at the end of the simulation. Table 5.5 presents the corresponding corrosion data.

Figure 5.6. Pitting corrosion on a reinforcing steel bar. Photograph taken from the Arcola Avenue Overpass at Ring Road barrier along the north side of the bridge, near the east abutment.

Chloride concentrations shown in Figure 5.7(a) have increased significantly from previous stages and are at the point where further increases will not produce a change in the kinetics of corrosion as outlined in Section 2.2.3 and Figure 2.13. In similar fashion to Stage 3, Figure 5.7(b) identifies that oxygen concentrations around the bar circumference are at a limiting condition, as the oxygen concentration within the pore solution adjacent to each segment is close to zero.

Figure 5.7(c) presents the corrosion potentials produced under the chloride and oxygen concentrations. At this point, corrosion potentials are essentially constant around the bar perimeter, with a decrease in corrosion potential with depth due to limits induced by mass transport of oxygen to the bar and their effect on the corrosion potential estimated by the Nernst Equations. The corresponding corrosion current densities are represented in Figure 5.7(d), which show a decreasing corrosion current with depth which is a result of oxygen mass transport limitations induced by the concrete cover. As depth increases, oxygen must be transported further, which causes a lowering of the limiting corrosion current.

While chloride concentrations around the bar in Stage 4 are the largest for all of the stages considered as outlined in Figure 5.7(a), the corrosion potential difference of 0.0033 V is very similar to that under Stage 1, resulting in an average coupled corrosion current density of 1.75 x 10^{-11} A/mm^2, with localized areas reaching 7.21 x 10^{-11} A/mm^2. Therefore, even though chlorides are present to increase the pore solution conductivity, the corrosion potential along the bar circumference is insufficient to overcome the pore solution ohmic resistance.

While corrosion potential differences and the resulting coupled corrosion current is quite low around the bar circumference, coupling could occur along the length of the bar if suitable conditions are present. Typical locations where environmental conditions could be present to produce longitudinal coupling would be in:

- Decks where top upper and top lower layer steel are in contact;
- Barriers with tapering sections creating variable cover; and
- At crack locations.

At any of these locations, coupling will occur between bars (intersections) or along the bar length as the electrolyte chemistry will produce different corrosion potentials which will allow current flow to occur through the pore solution.

5.2.5 Stage Summary

The four stages shown in the preceding sections highlight the change in corrosion potential and corrosion current as the environment around the bar changes with the presence of chloride and oxygen mass transport limitations induced by the concrete cover. The model also identifies that the greatest coupling between adjacent portions on the bar surface occurs when chlorides and significant corrosion potential differences are present. This occurs only in Cell 1 of Stage 3.

Models produced to simulate macro cell reinforcing steel corrosion in concrete assume conductivity of the concrete is constant throughout the model space and time period considered. For the model used in this research, the pore solution conductivity was related to the concentration of ions within the pore solution using Equation 2.36. This relationship permits solution conductivity to be adjusted by the presence of chloride and other species that diffuse to the reinforcing bar surface if these other species were included in the model. For this simulation, the effect that chloride has on the overall corrosion rate is evident from Figure 5.5(d) and Table 5.3 and 5.4 where areas with chloride (Cell 1) had an increase in the average corrosion current density of 17.2%, while areas without chloride (Cell 2) increased by only 4.8% even though the corrosion potential differences within these two cells were similar. Some of the reduction in corrosion current density can be attributed to the change in the corrosion potential difference of 36% from Cell 1 to Cell 2. However, it is apparent from these simple calculations that the increase in corrosion current density can be attributed to the chloride not only changing the local kinetics of corrosion but also changing the conductivity of the solution, thereby permitting additional current flow through the pore solution.

Table 5.5. Stage 4 - Corrosion potential differences, corrosion current density, supplementary anodic current, anodic and cathodic area. Bar Diameter = 20 mm, Bar Spacing = 200 mm, Cover = 50 mm, Relative Humidity = 90%.

	i_{anode} 10^{-9} (A/mm^2)	$i_{uncoupled}$ 10^{-9} (A/mm^2)	$i_{coupled}$ 10^{-9} (A/mm^2)	Δe_{corr} (volts)	Anode %	Cathode %
Maximum	0.0721	2.9124	2.9844			
Minimum	0.0008	2.6330	2.6338	0.0033	52%	14%
Average	0.0175	3.0403	3.0578			

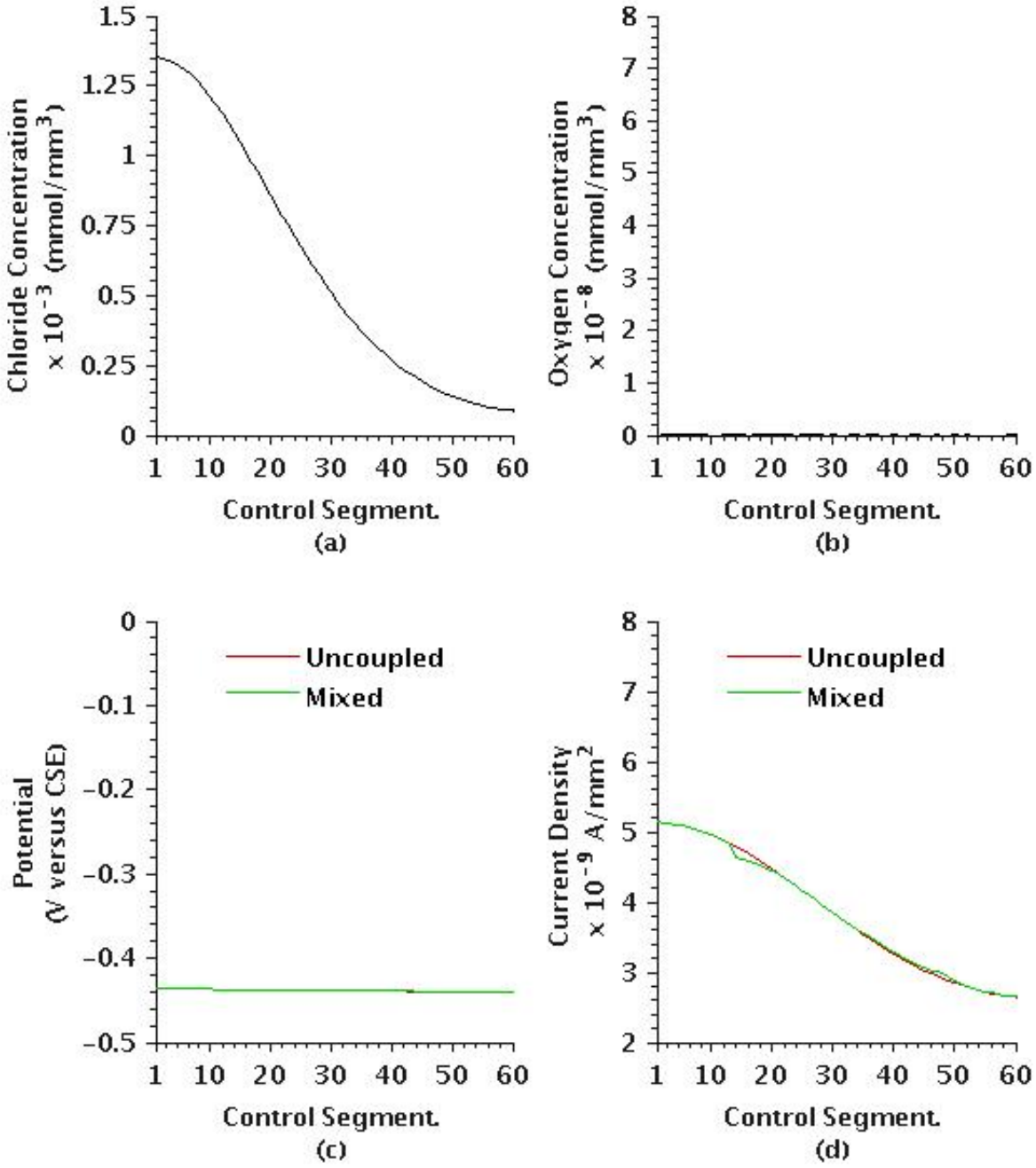

Figure 5.7. Stage 4 chloride concentration, oxygen concentration, corrosion potential and corrosion current density around the bar perimeter: (a) Chloride concentration. (b) Oxygen concentration. (c) Uncoupled and mixed corrosion potential; (d) Uncoupled and mixed corrosion current density. Month=1, Bar diameter = 20 mm, Bar spacing = 200 mm, Cover = 50 mm, Relative Humidity = 90%.

This observation has significant consequences for corrosion modeling in reinforced concrete as the concentration of species within the electrolyte and the effects these concentrations have on solution conductivity has been ignored in the reported models. As demonstrated by the results

of this simulation, electrolyte composition affects the quantity of current flow passing through the electrolyte, the neglect of which results in a potential underestimation of the total corrosion current density. Therefore, the adoption of Equation 2.36 in the current model represents a significant improvement for simulating corrosion current through the electrolyte.

Additionally, current passing through the pore solution increases the rate of localized section loss on the bar surface with a corresponding buildup of Fe^{2+} at the anodic locations and OH^- at the cathodic locations. In the case of the anodic reaction, the production of Fe^{2+} causes the local pore solution to become more acidic due to the creation of $Fe(OH)_2$, which is initially offset by hydrated cement dissolving into the pore solution. However, two mechanisms will be present that will ultimately cause the local pH to be reduced. These are:

1. $Fe(OH)_2$ precipitates from the pore solution, which results in the pore system being filled with $Fe(OH)_2$. As the pore system is filled, the ability of the system to replenish OH^- that is consumed in the corrosion process becomes limited; and

2. The dissolution of hardened cement to balance the removal of OH^- will reach a limiting condition similar to that experienced when carbonation occurs. Once this limiting condition is reached, the local environment will become acidified in relation to the remainder of the concrete, causing a shift in the thermodynamics and kinetics of corrosion.

Models for macro cell corrosion simulations assume coupling occurs between layers of reinforcing steel or along a bar which passes between repaired to unrepaired concrete (Maruya et al. (2007)). Therefore, circumferential corrosion coupling has been largely ignored in the current models. The model developed herein, however, allows cathodic and anodic zones to be identified based on corrosion potential differences and conductivity of the electrolyte on the bar/concrete interface. This improvement to the simulation demonstrates that when circumferential coupling occurs, the portion of bar supporting the cathodic site is smaller than that at the anodic site and the combined cathodic and anodic sites is smaller than the bar circumference. This result is consistent with field observations identified in Figures 1.1 and 5.4

which show corrosion by-product buildup present on the bar face closest to the barrier face with limited or non-existent corrosion by-product on the surfaces further away.

Therefore, allowing cathodic and anodic sites to form based on the corrosion potential differences and electrolyte concentrations represents an improvement over the current modeling which ignores circumferential coupling by setting the relative areas of cathode and anode. This improvement suggests that, when longitudinal coupling is present on a bar, the coupling distance will be limited to approximately the bar circumference.

However, this result will be affected if changes to the pore solution pH are incorporated. Under this scenario, when the pH is reduced, the electrochemistry will change, resulting in an increase in the total corrosion current and further corrosion potential changes. The increase in corrosion potential differences will then increase the distance that coupling will occur along the bar length. This scenario is addressed in subsequent sections.

Based on this initial assessment, the model developed as part of this research has demonstrated:

- Assuming constant conductivity for the concrete obscures the effect chloride has on the conductivity of the pore solution and how increased conductivity increases the corrosion current density within the affected area; and

- Macro-cell corrosion where anodic and cathodic processes on the bar surface become separated will be balanced within the bar circumference or along the bar length within a distance similar to the bar circumference. This observation suggests that macro-cell corrosion between layers of reinforcing steel or along the length of a bar that transitions between repaired and unrepaired areas will either not occur or be limited to the length of the bar circumference.

5.3 Surface Corrosion Potentials versus Bar/Concrete Corrosion

Corrosion potentials measured on the concrete surface are commonly recorded for monitoring the condition of a reinforced concrete element. The industry's belief is that regular monitoring of these values provide a strong indication of corrosion occurring at the bar/concrete interface and, as such, provide a powerful predictive tool for scheduling interventions (Alberta Transportation Technical Standards Branch 2007).

Mixed corrosion potentials on the bar/concrete interface generated from the simulation described previously were projected to the concrete surface using the model geometry identified in Figure 3.3 and the following relationship (Warkus and Raupach 2008, Isgor and Razaqpur 2005):

$$\nabla\Phi = 0 \qquad \text{Eq 5.1}$$

where Φ is the corrosion potential in V.

Table 5.5 reports the simulated corrosion potential values at the concrete surface and bar/concrete interface for each of the four stages identified in Section 5.2. For each case, corrosion potentials at the concrete surface are relatively uniform across the width of the section even when wide variations in corrosion potential are present on the bar/concrete interface. Additionally, average corrosion potentials on the concrete surface are nearly identical to the average corrosion potential on the bar surface under each stage considered. Therefore, averages measured at the concrete surface appear to provide a reasonable approximation of the average corrosion potential on the bar/concrete interface. However, these averages do not identify corrosion potential variations that occur on the bar/concrete interface which create an increase in the corrosion current density due to coupling around the bar perimeter.

Table 5.6 compares simulated average uncoupled ($i_{uncoupled}$) and coupled ($i_{coupled}$) corrosion current densities on the bar/concrete interface to the average corrosion potentials (e_{corr_s} (V versus CSE)) on the concrete surface. This table indicates that $i_{uncoupled}$ increases as corrosion potentials at the concrete surface become more negative until Stage 4 is reached, at which point the average uncoupled, anodic, and coupled corrosion current densities decrease due to oxygen limitations around the bar circumference. This result is related to coupling, which is maximized when the bar circumference is partially exposed to chlorides and the corrosion potential differences around the bar circumference are at a maximum, thereby producing the

Table 5.5. Surface Corrosion versus Bar/Concrete Interface Corrosion Potential

Stage	Concrete Surface (V vs CSE)			Bar/Concrete Interface (V vs CSE)		
	Maximum	Minimum	Average	Maximum	Minimum	Average
1	-0.133	-0.133	-0.133	-0.133	-0.133	-0.133
2	-0.177	-0.181	-0.179	-0.157	-0.196	-0.182
3	-0.294	-0.295	-0.294	-0.184	-0.367	-0.296
4	-0.438	-0.438	-0.438	-0.437	-0.440	-0.438

largest driving force for current flow through the pore solution.

Surface corrosion potentials are normally the main information collected from a bridge evaluation study and are then compared to industry recommendations outlined in references such as ASTM C876-09 or Alberta Transportations (AT) Bridge Inspection and Maintenance System – Level 2 Inspection Manual. Table 5.7 compares results from this simulation to these industry standards.

Using either of the ASTM or Alberta standard, corrosion likely does not occur until Stage 4 is reached. However, the simulation identified Stage 3 as generating the most corrosion current density, while Stage 4 showed a reduction in corrosion current density due to oxygen limitations created when the entire bar circumference is exposed to chloride. This simulation result would suggest that under the kinetics of corrosion assumed for this model, concrete surface corrosion potentials, which indicate a high probability of corrosion, cannot be reached. However, these

Table 5.6. Surface corrosion potentials and bar/concrete interface corrosion current density.

Stage/Cell	Average e_{corrs} (V vs CSE)	$I_{uncoupled}$ 10^{-9} (A/mm^2)	i_{anode} 10^{-9} (A/mm^2)	$i_{coupled}$ 10^{-9} (A/mm^2)
1	-0.1332	4.8482	0.0002	4.8484
2	-0.1788	4.2292	0.0374	4.2666
3 - Cell 1	-0.2940	5.4541	1.1296	6.5836
3 - Cell 2	-0.2940	2.9236	0.1497	3.0733
4	-0.4381	3.0403	0.0175	3.0578

Table 5.7. Comparison of simulated surface corrosion potentials with ASTM and Alberta Transportation interpretations.

Stage	Corrosion Potential Simulation Results (V vs CSE)	Corrosion Current Density (A/mm^2)	ASTM[1]	Albert Transportation [2]
1	-0.133	4.85×10^{-9}	No Corrosion	Inactive
2	-0.181	4.31×10^{-9}	No Corrosion	Inactive
3	-0.295	7.38×10^{-9}	Uncertain	Inactive
4	-0.438	6.03×10^{-9}	Corrosion	Active

Notes:
1. ASTM C876 Interpretation:
   More Positive than -0.200 V = Greater than 90% probability no corrosion occurring
   -0.201 V to -0.350 V = Corrosion activity is uncertain
   More Negative than -0.351 V = Greater than 90% probability corrosion is occurring
2. Alberta Transportation Interpretation:
   0.000 V to -0.300 V = Inactive (very low probability of active corrosion)
   -0.301 V to -0.400 V = Transition (good probability that corrosion is initiating)
   -0.401 V to -0.800 V = Active (very high probability of active corrosion).

corrosion potentials are commonly recorded in the field. Therefore, the kinetics of corrosion employed in this simulation must transition from high to lower pH values as discussed in Section 5.2.2. This transition is required to produce the high negative corrosion potential values associated with a high probability of corrosion.

However, the current model does not simulate the transition that occurs on the bar/concrete interface when coupling creates local acidification of the electrolyte. This aspect of the corrosion process will change the kinetics of corrosion in the affected area, which will produce larger corrosion current densities and more negative corrosion potentials as oxygen limitations are created due to the diffusion barriers developed by excess production of Fe^{2+} forming $Fe(OH)_2$. This aspect of the model is discussed in Section 5.5.

5.4 Geometry and Humidity Influence on the Bar/Concrete Interface Electrochemistry

The preceding sections presented results obtained from a single simulation that described corrosion potentials and corrosion current densities on the bar/concrete interface as oxygen and chloride concentrations change around a reinforcing bar. The purpose of this discussion was to present the relationship between kinetics of corrosion and thermodynamics on the electrochemistry occurring on the bar/concrete interface and how corrosion potentials produced on the bar surface were related to the concrete surface.

Within this section, system geometry as it relates to cover, bar diameter, and bar spacing, combined with relative humidity, are varied to determine the influence these parameters have on the corrosion processes on the bar/concrete interface. The base system considered, after which selected parameters are varied, assumes the following geometry and humidity which represent a typical bridge deck where ponding regularly occurs:

- Cover = 50 mm;
- Bar Diameter = 20 mm;
- Centre to Centre Bar Spacing = 200 mm; and
- Relative Humidity = 90%.

Results are reported at the four stages discussed previously using the following criteria:

- Stage 1 – Initial conditions representing a chloride free, but fully oxygenated pore solution;
- Stage 2 – Steady state condition representing the mid-way point between Stage 1 and Stage 3;
- Stage 3 – Chloride is present and has caused maximization of the corrosion current through the electrolyte; and
- Stage 4 – Chlorides have reached concentrations at all points on the bar/concrete interface beyond which there are no further changes in the kinetics of corrosion.

5.4.1 Bar Diameter

Nominal bar diameters considered ranged from 15 mm to 30 mm in increments of 5 mm as this covered the majority of bar diameters used in construction on most bridge decks. For the purpose of this study, bars were assumed to be smooth, so irregularities introduced by bar deformations were not considered. Figure 5.9 presents results from the numerical simulation for the concrete surface corrosion potentials and corrosion current density on the bar/concrete interface for each of the bar diameters considered.

The simulated concrete surface corrosion potentials identified in Figure 5.9(a) were recorded for each stage previously identified and discussed in Section 5.2. The trend for Stage 1, 2, and 4 indicate a decrease in corrosion potential with increasing diameter. This result is expected given that larger bars create a larger bar/concrete interface where the cathodic reactions extract oxygen from the electrolyte. With the rate of oxygen transport to this interface restricted by the concrete cover, the total oxygen concentration within the electrolyte decreases with increasing bar diameter producing a decrease in the reversible corrosion potential as predicted by the Nernst Equations. This lowered reversible corrosion potential then causes the mixed corrosion potential on the bar/concrete interface to become lower with increasing bar diameter.

For Stage 3, corrosion potentials on the concrete surface decrease over the range of bar diameters. However, the corrosion potential for the 25 mm bar is lower than the 30 mm bar. This result is likely caused by error minimization routines failing to converge to a global minimum for both the 25 and 30 mm bar. This convergence problem within the simulation was observed for any model geometry or humidity that created:

- Large uncoupled corrosion potential differences which normally occurred during Stage 3; and

- When oxygen concentrations within the electrolyte reached a limiting condition on portions of the bar/concrete interface.

This difficult in reaching a global minimization was related to the algorithm where changes to the corrosion current density were implemented to match the oxygen consumption rate on the bar/concrete interface with the mass transport of oxygen. As noted in Section 4.5, a high degree of difficulty was encountered with this aspect of the simulation and that during the model development several assumptions were adopted to balance computational effort with

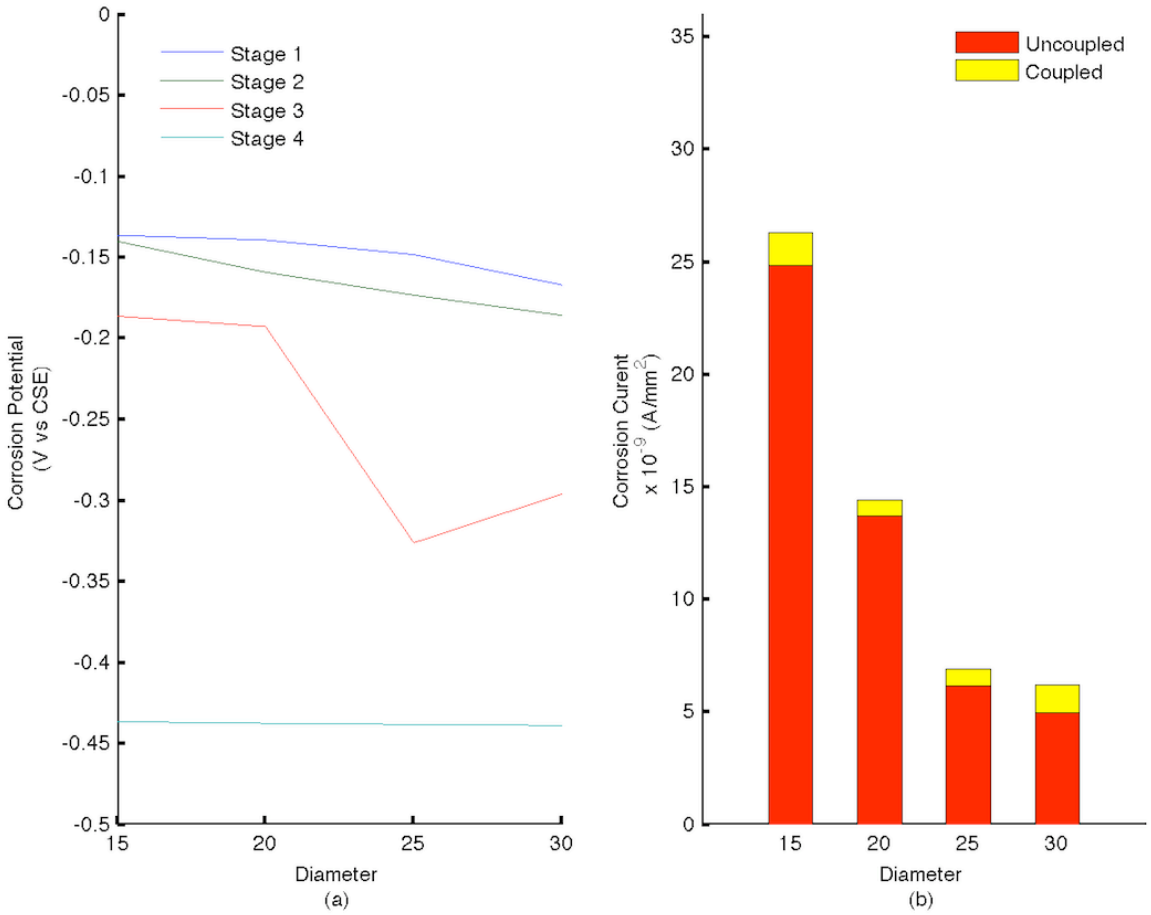

Figure 5.8. Corrosion potential on the concrete surface and corrosion currents on the bar/concrete interface versus bar diameter for Cover = 50 mm, Bar Spacing = 200 mm, Relative Humidity = 90%. Contours set at 0.01 V increments: (a) Corrosion potential on the concrete surface versus bar diameter for Stages 1 through 4, (b) Maximum average corrosion current on the bar/concrete interface for each diameter at Stage 3.

convergence.

Figure 5.9(b) presents the average simulated corrosion current density for Stage 3 as this stage represents the condition where the largest coupled corrosion currents are generated on the bar/concrete interface. Contributions from uncoupled and coupled corrosion current densities are identified with the uncoupled corrosion current density representing the largest component of the total corrosion current. The pattern of combined coupled and uncoupled corrosion current is similar to the corrosion potentials identified in Figure 5.9(a), with the total corrosion current under coupled conditions decreasing with increased bar diameter. This result is related to oxygen levels in the electrolyte being reduced, as the contact area between the bar and concrete increases, for the cathodic consumption of oxygen. As oxygen levels and resulting corrosion potentials are reduced, the uncoupled corrosion current is also reduced to comply with the kinetics of corrosion for the electrolyte chemistry. However, as the bar diameter increases, the coupled corrosion current remains relatively constant, which is a result of the corrosion potential differences on the bar/concrete interface remaining similar across the bar diameters considered.

The general outcome of this assessment suggests increases in bar diameter cause a reduction of the concrete surface corrosion potential. Corresponding with the decrease in corrosion potential is a lowering of the total corrosion current. However, the amount of coupled corrosion current is relatively constant for the reinforcing bar sizes considered. This observation suggests that field results obtained using ASTM C876-09 or Alberta Transportations Bridge Inspection and Maintenance System – Level 2 Inspection Manual for corrosion potential readings should include a correction factor to account for the lowering of corrosion potential with increased bar diameter.

5.4.2 Concrete Cover

Concrete cover depths considered ranged from 10 mm to 90 mm in increments of 10 mm. The low end was chosen as older structures were often constructed with minimal covers, and with construction tolerances resulting in bars being placed near the concrete surface. The high range of covers was chosen as current design standards and jurisdictional requirements are directing designers to employ larger covers to delay the diffusion of chloride to the bar surface. Figure 5.10 presents results from the numerical simulation for the concrete surface corrosion potentials and the corrosion current density on the bar/concrete interface for each of the concrete covers considered.

Figure 5.10(a) shows the concrete surface corrosion potentials at four stages versus the concrete cover depth. Concrete surface corrosion potentials decrease with cover, for Stages 1, 2, and 4, which is a result of restrictions to oxygen transport to the bar/concrete interface induced by the concrete cover, and the resulting corrosion potential drop as predicted by the Nernst Equations. However, this linear reduction in corrosion potential with increasing concrete cover is not evident when Stage 3 is considered. At this stage, the change in corrosion potential versus cover thickness results in the following observations:

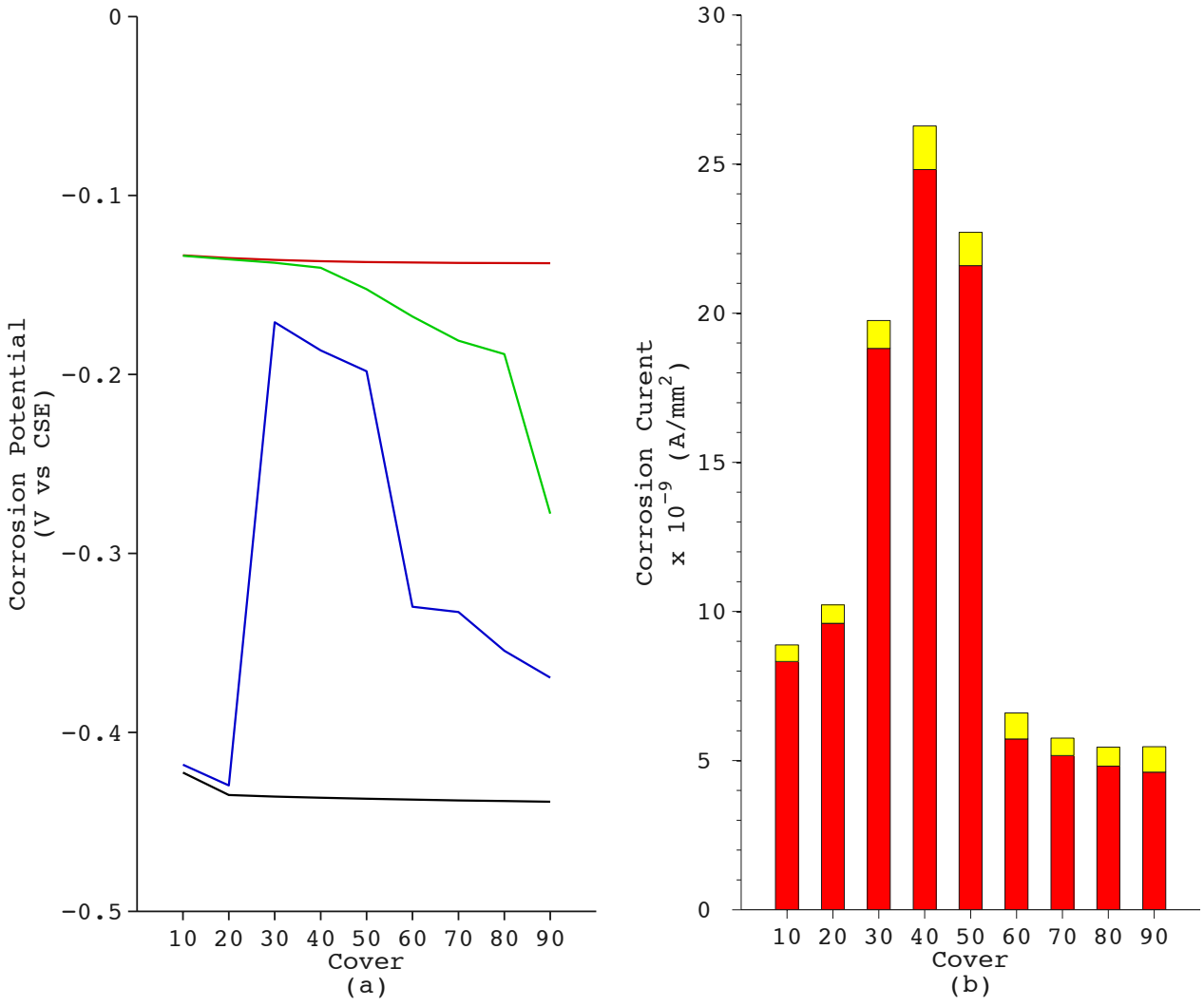

Figure 5.9. Corrosion potential on the concrete surface and corrosion currents on the bar/concrete interface versus concrete cover for Bar Spacing = 200 mm, Bar Diameter = 20 mm, Relative Humidity = 90%. Contours set at 0.01 V increments: (a) Corrosion potential on the concrete surface versus bar diameter for Stages 1 through 4, (b) Maximum average corrosion current on the bar/concrete interface for each cover at Stage 3.

- For concrete covers equal to 10 and 20 mm, the simulated corrosion potentials are similar to the corrosion potentials produced under Stage 4; and

- At 30 mm concrete cover, the corrosion potential increases to near the Stage 2 corrosion potential value and then decreases as concrete covers increase.

Figure 5.10(b) shows a similar pattern for the average uncoupled and coupled corrosion currents for Stage 3 for each cover considered. Similarities between Figures 5.10(a) and 5.10(b) are caused by corrosion potentials being related to corrosion current densities as high corrosion potentials produce high uncoupled corrosion current densities, while low corrosion potentials create low-uncoupled corrosion current densities.

Under Stage 3, the response of the simulated corrosion potential and corrosion current density with increasing cover are related to mass transport of chloride and oxygen. For values of concrete covers less than 20 mm, chloride concentrations around the bar circumference reach the entire bar surface relatively quickly and uniformly. As well, oxygen transport to the bar/concrete interface is not restricted to the same extent as with larger covers. Therefore, as corrosion and oxygen consumption rates increase with the presence of chloride, oxygen concentrations on the bar/concrete interface quickly replenish, minimizing corrosion potential differences and corrosion current flow through the electrolyte.

However once, the concrete cover increases to 30 mm, mass transport through the cover introduce gradients around the bar circumference with:

- Chlorides becoming concentrated on the bar surface closest to the concrete surface which causes the corrosion rate to increase as predicted by the kinetics of corrosion for this system; and

- Oxygen concentrations within the electrolyte begin to decrease with increasing corrosion rates caused by the chlorides.

These gradients in chloride and oxygen at the bar/concrete interface create the corrosion potential differences that increase the corrosion current density through the electrolyte which, at 30 mm of concrete cover, occur at higher average concrete surface corrosion potentials. However, as the cover increases beyond 30 mm, the concentration gradients caused by the

cover become less pronounced, which results in maximum-coupled corrosion currents occurring at more negative concrete surface corrosion potentials.

These results are consistent with the kinetics of corrosion; however, they identify an issue with the interpretations employed in standards for corrosion potential testing. These standards (ASTM C876-09 and Alberta Transportation – Bridge Inspection and Maintenance System – Level 2 Inspection Manual) do not adjust corrosion potential readings measured on the concrete surface as a function of cover. Measured potentials values may therefore provide misleading results related to the probability of corrosion occurring on the bar/concrete interface.

5.4.3 Bar Spacing

Bar spacing considered in the simulation ranged from 50 mm to 200 mm with increments of 50 mm. These spacings were selected to represent typical locations on a bridge deck and locations where bars are spliced, added for capacity reasons, or where features such as barriers and expansion joints are attached with doweled reinforcement.

Figure 5.10 presents the results from the simulations for corrosion potentials at each stage identified, along with the maximum average coupled corrosion current and corresponding uncoupled corrosion current for Stage 3. Figure 5.10(a) indicates simulated corrosion potentials are more negative for Stages 1, 2, and 3 at 50 mm spacing when compared to larger spacings, while corrosion potentials for Stage 4 remain relatively constant for all spacings. Stage 1, 2, and 3 results are produced by the corrosion current generated on the bar circumference consuming oxygen from the electrolyte faster than it can be replaced through mass transport from the exposed concrete surface. This mass transport limit causes oxygen concentrations within the electrolyte to decrease, which reduces the reversible corrosion potential and corrosion potential. This effect on the mass transport of oxygen is effectively eliminated when the centre-to-centre bar spacing increases to 100 mm or larger.

Figure 5.10(b) similarly shows the maximum average coupled corrosion current present on the bar/concrete interface. Once the bar spacing is equal to 100 mm or greater, there appears to be no effect on the corrosion current with bar spacing. However, at the 50 mm spacing, there is a noticeable decrease in the total corrosion current. Coupled corrosion current appears to be relatively constant across the entire bar range of spacings considered with a slight increase at the 200 mm spacing. This slight increase at the highest spacing considered may be a reflection of the search routines employed within the simulation failing to minimize.

From a field corrosion-testing standpoint, the effect of bar spacing on corrosion potentials has a significant impact on the results observed in the field. Field results often indicate areas adjacent to expansion joints and barriers as having more negative results than the remaining areas. This has, often times, been attributed to a failure in the protection systems at these locations or the presence of moisture, particularly in the case of the barrier/bridge deck interface. Therefore, similar to concrete cover and bar diameter, adjustment factors are necessary for corrosion potential readings where bar spacing is less than 100 mm centre-to-centre, which would be typically at locations near expansion joints, barriers, or in negative moment regions where additional reinforcement is required for structural reasons.

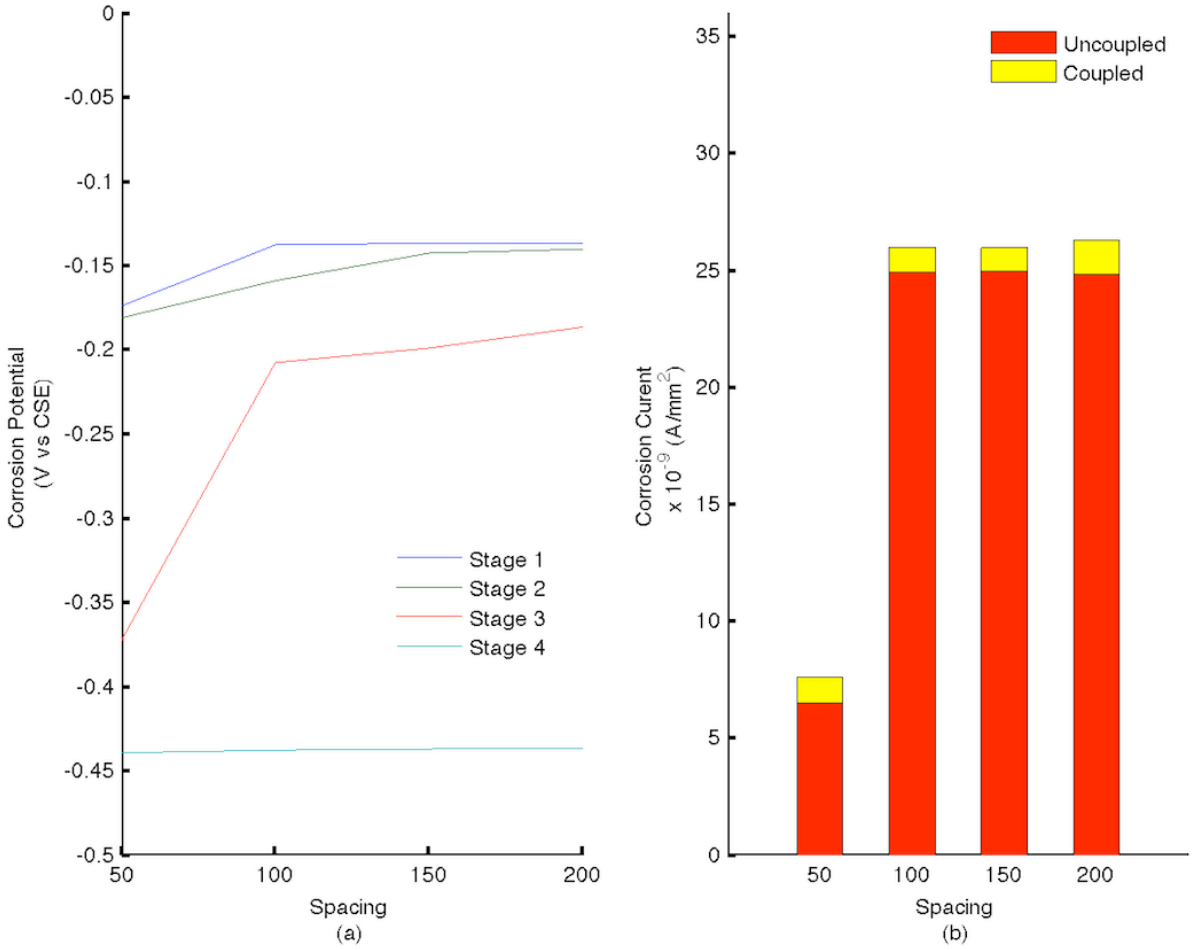

Figure 5.10. Corrosion potential on the concrete surface and corrosion currents on the bar/concrete interface versus bar spacing for Bar Cover = 50 mm, Bar Diameter = 20 mm, Relative Humidity = 90%. Contours set at 0.01 V increments: (a) Corrosion potential on the concrete surface versus bar diameter for Stages 1 through 4, (b) Maximum average corrosion current on the bar/concrete interface for each spacing at Stage 3.

5.4.4 Relative Humidity

Moisture conditions within the concrete were varied by changing the relative humidity from 50% to 90% with increments of 10%. This range was selected as it best represented the potential range of relative humidity present in the field without considering the fully saturated condition. The fully saturated condition was not evaluated as it is rarely observed on a bridge deck, and when it does occur, is generally present only for the duration of the rain event. Figure 5.11 presents the simulation results under the range of the selected relative humidities for corrosion potential under the stages considered and the maximum average coupled corrosion current calculated for Stage 3 which represents the conditions under which corrosion potential differences are maximized around the bar circumference.

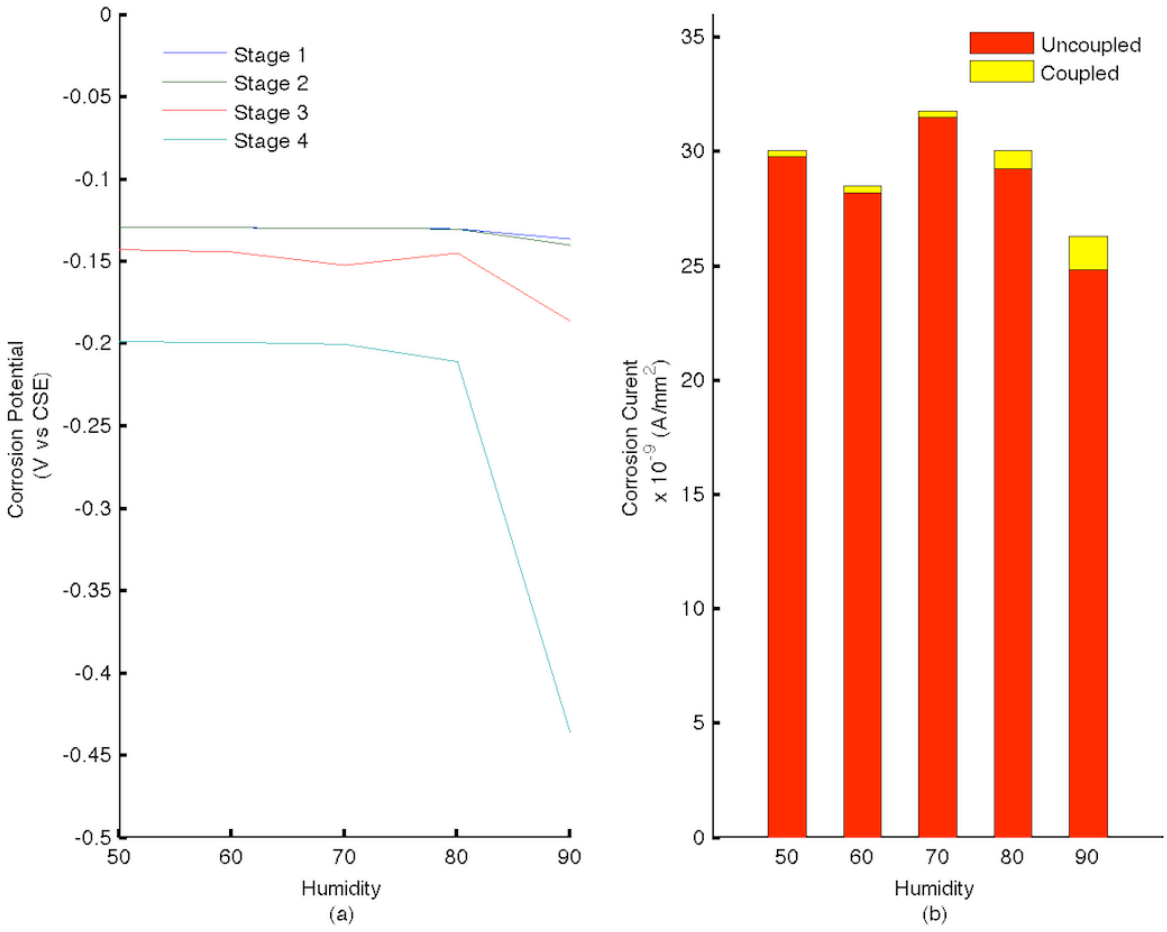

Figure 5.11. Corrosion potential on the concrete surface and corrosion currents on the bar/concrete interface versus relative humidity for Bar Cover = 50 mm, Bar Diameter = 20 mm, Bar Spacing = 200 mm. Contours set at 0.01 V increments: (a) Corrosion potential on the concrete surface versus bar diameter for Stages 1 through 4, (b) Maximum average corrosion

current on the bar/concrete interface for each relative humidity at Stage 3.
Figure 5.11(a) presents the corrosion potentials versus relative humidity for each of the four stages previously described. For relative humidity values between 50% and 80%, the corrosion potentials on the concrete surface at each stage remain relatively constant. However, beyond 80% relative humidity, corrosion potentials decrease slightly for Stages 1 and 2, by a larger amount for Stage 3, and decrease significantly for Stage 4. These results are consistent with moisture conditions at 90% relative humidity limiting the transfer of oxygen to the bar/concrete interface, so causing a decrease in the oxygen concentrations with a corresponding decrease in the corrosion potential.

Figure 5.11(b) presents the maximum average coupled corrosion current and the corresponding uncoupled corrosion current present under Stage 3 for each of the relative humidity levels investigated. While there is some variation in the uncoupled corrosion current density as the relative humidity increases, the value remains relatively constant between 50 and 80%. At 90%, the uncoupled corrosion current density begins to decrease due to limits imposed with oxygen transport to the bar/concrete interface. The coupled corrosion current flowing through the electrolyte is relatively small for values of relative humidities between 50 and 70%, a result related to the low conductivity of the solution that restricts the flow of ions through the electrolyte. However, once the relative humidity of 80% is reached, there is an increase in the coupled corrosion current, which increases when the relative humidity reaches 90%. This increase in coupled corrosion current is consistent with the increased moisture content creating a more conductive solution for current to flow within.

Another observation from this comparison is related to the maximum negative corrosion potential that was simulated using the kinetics of corrosion. Until the 90% relative humidity level was reached, the most negative corrosion potential at the concrete surface was approximately equal to -200 mV. This value would suggest a low probability that corrosion is present, in accordance with ASTM C876-09 or Alberta Transportation Bridge Inspection and Maintenance System – Level 2 Inspection Manual. Therefore, a second mechanism must be present to create negative potentials in the ranges observed in the field. This second mechanism is likely related to the acidification of the bar/concrete interface where coupled current is generated which is discussed in the following section.

5.5 Kinetic Modifications

The current model is based on kinetics of corrosion for a reinforcing steel bar in a 12.5 pH environment. At early stages of the model development, simulations attempted to address the change in local chemistry caused by the production of Fe^{2+} and OH^- in separate locations on the bar circumference. These initial attempts assumed all Fe^{2+} produced would consume the local OH^-, which would then be restored by diffusion of OH^- from the surrounding environment. Using these assumptions, results from the simulation produced highly acidic regions on the bar/concrete interface prior to when chlorides had reached this surface. This result was inconsistent with values recorded in the field that indicate this type of corrosion only occurs when chlorides are present.

The effect of acidification of the pore solution can be modeled by assuming that the local pH would change after chlorides reach the bar and attain a certain concentration. This change in local pH, while driven by the creation of Fe^{2+} and the consumption of OH^- in the formation of $Fe(OH)_2$, produces a similar result to that produced by carbonation. Therefore, kinetics of corrosion data developed for simulated carbonated concrete pore solutions could be applied to simulate the effect on coupling that this change in environment would create. However, when implemented in the current model, the immediate change in pH along a portion of the bar circumference created instabilities in the solution algorithms employed, creating results that were inconsistent with known behavior.

These inaccuracies were related to the algorithms developed for balancing the oxygen consumption rate with the mass transport of oxygen to the bar/concrete interface. Originally, these algorithms were developed and tested for the kinetics of corrosion expected for a pH of 12.5. When the lower pH of 9 was implemented, the kinetics of corrosion related to this environment produced corrosion potentials and current densities that were outside of the range previously used for validation. Initially, it was expected that the search algorithm should be able to handle the different range in kinetics. However, the difficulty observed in resolving the new kinetic information was not surprising given the difficulty encountered in the original development of the algorithm for the higher pH.

Therefore, the model with the current search algorithm could not be used to explore the effect that lower pH would have on the corrosion potential and current density. However, observations can still be made related to the expected localized pH and the chloride concentration necessary to produce damaging corrosion rates as follows:

- Use of the kinetics of corrosion for a carbonated concrete from published data produce corrosion potentials more negative than identified in ASTM C876-09. This would suggest the change in pH expected within the anodic zone on the bar/concrete interface will be somewhere between a carbonated and non-carbonated concrete; and

- A reduction in pH will occur when coupling on the bar/concrete interface allows excess Fe^{2+} to be produced at specific locations, thereby creating the necessary conditions for the consumption of OH^-. The magnitude of coupling, and the corresponding rate at which pH will be reduced, is related to the corrosion potential differences on the bar surface which, in turn, is a function of the pore solution chemistry, kinetics of corrosion, and oxygen mass transport.

This last observation has significant implications related to service life prediction for a reinforced concrete element. Many practitioners and researchers have assumed that a set chloride concentration is required before corrosion can initiate within a reinforced concrete element. The results of the simulations employed herein have identified that low levels of corrosion are present at all times which only cause a reduction in pH when coupling occurs around the bar circumference. This coupling occurs when corrosion potential differences are present which can occur due to a combination of factors, one of which is chloride concentrations. The other factors include OH^- concentrations and the ability of the hydrated cement paste to replenish OH^- in the pore solution, kinetics of corrosion which are tied to the pore solution chemistry, and oxygen transport which is a function of the bar spacing, bar diameter, cover, and moisture conditions within the concrete.

The practical significance of this observation obtained from the simulations is that basing the timing of a maintenance or rehabilitation plan on a single value of chloride concentration within the concrete will produce inaccurate results and increased costs due to either implementing repairs before they are necessary or missing the optimum timing for repair. As well, the methodology used in the development of this simulation can be adapted to include features to address the consumption of OH^- and the evolution of the pore solution chemistry with time which will result in improvements to for service life modeling and scheduling rehabilitations.

5.6 Discussion

The preceding simulations indicate that corrosion potentials on the concrete surface are not sufficiently sensitive to identify variations in corrosion potentials on the bar/concrete interface or

identify absolute values of corrosion current density. However, the simulations demonstrate corrosion coupling is possible around the bar perimeter and that coupling between the cathodic and anodic zones occurs within one-half of the bar circumference. This result suggests that coupling on the bar surface either circumferentially or longitudinally will also be confined to a distance equal to one-half the bar circumference. Therefore, coupling over longer distances will not occur as ohmic potential drops through the electrolyte combined with the available corrosion potential differences will prevent this current flow from occurring.

Also, corrosion potentials at the concrete surface produced by the simulation did not reach the values identified in ASTM C876-09 unless the simulation was completed under a high relative humidity with chloride reaching all points on the bar circumference in sufficient concentrations to affect the kinetics. Similar conclusions have been identified for models that simulate the transport of oxygen to the corroding surface (Huet et al. 2007, Pour-Ghaz et al. 2009) which indicate concrete cover does not cause oxygen limitations and the resulting high negative corrosion potentials unless moisture conditions are greater than 90% relative humidity. These observations would suggest that relative humidity conditions in concrete in the field must then be greater than 90% in order for corrosion potentials to reach similar values to those identified in the relevant testing standards. However, Andrade et al. (2003) described how the internal relative humidity of concrete decreases from fully saturated at casting, transitioning to the relative humidity of the external environment over time. Therefore, using climatic data for North American, the expected concrete relative humidity for bridge structures will vary between 10% and 90% with lower values predominant in desert regions and higher values in coastal regions (National Climate Data and Information Archive, National Climatic Data Centre).

Combining this climatic data with observations from the literature and simulations completed herein suggest field recorded values in the ranges identified in the corrosion potential standards should not be occurring. However, these values are commonly observed and have been correlated to corrosion occurring in a reinforced concrete element (ASTM C876-09). Therefore, it is expected that a secondary mechanism must be present to cause portions of the concrete in contact with the bar circumference to become acidified in order for the kinetics of corrosion to produce negative corrosion potentials in the ranges identified in the relevant corrosion testing standards. From the simulations completed as part of this work, it was noted that this change in pH would fall between a pH of 12.5 and a fully carbonated concrete with a pH of 9. This observation has significant implications to the development of maintenance plans for reinforced concrete structures exposed to chloride, as current practice has been to identify a chloride

threshold value above which corrosion is expected to be present. This research has confirmed that a single chloride threshold value does not exist. Rather, chloride levels and the chemistry of the pore solution combined with concrete cover, bar spacing, bar diameter, and relative humidity will dictate the duration between when chlorides first reach the reinforcement and when damaging levels of corrosion by-product will be produced.

In addition to this secondary mechanism, the author has observed situations where low negative corrosion potentials are recorded without a corresponding buildup of corrosion by product on the bar surface once the concrete had been removed to expose the reinforcement. In these situations, conditions related to excessive concrete cover (greater than 100 mm) or supplementary protection systems such as epoxy coated reinforcement or asphalt based membranes have been present which appear to influence the corrosion potentials recorded on the concrete surface. Using the observations derived from the research completed herein, these field situations of high negative corrosion potentials without corresponding corrosion by-product on the bar/concrete interface is related to:

- Diffusion barriers in the form of the concrete cover or asphalt membrane which restrict the movement of oxygen to the bar/concrete interface causing the kinetics of corrosion to shift towards a oxygen limited condition; and

- Localized breakdown (holidays) in the epoxy coated surface becoming coupled with the surrounding coated bar,causing the area with the disturbed coating to consume the available oxygen in the pore solution, following which mass transport limitations result in an oxygen limit being reached.

The first issue related to diffusion barriers has been identified in field evaluations conducted on polymer modified asphalt (PMA) protected bridge decks that have similar characteristics to asphalt membrane systems. Carter and Hamilton (2007) reviewed corrosion potential data from four sites in the City of Calgary by performing corrosion potential tests on the surface of the PMA following which tests were repeated with the PMA removed or penetrated to provide a direct electrical contact between the reference half cell and the concrete deck. Results from this study recommended an adjustment factor for increasing surface recorded corrosion potential values by 150 mV for new PMA, which decreased to a value of 0 for failed PMA. This recommendation by Carter and Hamilton (2007) is expected given the properties of the PMA and the results of the simulations completed herein which link increased cover (asphalt and

concrete) with reaching corrosion limitations due to oxygen transport to the embedded reinforcement.

5.7 Summary

The results of the simulation presented in previous sections were identified and discussed. The simulation indicates that coupling is possible around the bar circumference due to variations in the pore solution chemistry induced by chloride and oxygen concentrations. As well, the simulation suggested that a secondary mechanism must be present within the corrosion cell. This mechanism causes the localized regions of negative corrosion potential to become acidified in order for the kinetics of corrosion to produce the concrete surface corrosion potentials identified in ASTM C876-09 that indicate a high probability of corrosion.

Additionally, the model has identified that specifying a single chloride concentration above which corrosion will initiate does not address the influence of concrete cover, bar spacing, bar diameter, relative humidity, and electrolyte on the corrosion process. However, the mechanistic model developed in this research can be used to simulate the corrosion processes on a bar embedded in concrete to identify the effect each variable has on the corrosion process and when corrosion will reach a stage where damaging levels of corrosion by-product are produced. This model provides the potential to improve the accuracy of service life prediction, which will lower the cost of maintenance and rehabilitation as work can now be optimized to the condition of the element.

6 SUMMARY AND CONCLUSIONS

6.1 Summary

This thesis investigated corrosion of a reinforcing steel bar embedded in concrete and the effect of corrosion coupling on the bar/concrete interface induced by the variation of corrosion potentials with concrete depth. Two separate models were used which included:

- A two-dimensional finite element model, which simulated oxygen and chloride transport to the bar/concrete interface; and
- A one-dimensional model which simulated the current flow induced by the corrosion process occurring on the bar/concrete interface.

For each time step considered, the kinetics of corrosion on the bar/concrete interface were adjusted to align with the chloride and oxygen concentrations within the pore solution in order that the fundamentals of corrosion and mass conservation were satisfied. Once corrosion potentials on the bar/concrete interface were established, the potential for coupling was evaluated using a novel approach to corrosion modeling in reinforced concrete that had not been identified in the literature. This new approach, incorporated:

- A variable solution conductivity that was developed based on concentrations within the pore solution for each discretized segment on the bar/concrete interface;
- Establishing the size of the anode and cathode within the corrosion cell by varying the size of the anodic and cathodic regions until a maximum coupled corrosion current was produced; and
- The ability to modify the kinetics of corrosion based on the pore solution chemistry. This more accurately reflects the mechanism occurring in practice where a pitting corrosion cell is formed in areas where active corrosion is present.

6.2 Conclusions

Several conclusions can be reached from this work which are related to:

- The formation of corrosion cells on the bar/concrete interface;

- Spatial separation of cathodic and anodic zones on the bar/concrete interface;
- The influence of bar spacing, bar diameter, concrete cover, and moisture conditions on the corrosion occurring on the bar/concrete interface and the corresponding corrosion potential measured on the concrete surface; and
- Localized acidification of the electrolyte.

6.2.1 Corrosion Cell Formation

By simulating the transport of chloride and oxygen to the bar/concrete interface in the two-dimensional model selected for this research, variable concentrations of chloride and oxygen were produced. These variable concentrations were related to the kinetics of corrosion for a concrete pH of 12.4, which resulted in the production of a variable corrosion potential, and corrosion current density around the bar. The effect of chloride concentrations and oxygen concentrations were shown to independently influence corrosion potentials at moisture conditions where the relative humidity was less than 90%. This was an unexpected result given that observations published in current literature stated variations due to oxygen limitations were not present unless moisture conditions were close to a saturated condition. The end conclusion of this aspect of the research was the confirmation that circumferential variations of oxygen and chloride concentrations produce variations in corrosion potential and corrosion current density around the bar circumference.

6.2.2 Spatial Separation of Cathode and Anode

Circumferential variations in corrosion potentials produce the driving force necessary for cathodic and anodic processes on the bar/concrete interface to be accelerated, thereby creating current flow through the connecting electrolyte. Previous research related to this phenomenon, had assumed separation of the anodic and cathodic regions would consume the entire bar circumference, thereby forcing separation of these cells to occur on the longitudinal axis of the reinforcing steel bar. Simulations conducted herein indicated that current flow from the anodic region was balanced by the corresponding cathodic reaction within one-half of the bar circumference. This result suggests that, under the corrosion potential differences simulated, combined with the pore solution conductivity, coupling along the bar axis would be limited to approximately one-half the bar circumference as well. Coupling over longer distances would be prevented, as ohmic potential drops through the pore solution would require larger corrosion potential differences than are generally possible from the kinetics of corrosion. This result is

consistent with previous studies, which evaluated the relative contribution of macro-cell and micro-cell corrosion on the total corrosion occurring for a reinforcing steel bar embedded in concrete exposed to chloride. In these studies measuring techniques consistently underestimated the total corrosion current generated as methods employed to measure the corrosion current assumed coupling over short distances similar to that evaluated in this work would not occur.

6.2.3 Influence of System Geometry and Moisture Conditions on Corrosion

Variations introduced into the model related to bar spacing, bar diameter, concrete cover, and moisture conditions affected the corrosion potentials measured on the concrete surface. As bar spacing decreased below 100 mm, bar diameters increased from 15 mm, and covers increased, the removal of oxygen from the pore solution caused by the corrosion process could not be replenished. This caused the total oxygen concentration on the bar/concrete interface to be reduced, in some situations reaching a limiting condition, resulting in lower corrosion potentials and corrosion current density. This result is consistent with field observations of half-cell testing experienced by the author. On many structures where locations of congested reinforcement, high cover, or high bar diameter were present, recorded corrosion potential results were inconsistent with other test results related to chloride concentrations or physical damage such as delaminations. As well, when concrete was removed as part of the rehabilitation process, minimal signs of corrosion by-product were observed.

Moisture conditions had the greatest influence on concrete surface corrosion potentials when compared to other variable considered in this research. When relative humidity values less than 90% were employed with high chloride concentrations, the resulting concrete surface corrosion potentials did not reach the values, which indicate a high level probability of corrosion identified in the applicable standards. This result is inconsistent with field observations where high corrosion potentials are experienced even when moisture conditions are well below the 90% level. This observation resulted in the identification of a secondary mechanism, which is presented in the following section, that will cause corrosion potentials to reach values indicative of damaging corrosion rates.

The outcome of this sensitivity analysis was that adjustment factors are necessary to modify concrete surface corrosion potentials in order to address the influences introduced by concrete cover, bar diameter, bar spacing, and relative humidity. Such factors are not currently available,

suggesting that existing procedures for evaluation possible corrosion activity may give misleading results.

6.2.4 Pore Solution Acidification

It was determined that a secondary mechanism must be present on the bar/concrete interface that causes local acidification of the pore solution in order for corrosion potentials to reach the values that indicate a high probability of corrosion. This mechanism has been discussed in the literature; however, no clear methodology has been identified to describe the process.

The mechanism proposed which results in the pore solution acidification is related to coupling that occurs along and around the bar circumference. When coupling occurs, zones are developed where Fe^{2+} is produced, thereby consuming the local OH^-. Once consumed, the local reduction in OH^- causes OH^- to diffuse into the affected zone from other locations, or from the dissolution of hardened portions of the pore structure. The relative contribution of each of these mechanisms was evaluated by initially assuming changes to local pH would be mitigated by diffusion of OH^- into or out of the area depending on whether the area was experiencing an increase in cathodic or anodic processes. These simulations produced a significant drop in pH at the anodic zones even when chloride was not present, a finding that was not consistent with observations from laboratory or field settings. Therefore, a second mechanism related to equilibrium between the pore solution and hardened pore structure was identified as being the most likely controlling mechanism for maintaining the pore solution pH.

Initially the equilibrium between the pore solution and hardened pore structure results in a relatively uniform pH through time. However, as Fe^{2+} reacts with OH^- to form $Fe(OH)_2$, the local pore structure becomes filled with corrosion by-product, reducing the contact area between the pore solution and the pore structure. This filling process has been commonly observed in the field and laboratory settings as the precursor to delaminations. As the pore structure fills, the contact area between the pore structure and the pore solution is reduced, which then limits the ability of the system to remain in equilibrium. Therefore, as the production of $Fe(OH)_2$ continues, the local pore solution gradually becomes more acidic, which changes the pore solution from a high pH to a pH closer to a carbonated concrete. This change, combined with the kinetics of corrosion, cause local corrosion rates to increase between 20 to 2000 times relative to that for the high pH case, resulting in a localized high rate of metal dissolution commonly observed on reinforcement in the field.

6.3 Recommendations for Future Research

The model developed forced coupling to occur on the circumference of the reinforcing steel bar. This assumption is correct when cover to the reinforcing steel bar and the concrete surrounding the bar is uniform. However, this uniformity is rarely present as cover thickness and concrete are quite variable due to material inconsistencies or construction tolerances.

As well, the current model limited variations in pore solution chemistry when coupling occurred. This assumption was based on the belief that all excess Fe^{2+} would be consumed by free OH^- within the pore solution, which would cause hardened portions of the pore structure to dissolve in order to maintain the solution pH. However, the simulations performed indicated a change in pore solution pH was necessary to produce corrosion potentials on the concrete surface that reached the values identified in current standards.

The following components of the simulation should therefore be updated to better reflect how corrosion would develop on a reinforcing steel bar embedded in concrete:

- Variation in local chemistry caused by addition of OH^- and extraction of Fe^{2+}. Including these effects will result in cathodic zones becoming increasingly caustic while anodic zones become acidified. The inclusion of this feature will require extensive modeling of the balance between pore solution and hardened portions of the pore structure as this interaction is critical to how the pore solution will acidify as the anodic zone creates excess Fe^{2+}. Additionally, this interaction between the pore solution and pore structure will need to include various types of concrete, supplementary cementitious materials, admixtures, aggregates, and water to cement ratios;

- When local variations in chemistry are evaluated, potential drops through the pore solution induced by concentrations changes will need to be included by accounting for concentration potential drops;

- The accommodation of local chemistry changes in the pore solution will require the development of kinetic of corrosion diagrams for a range of pH and pore solution concentrations in order to capture transition points as concentrations change. Kinetic of corrosion diagrams could include conventional reinforcing steel, stainless steel, and other types of corrosion resistant materials;

- Creation of a three dimensional model to simulate coupling on the bar surface both circumferentially and longitudinally combined with the transport of chloride and oxygen to this surface surface;

- Modification of the bar surface from a smooth element to a deformed bar to better reflect the surface condition employed in most reinforced concrete structures; and

- The ability to add different membrane systems so that the transport of oxygen and chloride to the concrete and embedded reinforcement better reflects many of the modern protection systems employed by bridge owners.

REFERENCES

Alberta Transportation Technical Standards Branch, 2007, Bridge inspection and maintenance system – Level 2 inspection manual – Release 1.1, Technical Standards Branch, Alberta Transportatin, Government of Alberta, Edmonton, Alberta.

Alonso, C., Andrede C., Castellote, M., Castro, P. 2000, Chloride Threshold Values to Depassivate Reinforcing Bars Embedded in a Standardized OPC Mortar, Cement and Concrete Research, 30: 1047 - 1055.

Alonso, C., Castellote, M., Andrade, C., 2002, Chloride threshold dependence of pitting potential of reinforcements, Electrochimica Acta, 47: 3469-3481.

Andrade, C., Page, C., 1986, Pore solution chemistry and corrosion in hydrated cement systems containing chloride salts, Cement and Concrete Research, 21:49-53.

ASTM Standard C876-09, Standard Test Method for Half-Cell Potentials of Uncoated Reinforcing Steel in Concrete, ASTM International, West Conshohocken, PA, 2003, DOI: 10.1520/C08.76-09, www.astm.org.

Balabanic, G., Bicanic, N., Durekovic, A., 1995, Numerical analysis of corrosion cell in concrete, Engineering Modelling, 8:1-5.

Balafas, I., Burgoyne, C., 2010, Environmental effects on cover cracking due to corrosion, Cement and Concrete Research, 40:1429-1440.

Basheer, L., Basheer, P., Long, A., 2005, Influence of coarse aggregate on the permeation, durability and the microstructure characteristics of ordinary Portland cement concrete, Construction and Building Materials, 19:682-690.

Battino, R., Rettich, T., Tominaga, T., 1983, The solubility of oxygen and ozone in liquids, Journal of Physical Chemistry, 12:163-178.

Bentour, A., Diamond, S., Berke, N.S. 1997, Steel Corrosion in Concrete, E & FN Spon, an imprint of Chapman & Hall, 2-6 Boundary Row, London Se1 8HN, UK. 1997.

Boulfiza, M., Sakai, K., Banthia, N., Yoshida, H., 2003, Prediction of chloride ions ingress in uncracked and cracked concrete, American Concrete Institute Materials Journal, 100: 38-48.

Canadian Highway Bridge Design Code, 2006, CAN/CSA-S6-06, Canadian Standards Association, Mississauga, Ontario.

Carter, P.D., Hamilton, D., 2007, Final Report – Deck Testing Modifications, Report to Alberta Transportation Infrastructure and Transportation Bridge Engineering Branch.

Chapra, S., Canale, R., 2006, Numerical methods for engineers, fifth edition, McGraw-Hill International, New York, NY.

Chin, J., Aouadi, K., Haight, M., Hughes, W., Nguyen, T., 2001, Effects of water, salt solution and simulated concrete pore solution on the properties of composite matrix resins used in civil engineering applications, Polymer Composites, 22:282-298.

Council of Ministers Responsible for Transportation and Highway Safety, 2012, Canada's National Highway System – Annual Report 2011, available from http://www.comt.ca/english/reports-e.htm [cited April 15, 2013].

Debelius, B., Gomez-Parra, A., Forja, J., 2009, Oxygen solubility in evaporated seawater as a function of temperature and salinity, Hydrobiologia, 632:157-165.

Elsener, B., 2001, Half-cell potential mapping to assess repair work on RC structures, Construction and Building Materials, 15:133-139.

Elsener, B., 2002, Macrocell corrosion of steel in concrete – implications for corrosion monitoring, Cement and Concrete Composites, 24:65-72.

Evitts, R., 1997, Modelling of crevice corrosion, PhD Thesis, Department of Chemical Engineering, University of Saskatchewan, Saskatoon, Saskatchewan, Canada.

fib bulletin 34, 2006, Model code for service life design, International Federation for Structural Concrete, Lausanne, Switzerland.

Garboczi, E., Bentz, D., 1998, Multiscale analytical/numerical theory of the diffusivity of concrete, Advanced Cement Based Materials, 8:77-88.

Garcia, H., Gordon, L., 1992, Oxygen solubility in seawater: Better fitting equaitons, Journal of Limnology and Oceanography, 37:1307-1312.

Garćes, P., Andrade, M., Saez, A., Alonso, M., 2005, Corrosion of reinforcing steel in neutral and acid solutions simulating the electolytic envornments in the micropores of concrete in the propagation period, Corrosion Science, 47:289-306.

Ge, J., Isgor, O., 2007, Effects of tafel slope, exchange current density and electrode potential on the corrosion of steel in concrete, Materials and Corrosion, 58:573-582.

Gojkovic, S., Zecevic, S., Drazic, D., 1994, Oxygen reduction on iron – Part VI, processes in alkaline solutions, Electrochimica Acta, 39:975-982.

Goni, S., Andrade, C., 1990, Synthetic concrete pore solution chemistry and rebar corrosion rate in the presence of chlorides, Cement and Concrete Research, 20:525-539.

Gouda, V., 1978, Corrosion and inhibition of reinforcing steel, British Corrosion Journal, 5:198-203.

Gouda, V., Halaka, W., 1970, Corrosion and corrosion inhibition of reinforcing steel, British Corrosion Journal, 5:204-208.

Han, S., 2007, Influence of diffusion coefficient on chloride ion penetration of concrete structure, Construction and Building Materials, 21:370-378.

Hansson, C., Poursaee, A., Laurent, A., 2006, Macrocell and microcell corrosion of steel in ordinary Portland cement and high performance concretes, Cement and Concrete Research, 36:2098-2102.

Hansson, C., Sorensen, B., 1990, The threshold concentration of chloride in concrete for initiation of reinforcement corrosion, Corrosion Rates of Steel in Concrete, N. Berke, V. Whiting (eds.), ASTM Special Technical Publication, 1065, 3-16.

Haque, M., Kayyali, O., 1995, Free and water soluble chloride in concrete, Cement and Concrete Research, 25:531-542.

Hartt, W.H., Powers, R. G., Leroux, V., Lysogorski, D.K. 2004, Critical Literature Review of High-Performance Corrosion Reinforcements in Concrete Bridge Applications Final Report, Report FHWA-HRT-04-093, McLean, Virginia.

Hausmann, D., 1967, Steel corrosion in concrete. How does it occur?, J. Mater. Prot., 6:19-23.

Heppner, K., 2006, Development of predictive models of flow induced and localized corrosion, PhD Thesis, Department of Chemical Engineering, University of Saskatchewan, Saskatoon, Saskatchewan, Canada.

Hope, B., Ip, A., 1987, Chloride corrosion threshold in concrete, American Concrete Institute Materials Journal, 84:306-314.

Huet, B., L'Hostis, V., Miserque, F., Hassane, I., 2005, Electrochemical behavior of mild steel in concrete: Influence of pH and carbonate content of concrete pore solution, electrochimica Acta, 51: 172-180.

Huet, B., L'hostis, V., Santarini, G., Feron, D., Idrissi, H., 2007, Steel corrosion in concrete: Determinist modeling of cathodic reaction as a function of water saturation degree, Corrosion Science, 49: 1918-1932.

Hurley, M.F., Scully, J.R. 2002, Chloride Threshold Levels in Clad 316L and Solid 316LN Stainless Steel Rebar, Paper No. 02224 presented at CORROSION/02, Denver, CO.

Hussain, R., Ishida, T., 2010a, Development of numerical model for FEM computation of oxygen transport through porous media coupled with micro-cell corrosion model of steel in concrete, Computers and Structures, 88: 639-647.

Hussain, R., Ishida, T., 2010b, Influence of connectivity of concrete pores and associated diffusion of oxygen on corrosion of steel under high humidity, Construction and Building Materials, 24:1014-1019.

Hussain, S., Rasheduzzafar, S., Al-Mussallam, A., Al-Gahtani, A., 1995, Factors affecting threshold chloride for reinforcement corrosion in concrete, Cement and Concrete Research 25:1543-1555.

Isgor, O., Razaqpur, A., 2006a, Modeling steel corrosion in concrete structures, Materials and Structures, 39:291-302.

Isgor, O., Razaqpur, A., 2006b, Advanced modelling of concrete deterioration due to reinforcement corrosion, Canadian Journal of Civil Engineering, 33: 707-718.

Izquierdo, D., Alonso, C., Andrade, C., Castellote, M. 2004, Potentiostatic determination of chloride threshold values for rebar depassivation - experimental and statistical study Electrochimica Acta, 49: 2731–2739.

Ji, Y., Shen, J., Wang, L., Xu, C., 2011, Corrosion characteristics and corrosion current distribution of steel bar in carbonated concrete, Advanced Materials Research, 239-242:3371-3376.

Jones, D., 1996, Principles and prevention of corrosion, 2nd Edition, Prentice Hall, Upper Saddle River, New Jersey.

Kayyali, O., Haque, M., 1995, The ratio of Cl^-/OH^- in chloride contaminated concrete. A most important criterion, Magazine of Concrete Research, 47:235-242.

Kennel, G., 2012, Electrolytic transport, electric fields, and the propensity for charge density in electrolytes, PhD Thesis, Department of Chemical Engineering, University of Saskatchewan, Saskatoon, Saskatchewan, Canada.

Kennell, G., Evitts, R., 2009, Crevice corrosion cathodic reactions and crevice scaling laws, Electrochemica Acta, 54:4696-4703.

Kennell, G., Evitts, R., Heppner, K., 2008, A critical crevice solution and IR drop crevice corrosion model, Corrosion Science, 50:1716-1725.

Kim, C., Kim, J., 2008, Numerical analysis of localized steel corrosion in concrete, Construction and Building Materials, 22:1129-1136.

Koretsky, M., Abooameri, F., Westall, J., 1999, Effect of concrete pore saturation on cathodic protection of steel-reinforced concrete bridges, Corrosion, 55:52-64.

Kranc, S., Sagues, A., 2001, Detailed modeling of corrosion macrocells on steel reinforcing in concrete, Corrosion Science, 43:1355-1372.

Lambert, P., Page, C., Vassie, P., 1991, Investigation of reinforcement corrosion. Electrochemical monitoring of steel in chloride contaminated concrete, Materials and Structures, 24:351-358.

Li, C.Q., 2001, Initiation of chloride-induced reinforcement corrosion in concrete structural members – experimentation, American Concrete Institute Structural Journal, 98: 502-510.

Li, C.Q., 2002, Initiation of chloride-induced reinforcement corrosion in concrete structural members – prediction, American Concrete Institute Structural Journal, 99: 133-140.

Li, L., Sagues, A, 2001, Chloride corrosion threshold of reinforcing steel in alkaline solutions – Open-circuit immersion tests, Corrosion 57:19-28.

Liu, Y., Weyers, R., 1998, Modeling the time-to-corrosion in chloride contaminated reinforced concrete structures, American Concrete Institute Materials Journal, 95:675-681.

Macias, A., Andrade, C., 1987, Corrosion of galvanized steel reinforcements in alkaline solutions, British Corrosion Journal, 22:113-118.

Martin-Perez, B., Zibara, H., Hooton, R., Thomas, M., 2000, A study of the effect of chloride binding on service life predictions, Cement and Concrete Research, 30:1215-1223.

Martin-Perez, B., Pantazopoulou, S., Thomas, M., 2001, Numerical solution of mass transport equations in concrete structures, Computers and Structures, 79: 1251-1264.

Maruya, T., Takeda, H., Horiguchi, K., Koyama, S., Hsu, K., 2007, Simulation of steel corrosion in concrete base on the model of macro-cell corrosion circuit, Journal of Advanced Concrete Technology, 5:343-362.

Mathworks, Inc., 2009, MATLAB™ users manual, Massechusetts, USA.

MATLAB™ (2009a) 2009, The Mathworks, Inc.

Millard, S., Law, D., Bungey, J., Cairns, J., 2001, Environmental influences on linear polarization corrosion rate measurement in reinforced concrete, NDT&E International, 34:409-417.

Mohammed, T., Hamada, H., 2001, Corrosion of steel bars in concrete with various steel surface conditions, American Concrete Institute Materials Journal, 103:233-242

Mohammed, T., Hamada, H., 2003, Relationship between free chloride and total chloride contents in concrete, Cement and Concrete Research, 33:1487-1490.

Moreno, M., Morris, W., Alvarez, M., Duffo, G., 2004, Corrosion of reinforcing steel in simulated concrete pore solutions. Effect of carbonation and chloride content, Corrosion Science, 46:2681-2699.

Moser, R., Singh, P., Kahn, L., Kurtis, K., 2011, Chloride-induced corrosion of prestressing steels considering crevice effects and surface imperfections, Corrosion, 67:065001-1:065001-14.

National Climate Data and Information Archive available from http://climate.weatheroffice.gc.ca [cited April 12, 2013].

National Climatic Data Centre, National Oceanic and Atmospheric Administration, available from http://www.ncdc.noaa.gov [cited April 12, 2013].

Newman, J., Thomas-Alyea, K., 2004, Electrochemical Systems, 3rd Edition, Prentice-Hall, Englewood Cliffs, New Jersey.

Novak, P., Mala, R., Joska, L., 2001, Influence of pre-rusting on steel corrosion in concrete, Cement and Concrete Research, 31:589-593.

Papadakis, V., Yayenas, C., Fardis, M., 1991, Physical and chemical characteristics affecting the durability of concrete, ACI Materials Journal, 8: 186-196.

Papadakis, V., Roumeliotis, A., Fardis, M., Vagenas, C., 1996, Mathematical modeling of chloride effect on concrete durability and protection measures, in Concrete Repair, Rehabilitation and Protection, Edited by R.K.Dhir and M.R. Jones, Published by E & FN Spon, London, UK, 165-174.

Peterson, K., 1992, Chloride threshold vale and the corrosion rate in reinforced concrete, CBI Report 2:92, Stockholm, Sweden.

Peterson, K., 1994, Chloride threshold value and the corrosion rate in reinforced concrete, Proceedings of the International Conference on Corrosion Protection of Steel in Concrete, R.N. Swamy (ed.), Academic Press, Sheffield, 461.

Petterson, K., 1996, Factors influencing chloride induced corrosion of reinforced concrete, Durability of Building Materials and Components, Vol 1, Chapman & Hall, London, 334-341.

Pourbaix, M., 1973, Lectures on electrochemical corrosion, Plenum Press, New York-London.

Pour-Ghaz, M., Isgor, O., Ghods, P., 2009, Quantitative interpretation of half-cell potential measurements in concrete structures, Journal of Materials in Civil Engineering, 21:467-475.

Poursaee, A., 2010, Determining the appropriate scan rate to perform cyclic polarization test on the steel bars in concrete, Electochimica Acta, 55:1200-1206.

Poursaee, A., Hansson, C., 2007, Reinforcing steel passivation in mortar and pore solution, Cement and Concrete Research, 37:1127-1133.

Raupach, M., 1996a, Investigations on the influence of oxygen on corrosion of steel in concrete – Part 1, Materials and Structures, 29:174-184.

Raupach, M., 1996b, Investigations on the influence of oxygen on corrosion of steel in concrete – Part 2, Materials and Structures, 29:226-232.

Raupach, M., 2006, Patch repairs on reinforced concrete structures – Model investiations on the required size and practical consequences, Cement and Concrete Composites, 28:679-684.

Raupach, M., Schiessl, P., 1997, Monitoring system for the penetration of chlorides, carbonation and the corrosion risk for the reinforcement, Construction and Building Materials, 11:207-214.

Revie, R., 2006, Uhlig's Corrosion Handbook – 2nd Edition, Wiley Interscience, Hoboken, New Jersey.

Rodriguez, P., Ramirez, R., Feliu, S., Gonzalez, J., Lopez, W., 1999, Significance of coplanar macrocells to corrosion in concrete-embedded steel, Corrosion, 55, 319-325.

Qian, S., Zhang, J., Qu, D., 2006, Theoretical and experimental study of microcell and macrocell corrosion in patch repairs of concrete structures, Cement and Concrete Composites, 28:685-695.

Saetta, A., Scotta, R., Vitaliani, R., 1993, Analysis of chloride diffusion into partially saturated concrete, American Concrete Institute Materials Journal, 90:441-451.

Saetta, A., Vitaliani, R., 2004, Experimental investigation and numerical modeling of carbonation process in reinforced concrete structures. Part I: Theoretical formulation, Cement and Concrete Research, 34:571-579.

Schiessl, P., Breit, W., 1996, Local repair measures at concrete structures damaged by reinforcement corrosion, Proceedings of the Fourth International Symposium on Corrosion of Reinforcement in Concrete Construction, SCI, Cambridge, 525-534.

Scrivener, K., Crumbie, A., Laugesen, P., 2004, The interfacial transition zone (ITZ) between cement paste and aggregate in concrete, Interface Science, 12:411-421.

Shi, C., Stegemann, J., Caldwell, R., 1998, Effect of supplementary cementing materials on the specific conductivity of pore solution and its implications on the rapid chloride permeability test (AASHTO T277 and ASTM C1202) Results, American Concrete Institute Materials Journal, 95:389-393.

Skeet, J.A., Kriviak, G.W., and Carter, P.D. 1994, Service Life Prediction of Protective Systems for Concrete Bridge Decks in Alberta, Report No. ABTR/RD/RR-94/01, Alberta Transportation and Utilities, Edmonton, Alberta.

Shoup, L., Donohue, N., Lang, M., 2011, The fix we're in for: The state of our nation's bridges, Transportation for America.

Soleimani, S., Ghods, P., Isgor, O., Zhang, J., 2010, Modeling the kinetics of corrosion in concrete patch repairs and identification of governing parameters, Cement and Concrete Composites, 32:360-368.

Steffens, A., Dinkler, D., Ahrens, H. 2002, Modeling carbonation for corrosion risk prediction of concrete structures, Cement and Concrete Research, 32: 935-941.

Stratfull, R., F., 1973, Half-cell potentials and the corrosion of steel in concrete, Highway Research Record, 433: 12-35.

Subramaniam, K., Bi, M., 2010, Investigation of steel corrosion in cracked concrete: Evaluation of macrocell and microcell rates using Tafel polarization response, Corrosion Science, 52:2725-2735.

Sun, G., Zhang, Y., Sun, W., Liu, Z., Wang, C., 2011, Multi-scale prediction of the effective chloride diffusion coefficient of concrete, Construction and Building Materials, 25:3820-3831.

Thangavel, K., Rengaswamy, N., 1998, Relationship between chloride/hydroxide ratio and corrosion rate of steel in concrete, Cement and Concrete Composites, 20: 283-292.

Thomas, M., Matthews, J., Hanes, C., 1990, Chloride diffusion and reinforcement corrosion in marine exposed concretes containing PFA, Corrosion of Reinforcement in Concrete, Elsevier, Warwickshire, UK, 198-212.

Thomas, M., 1996, Chloride thresholds in marine concrete, Cement and Concrete Research, 26:513-519.

Wang, Yu, Li, Long-yuan, Page, C.L., 2005, Modelling of chloride ingress into concrete from a saline environment, Building and Environment, 40: 1573–1582.

Warkus, J., Raupach, M., 2008, Numerical modeling of macrocells occurring during corrosion of steel in concrete, Materials and Corrosion, 59:122-130.

Watson, M., 1989, Numerical simulation of crevice corrosion, PhD Thesis, Department of Chemical Engineering, University of Saskatchewan, Saskatoon, Saskatchewan, Canada.

Watson, M., Postlethwaite, J. ,1990a, Numerical simulation of crevice corrosion of stainless steels and nickel alloys in chloride solutions, Corrosion, 46:522–530.

Watson, M., Postlethwaite, J., 1990b, Numerical simulation of crevice corrosion, Proceedings of the Corrosion/90, Las Vegas, NV, April 23–27, NACE International, Houston, TX, 156:1–156:19.

Watson, M., Postlethwaite, J., 1991, Numerical simulation of crevice corrosion: the effect of the crevice gap profile, Corrosion Science, 32:1253–1262.

Williamson, G.,S., Weyers, R., E., Sprinkel, M., M., Brown, M., C., 2009, Concrete and steel type influence on probabilistic corrosion service life, ACI Materials Journal, 106: 82-88.

Ye, G., van Breugel, K., 2009, Simulation of connectivity of capillary porosity in hardening cement based systems made of blended materials, Heron, 54:163-184.

Yokota, M., Kyung, J., Lee, H., 2008, Environmental influence on the corrosion rate of steel bars embedded in concrete, ISIJ International, 48:230-234.

Yu, H., Chiang, K., Yang, L., 2012, Threshold chloride level and characteristics of reinforcement corrosion initiation in simulated concrete pore solutions, Construction and Building Materials, 26:723-729.

Zhang, R., Castel, A., Francois, R., 2009, The corrosion pattern or reinforcement and its influence on serviceability of reinforced concrete members in chloride environment, Cement and Concrete Research, 39: 1077-1086.

Zhang, J., Mailvaganam, N., 2006, Corrosion of concrete reinforcement and electrochemical factors in concrete patch repair, Canadian Journal of Civil Engineering, 33:785-793.

Zhitnikov, Y., Mozhegov, N., Matrosova, Y., 2002, Physicochemical Measurements - Determining the porosity of concrete, Measurement Techniques, 45:305-310.

Zhou, K., Martin-Perez, B., Lounis, Z., 2005, Finite element analysis of corrosion-induced cracking, spalling and delamination of RC bridge decks, 1st Canadian

Conference on Effetive Design of Structures, McMaster University, Hamilton, Ontario, Canada.

APPENDIX A. COUPLING EQUATIONS

A.1 Overview.

Figure 3.6 presents the model used to simulate corrosion current produced on the bar/concrete interface and the portion that flows through the pore solution. Within this section, the derivation of the non-linear equations used to identify the corrosion current from each contributing segment is presented.

The model formulation of Figure 3.6 divides the corrosion cell into two sections, namely the anode and cathode. Figure A.1 superimposes the model formulation from Figure 3.6 onto the kinetics of corrosion diagram used within the simulation. Two points are identified labeled Zone A and Zone B which represent portions of the bar that are either in contact with chloride (Zone A), or chloride free (Zone B). Other zones are created depending on the localized chloride concentration, however, for the purposes of this derivation, only two zones are considered.

From Figure A.1, it is apparent that different corrosion potentials are produced at these locations resulting from the different chloride and oxygen concentrations present. If sufficient corrosion potential difference is present, current will flow between these zones creating increased metal dissolution at the point at lower corrosion potential and either increased consumption of oxygen or a decreased metal dissolution rate at the zone of higher corrosion potential.

A transition point is identified in Figure 3.6 and Figure A.1 that separates the anode and cathode. This transition point is required to simplify the solution process by first solving for the current flow that is developed from the anodic site. Once this initial corrosion current is identified, the equations related to the cathodic side can be directly solved.

Beginning with zone A, potential drops through the electrolyte between the transition zone and the uncoupled corrosion potential are identified as Φ_a and $\Phi_{a,\Omega}$ which represent the overpotential and ohmic potential drops through the electrolyte caused by increase current flow at the anode. Similar overpotentials and ohmic potential drops are created on the cathodic side of the corrosion cell which are represented by Φ_c and $\Phi_{c,\Omega}$. However, within the cathode, two separate reactions may occur depending on the oxygen concentrations available within the pore solution. If excess oxygen is available,

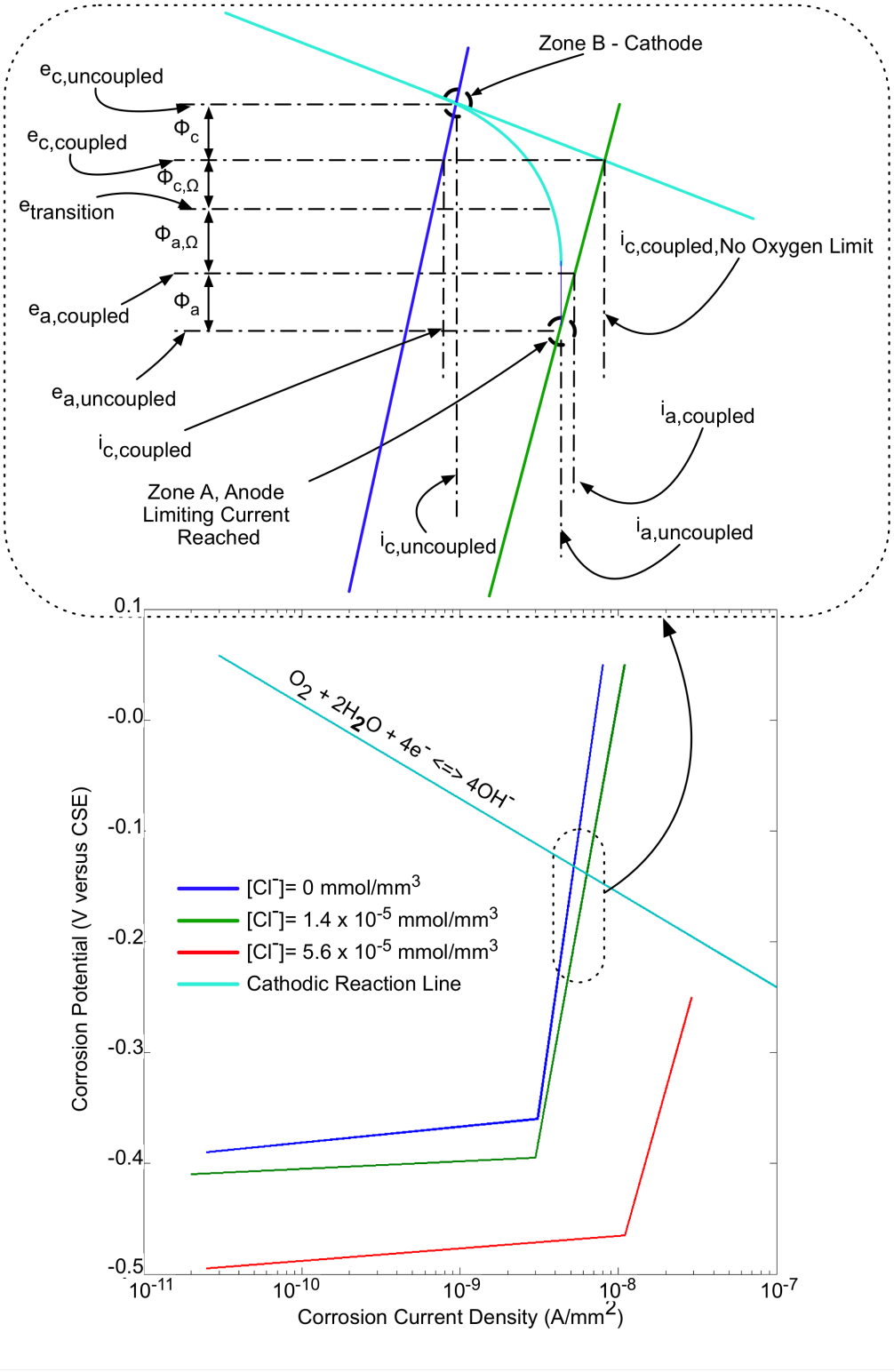

Figure A.1. Corrosion potential drops through the electrolyte and on the bar/concrete interface related to the kinetics of corrosion.

then overpotentials caused by coupling will create an increase in the cathodic reaction by consuming oxygen. If oxygen is at a limiting condition, then the local metal dissolution rate is suppressed in a similar manner to cathodic protection where the sacrificial anode reduces the corrosion rate at the cathode.

In the following sections, the equations are developed which are used in the simulation to solve for the corrosion current flowing through the pore solution on the bar/concrete interface are presented. Initially, the anodic region is developed along with the solution process, which employs the Gauss-Seidel method for solving non-linear transcendental systems of equations. After the anodic side is presented, the two conditions which control the countering cathodic reaction is presented.

A.2 Anodic Region

Equation development for the anodic side of the corrosion cell begins by identifying the corrosion potential drop from the transition point to the uncoupled corrosion potential present at the bar/concrete interface. The resulting difference is then equated to the ohmic potential drop and resulting overpotential that is formed when these two points are coupled through the pore solution. Beginning with the first segment denoted by the subscript 1, these corrosion potential differences and corresponding ohmic and overpotential drops result in Equation A.1 as follows:

$$e_{transition} - e_{1a,uncoupled} = \phi_{1a,\Omega} + \phi_{1a} \qquad [A.1]$$

where $e_{transition}$ is the corrosion potential at the transition point between the anodic and cathodic sites (volts), $e_{1a,uncoupled}$ is the uncoupled corrosion potential at segment 1 of the anode (volts), $\Phi_{1a,\Omega}$ is the ohmic potential drop caused by the total current flow through the electrolyte present at this segment (volts), and Φ_{1a} is the overpotential created at the segment when the segment is coupled (volts).

The ohmic corrosion potential drop that occurs at the first segment ($\Phi_{1a,\Omega}$) begins with Equation 3.1 which is then expanded to Equation A.2 to capture the total corrosion current flowing through the electrolyte:

$$\phi_{1a,\Omega} = \frac{I_{1a} + I_{2a} + \cdots + I_{(n-1)a} + I_{na}}{\kappa_{1,a}} = \frac{\sum_{s=1}^{n} I_{sa}}{\kappa_{1a}} \quad [A.2]$$

where I_{1a}, I_{2a}, $I_{(n-1)a}$ and I_{na} represents the current flow through the electrolyte contributed from each segment (Amps) represented by Equation A.3, $\kappa_{1,a}$ represents the conductivity of the solution within segment 1 on the anodic side (1/Ω) represented by Equation 2.36, and n is the number of segments.

$$I_{na} = I_{na,coupled} - I_{na,uncoupled} \quad [A.3]$$

where $I_{na,coupled}$ and $I_{na,uncoupled}$ represent the current generated for each segment converted to amps by multiplying the corrosion current density by the segment area.

Equation A.4 represents the overpotential created at the first segment within the anode when coupling through the connecting pore solution occurs. This overpotential is the difference between uncoupled and coupled corrosion potentials, which are represented by Equation A.4, A.5, and A.6:

$$e_{1a,uncoupled} = \tau_{1a,Fe} \log\left(i_{1a,uncoupled}\right) - b_1 \quad [A.4]$$

$$e_{1a,coupled} = \tau_{1a,Fe} \log\left(i_{1a,coupled}\right) - b_1 \quad [A.5]$$

$$\phi_{1a} = e_{1a,coupled} - e_{1a,uncoupled} \quad [A.6]$$

where $e_{1a,uncoupled}$ is the uncoupled corrosion potential at segment 1 of the anode (Zone A) (volts), $\tau_{1a,Fe}$ is the Tafel slope of the Fe dissolution curve represented in Figure A.1, $I_{1a,uncoupled}$ is the uncoupled corrosion current occurring at the first segment (Amps), and b_1 is the y-intercept, $e_{1a,coupled}$ is the coupled corrosion potential at segment 1 of the anode (Zone A) (volts), $I_{1a,coupled}$ is the coupled corrosion current occurring at the first segment (Amps).

Substituting Equation A.4 and A.5 into A.6 and simplifying, produces Equation A.7:

$$\phi_{1a} = \tau_{1a,Fe} \log\left(\frac{I_{1a,coupled}}{I_{1a,uncoupled}}\right) \qquad [A.7]$$

Substituting Equations A.2, A.3, and A.7 into A.1, produces Equation A.8, which represents the current flow produced at the first segment when a corrosion potential difference is present which includes current contributions from adjacent segments:

$$e_{transition} - e_{1a,uncoupled} = \frac{\sum_{s=1}^{n} I_{sa}}{\kappa_{1a}} + \tau_{1a,Fe} \log\left(\frac{I_{1a,coupled}}{I_{1a,uncoupled}}\right) \qquad [A.8]$$

Equation A.5 represents the single equation that relates the corrosion potential differences between the first segment and the transition point to the corrosion current produced at that segment and flowing from adjacent segments. Using the logic employed to develop Equation A.8, the expression for segment "n" can be produced as shown in Equation A.9:

$$e_{transition} - e_{na,uncoupled} = \frac{\sum_{s=1}^{n} I_{sa}}{\kappa_{1a}} + \frac{\sum_{s=2}^{n} I_{sa}}{\kappa_{2a}} \cdots + \frac{\sum_{s=n}^{n} I_{sa}}{\kappa_{na}} + \tau_{na,Fe} \log\left(\frac{I_{na,coupled}}{I_{na,uncoupled}}\right) \qquad [A.9]$$

Summarizing, for the anodic side of the electrochemical cell, the system of non-linear equations are presented in Table A.1 for 1 to "n" segments contributing. The number of segments that contribute to the overall electrochemical cell is established by assuming initially that only the first segment adjacent to the transition between the anode and cathode is contributing. Once this initial calculation is completed, potential drops are determined and if sufficient potential remains for the next segment to contribute then a subsequent evaluation-using segment 1 and 2 is performed. This cycle is repeated until the potential drops from the transition point to the last segment become sufficiently large that the last segment is no longer connected. At this point, the total current flow produced from the anodic side is identified as $I_{a,total}$ which is used in the following section to determine the consumption of current within the cathodic zone.

Obtaining solutions for these systems of equations required iterative techniques, which are discussed in Section A.4.

A.3 Cathodic Region

As noted earlier, within the cathodic region, two distinct processes may exist when the cathodic region is coupled with the anodic region. When oxygen is available, excess electrons produced by coupling between the cathode and the anode can be consumed by increasing the local oxygen consumption rate in accordance with Equation 2.2. In some instances, oxygen at the cathodic site has reached a limiting condition or the increased oxygen demand caused by coupling results in a limiting condition being reached. When either of these conditions are present, coupling results in the local metal dissolution rate represented by Equation 2.1 being suppressed so that additional electrons produced by coupling can be consumed by the cathodic reaction represented by Equation 2.2. Li

Therefore, since two independent conditions can be present within the cathodic region separate equations were required to describe these processes mathematically which are described in the following sections.

A.3.1 Cathodic Region – Oxygen is Limited

When oxygen concentrations on the bar/concrete interface reach a limiting condition and coupling is present through the pore solution, oxygen consumption rates within the cathode cannot increase. However, coupling still occurs as excess ions and electrons

Table A.1. Summary of non-linear equations for each segment within the anodic region.

Segment	Relationship
1	$E_{transition} - E_{1a,uncoupled} = \frac{\sum_{s=1}^{n} I_{sa}}{\kappa_{1a}} + \tau_{1a,Fe} \log\left(\frac{I_{1a,coupled}}{I_{1a,uncoupled}}\right)$
2	$E_{transition} - E_{2a,uncoupled} = \sum_{p=1}^{2}\left(\frac{\sum_{s=p}^{n} I_{sa}}{\kappa_{pa}}\right) + \tau_{2a,Fe} \log\left(\frac{I_{2a,coupled}}{I_{2a,uncoupled}}\right)$
⋮	⋮
n	$E_{transition} - E_{na,uncoupled} = \sum_{p=1}^{n}\left(\frac{\sum_{s=p}^{n} I_{sa}}{\kappa_{pa}}\right) + \tau_{na,Fe} \log\left(\frac{I_{na,coupled}}{I_{na,uncoupled}}\right)$

produced at the anodic region affect the corrosion processes at the cathodic zone by suppressing metal dissolution rates represented by Equation 2.1. When Equation 2.1 is suppressed, Equation 2.2 can then consume the excess electrons produced at the anodic site without a affecting the underlying oxygen limited condition.

With this understanding, equations that describe the electrochemistry occurring within the cathodic zone are very similar to the equations described previously for the anodic zone. Beginning with the first segment, Equation A.10 can be produced:

$$e_{1c,uncoupled} - e_{transition} = \phi_{1c,\Omega} + \phi_{1c} \qquad [A.10]$$

where $e_{transition}$ is the corrosion potential at the transition point between the anodic and cathodic sites (volts), $e_{1c,uncoupled}$ is the uncoupled corrosion potential at segment 1 of the cathode (volts), $\Phi_{1c,\Omega}$ is the ohmic potential drop caused by the total current flow through the electrolyte present at this segment (volts), and Φ_{1c} is the overpotential created at the segment when the segment is coupled (volts).

The ohmic corrosion potential drop that occurs at the first segment ($\Phi_{1c,\Omega}$) begins with Equation 3.1. In contrast to Equation A.2, the ohmic potential drop through the first segment on the cathodic side can be directly solved, as the total current flow from the anodic side is known. Therefore Equation A.2 is modified as follows:

$$\phi_{1c,\Omega} = \frac{I_{a,total}}{\kappa_{1c}} \qquad [A.11]$$

where $I_{a,total}$ represents the total current flowing from the anodic side of the corrosion cell (Amps), and κ_{1c} represents the conductivity of the solution within segment 1 on the cathodic side (1/Ω) represented by Equation 2.36. For subsequent segments, the total current flow through the electrolyte will be reduced as current is consumed by the cathodic reactions. Therefore, Equation A.11 is modified as follows:

$$\phi_{nc,\Omega} = \frac{I_{a,total} - \sum_{s=1}^{n-1} I_{nc}}{\kappa_{nc}} \qquad [A.12]$$

where n is the number of segments on the cathodic side, I_{nc} is the cathodic current produced at segment "n" (amps), and κ_{nc} is the conductivity of the solution in segment "n".

Overpotentials created at the cathode due to coupled current flow is similar to Equation A.7 with the subscripts changed to reflect reactions occurring within the cathodic zone rather than the anodic zone as follows:

$$\phi_{1c} = \tau_{1c,Fe} \log\left(\frac{I_{1c,coupled}}{I_{1c,uncoupled}}\right) \quad [A.13]$$

Ohmic potential drops and overpotentials for subsequent segments on the cathodic side are calculated by first solving for the coupled corrosion current density occurring at the first segment. This result is then subtracted from the total current flow produced from the anodic side, which then represents the current flowing into the next cathodic segment. This process is repeated until the cathodic processes occurring within the cathodic zone consume the total current produced from the anodic side.

A.3.2 Cathodic Region – Oxygen is Available

In this scenario, oxygen is present which can be consumed at the cathode. The derivation of equations for this scenario is similar to the previous derivations except Tafel slopes for Equation 2.2 are used rather than for the metal dissolution represented by Equation 2.1. Therefore, when oxygen is present, Equations A.10 to A.12 remain the same with Equation A.13 modified as follows:

$$\phi_{1c} = \tau_{1c,O_2} \log\left(\frac{I_{1c,coupled}}{I_{1c,uncoupled}}\right) \quad [A.14]$$

where τ_{1,c,O_2} is the Tafel slope for the oxygen reduction represented by Equation 2.2.

A.4 Anodic Equation Solution

Two approaches to solving the system of non-linear equations were considered. The first was based on solving the system of equations for a direct solution to each segment's current contribution. This approach was found to be computationally expensive once the number of segments increased past 5. Therefore an alternative solution process was developed which used Newton-Raphson's method to arrive at an approximate solution.

The first step in this approach solved for the current generated in the first segment assuming that this segment was the only segment contributing current. The second segment was then added assuming the current contribution from the first segment would not be affected. The second segment current contribution was then solved directly

which was then used to estimate the potential drops that occurred within the two-segment system. If the potential drops at the coupled potentials for segment 1 and segment 2 matched the current generated at that location then another segment was added. If the potential drops did not match the current generated, then Newton-Raphson's method was employed to adjust the corrosion currents until the corrosion potential drops through the electrolyte matched the overpotentials created on the bar/concrete interface.

Newton-Raphson's methods for solving nonlinear equations employs an iterative approach to finding a solution by modifying the initial guess using (Chapra and Canale 2006):

$$x_{k+1} = x_k - J_f^{-1} f(x_k) \qquad \text{[A.15]}$$

where x_k is the initial guess, J_f^{-1} is the Jacobian matrix developed from the system of equations, $f(x_k)$ is the system of equations and x_{k+1} is the new guess.

The Jacobian matrix represents the first derivative of the system of equations as follows:

$$J_f = \begin{bmatrix} \frac{\partial f_1(x)}{\partial x_1} & \frac{\partial f_1(x)}{\partial x_2} & \cdots & \frac{\partial f_1(x)}{\partial x_n} \\ \frac{\partial f_2(x)}{\partial x_1} & \frac{\partial f_2(x)}{\partial x_2} & \cdots & \frac{\partial f_2(x)}{\partial x_n} \\ \vdots & \vdots & \ddots & \vdots \\ \frac{\partial f_n(x)}{\partial x_1} & \frac{\partial f_n(x)}{\partial x_2} & \cdots & \frac{\partial f_n(x)}{\partial x_n} \end{bmatrix} \qquad \text{[A.16]}$$

The Newton-Raphson method for solving the series of non-linear transcendental equations is only applied in the anodic region, as this region requires the solution of a system of equations in the development of the total anodic current generated from coupling. In order to demonstrate the formation of the Jacobian matrix, a three-segment model was constructed from the equations identified in Table A.1 which were rearranged as functions resulting in:

$$f_1(x) = \frac{(I_{1a} + I_{2a} + I_{3a})}{\kappa_1} + \frac{\tau_{1,Fe}}{\ln(10)} \ln\left(\frac{I_{1a} + I_{1a,uncoupled}}{I_{1a,uncoupled}}\right) + e_{1a,uncoupled} - e_{transition} \quad [A.17]$$

$$f_2(x) = \frac{(I_{1a} + I_{2a} + I_{3a})}{\kappa_1} + \frac{(I_{2a} + I_{3a})}{\kappa_2} + \frac{\tau_{2,Fe}}{\ln(10)} \ln\left(\frac{I_{2a} + I_{2a,uncoupled}}{I_{2a,uncoupled}}\right) + e_{2a,uncoupled} - e_{transition} \quad [A.18]$$

$$f_1(x) = \frac{(I_{1a} + I_{2a} + I_{3a})}{\kappa_1} + \frac{(I_{2a} + I_{3a})}{\kappa_2} + \frac{(I_{3a})}{\kappa_3} + \frac{\tau_{3,Fe}}{\ln(10)} \ln\left(\frac{I_{3a} + I_{3a,uncoupled}}{I_{3a,uncoupled}}\right) + e_{3a,uncoupled} - e_{transition} \quad [A.19]$$

Taking the first derivative of equations $f_1(x)$, $f_2(x)$, and $f_3(x)$ with respect to the three unknowns of I_1, I_2, and I_3 results in the following:

$$\frac{\partial f_1(x)}{\partial I_{1a}} = \frac{1}{\kappa_1} + \frac{\tau_{1,Fe}}{\left(I_{1a} + I_{1a,uncoupled}\right)\ln(10)} \quad [A.20]$$

$$\frac{\partial f_1(x)}{\partial I_{2a}} = \frac{1}{\kappa_1} \quad [A.21]$$

$$\frac{\partial f_1(x)}{\partial I_{3a}} = \frac{1}{\kappa_1} \quad [A.22]$$

$$\frac{\partial f_2(x)}{\partial I_{1a}} = \frac{1}{\kappa_1} + \frac{1}{\kappa_2} \quad [A.23]$$

$$\frac{\partial f_2(x)}{\partial I_{2a}} = \frac{1}{\kappa_1} + \frac{1}{\kappa_2} + \frac{\tau_{2,Fe}}{\left(I_{2a} + I_{2a,uncoupled}\right)\ln(10)} \quad [A.24]$$

$$\frac{\partial f_2(x)}{\partial I_{3a}} = \frac{1}{\kappa_1} + \frac{1}{\kappa_2} \quad [A.25]$$

$$\frac{\partial f_3(x)}{\partial I_{1a}} = \frac{1}{\kappa_1} + \frac{1}{\kappa_2} + \frac{1}{\kappa_3} \quad [A.26]$$

$$\frac{\partial f_3(x)}{\partial I_{2a}} = \frac{1}{\kappa_1} + \frac{1}{\kappa_2} + \frac{1}{\kappa_3} \qquad [A.27]$$

$$\frac{\partial f_3(x)}{\partial I_{3a}} = \frac{1}{\kappa_1} + \frac{1}{\kappa_2} + \frac{1}{\kappa_3} + \frac{\tau_{3,Fe}}{\left(I_{3a} + I_{3a,uncoupled}\right)\ln(10)} \qquad [A.28]$$

Combining equations A.20 to A.28 produces the following Jacobian matrix for a three segment anode:

$$J_f = \begin{bmatrix} \frac{1}{\kappa_1} + \frac{\tau_{1,Fe}}{I_{1a}\log(10)} & \frac{1}{\kappa_1} & \frac{1}{\kappa_1} \\ \frac{1}{\kappa_1} & \frac{1}{\kappa_1} + \frac{1}{\kappa_2} + \frac{\tau_{2,Fe}}{I_{2a}\log(10)} & \frac{1}{\kappa_1} + \frac{1}{\kappa_2} \\ \frac{1}{\kappa_1} & \frac{1}{\kappa_1} + \frac{1}{\kappa_2} & \frac{1}{\kappa_1} + \frac{1}{\kappa_2} + \frac{1}{\kappa_3} + \frac{\tau_{3,Fe}}{I_{3a}\log(10)} \end{bmatrix} \qquad [A.29]$$

Equation A.29 can be generalized to the matrix shown as Equation A.30 below:

$$J_f = \begin{bmatrix} -\frac{1}{\kappa_1} - \frac{\tau_{1a,Fe}}{\ln(10)(I_{1a} + I_{1a,uncoupled})} & -\frac{1}{\kappa_1} & -\frac{1}{\kappa_1} & \cdots & -\frac{1}{\kappa_1} \\ -\frac{1}{\kappa_1} & -\sum_{j=1}^{2}\frac{1}{\kappa_j} - \frac{\tau_{2a,Fe}}{\ln(10)(I_{2a} + I_{2a,uncoupled})} & -\sum_{j=1}^{2}\frac{1}{\kappa_j} & \cdots & -\sum_{j=1}^{2}\frac{1}{\kappa_j} \\ -\frac{1}{\kappa_1} & -\frac{1}{\kappa_1} - \frac{1}{\kappa_2} & -\sum_{j=1}^{3}\frac{1}{\kappa_j} - \frac{\tau_{3a,Fe}}{\ln(10)(I_{3a} + I_{3a,uncoupled})} & \cdots & -\sum_{j=1}^{3}\frac{1}{\kappa_j} \\ \vdots & \vdots & \vdots & \vdots & \vdots \\ -\frac{1}{\kappa_1} & -\frac{1}{\kappa_1} - \frac{1}{\kappa_2} & -\frac{1}{\kappa_1} - \frac{1}{\kappa_2} - \frac{1}{\kappa_3} & \cdots & -\sum_{j=1}^{n}\frac{1}{\kappa_n} - \frac{\tau_{na,Fe}}{\ln(10)(I_{na} + I_{na,uncoupled})} \end{bmatrix} \qquad [A.30]$$

Using this process, the Jacobian matrix was developed as segments were added to the anodic side of the half-cell. A similar matrix was not required for the cathodic side as a direct solution was possible as the total current flow was known from the anodic calculations.

APPENDIX B. DISSOLVED OXYGEN

Mass transport of oxygen to the corroding surface occurs by two processes, namely, diffusion in the gas phase or diffusion in the liquid phase. The complicating issue is that consumption of oxygen on the corroding surface occurs from the liquid phase while the mass transport of oxygen to the corroding surface is a blend of diffusion through gas and liquid phases. Therefore, an approach to deal with these different phases is required in order that the two-dimensional model that assumes a homogeneous material can be used.

The relationships that describe the interaction of oxygen between these phases include the ideal gas law:

$$PV = nRT \qquad [B.1]$$

Where P is the partial pressure of the gas in Pa, V is the volume (m3), n is the number of moles of gas, R is the ideal gas constant and T is the temperature in Kelvin. Since we are interested in the oxygen content of the air (mol/m^3) in contact with the concrete and pore solution, Equation B.1 can be re-written as:

$$P_{O_2} = [O_2]_g RT \qquad [B.2]$$

Where P_{O_2} is the partial pressure of oxygen above the pore solution in Pa, and $[O_2]_g$ is the oxygen concentration in the atmosphere in mol/m^3.

Since oxygen will be in equilibrium between the gas and liquid phases Henry's Law will be used to establish the relationship between the partial pressure of oxygen in the pore space with the dissolved oxygen in the pore solution as follows:

$$P_{O_2} = \frac{[O_2]_d}{H} \qquad [B.3]$$

H is Henry's constant for the pore solution (Pa•m^3/mols), and $[O_2]_d$ is the dissolved oxygen concentration in mols/m^3.

The 2 dimensional model employed for evaluating oxygen transport to the corroding surface assumes a homogeneous material is present between the atmosphere and the bar. However, concrete consists of solid and pore phases that complicate the transport modeling, as oxygen is present in the pore phases only (Huet et al. 2004). Therefore, a relationship is required which converts oxygen concentration within the pore phase to the global oxygen content of the concrete including the solid phase. In this way, the 2 dimensional based on a homogeneous material can be employed to simulate the transport of oxygen to the corroding surface. The model employed for this relationship is based on (Papadakis et al. 1991 and Huet et al. 2004):

$$[O_2]_{blended} = \phi\left(PS[O_2]_d + (1-PS)[O_2]_g\right) \qquad [B.4]$$

Where $[O_2]_{blended}$ is the oxygen content in mol/m^3 for the concrete volume, ϕ is the pore volume relative to the concrete volume, PS is the pore saturation, $[O_2]_d$ is the dissolved oxygen concentration in the pore solution, and $[O_2]_g$ is the oxygen concentration in the gaseous phase within the pore structure.

The cathodic corrosion process reduces oxygen contained within the pore solution, therefore, a relationship between the oxygen concentrations within the pore solution and the bulk concrete is necessary. Combining Equations B.2, B.3 and B.4 and writing in terms of the blended oxygen content and dissolved oxygen contents we arrive at the following relationship:

$$[O_2]_d = \frac{[O_2]_{blended}}{\phi\left(PS + \frac{(1-PS)}{RTH}\right)} \qquad [B.5]$$

Equation B.5 is used to convert the bulk oxygen concentrations which are simulated within the two-dimensional model to the available oxygen within the pore solution on the bar/concrete interface.

APPENDIX C. ALGORITHMS

C.1 Introduction

All code presented in this Appendix was produced using MATLAB version R2009 and the Partial Differential Equation Tool Box. Execution of this code, requires the function titled “constants” to be updated to reflect the geometry of the model, material properties, and relative humidity conditions. Currently, kinetics of corrosion data is set in accordance with the data published by Moreno et. al (2004) in the routine labeled “kineticsSlab”. Diffusion coefficients are set in the “coefficients” function.

Once the appropriate values are identified the main program titled “FBASlabOxygen” can be executed to produce the simulation results.

C.2 anode_coupling

```
function [ix_all,i_anodic,ecorr]=anode_coupling(ecorr,k,icorr,kg,start,stop,step,cv,perror)

%Function to iteratively solve the system of nonlinear equations describing the flow of
%ions through the electrolyte between two corrosion cells. Equations to solve are based
%on the following simplified formulas which ignore concentration effects as it is assumed
%that the concrete pore solution will buffer any production or consumption of OH-.
%
%Equation 1 - Represents the potential drop from the transition to the bar surface on
Segment 1
%         i1 + i2 + i3                i1
%Eq1 = ------------ + tafel*log---- + C1 - etransition + euncoupled1
%          k1                       i1uc
%
%Equation 2 - Represents the potential drop from the transition to the bar surface on
Segment 2
%         i1+i2+i3       i2+i3                  i2
%Eq2 = ------------ + --------- + tafel*log---- + C1 + C2 - etransition + euncoupled2
%           k1             k2                  i2uc
%
%Equation 3 - Represents the potential drop from the transition to the bar surface on
Segment 2
%         i1+i2+i3      i2+i3       i3                 i3
%Eq3 = ------------ + -------- + --- + tafel*log---- + C1 + C2 + C3 - etransition +
euncoupled3
%           k1              k2       k3              i3uc
%
%Where:
%       i1uc + i2uc + i3uc
%C1 = - -------------------
%             k1
```

```
%
%       i2uc + i3uc
%C2 = - ------------
%          k2
%
%       i3uc
%C3 = - ------
%        k3
%
%Initially, the system assumes that one segment will contribute current to
%the anode.  This simple system allows for the direct solution of icorr.
%If icorr is greater than iuncoupled, then another segment is added using
%icorr from the first segment to initiate the calculations and solve for
%icorr from the second segment.  The resulting icorr from the second
%segment is then used to determine the potential drops within the first
%segment which changes the icorr from the first segment.  Iterations are
%performed until the current calculation resulting from the inclusion of
%the second segment produces the correct potential drops across the circuit
%to match the current produced from the second segment.

%Preallocate arrays for speed.

ix_all=zeros(cv.segments,1);
slope=ix_all;
y_int=ix_all;
guess.high=icorr.uncoupled(start.anode);
ecorr.coupled=ecorr.uncoupled; %Set coupled to be equal to uncoupled and
                               %only change segments which are coupled.
potentials.IRDrop=ix_all;
potentials.eCoupled=ecorr.uncoupled;
first_coupled=start.anode;
last_coupled=start.anode-step.anode;

%Start loop to check each node in series starting from the start.anode and
%increasing until the node becomes uncoupled or we run into the stop.anode
%criteria.

while last_coupled~=stop.anode

   %Increment node.

   last_coupled=last_coupled+step.anode;

   %For first set of calculation use the previous segment as the starting
   %point.  Output will set the maximum and minimum boundaries for the
   %current being generated at each segment.

         cumulativeIRDrop=potentials.IRDrop(end);

         %Calculate the current flow generated at this node using the
         %current flow generated at the previous nodes as fixed values.  If
```

```
        %potentials differences exist calculate the new current.  Otherwise
        %pass.

if ecorr.transition-ecorr.uncoupled(last_coupled)>cumulativeIRDrop

    %Sufficient potential exists for coupling to occur.

    [ix_all(last_coupled),slope,y_int]=anode_solver(kg,last_coupled,...
        ecorr,k,cumulativeIRDrop,icorr.uncoupled,slope,y_int,guess);

    %Determine potential drops through the electrolyte and corrosion cell.

    [ratio,potentials]=compare(ix_all,first_coupled,last_coupled,k,...
        slope,y_int,icorr,perror,ecorr);

else

    %Insufficient potential differences exist to permit coupling at
    %this segment.  If this is the first segment, increment
    %first_coupled and check if next segment can couple.  If this is
    %not the first segment, then return to current balance algorithm.

    ix_all(last_coupled)=0;

    if first_coupled==start.anode && ix_all(last_coupled-step.anode)==0

        %Increment first coupled.

        first_coupled=first_coupled+step.anode;

        start.anode=first_coupled;

        %Set ratio to zero.

        ratio=0;

        %Set potential drop through the electrolyte to zero.

        potentials.term1=0;

    else

        %Potential drops through the electrolyte have now exceeded the
        %potential difference along the bar so exit the loop.

        break;

    end

end
```

```
%Check if error limits on the ratio between the potential drops through
%the electrolyte versus the corrosion cell potential drops have been
%met.

while numel(find(ratio>0))>0

   %Error limits have not been met so create the jacobian matrix which
   %doesn't change with changes to the current.  J is an r x r matrix
   %where r is the number of segments on the anodic side.  If during
   %adjustment, negative values result, these are kept in to complete
   %the balancing and then zeroed out as the do not generally
   %contribute a significant amount of current to the overall result.

   j=jacobianMain(last_coupled,first_coupled,step.anode,k);

      %Create the diagonal portion of the jacobian which changes as
   %the current flows change.  First check if we have anode over
   %cathode or cathode over anode.

   if start.anode>last_coupled

      %We have an anode over the cathode.

      slopeFlipped=flipud(slope);
      icorrFlipped=flipud(icorr.uncoupled);
      ixAllFlipped=flipud(ix_all);

      %Reset start and ending points.

      firstSegment=cv.segments+1-first_coupled;
      lastSegment=cv.segments+1-last_coupled;

      %Establish j_diag for the modified matrices.

      j_diag=slopeFlipped(firstSegment:lastSegment)./(2.303*...
            (icorrFlipped(firstSegment:lastSegment)...
            +ixAllFlipped(firstSegment:lastSegment)));

   else

      %We have a cathode over an anode.

      j_diag=slope(first_coupled:last_coupled)./(2.303*...
            (icorr.uncoupled(first_coupled:last_coupled)...
            +ix_all(first_coupled:last_coupled)));

   end

   %Find the number of rows/columns in the jacobian as this is used to
   %duplicate the diagonals a sufficient number of times.
```

```
cols=abs(last_coupled-first_coupled)+1;

%Create a matrix of the values that will form the diagonal.

j_diag=repmat(j_diag,1,cols);

%Only take the values on the diagonal.

j_diag=eye(cols).*j_diag;

%Assemble the final jacobian from the matrix of k's which don't
%change with current and the diagonal which changes with current.

j_working=-j-j_diag;

%Establish the change in current flow identified by the
%Jacobian.

delta_i=j_working\potentials.Equation;

%Save ix_all prior to modifying as we may need to go back and
%modify if negative values occur.

ix_working=ix_all;

%Modify ix_all using the established current flow modifications.
%As part of the modification, check if negative currents will be
%created and if so, modify the adjustment to ensure we move slowly
%to the correct value otherwise negative values cause the program
%to fail!

%Check if we have anode over cathode or cathode over anode.

if start.anode>last_coupled

   %We have an anode over cathode.  Establish adjustment factors
   %for each segment.

   adjust=adjustment(icorrFlipped(firstSegment:lastSegment),...
      ixAllFlipped(firstSegment:lastSegment),delta_i);

   %Apply adjustment factor.

   ixAllFlipped(firstSegment:lastSegment)=...
      ixAllFlipped(firstSegment:lastSegment)+adjust*delta_i;

   %Now flip adjusted values back.

   ix_working=flipud(ixAllFlipped);

else
```

```
        %We have a cathode over anode. Establish adjustment factors
        %for each segment.

        adjust=adjustment(icorr.uncoupled(first_coupled:last_coupled),...
           ix_working(first_coupled:last_coupled),delta_i);

        %Apply adjustment factor.

        ix_working(first_coupled:last_coupled)=...
              ix_working(first_coupled:last_coupled)+adjust*delta_i;

    end

    %ix_all for future calculations.

    ix_all=ix_working;

    %Check if current adjustments have resulted in meeting the
    %tolerances.

    [ratio,potentials]=compare(ix_all,first_coupled,...
              last_coupled,k,slope,y_int,icorr,perror,ecorr);

end

%Check if adjustments have resulted in negative values being
%generated. If so, then eliminate negative values and modify the first
%coupled accordingly.

if numel(find(ix_all<0))>0

    %Set all negative values to zero.

    ix_all(ix_all<0)=0;

    %Reset the location for first_coupled as this sets the size of the
    %jacobian and other functions for future calculations.

    if start.anode>last_coupled

        %We have anode over cathode.

        first_coupled=find(ix_all>0,1,'last');

    else

        %We have cathode over anode.

        first_coupled=find(ix_all>0,1,'first');
```

```
        end

        %Update potential drops.

        [ratio,potentials]=compare(ix_all,first_coupled,...
                last_coupled,k,slope,y_int,icorr,perror,ecorr);

    end

    %Set guess for next round.

    if ix_all(last_coupled)==0

        guess.high=1e-14;

    else

        guess.high=ix_all(last_coupled);

    end

end

i_anodic=sum(ix_all);

%Find which segments have coupled.

coupledSegments=ix_all>0;

%Find total current in these segments.

totalCoupledCurrent=ix_all+icorr.uncoupled;

%Update ecorr.coupled.

ecorr.coupled(coupledSegments)=slope(coupledSegments)...
    .*log10(totalCoupledCurrent(coupledSegments))+y_int(coupledSegments);

%
end
%
%
%
function [ratio,pot]=compare(ix_all,first_coupled,last_coupled,...
    k,slope,yIntercept,icorr,perror,ecorr)

%Routine to calculate the potential drops through the electrolyte and
%overpotential caused by the corrosion couple by solving the potential drop
%equations on the bar surface.  Three terms are created as follows:
%
%Term 1 - This term represents the potential drops through the electrolyte.
```

```
%Term 2 - This term represents the coupled potential.
%
%These terms are summed together and the result must be within the
%error tolerance, otherwise we go to the jacobian matrix to search for a
%solution.

%Determine if we have an anode over cathode cell or a cathode over anode
%cell.

if first_coupled>last_coupled

   %We have an anode over cathode cell configuration therefore, flip the
   %input information so that we have the information properly aligned.

   ixAll=flipud(ix_all(last_coupled:first_coupled));
   slopeModified=flipud(slope(last_coupled:first_coupled));
   yInterceptModified=flipud(yIntercept(last_coupled:first_coupled));
   iUncoupled=flipud(icorr.uncoupled(last_coupled:first_coupled));
   kModified=flipud(k.each(last_coupled:first_coupled));

else

   %We have a cathode over anode cell configuration.

   ixAll=ix_all(first_coupled:last_coupled);
   slopeModified=slope(first_coupled:last_coupled);
   yInterceptModified=yIntercept(first_coupled:last_coupled);
   iUncoupled=icorr.uncoupled(first_coupled:last_coupled);
   kModified=k.each(first_coupled:last_coupled);

end

%Develop Term 1 - Potential Drops Through the Electrolyte.

pot.IRDrop=firstTerm(ixAll,kModified);

%Develop Term 2 - Coupled potential on the bar surface.

pot.eCoupled=slopeModified.*log10(ixAll+iUncoupled)+yInterceptModified;

%Final equation equals term1 + term2.

pot.Equation=pot.IRDrop+pot.eCoupled-ecorr.transition;

%Identify if results are within error tolerance.

ratio=abs(pot.Equation)>perror.pot;

end
%
%
```

```
%
function term1=firstTerm(ixAll,kEach)

%Function to create the first term of the potential equation which
%represents the potential drop through the electrolyte.

%Identify the size of the matrices passed.

rows=size(ixAll,1);

%Create term1.

term1=zeros(rows,1);

%Start loop to calculate the potential drops created through the
%electrolyte.

for row=1:rows

   %Check if we are at the first row.

   if row==1

      %First term so create the first segment.

      term1(row)=sum(ixAll(row:rows))/kEach(row);

   else

      %We are passed the first term so add subsequent terms to this term.

      term1(row)=sum(ixAll(row:rows)/kEach(row))+term1(row-1);

   end

end

end
%
%
%
function j=jacobianMain(lastCoupled,firstCoupled,segmentStep,k)

%Routine to build the jacobian matrix related to the Newton Ralphson method
%of solving non-linear simultaneous equations.  Only the portion related to
%the IR drop through the electrolyte is considered at this time.  The
%potential drops caused by the overpotential at each segment are added in
%later.

%The matrix will take the form of:
%
```

```
%|-1/k1  -1/k1 ---------------------------------------- -1/k1 |
%|-1/k1  -1/k1-1/k2 ------------------------------ -1/k1-1/k2 |
%|-1/k1  -1/k1-1/k3 -1/k1-1/k2-1/k3 -------------1/k1-1/k2-1/k3 |
%|  | ---------------------------------------          |      |
%|-1/k1  -1/k1-1/k2 -1/k1-1/k2-1/k3 --------- -1/k1-1/k2...-1/kn|

%Identify counters.

counter=1;

%Determine size of matrix.  Since we can have cathode over anode or anode
%over cathode we need to check for which one we have and select
%accordingly.

numberRows=abs(lastCoupled-firstCoupled)+1;

%Create initial matrix

k_row=repmat(1/k.all(firstCoupled),1,numberRows);
k_col=repmat(1/k.all(firstCoupled),numberRows-1,1);
j=[k_row;[k_col,zeros(numberRows-1)]];

%Assemble remainder of 1/k matrix.

for segment=firstCoupled+segmentStep:segmentStep:lastCoupled

   %Start counter.

   counter=counter+1;

   %Create the row and columns which have the correct k values.

   k_row=repmat(1/k.all(segment),1,numberRows-counter+1);
   k_col=repmat(1/k.all(segment),numberRows-counter,1);

   %Create the main k-matrix using the above row and column.

   j=j+[zeros(counter-1,numberRows);[zeros(1,counter-1),k_row];...
      [zeros(numberRows-counter,counter-1),[k_col,zeros(numberRows-
counter,numberRows-counter)]]];

end

end
%
%
%
function adjFactor=adjustment(iUncoupled,deltaICoupled,deltaI)

%Routine to modify adjustment factors to ensure negative values do not
%occur.
```

```
deltaAdjust=(iUncoupled+deltaICoupled)./abs(deltaI);

%Select the smallest adjustment factor.  First find the smallest value that
%we have to round.

minValue=min(deltaAdjust);

%Take the log of the minValue;

logMinValue=log10(minValue);

%Rounddown if positive, round up if negative.

if logMinValue>0

   %Create adjustment coefficient.

   adjCoefficient=floor(logMinValue)-1;

else

   %Create adjustment factor.

   adjCoefficient=-(ceil(abs(logMinValue))+1);

end

%Create adjustment factor.

adjFactor=floor(minValue/10^adjCoefficient)*10^adjCoefficient;

%Ensure the smallest adjustment factor is no greater than 1.

if adjFactor>1

   adjFactor=1;

end

end
```

C.3 anode_solver

```
function
[icorr_c,slope,y_int]=anode_solver(kg,segment,ecorr,k,conc,i_uc,slope,y_int,guess)

%Function to build the non-linear system of equations to solve for the
%current flow that is created at each segment.
%   e=structured variable with the critical potentials at each segment:
%          ecorr.transition=potential at the transition between the anode and cathode.
```

```
%         ecorr.uncoupled=uncoupled potentials at each segment.
%   corrosion=structured variable with constants that are used in the
%   calculations below:
%         corrosion.r= gas constant
%         corrosion.t= temperature in kelvin
%         corrosion.faraday = faraday's constant.
%   k_s=matrix of solution conductivities for each segment.
%   conc=potential drop in each segment due to differences in ionic
%   concentrations between segments.
%   i_uc=uncoupled corrosion current for each segment.
%   ecorr.uncoupled=uncoupled potentials for each segment.
%   anodic_counter=counter which indicates how many segments are being
%   evaluated at this cycle.
%   icorr_c=coupled corrosion current.
%   icorr_delc=difference between the coupled and uncoupled corrosion
%   current.
%   potential_c=coupled potential at the cell/electrolyte interface.


%Anodic current is calculated using:
%ecorr.transition-Elim=conc drop+ohmic drop+corrosion drop for each segment
%that is contributing current.
%Where
%              F
%   Conc Drop = --- sum(zjDjdelCj)
%              k
%              i_c-i_uc
%   ohmic Drop = ----------
%                 k
%                        i_c
%   Corrosion Drop = ts log -----
%                       i_uc
%where:
%   Etransition = current potential at the between the anode and
%   cathode.
%   Elim = corrosion potential at the limiting current density
%   F = faraday's constant.
%   k= conductivity of the solution.
%   zjDjdelCj = concentration flux between adjacent nodes.
%   i_c = coupled corrosion current density at the segment.
%   i_uc = uncoupled corrosion current density at the segment.
%   ts= tafel slope of the anodic reaction.

%Set the tolerance.

optim=optimset('TolX',2*eps(i_uc(segment)));

%Set guess.high if the current guess.high=0.

%if guess.high==0
```

```
%    guess.high=1e-14;

%end

%Since there are two curves describing the anodic reactions we must
%check which curve we are on.

if ecorr.transition-conc>=kg.e_int(segment)

   %Potentials are above the intersection of the two curves so use Curve 2
   %geometry but check to see if IR drop is sufficient to cause
   %potentials to fall into Curve 1.

   equation=@(i_c)i_c+i_uc(segment)-10^((ecorr.transition-conc-i_c/k.all(segment)...
            -kg.b2(segment))/kg.m2(segment));

   icorr_c=fzero(equation,guess.high,optim);

   %Check if IR drop has caused e_couple to fall below e_int. If it has
   %then Curve 1 geometry will govern.

   e_couple=kg.m2(segment)*log10(icorr_c+i_uc(segment))+kg.b2(segment);

   %Check if negative value is present...if so, then skip to end and set
   %to zero.

   if icorr_c>0

      if e_couple<kg.e_int(segment)

         %Then use Curve 1 geometry and recalculate icorr_c.

         equation=@(i_c)i_c+i_uc(segment)-10^((ecorr.transition-conc-
i_c/k.all(segment)...
                  -kg.b1(segment))/kg.m1(segment));

         icorr_c=fzero(equation,guess.high,optim);

         slope(segment)=kg.m1(segment);

         y_int(segment)=kg.b1(segment);

      else

         %Pass corresponding slope back to the main program as this is used
         %in subsequent calculations.

         slope(segment)=kg.m2(segment);

         y_int(segment)=kg.b2(segment);
```

```
        end

    end

else

    %Potentials are below the intersection of the two curves so use Curve 1
    %geometry.

    equation=@(i_c)i_c+i_uc(segment)-10^((ecorr.transition-conc-i_c/k.all(segment)...
            -kg.b1(segment))/kg.m1(segment));

    icorr_c=fzero(equation,guess.high,optim);

    %Pass corresponding slope back to the main program as this is used
    %in subsequent calculations.

    slope(segment)=kg.m1(segment);

    y_int(segment)=kg.b1(segment);

end

%Check if returning value is negative.  If a negative value results this is
%an indication that insufficient potential differences exist between the
%transition and the segment to permit coupling to occur.  Set this value to
%zero and subsequent calculations will need to be modified accordingly.

if icorr_c<0

    icorr_c=0;

end

end
```

C.4 blendedO2

```
function corrosion=blendedO2(corrosion)

%[O2]blended=Porosity x (PS x [O2]d + (1-PS) x [O2]g)
%where:
    %Porosity = is the concrete porosity from Figure 3 of Zhitnikov, Y.,
    %Mozhegov, N., Matrosova, Y., 2002, Physicochemical measurements,
    %determining the porosity of concrete, Measurement Techniques,
    %45:305-310
    %PS = degree of pore saturation from figure 6, Papadakis, V., Vayenas,
    %C., Fardis, M., 1991, Physical and chemical characteristics affecting
    %the durability of concrete, American Concrete Institute Materials
    %Journal,8:186-196.
```

```
   %[O2]g = 9.35 x 10-6 mmol/mm3 (assuming 20.95% O2 in atmosphere.
   %[O2]d = 2 x 10-8 mmol/mm3 from Zhang et al 2009 as outlined above.

corrosion.PS=corrosion.PSslope*corrosion.RH+corrosion.PSintercept;

corrosion.o2=corrosion.porosity*(corrosion.PS*...
   corrosion.dissolvedO2+(1-corrosion.PS)*corrosion.gasO2);
corrosion.saturation=corrosion.o2;

end
```

C.5 boundary_column_add_zeros

```
function [new_column_revised]=boundary_column_add_zeros(new_column,new_row)

%Routine to add rows to the new boundary condition column before merging
%with the old boundary condition matrix.

%Find out how big the new column is.

old_row=size(new_column);

%Subract the old number of rows from the new number of rows required.

number_zeros=new_row-old_row(1);

%Create new column of rows filled with zeros.

add_row=zeros(number_zeros,1);

%Create new column with the correct number of rows.

new_column_revised=[new_column;add_row];
```

C.6 boundary_column

```
function [bc]=boundary_column(bc, dirichlet, dimension, column, values)

%Subroutine to create one column of the boundary condition matrix.
%Values used are:
%   dirichlet   = boundary type
%                 0=dirichlet;
%                 1=neumann.
%   dimension   = 1 as one dimension, 2 as two dimensions.
%   column      = column we are creating.
%   values      = values to be used at the boundary for the dirichlet or neumann
%                 boundaries.

%   bc=boundary condition matrix.  Number of columns equates to the number
%   of different boundary elements.  Each row describes the boundary
%   conditions as follows:
```

```
%   Row 1=number of dimensions N.
%   Row 2=number of dirichlet boundary conditions if 0 then only neumann.
%   Row 3=length of string for q.
%   Row 4=length of string for g.
%   Row 5=length of string for h.
%   Row 6=length of string for r.

%Check if Dirichlet or Neumann

if dirichlet==1 %Then its a dirichlet boundary condition.

   %Convert numeric value to string value.

   q_val=abs(num2str(values(1)))';
   g_val=abs(num2str(values(2)))';
   h_val=abs(num2str(values(3)))';
   r_val=abs(num2str(values(4)))';

   %Determine size of each string.

   h_size=size(h_val);
   r_size=size(r_val);
   q_size=size(q_val);
   g_size=size(g_val);

   %Create new boundary condition column.
   new_column=…
         [dimension;dirichlet;q_size(1);g_size(1);h_size(1);r_size(1);q_val;g_val;h_val;r_v
al];

   %Compare new column to old boundary matrix and add zeros as required to
   %keep both old and new with a consistent number of rows.

   bc=boundary_modify_column(bc,new_column,column);

else %Then its a neumann boundary condition.

   %Convert numeric value to string value.

   q_val=abs(num2str(values(1)))';
   g_val=abs(num2str(values(2)))';
   row_7=abs(num2str(0))';
   row_8=abs(num2str(0))';
   row_9=abs(num2str(1))';
   row_10=abs(num2str(0))';

   %Determine size of each string.

   q_size=size(q_val);
   g_size=size(g_val);
```

```
   %Create new boundary condition column.

new_column=[dimension;dirichlet;q_size(1);g_size(1);q_val;g_val;row_7;row_8;row_9;ro
w_10];

   %Compare new column to old boundary matrix and add zeros as required to
   %keep both old and new with a consistent number of rows.

   bc=boundary_modify_column(bc,new_column,column);

end
```

C.7 boundary_matrix_add_zeros

```
function [bc_revised]=boundary_matrix_add_zeros(bc,new_row)

%Subroutine to add zeros to the original boundary matrix so that it is
%dimensionally the same as the new boundary to be added.

%   bc = boundary condition matrix to be modified.
%   new_row=number of rows in the new column to be added.

%Determine size of the old matrix.

[bc_row,bc_col]=size(bc);

%Subtract the boundary condition number of rows from the new columns rows.

number_zeros=new_row-bc_row;

%Create matrix of zeros to be added to the old boundary condition matrix.

add_row=zeros(number_zeros,bc_col);

%Create new boundary condition matrix with the correct number of rows.

bc_revised=[bc;add_row];

end
```

C.8 boundary_modify_column

```
function [bc]=boundary_modify_column(bc,new_column,column_number)

%Subroutine to check if new and old boundary condition matrix is of the
%same size and if not modify either the old matrix or new column.

%   bc = boundary condition matrix
```

```
%   new_column = new column of values to be added to the bc.
%   column_number = column number we are working in.

[number_rows_bc]=size(bc);
[new_row]=size(new_column);

if column_number==1 %Then this is the first column so no modification required.

      bc=new_column;

   elseif new_row(1)==number_rows_bc(1);
     %If the new and old are the same size then just add the new column.

      bc(:,column_number)=new_column;

   elseif new_row(1)>number_rows_bc(1)
     %If new column is bigger than old then add zeros to the old matrix.

      bc=boundary_matrix_add_zeros(bc,new_row(1));

      bc(:,column_number)=new_column;

   else %If new column is smaller than old then add zeros to new.

      new_column=boundary_column_add_zeros(new_column,number_rows_bc(1));

      bc(:,column_number)=new_column;

end
```

C.9 boundaryNodesSlab

```
function [nodes]=boundaryNodesSlab(p,e,slab)

%Subroutine to sort the boundary nodes around the bar, surface and at
%normal testing depths so that the results can be plotted.
%p = point matrix - First and second rows contain x- and y-coordinates of
%the points in the mesh.
%e = edge matrix - First and second rows contain indices of the starting and
%ending point, the third and fourth rows contain the starting and ending
%parameter values, the fifth row contains the edge segment number,
%and the sixth and seventh row contain the left- and right-hand side
%subdomain numbers.
%nodes.bar = sorted array with nodes starting on the top and ending on the
%bottom of the bar.
%nodes.distance = location of each node on the perimeter of the bar
%starting on the top at "0" and ending on the bottom.
%nodes.surface= sorted array of nodes along the top surface which is used
%in later components to plot the surface potential.
%nodes.sample_x=range of nodes which are used to determine chloride
```

```
%concentrations at the typical sampling depths used in practice.

nodes.bar=sortrows(e',5);

%Find all rows within nodes.bar which are on line elements that are at 21
%or higher as these are the elements which form the bar.

row=find(nodes.bar(:,5)>=21);

m=size(row);

%Select only nodes on the bar

nodes.bar=unique([nodes.bar(row(1):row(m,1),1);nodes.bar(row(1):row(m,1),2)]);

%Attache x and y coordinate to each node on the bar boundary.

nodes.bar=[nodes.bar,p(1,nodes.bar)',p(2,nodes.bar)'];

%Sort on the y coordinate from highest to lowest as this represents the
%node sequence which starts at the top and rotates towards the bottom.

nodes.bar=sortrows(nodes.bar,-3);

%Determine spacing of nodes around the bar circumference and return values
%to main program.

m=size(nodes.bar,1);

x2=nodes.bar(2:m,2);
x1=nodes.bar(1:m-1,2);

y2=nodes.bar(2:m,3);
y1=nodes.bar(1:m-1,3);

nodes.distance=linspace(1,m-1,m-1)';

nodes.distance=[0;nodes.distance.*((x2-x1).^2+(y2-y1).^2).^.5];

%Return the node sequence along the bar circumference.

nodes.bar=nodes.bar(:,1);

%Sort nodes that form the top surface boundary.

%All nodes that intersect the top surface boundary are at the maximum
%height of the model.  Therefore, sort the point matrix along row 2
%which is the y position for each node.

surface=find(p(2,:)==slab.thickness);
```

```
surface=[surface;p(1,surface)]';

nodes.surface=sortrows(surface,-2);

nodes.surface(:,2)=slab.bar_spacing/2-nodes.surface(:,2);

%Determine nodes in within the chloride sampling areas which are 10 mm wide
%(representing a 20 mm drill bit) and taken at the following depths.
%   Depth 1 = 10 to 25 mm depth
%   Depth 2 = 50 to 65 mm depth
%   Depth 3 = 100 to 115 mm depth
%All nodes within this volume of 10 x 15 mm will be averaged in future
%calculations and compared to the chlorides that exist around the bar.

%Model has the height of the slab starting at the lower right so convert
%the sample depths to a dimension measured from the bottom of the slab.

depth_10=slab.thickness-10;
depth_25=slab.thickness-25;
depth_50=slab.thickness-50;
depth_65=slab.thickness-65;
depth_100=slab.thickness-100;
depth_115=slab.thickness-115;

%Sort the nodes that form the boundary at the edge of the sample
%zone.

sample_x2=find(p(1,:)<=10);

%Find nodes that fall between the edge at '0' and the sample width of '10'.

sample=[sample_x2;p(2,sample_x2)]';

sample=sortrows(sample,-2);

%Locate the nodes that fall within the sample depths identified above.

nodes.sample_1=sample(sample(:,2)<=depth_10 & sample(:,2)>=depth_25);

nodes.sample_2=sample(sample(:,2)<=depth_50 & sample(:,2)>=depth_65);

nodes.sample_3=sample(sample(:,2)<=depth_100 & sample(:,2)>=depth_115);

end
```

C.10 boundarySlab

```
function [bc]=boundarySlab(species,segments,g,corrosion)

%Routine to establish boundary conditions.
```

```
%   species=boundary condition species as follows:

%   1=  chloride - all surfaces are neumann except for the top surface.
%   2=  oxygen - all surfaces are neumann except for the top and bottom
%       surface which are at a fixed value and the bar surface which varies
%       with the corrosion rate.
%   3=  hydroxide - all surfaces are neumann except for the bar surface
%       which is dirichlet and varies with corrosion rate.
%   4=  Fe2+ - same as hydroxide.
%   100 = Used for determining the potential within the model space.
%   number_boundary=number of different boundary conditions.
%   bc=boundary condition matrix.  Number of columns equates to the number
%   of different boundary elements.  Each row describes the boundary
%   conditions as follows:
%   Row 1=number of dimensions N.
%   Row 2=number of dirichlet boundary conditions if 0 then only neumann.
%   Row 3=length of string for q.
%   Row 4=length of string for g.
%   Row 5=length of string for h.
%   Row 6=length of string for r.

%Dimension is equal to 1 for all exterior portions of the model and 0 for
%the boundary's related to the chloride sample locations.

bc=0;

switch species

   case 1 %Chloride boundary conditions.

      %Set boundary 1 - bottom of slab.  For all dirichlet conditions,
      %you must include a value(3) and value(4) to setup the boundary
      %condition file properly. If neumann conditions, then only
      %values(1) and values(2) required.

      dimension=1;
      dirichlet=0;
      column=1;
      values(1)=0;
      values(2)=0;
      values(3)=1;
      values(4)=0;

      %Create first column in the boundary condition file.

      bc=boundary_column(bc,dirichlet,dimension,column,values);

      %Set boundary 2 - top surface exposed to chlorides.

      dimension=1;
      dirichlet=1;
```

```
  column=2;
  values(1)=0;
  values(2)=0;
  values(3)=1;
  values(4)=corrosion.expressed;

  %Create second column in the boundary condition file.

  bc=boundary_column(bc,dirichlet,dimension,column,values);

  %Create third through eleventh column which are related to the
  %chloride sample locations.

  for i=3:11

     dimension=0;
     dirichlet=0;
     column=i;
     values(1)=0;
     values(2)=0;
     values(3)=1;
     values(4)=0;

    %Create columns in the boundary condition file.

    bc=boundary_column(bc,dirichlet,dimension,column,values);

  end

  %Set remaining boundary conditions including the bar surface.

  for i=12:20+segments

     dimension=1;
     dirichlet=0;
     column=i;
     values(1)=0;
     values(2)=0;
     values(3)=1;
     values(4)=0;

     %Create remaining columns in boundary conditions matrix.

     bc=boundary_column(bc,dirichlet,dimension,column,values);
  end

case 2 %Oxygen boundary conditions.

  %Boundary conditions are set

  %Set boundary 1 - bottom of slab exposed to oxygen
```

```
dimension=1;
dirichlet=0;
column=1;
values(1)=0;
values(2)=0;
values(3)=1;
values(4)=0;

%Create first column in the boundary condition file.

bc=boundary_column(bc,dirichlet,dimension,column,values);

%Set boundary 2 - top surface exposed to oxygen.

dimension=1;
dirichlet=1;
column=2;
values(1)=0;
values(2)=0;
values(3)=1;
values(4)=corrosion.saturation;

%Create second column in the boundary condition file.

bc=boundary_column(bc,dirichlet,dimension,column,values);

%Create third through eleventh column which are related to the
%chloride sample locations.

for i=3:11

   dimension=0;
   dirichlet=0;
   column=i;
   values(1)=0;
   values(2)=0;
   values(3)=1;
   values(4)=0;

  %Create columns in the boundary condition file.

  bc=boundary_column(bc,dirichlet,dimension,column,values);

end

%Set boundary conditions on side surfaces which exclude the bar
%surface.

for i=12:20
```

```
        dimension=1;
        dirichlet=0;
        column=i;
        values(1)=0;
        values(2)=0;
        values(3)=1;
        values(4)=0;

        %Create remaining columns in boundary conditions matrix.

        bc=boundary_column(bc,dirichlet,dimension,column,values);
    end

    %Set boundary conditions on the bar.

    for i=1:segments

        %Create remaining columns in boundary conditions matrix.

        dimension=1;
        dirichlet=0;
        column=i+20;
        values(1)=0;
        values(2)=g(i,species);
        values(3)=1;
        values(4)=0;

        bc=boundary_column(bc,dirichlet,dimension,column,values);

    end

case 100 %Location for potential boundary conditions.

    %Create first column in the boundary condition matrix.

    bc=0;

    %All exterior faces of the model are neumann boundaries with 0
    %flux.  Portions of the model directly against the bar are
    %dirichlet using the boundary conditions established from the
    %ecorr_point from the Potential sub-routine.

    %Set boundary conditions to neumann for all boundaries.

    for i=1:2

        dimension=1;
        dirichlet=0;
        column=i;
        values(1)=0;
        values(2)=0;
```

```
    values(3)=1;
    values(4)=0;

    %Create remaining columns in boundary conditions matrix.

    bc=boundary_column(bc,dirichlet,dimension,column,values);

end

%Set boundaries around sample areas to dimension 0 so that they
%don't affect the calculations.

for i=3:11

    dimension=0;
    dirichlet=0;
    column=i;
    values(1)=0;
    values(2)=0;
    values(3)=1;
    values(4)=0;

    %Create remaining columns in boundary conditions matrix.

    bc=boundary_column(bc,dirichlet,dimension,column,values);

end

%Set boundary conditions for remaining elements except for the bar
%surface.

for i=12:20+segments

    dimension=1;
    dirichlet=0;
    column=i;
    values(1)=0;
    values(2)=0;
    values(3)=1;
    values(4)=0;

    %Create remaining columns in boundary conditions matrix.

    bc=boundary_column(bc,dirichlet,dimension,column,values);

end

for i=1:segments

    %Create remaining columns in boundary conditions matrix.
```

```
    dimension=1;
    dirichlet=1;
    column=i+20;
    values(1)=0;
    values(2)=0;
    values(3)=1;
    values(4)=g.coupled(i);

    bc=boundary_column(bc,dirichlet,dimension,column,values);

end

case 110 %Location for potential boundary conditions.

%Create first column in the boundary condition matrix.

bc=0;

%All exterior faces of the model are neumann boundaries with 0
%flux.  Portions of the model directly against the bar are
%dirichlet using the boundary conditions established from the
%ecorr_point from the Potential sub-routine.

%Set boundary conditions to neumann for all boundaries.

for i=1:2

    dimension=1;
    dirichlet=0;
    column=i;
    values(1)=0;
    values(2)=0;
    values(3)=1;
    values(4)=0;

    %Create remaining columns in boundary conditions matrix.

    bc=boundary_column(bc,dirichlet,dimension,column,values);

end

%Set boundaries around sample areas to dimension 0 so that they
%don't affect the calculations.

for i=3:11

    dimension=0;
    dirichlet=0;
    column=i;
    values(1)=0;
    values(2)=0;
```

```
        values(3)=1;
        values(4)=0;

        %Create remaining columns in boundary conditions matrix.

        bc=boundary_column(bc,dirichlet,dimension,column,values);

    end

    %Set boundary conditions for remaining elements except for the bar
    %surface.

    for i=12:20+segments

        dimension=1;
        dirichlet=0;
        column=i;
        values(1)=0;
        values(2)=0;
        values(3)=1;
        values(4)=0;

        %Create remaining columns in boundary conditions matrix.

        bc=boundary_column(bc,dirichlet,dimension,column,values);

    end

    for i=1:segments

        %Create remaining columns in boundary conditions matrix.

        dimension=1;
        dirichlet=1;
        column=i+20;
        values(1)=0;
        values(2)=0;
        values(3)=1;
        values(4)=g.uncoupled(i);

        bc=boundary_column(bc,dirichlet,dimension,column,values);

    end

end

end
```

C.11 dissolvedO2

```
function dissolvedO2=bulk2dissolved(corrosion,barResult)
```

```
%Function to convert the bulk oxygen content to the dissolved oxygen
%content.

dissolvedO2=barResult(:,2)/(corrosion.porosity*(corrosion.PS+...
   (1-corrosion.PS)/(corrosion.r*corrosion.temp*corrosion.henry*1000)));

end
```

C.12 cathodeCoupling

```
function [ecorr,iCathodeOxygen,iCathodeNoOxygen]=...
   cathodeCoupling(ecorr,i_c,segment,step,cflag,k,corrosion,kg,cv,icorr)

%Function to calculate the cathodic current that will balance the anodic
%current flowing out of the anodic region.

%Establish variables used in this routine.

edrop=0;
iCathodeOxygen=zeros(cv.segments,1);
iCathodeNoOxygen=iCathodeOxygen;

while segment~=cflag.lastCathode+step.cathode && i_c>0

        %Determine ohmic and concentration potential drops at this segment.

   edrop=edrop+i_c/k.each(segment);

   %Establish the coupled potential.

   ecorr.coupled(segment)=ecorr.transition+edrop;

   %Check if this segment is coupled.

        if ecorr.coupled(segment)<ecorr.uncoupled(segment)

        %A potential drop exists sufficient to cause coupling at this
      %segment.Check if oxygen is limited in this segment and if it is
      %use the appropriate overpotential calculation.

      if cflag.depletion(segment)==1

         %Cathode is oxygen deprived so this segment becomes
         %cathodically protected by the anodic region ie: the local
         %corrosion rate is reduced as the by products of the oxygen
         %reduction reaction are used to sustain the anodic reaction at
         %the coupled location.

         %Check if coupled potential lies above or below the
```

```
        %intersecting potential for the two kinetic curves.

        if ecorr.coupled(segment)>kg.e_int(segment)

            %Coupled potential lies above the intersection.  Therefore,
            %use the second curve.

            iCathodeNoOxygen(segment)=icorr.uncoupled(segment)...
                    -10^((ecorr.coupled(segment)-kg.b2(segment))...
                        /kg.m2(segment));

        else

                %Coupled potential lies below the intersection.  Therefore,
            %use the first curve.

            iCathodeNoOxygen(segment)=icorr.uncoupled(segment)...
                        -10^((ecorr.coupled(segment)-kg.b1(segment))...
                        /kg.m1(segment));

        end

    else

        %Cathode has oxygen therefore use the cathodic branch of
        %the oxygen reduction reaction.

        iCathodeOxygen(segment)=10^((ecorr.coupled(segment)-
corrosion.b_o2(segment))/corrosion.m_o2)...
            -10^((ecorr.uncoupled(segment)-corrosion.b_o2(segment))/corrosion.m_o2);

        %Check if i_cathode(segment) has exceeded the available [O2].

        if iCathodeOxygen(segment)+icorr.uncoupled(segment)>icorr.max(segment)

                %i_cathode is sufficiently large to cause negative [O2].
            %Therefore, limit i_cathode to the maximum available which
            %is limited by the O2 availability.

            iCathodeOxygen(segment)=icorr.max(segment)-icorr.uncoupled(segment);

        end

    end

    if iCathodeNoOxygen(segment)<0 || iCathodeOxygen(segment)<0

        display ('negative');

    end
```

```
        if isnan(iCathodeNoOxygen(segment)) || isnan(iCathodeOxygen(segment))

            display ('NaN');

        end

        %Deduct the current generated in this segment from the total
        %current generated in the cathode.

        i_c=i_c-iCathodeNoOxygen(segment)-iCathodeOxygen(segment);

            end

    %Increment segment to the next cathodic segment.

    segment=segment+step.cathode;

end

end
```

C.13 chloride_conversion

```
function [chloride]=chloride_conversion(chloride)

%Function to convert chlorides concentrations from % to mmol/mm3.
%Conversion based on the following:
%   1 mol of Cl-=35.5 grams.
%   1% of Cl- = 281.7 mmol/l or 2.817e-4 mmol/mm3

chloride=2.817e-4*chloride;

end
```

C.14 chloride_ratio

```
function [m1,b1,m2,b2]=chloride_ratio(chloride,corrosion,count)

%Function to calculate the location of the kinetic curve given the chloride
%concentration and the kinetic test data.

%Establish position of the new curve using the calculated and test chloride
%values passed to this routine.

ratio=(chloride-corrosion.chloride(count-1))...
    /(corrosion.chloride(count)-corrosion.chloride(count-1));

%Determine slope and y-intercept of the new curve (bi-linear).
```

```
m1=ratio*(corrosion.m1(count)-corrosion.m1(count-1))+corrosion.m1(count-1);
b1=ratio*(corrosion.b1(count)-corrosion.b1(count-1))+corrosion.b1(count-1);
m2=ratio*(corrosion.m2(count)-corrosion.m2(count-1))+corrosion.m2(count-1);
b2=ratio*(corrosion.b2(count)-corrosion.b2(count-1))+corrosion.b2(count-1);

end
```

C.15 chloride_slope

```
function
[m1,b1,m2,b2,icorr_intersection,ecorr_intersection]=chloride_slope(corrosion,chloride)

%Function to determine the slope of the corrosion kinetic curve when the
%chloride levels are between the test data.  Test data used was obtained
%from Moreno, M., Morris, W., Alvarez, M., Duffo, G. 2004, Corrosion of
%reinforcing steel in simulated concrete pore solutions.  Effect of
%carbonation and chloride content, Corrosion Science, 46:2681-2699.

%Five chloride levels were presented in the test data.  Locate current
%chloride level relative to the test values.  From there determine the new
%slopes and y-intercepts by using a ratio of actual to test chloride as
%follows:

%   (Clact-Cltest1)    (mact-mtest)
%   ---------------  = ------------
%   Cltest2-Cltest1    mtest2-mtest1

%Find where calculated chloride concentration is relative to the test
%values.

if chloride>corrosion.chloride(size(corrosion.chloride,2))

   count=5;

else

   count=find(corrosion.chloride>=chloride,1,'first');

end

%Select or calculate corresponding slopes of the bi-linear curve.

if count==1

   %Chloride is less than the lowest value reported.  Therefore, use
   %the lowest chloride value information.

   m1=corrosion.m1(1);
   m2=corrosion.m2(1);
   b1=corrosion.b1(1);
```

```
    b2=corrosion.b2(1);

elseif count==5

    %Chloride is above the highest value, therefore, use the highest value.

    m1=corrosion.m1(5);
    m2=corrosion.m2(5);
    b1=corrosion.b1(5);
    b2=corrosion.b2(5);

else

    %Calculated chloride falls between the max and min values.

    [m1,b1,m2,b2]=chloride_ratio(chloride,corrosion,count);

end

%Find intersection of the two new curves.  Use this intersection to
%determine if icorr should be applied to curve 1 or curve 2.

icorr_intersection=10^((b2-b1)/(m1-m2));

ecorr_intersection=m1*log10(icorr_intersection)+b1;

end
```

C.16 chlorideMod

```
function chlReturnSegs=chlorideMod(chlOriginal,cv,nodes)

%Routine to extract each years worth of chloride data and eliminate the
%negative values around the bar followed by smoothing of the data so we
%don't have any gaps in chloride concentrations around the bar.

%Extract data from around the bar.

chlOriginalBar=chlOriginal(nodes.bar,:);

%Convert nodes values to segment values.

chlReturnSegs=node2seg(cv.segments,chlOriginalBar);

%Scale results back to original.

chlReturnSegs=chlReturnSegs*cv.scale;

%Set all values less than where chlorides cause corrosion to increase to 0.
```

```
chlReturnSegs(chlReturnSegs<5e-6)=0;

end
```

C.17 coefficients

```
function [c,a,f,d]=coefficients(corrosion)

%Subroutine to establish the pde coefficients for the following pde:
%   d*u'-div(c*grad(u))+a*u=f

%   Where:

%   u = the concentration of the element being considered.
%   d = coefficient applied to the element concentration with respect to
%   time.
%   c = diffusion coefficient.
%   a = coefficient applied to the element concentration.
%   f = outside source of the element.

%   option = element being considered:

%   1=  chloride
%   2=  oxygen
%   3=  hydroxide
%   4=  Fe2+

%Chloride PDE Coefficients.

%Diffusion coefficients estimated using the research of Sang-Hun,
%H., 2007, Influence of diffusion coefficient on chloride ion
%penetration of concrete structure, Construction and Building
%Materials, 21:370-378

%Dcl=Dcref x f1 x f2 x f3

%   Dcref = DH2O x 0.15 x (1+pc(w/c))/(1+pc(w/c)+(pc/pa)(a/c)) x
%           (pc(w/c)-0.85/(1+pc(w/c)))^3
%   DH2O = 1.6 x 10-3 mm2/s
%   pc = specific gravity of cement = 3.15 (PCA website)
%   w/c = water to cement ratio = 0.42 (current AT standard)
%   pa = specific gravity of aggregate =2.7 for limestone.
%   a = aggregate content (kg/m3) = 2400-335-0.42*335 = 1924 kg/m3
%   c = cement content (kg/m3) = 335 kg/m3
%   f1 = gamma+(1-gamma)/(1+(1-H))/(1-Hc))^4
%   f2 = exp((E/R) x (1/To - 1/T))
%   f3 = 1+(1/b3 - 1)(28/t)^0.5 - for modeling purposes ignored as
%   t becomes so large that f3 approaches 1.0.
%   where:
%       H = relative humitidy.
```

```
%       Hc = critical humidity level.  Assumed to be 0.75.
%       E = activation energy of the diffusion process.
%       R = gas constant = 8.314 J/M/K
%       To = reference temperature = 296 K
%       T = current temperature.  Assumed to be 296 K for model.
%       b3 = coefficient to estimate curing effects on diffusion.
%       Neglected as t becomes so large that f3 approaches 1.0.
%       gamma=0.03

%Coefficient definitions.

U=44;
R=corrosion.r;
T=corrosion.temp;
a1=1924;
cem=corrosion.cem;
dh2o=1.6e-3;
pc=3.15;
pa=2.700;
w_c=corrosion.wc;
pwc=pc*w_c;
hc=75;
To=296;

%Chloride diffusion coefficient.

dcref=dh2o*0.15*((1+pwc)/(1+pwc+(pc/pa)*a1/cem)*((pwc-0.85)/(1+pwc))^3);

%Humidity correction;

f1=0.03+(1-0.03)/(1+((1-corrosion.RH/100)/(1-hc/100))^4);

%Temperature correction;

f2=exp((U/R)*(1/To-1/T));

%PDE coefficients.

d(1)=1;
c(1)=dcref*f1*f2; %reported as mm2/s.
a(1)=0;
f(1)=0;

%Oxygen pde coefficients.

%Values for diffusion are estimated from: Papadakis, V., Vayenas,C.,
%Fardis, M., 1991, Physical and chemical characteristics affecting the
%durability of concrete, ACI Materials Journal, 8:186-196.

%DO2=1.92e-6 x e^1.8 x (1-RH/100)^2.2
%   DO2 = diffusion coefficient in m2/sec.
```

```
%   e= porosity of the hardened cement paste, assumed to be 0.22 for
%   w/c of 0.4 and after 1000 days of hydration, refer to Figure 4.
%   RH = relative humidity in percent.

d(2)=1;
c(2)=1.92*0.22^1.8*(1-corrosion.RH/100)^2.2;%Converted to mm2/s
a(2)=0;
f(2)=0;

%Papers used for developing hydroxide diffusion coefficient is Johannesson,
%B., Hosokawa, Y., Yamada,K., 2009, Numerical calculations of the effect of
%moisture content and moisture flow on ionic multi-species diffusion in the
%pore solution of porous materials, Computers and Structures, 87:39-46
%(species diffusion coefficient)and Nguyen, T. Baroghel-Bouny, V., 2006,
%Prediction of chloride ingress into saturated concrete on the basis of a
%multi-species model by numerical calculations, Computers and Concrete,
%3:401-422 (conversion of bulk water diffusion coefficient to concrete
%diffusion coefficient.

%Bulkwater to concrete diffusion coefficient conversion:
%   Deff/Di = Dclo/Dio
%Where:
%   Dcl0 and Dio = diffusion coefficient in an infinitely dillute solution
%   for each ion.
%   Deff = effective diffusion coefficient for the chloride ion calculated
%   above.
%   Di = diffusion coefficient for the reference ion in concrete.

%Reference diffusion coefficient in bulk water (m2/s):
%   Cl- = 2.03e-9
%   Na+ = 1.33e-9
%   OH- = 5.3e-9
%   Ca2+ = 0.79e-9
%   K+ = 1.96e-9
%   SO4 (2-) = 1.07e-9

d(3)=1;
c(3)=c(1)*5.3/2.03;
a(3)=0;
f(3)=0;

%Fe2+ coefficients.
d(4)=1;
c(4)=c(1)*0.79/2.03;%Still to update.
a(4)=0;
f(4)=0;

%Ca2+
d(5)=1;
c(5)=c(1)*0.79/2.03;
a(5)=0;
```

```
f(5)=0;

%Fe(OH)2,aq.
d(6)=1;
c(6)=c(1)*0.79/2.03;
a(6)=0;
f(6)=0;

end
```

C.18 constants

```
function [corrosion,slab,cv,perror,time]=constants

%Function to establish constants used throughout the algorithm.

%Assume 25 Centigrade for all calculations;

corrosion.temp=25+273.15;

corrosion.r=8.3144621/1000; %Ideal gas constant J/K/mmol.

corrosion.RH=80; %Relative Humidity.

corrosion.faraday=96.485; %Faraday's constant in C/mmol.

%Number of electrons transferred for each species considered in the
%corrosion process.

corrosion.o2_number=4; %1 - O2 consumed for every 4 electrons consumed.

corrosion.oh_number=2; %2 - OH- produced for every 4 electrons consumed in reducing
O2.

corrosion.fe_number=4; %1 - Fe2+ produced for every 2 OH- produced or every O2
consumed.

corrosion.ca_number=0; %Ca2+ does not participate but must be included for
compatibility reasons.

%irev, Erev for cathodic reaction. %Obtained from Ge, J., Isgor, O., 2007
%Effects of Tafel slope, exchange current density and electrode potential
%on the corrosion of steel in concrete, Materials and Corrosion,
%58:573-582.

corrosion.SHEconvert=0.318;
corrosion.SCEconvert=0.077;

corrosion.eoO2Std=0.401-corrosion.SHEconvert;

corrosion.irev_o2=6e-12; %multiple values reported.
```

```
%Tafel slope for oxygen reduction was obtained from Gojkovic, S., Zecevic,
%S., Drazic, D., 1994, Oxygen reduction on iron - Part VI, processes in
%alkaline solutions, Electrochimica Acta, 39:975-982, where a tafel slope
%for oxygen reduction in pH > 11 of 0.085V is proposed.

corrosion.tafel_o2=0.085;

%corrosion.tafel_o2=0.160; %Ge and Isgor

%Concrete parameters.  Porosity taken from Zhitnikov, Y., Mozhegov, N.,
%Matosova, Y., 2002, Determining the porosity of concrete, Measurement
%Techniques, 45:305-310.

corrosion.porosity=0.11;
corrosion.wc=0.42;
corrosion.cem=335; %kg

%Solubility of O2 in high pH system is based on O2 in seawater.  Which is
%then converted to a blended oxygen concentration for the entire concrete
%mass using the following relationship:
%[O2]blended=Porosity x (PS x [O2]d + (1-PS) x [O2]g)
%where:
   %Porosity = is the concrete porosity from Figure 3 of Zhitnikov, Y.,
   %Mozhegov, N., Matrosova, Y., 2002, Physicochemical measurements,
   %determining the porosity of concrete, Measurement Techniques,
   %45:305-310
   %PS = degree of pore saturation from figure 6, Papadakis, V., Vayenas,
   %C., Fardis, M., 1991, Physical and chemical characteristics affecting
   %the durability of concrete, American Concrete Institute Materials
   %Journal,8:186-196.
   %[O2]g = 9.35 x 10-6 mmol/mm3 (assuming 20.95% O2 in atmosphere.
   %[O2]d = 2 x 10-8 mmol/mm3 from Zhang et al 2009 as outlined above.

%Chemistry of the concrete pore solution is based on a simplification using
%Ca(OH)2.

corrosion.pH=12.5; %Initially set pH for passivated condition.
corrosion.dissolvedO2=2.25e-7; %mmol/mm3 in sea water - Balabanic et al. 1996.
corrosion.gasO2=8.5631e-6; %mmol/mm3. Based on 20.95% by volume in atmosphere.

%Establish pore saturation of concrete.  Using relationship developed from
%Papadakis et al. 1991.
%
%PS=0.0157 x RH - 0.789.

corrosion.PSslope=0.0157;
corrosion.PSintercept=-0.789;

corrosion.PS=corrosion.PSslope*corrosion.RH+corrosion.PSintercept;
```

```
%Establish mole fractions of oxygen in atmosphere of the constituents:
%N2 = 78.1%
%O2 = 20.95%
%Ar = 0.95%

corrosion.pressure=.101325; %MPa or N/mm2
corrosion.moleO2=0.2095*corrosion.pressure/corrosion.r/corrosion.temp;
corrosion.moleAll=corrosion.pressure/corrosion.r/corrosion.temp;

%Establish Henry's constant for oxygen in pore solution.

corrosion.henry=corrosion.dissolvedO2/(corrosion.pressure*0.2095);

%Establish molarity of oxygen in the atmosphere as the starting point.

corrosion.o2=corrosion.porosity*(corrosion.PS*corrosion.dissolvedO2+(1-
corrosion.PS)*corrosion.gasO2);
corrosion.saturation=corrosion.o2;
corrosion.fe2=0;
corrosion.oh=10^(-(14-corrosion.pH))/1000; %Divide by 1000 to get mmol/mm3.
corrosion.ca=corrosion.oh*.5;%1 Ca+ for every 2OH-.
corrosion.cl=0;
corrosion.surfDiffusion=0.4; %Modification value to account for the increase in
                        %diffusion coefficient on the bar surface caused by the ITZ.
%corrosion.feoh2aq=0;

%Initialize starting conditions.

corrosion.concentration=[corrosion.cl,corrosion.o2,corrosion.oh,...
   corrosion.fe2,corrosion.ca];

%Identify kinetic reaction coefficients for Fe(OH)2==Fe2+ + 2OH-.  From
%Evitt's p80 log(k)=-15.1 for the reaction.

%corrosion.keq_eq1=10^(-19.4); %Fe2+ + 2OH- == FE(OH)2<aq>
corrosion.keq_eq2=10^(-15.1); %Fe(OH)2<s>==Fe2+ + 2OH-
corrosion.keq_h2o=1e-14; %H+ + OH- == H2O -- Assumed at 25C

%Charge Transfer for species underconsideration.
%Cl-, O2, OH-, Fe2+, Ca2+.

corrosion.charge_transfer=[-1,0,-1,2,2];
corrosion.number_species=size(corrosion.charge_transfer,2);

%PDE Errors.

perror.rtol=1e-6; %rtol and atol are required for the pde.
perror.atol=1e-7;
perror.ratio=0.01;
perror.o2=1e-11; %Allowable dissolved O2 concentration for establishing the ilim
condition.
```

```
perror.cl=1e-9; %Error limit to remove small values that are generated by the pde.
perror.cl_x=0.02*2.817e-4; %Chloride concentration which changes the kinetics.
perror.icorr=1e-12; %Coupled currents less than this are considered de-coupled.
perror.pot=0.0005; %Potential limits for search algorithms.

%Identify max and min chlorides.  Max chloride is the value above which no
%change in kinetics occur while min chloride is the value below which no
%change in kinetics occurs.

corrosion.MaxChl=chloride_conversion(0.20);
corrosion.MinChl=chloride_conversion(0.02);

%PDE and Mass Transport time steps.

time.year=365*24*3600; %Length of one year in seconds.
time.year_rep=201; %Number of years the routine will cycle through.
time.step_rem=10; %Subdivision of time for species other than chloride.
time.month_rep=12; %Number of months in the year.

%Model geometry.

slab.thickness=215; %slab thickness.
slab.bar_spacing=150; %bar spacing.
slab.bar_diameter=20; %bar diameter.
slab.cover=90; %Concrete cover to the bar.

%Control volume geometry.

cv.dx=.5; %Segment length.

%Chloride surface concentrations.
%Typical ranges of surface concentration range from 5 kg/m3 to 13 kg/m3 of
%concrete measured using a chloride extraction technique using powdered
%concrete and acid.  Assuming 350kg of cement per m3 of concrete and 2400
%kg/m3 for concrete results in a range of surface concentrations of 1.4286
%to 3.7143% by weight of cement.  Using the following conversion developed
%from research outlined in Haque, M. N., Kayyali, O. A., 1995, Free and
%water soluble chloride in concrete, Cement and Concrete Research,
%25:531-542:
        %For % Decanted <0.385% by weight of concrete:
  %   Expressed = 10^(0.4809153 x Decanted + 0.396772)
        %For % Decanted >=0.385% by weight of concrete:
  %   Expressed = 10^(1.16254319 x Decanted + 1.5285832)
     %   Expressed = chloride concentration in mM/l.
     %   Decanted = chloride concentration in % by weight of cement.

%Start with the high end of surface chlorides.

corrosion.clSurface=100*13/350;

cv.scale=1e12;
```

```
expressed=10^(1.0965*corrosion.clSurface+1.0875); %mM/l
corrosion.expressed=expressed/1e6/cv.scale; %mM/mm3

end
```

C.19 coupling_multi

```
function [icorr,ecorr,g,cflag]=…
        coupling_multi(result,corrosion,cflag,coef,dx,g,ecorr,perror,kg,cv,icorr)

%Routine to determine if coupling is occurring between the anodic and
%cathodic sites using the procedure outlined in Kennell, G., Evitts. R.,
%Heppner, K., 2008, A critical crevice solution and IR drop crevice
%corrosion model, Corrosion Science, 50, 1716-1725.  The routine returns
%the corrosion current density (icorr) at each segment along the bar surface.

%Algorithm starts by evaluating the anodic current at the anodic side.  Potential
%at the transition point between the cathode and anode is considered to be
%0 and will be varied at future stages to ensure andodic and cathodic
%currents are balanced.

%Algorithm is based on a simplified set of equations derived from Kennell
%et al. 2008.  The simplification resides in that concentration effects are
%ignored as the concrete pore solution is buffered so any local changes of
%pH caused by the creation of OH- or Fe2+ are absorbed the chemical
%equilibrium of the pore solution....further research needed to verify
%this.

%At the anodic side of the corrosion cell.
%            ia-ilim            ia
%Etransition=  ------- + ts x log ----
%               k              ilim

%At the cathodic side of the corrosion cell.
%             ic-i1             ic
%Etransition=  ------- + ts x log ---
%               k              i1

%Establish the corrosion current and corrosion potential in each segment
%based on the oxygen consumption rate in the un-coupled condition.

icorr.uncoupled=-g.uncoupled(:,2)*(corrosion.o2_number*corrosion.faraday);

%Establish coefficients used in this module.

%end_loop=1;
k.b_all=zeros(cv.segments,1);
k.t_all=k.b_all;
%icorrCoupleCathodeOld=0;
```

```
%icorrCoupleAnodeOld=0;
icorrCathodeOverAnode1.maxAnode=k.b_all;
icorrCathodeOverAnode1.maxCathodeOxygen=k.b_all;
icorrCathodeOverAnode1.maxCathodeNoOxygen=k.b_all;
icorrCathodeOverAnode2.maxAnode=k.b_all;
icorrCathodeOverAnode2.maxCathodeOxygen=k.b_all;
icorrCathodeOverAnode2.maxCathodeNoOxygen=k.b_all;
icorrAnodeOverCathode.maxAnode=k.b_all;
icorrAnodeOverCathode.maxCathodeOxygen=k.b_all;
icorrAnodeOverCathode.maxCathodeNoOxygen=k.b_all;
%anodicMax=1;
%cathodicMax=1;

%Determine the conductivity of the solution (k) for each segment.
%   k=conductivity of the solution = F^2 Sum zj^2 uj Cj

k.each=corrosion.faraday^2*result.bar_seg(:,1:corrosion.number_species)*coef.zj2_uj';

%Units for conductivity are in 1/ohm metre.  Therefore a modification is
%required to address the changes in cross sectional area and length of each
%control volume.  From first principles:
%   V=IR
%where:
%   I=i x A (i is the current density and A is the area contributing).
%   R=rho x L/A (rho is the resistivity in ohm metre, L is the length of
%   the resistor and A is the cross sectional area of the resistor).
%   rho = 1/k.
%Therefore the final mathematical equation is:
%   V=i x A x L / A / k
%which simplifies to:
%   V=i x L / k with units of volts.

k.each=k.each/dx;

%Determine the sum of the conductivity's for the anodic and cathodic
%regions as these are used in the calculations for IR drop due to current
%flow.  Since we can have either the top or bottom of the bar be the anode
%the following calculations will determine the conductivity of the top and
%bottom portion of the bar separately.  A later evaluation will determine
%if the top is anodic or cathodic.

%Start loop to check if coupling is occurring on the corrosion cells that
%have formed on the bar surface.  Orientation on the bar for the anodic and
%cathodic zones is as follows:
%
%Anode:
   %start.anode=first segment on the anodic side.
   %stop.anode=last segment on the anodic side.
   %step.anode=increment allowing the anode to grow from the first to the
   %last segment on the anodic side.
%Cathode:
```

```
   %start.cathode=first segment on the cathodic side.
   %stop.cathode=last segment on the cathodic side.
   %step.cathode=increment allowing the cathode to grow from the first to
   %the last segment on the cathodic side.

%while (anodicMax==1 || cathodicMax==1) && end_loop==1

   if cflag.type~=3

      %The cell configuration has a cathode over anode component.  In the
      %case of Type 4, 5, or 6, anode over cathode cells also form which
      %are evaluated later.  More than one cathode over anode cell can
      %form on the bar surface so check for the number of cells and
      %adjust calculations accordingly.

      numberCells=size(cflag.lastCathodeCathodeOverAnode,2);

      for cellNumber=1:numberCells

         %Anode information.

         start.anode=cflag.transitionCathodeOverAnode(cellNumber);
         stop.anode=start.anode; %Last physical anodic element.
         step.anode=1;
         cflag.lastAnode=cflag.lastAnodeCathodeOverAnode;

         %Cathode information.

         start.cathode=cflag.transitionCathodeOverAnode(cellNumber)-1;
         stop.cathode=cflag.lastCathodeCathodeOverAnode(cellNumber);
         step.cathode=-1;

         %Set last cathode.

         cflag.lastCathode=cflag.lastCathodeCathodeOverAnode(cellNumber);

         %Send to current balancing routine to balance the anode and
         %cathodic currents.

         if cellNumber==1

            %First cell which covers all of the cell configurations.

            [icorrCathodeOverAnode1,cflag,ecorr]=current_balance_all(ecorr,k,kg,...
              start,stop,step,cv,perror,cflag,corrosion,icorr);

            %Check if the last anodic segment ran up against the anodic
            %segment limit.

            cflag.anodeHitLimitCathodeOverAnode=…
                        icorrCathodeOverAnode1.maxAnode(stop.anode)>0;
```

```
            %Check if last cathodic segment ran up against the cathodic
            %segment limit.

            cflag.cathodeHitLimitCathodeOverAnode=…
                        icorrCathodeOverAnode1.combinedCathode(stop.cathode)>0;

        else

            %Second cell which only occurs with Type 5.

            [icorrCathodeOverAnode2,cflag,ecorr]=…
                current_balance_all(ecorr,k,kg,start,stop,step,cv,perror,cflag,corrosion,ico
        rr);

            %Check if the last cathodic segment ran up against the cathodic
            %segment limit.

            cflag.cathodeHitLimitCathodeOverAnode=…
                icorrCathodeOverAnode2.combinedCathode(stop.cathode)>0;

        end

    end

end

        %Check for anode over cathode cells.

   if cflag.type~=2

        %We have cell types with anodes over cathodes.  In the case of
        %Type 4, 5 and 6, the cathode over anode configuration has been
        %evaluated previously.

        %Anode information;

        start.anode=cflag.transitionAnodeOverCathode;
        stop.anode=start.anode;
        step.anode=-1;
        cflag.lastAnode=cflag.lastAnodeAnodeOverCathode;

        %Cathode information;

        start.cathode=cflag.transitionAnodeOverCathode+1;
        stop.cathode=cflag.lastCathodeAnodeOverCathode;
        step.cathode=1;

        %Set last cathode.

        cflag.lastCathode=cflag.lastCathodeAnodeOverCathode;
```

```
        %Send to current balancing routine to balance the anode and
        %cathodic currents.

        [icorrAnodeOverCathode,cflag,ecorr]=current_balance_all(ecorr,k,kg,...
          start,stop,step,cv,perror,cflag,corrosion,icorr);

        %Check if the last cathodic segment ran up against the cathodic
        %segment limit.

        cflag.cathodeHitLimitAnodeOverCathode=…
          icorrAnodeOverCathode.combinedCathode(stop.cathode)>0;

        cflag.anodeHitLimitAnodeOverCathode=…
          icorrAnodeOverCathode.maxAnode(stop.anode)>0;

    end

%Update icorr with the final coupled currents. The first three icorr's are
%used to update each species consumption or production rate on the bar
%surface while icorr.coupled is used for plotting purposes.  icorr.coupled is
%just the sum of maxAnode and maxCathodeOxygen as maxCathodeNoOxygen does
%not result in an increase in current due to coupling, rather it causes a
%reduction in the local consumption of Fe2+ which provides the necessary
%OH- to complete the coupling.

icorr.maxAnode=icorrCathodeOverAnode1.maxAnode+...
    icorrCathodeOverAnode2.maxAnode+icorrAnodeOverCathode.maxAnode;
icorr.maxCathodeOxygen=icorrCathodeOverAnode1.maxCathodeOxygen+...
    icorrCathodeOverAnode2.maxCathodeOxygen+...
    icorrAnodeOverCathode.maxCathodeOxygen;
icorr.maxCathodeNoOxygen=icorrCathodeOverAnode1.maxCathodeNoOxygen+...
    icorrCathodeOverAnode2.maxCathodeNoOxygen+...
    icorrAnodeOverCathode.maxCathodeNoOxygen;
icorr.coupled=icorr.uncoupled+icorr.maxAnode+icorr.maxCathodeOxygen;

%Update g for the new coupled corrosion currents.  Anodic regions will not
%consume anymore oxygen than is currently present so g for those areas
%remains unchanged.  Cathodic regions without oxygen have no change to the
%total oxygen consumption rate as it is just being used by two processes
%(micro and macro cell corrosion).  So the only change to g is in the
%regions where oxygen is present along with coupling.

g.coupled=g.uncoupled;

%Identify locations where oxygen is present with coupling.
cathodicCurrent=icorr.maxCathodeOxygen>0;

%Update g at these locations.

g.coupled(cathodicCurrent,2)=g.coupled(cathodicCurrent,2)-...
```

```
   icorr.maxCathodeOxygen(cathodicCurrent)/corrosion.o2_number/corrosion.faraday;

if numel(find(isnan(icorr.maxCathodeOxygen)==1))>0 ...
   || numel(find(isnan(icorr.maxCathodeNoOxygen)==1))>0 ...
   || numel(find(isnan(icorr.maxAnode)==1))>0

   display ('NaN present');

   pause;

end

end
```

C.20 current_balance

```
function [icorr,cflag,cell_type,ecorr]=current_balance(pconc,ecorr,k,...
   kg,start,stop,step,cv,perror,cflag,corrosion,icorr)

%Routine which calculates the current flow from the anode to the cathode
%and balances the currents so that they are equal by adjusting the
%transition potential between the anode and cathode.

%Establish constants used in this routine.

i_cathodic=0;
o2.transition=0;
o2.segment=0;
edrop=0;
cell_type=zeros(cv.segments,1);
ratio=2;
dir_old=0;

while ratio>1+perror.ratio || ratio<1-perror.ratio

        %Call solver to determine the anodic current being generated from the
   %anodic side of the cell.

   [ix_all,i_anodic,ecorr]=anode_coupling(pconc,ecorr,k,icorr,...
               kg,start,stop,step,cv.segments,perror);

   %Set segment location to starting point for use in the cathodic calculation.

   segment=cflag.transition+step.cathode;

   %Set total cathodic current for the starting segment;

   i_c=i_anodic;

   %Start loop to calculate the current density and potential on the cathode.
```

```
while segment~=cflag.lastCathode+step.cathode && i_c>0

    %Determine ohmic and concentration potential drops at this segment.

  edrop=edrop+i_c/k.each(segment)+pconc(segment);

  %Establish the coupled potential.

  ecorr.coupled(segment)=ecorr.transition+edrop;

  %Check if this segment is coupled.

  if ecorr.coupled(segment)<ecorr.uncoupled(segment)

    %A potential drop exists sufficient to cause coupling at this
    %segment.

    %Check if oxygen is limited in this segment and if it is use
    %the appropriate overpotential calculation.

    if cflag.depletion(segment)==1

      %Oxygen is limited at this segment.  Therefore, set cell
      %flag as this is used in later algorithms to determine the
      %oxygen consumption rates.

      cell_type(segment)=3;

      %Cathode is oxygen deprived so this segment becomes
      %cathodically protected by the anodic region ie: the local
      %corrosion rate is reduced as the by products of the oxygen
      %reduction reaction are used to sustain the anodic reaction
      %at the coupled location.

      %Check if coupled potential lies above or below the
      %intersecting potential for the two kinetic curves.

      if ecorr.coupled(segment)>kg.e_int

          %Coupled potential lies above the intersection.  Therefore,
        %use the second curve.

        ix_all(segment)=icorr.uncoupled(segment)...
            -10^((ecorr.coupled(segment)-kg.b2(segment))...
              /kg.m2(segment));

      else

        %Coupled potential lies below the intersection.  Therefore,
        %use the first curve.
```

```
            ix_all(segment)=icorr.uncoupled(segment)...
                    -10^((ecorr.coupled(segment)-kg.b1(segment))...
                    /kg.m1(segment));

        end

    else

        %Oxygen is available at this location.  Therefore, set cell
        %flag as this is used in later algorithms to determine the
        %oxygen consumption rates.

        cell_type(segment)=2;

        p_op=ecorr.uncoupled(segment)-ecorr.coupled(segment);

        %Cathode has oxygen therefore use the cathodic branch of
        %the oxygen reduction reaction.

        ix_all(segment)=icorr.uncoupled(segment)*(10^(-p_op/corrosion.m_o2)-1);

        %Check if ix_all(segment) has exceeded the available [O2].

        if ix_all(segment)+icorr.uncoupled(segment)>icorr.max(segment)

            %ix_all is sufficiently large to cause negative [O2].
            %Therefore, limit ix_all to the maximum available which
            %is limited by the O2 availability.

            ix_all(segment)=icorr.max(segment)-icorr.uncoupled(segment);

        end

    end

    %Deduct the current generated in this segment from the total
    %current generated in the cathode.

    i_c=i_c-ix_all(segment);

    %Keep a running tally of the total cathodic current generated.

    i_cathodic=i_cathodic+ix_all(segment);

  end

  %Increment segment to the next cathodic segment.

  segment=segment+step.cathode;

end
```

```
%Check if the assumed potential at the interface between the anode and
%cathode has resulted in the anodic and cathodic currents being
%balanced.  If they haven't ie: there is more anodic current than
%cathodic or more cathodic than anodic, then adjust the interface
%potential.  If anodic currents exceed the cathodic current, then lower
%the interface potential.  If the cathodic current exceeds the anodic
%current then increase the interface potential.

if i_anodic>i_cathodic

   %Lower ecorr.transition.

   dir_new=-1;

   if dir_old==dir_new || dir_old==0

      %Move the transition towards the anodic region.

      cflag.transition=cflag.transition+step.anode;

      %Set the boundary potentials to the uncoupled potentials
      %bounding this segment.

      ecorr.uc_1=ecorr.uncoupled(cflag.transition+step.cathode);

      ecorr.uc_2=ecorr.uncoupled(cflag.transition);

      %Set flags.

      dir_old=dir_new;

      %Since the transition point has moved, k.all must be updated.
      %First update the anode.

      start.anode=cflag.transition;

      [k]=k_multi(start.anode,stop.anode,step.anode,k);

      %Update the cathode.

      start.cathode=cflag.transition+step.cathode;

      [k]=k_multi(start.cathode,stop.cathode,step.cathode,k);

   else

      %The last change in etransition was caused by raising. Now we
      %must lower etransition as we have moved past the balance
      %point. Check if e.uc1 is less than e.uc2.  If it is then we
      %can lower etransition by moving towards e.uc1.  If it isn't
```

```
        %then we must lower by moving towards e.uc2.

        if ecorr.uc_1>ecorr.uc_2

            %Cathodic segment is more positive than anodic  Therefore,
            %set e.uc1 to be equal to ecorr.transition capturing the
            %lower bound).  Then set e.uc2 to the old transition.

            ecorr.uc_1=ecorr.transition;

            %Check if lower bound needs to move.

            if dir_old~=3

                %Set lower bound to the old transition.

                ecorr.uc_2=ecorr.transition_old;

            end

         else

            %We are on a decreasing portion of the curve.  Set e.uc2 at
            %ecorr.transition.

            ecorr.uc_2=ecorr.transition;

            if dir_old~=3

                %Set upper bound to the old transition.

                ecorr.uc_1=ecorr.transition_old;

            end

        end

        %Set flag so that we only return to this portion of the
        %algorithm.  ie: we only want to bounce back and forth near
        %this segment.

        dir_old=3;

    end

else

    %Raise ecorr.transition.

    dir_new=1;
```

```
if dir_old==dir_new || dir_old==0

    %Move the transition towards the cathodic region.

    cflag.transition=cflag.transition+step.cathode;

    %Set the boundary potentials to the uncoupled potentials
    %bounding this segment.

    ecorr.uc_1=ecorr.uncoupled(cflag.transition+step.cathode);

    ecorr.uc_2=ecorr.uncoupled(cflag.transition);

    %Set flags.

    dir_old=dir_new;

    %Since the transition point has moved, k.all must be updated.
    %First update the anode.

    start.anode=cflag.transition;

    [k]=k_multi(start.anode,stop.anode,step.anode,k);

    %Update the cathode.

    start.cathode=cflag.transition+step.cathode;

    [k]=k_multi(start.cathode,stop.cathode,step.cathode,k);

else

    %The last change in etransition was caused by raising. Now we
    %must lower etransition as we have moved past the balance
    %point. Check if e.uc1 is less than e.uc2.  If it is then we
    %can lower etransition by moving towards e.uc1.  If it isn't
    %then we must lower by moving towards e.uc2.

    if ecorr.uc_1>ecorr.uc_2

        %We are on an increasing portion of the curve.  Therefore,
        %set e.uc2 to be equal to ecorr.transition (capturing the
        %lower bound).  Then set e.uc1 to the old transition.

        ecorr.uc_2=ecorr.transition;

        %Check if upper bound needs to move.

        if dir_old~=2

            %Set upper bound to the old transition.
```

```
            ecorr.uc_1=ecorr.transition_old;

        end

    else

        %We are on a decreasing portion of the curve.  Set e.uc2 at
        %ecorr.transition.

        ecorr.uc_1=ecorr.transition;

        %Check if lower bound needs to move.

        if dir_old~=2

            %Set lower bound to the old transition.

            ecorr.uc_2=ecorr.transition_old;

        end

    end

    %Set flag so that we only return to this portion of the
    %algorithm.  ie: we only want to bounce back and forth near
    %this segment.

    dir_old=2;

  end

end

%Store the old etransition and establish the new.

ecorr.transition_old=ecorr.transition;

ecorr.transition=(ecorr.uc_1+ecorr.uc_2)/2;

%Establish ratio for checking if it meets the requirements.

if i_anodic==0

  %No anodic current was generated so go to the next segment.

  ratio=2;

else

  %Anodic current was generated so check if a balance has been
```

```
        %achieved between the anodic and cathodic regions.

        ratio=i_cathodic/i_anodic;

    end

    %Reset variables.

    i_cathodic=0;

    edrop=0;

end

%Set icorr for transfer to other routines.

icorr.delta=ix_all;
icorr.coupled=icorr.uncoupled+ix_all;

end
```

C.21 dissolved2bulk

```
function bulkO2=dissolved2bulk(corrosion,resultDissolvedO2)

%Function to convert the bulk oxygen content to the dissolved oxygen
%content.

bulkO2=resultDissolvedO2*(corrosion.porosity*(corrosion.PS+...
    (1-corrosion.PS)/(corrosion.r*corrosion.temp*corrosion.henry*1000)));

end
```

C.22 dissolvedOxygen

```
function [dissolvedO2]=dissolvedOxygen(result,corrosion)

%Routine to convert the bulk oxygen concentration to an equivalent oxygen
%concentration in the pore solution.  Conversion uses the following
%relationships:
%           [O2]model
%PO2 = ---------------------              Eq 1
%                PS      1-PS
%       Porosity (-----  + -------)
%                H        RT
%
%PS = pore saturation.
%H = Henry's constant.
%[O2]model = oxygen concentration obtained from the 2-d model.
%PO2 = partial pressure of oxygen in the atmosphere at the bar level.
%
```

```
%Results from equation 1 are used to determine the oxygen concentration in
%the electrolyte adjacent to the bar.  When this concentration reaches our
%error limits we then stop the analysis and assume an ilim condition has
%been reached.  The relationship between PO2 and the dissolved oxygen
%concentration is:
%                    PO2
%[O2]dissolved=-----
%                     H
%
%where H is Henry's constant which is determined from the initial
%conditions where PO2 is set based on the following volume fraction for
%air:
%
%N2 = 78.1%
%O2 = 20.95%
%Ar = 0.95%

partialPressureO2=result.bar_seg(:,2)/corrosion.porosity...
   /(corrosion.PS*corrosion.henry+(1-corrosion.PS)/corrosion.r/corrosion.temp);

dissolvedO2=partialPressureO2*corrosion.henry;

end
```

C.23 fbaSlabOxygen

```
function fbaSlabOxygen

%Clear all variables

clear

%Program to setup the finite element analysis of a 1/2 bar embedded in
%concrete in order to evaluate the effects of cover, bar spacing, and
%humidity levels on the ilim conditions around the bar.

%Units used in the program are:
%   Dimensions - mm.
%   Concentrations - mmol/mm3

%Setup counters.

countHumidity=0;
countCover=0;
countSpacing=0;
countBarDiameter=0;
year=0;

%Define constants.
```

```
[corrosion,slab,cv,perror,time]=constants;

%Setup arrays for speed.

humidityAll=zeros(6,1);
coverAll=zeros(10,1);
spacingAll=zeros(7,1);
barDiameterAll=zeros(6,1);

%Start loop to vary bar diameter, spacing, cover, and humidity.

for barDiameter=20:5:20

   countBarDiameter=countBarDiameter+1;

   barDiameterAll(countBarDiameter)=barDiameter;

   slab.bar_diameter=barDiameter;

   %Set segment size and number around bar circumference.

   cv.segments=round(barDiameter*pi()/2/cv.dx);
   cv.dz=cv.dx; %Height of the control volume.
   cv.dy=cv.dx; %Set the width to equal the height.

   %Set identifier for locations where [O2]d is less than saturated.
   %Initially all are at the saturated condition.

   cflag.lowO2=zeros(cv.segments,1);

   %Set array to match the number of segments.

   numberMonths=time.month_rep*time.year_rep;

   for spacing=200:-50:200

      countSpacing=countSpacing+1;

      spacingAll(countSpacing)=spacing;

      slab.bar_spacing=spacing;

      %Define covers.

      for cover=50:10:50

         countCover=countCover+1;

         coverAll(countCover)=cover;

         slab.cover=cover;
```

```
%Setup corrosion kinetic parameters.

[corrosion]=kineticSlabOxygen(corrosion,cv);

%Define Geometry - Call Function Geometry using the geometry
%set in the constants sub-routine.

[gd,sf,ns]=geometrySlab(slab);

%Develop decomposed geometry matrix.

[dl]=decsg(gd,sf,ns);

%Modify the decomposed geometry matrix to add more segments
%along the bar. Segments are added starting at the top nearest
%the concrete surface and rotated counter-clockwise to the
%bottom closest to the slab soffit.

[dl]=modify_geometry(dl,cv.segments);

%Initialize pdemesh

[pdemesh.p,pdemesh.e,pdemesh.t]=initmesh(dl);

%Identify the number of nodes in the points matrix as this is used later
%on to setup the initial conditions for all species.

numberRows=size(pdemesh.p,2);

%Identify nodes that are on the bar boundary as these are the nodes of
%interest.

[nodes]=boundaryNodesSlab(pdemesh.p,pdemesh.e,slab);

%Setup time vector for chloride and oxygen PDE.

time.tlist_chl=linspace(1,time.year_rep,time.year_rep);
time.tlist=linspace(time.year/time.month_rep/time.step_rem,...
            time.year/time.month_rep,time.step_rem);

for humidity=90:10:90

   %Setup array for surface potentials.

   ecorrCoupledSurface=zeros(size(nodes.surface,1),numberMonths);
   ecorrUnCoupledSurface=ecorrCoupledSurface;

   %Preallocate and initialize result arrays.

   result.uChl=zeros(numberRows,size(time.tlist_chl,2));
```

```
result.uO2=zeros(numberRows,size(time.tlist,2));

%Store values for this step.

corrosion.RH=humidity;

countHumidity=countHumidity+1;

humidityAll(countHumidity)=humidity;

%Establish bulk oxygen content for the current humidity.

corrosion.PS=corrosion.PSslope*corrosion.RH+...
   corrosion.PSintercept;
corrosion.o2=corrosion.porosity*(corrosion.PS*...
   corrosion.dissolvedO2+(1-corrosion.PS)*corrosion.gasO2);
corrosion.saturation=corrosion.o2;
corrosion.concentration(2)=corrosion.o2;

%Set error limit for the bulk dissolved oxygen condition.

perror.o2Bulk=dissolved2bulk(corrosion,perror.o2);

%Initialize starting conditions.

result.u0=repmat(corrosion.concentration,numberRows,1);
cflag.transition=0;
cflag.depletion=zeros(cv.segments,1);
result.bar_seg=node2seg(cv.segments,result.u0(nodes.bar,:));
corrosion.oldDissolvedO2=corrosion.saturation*ones(cv.segments,1);

%Initialize g for each segment using icorr at 0 chloride.
%Setup matrix which includes g for each species.

g.uncoupled=zeros(cv.segments,2);
g.working=g.uncoupled;

%Initialize arrays used for saving data.

ecorrCoupled=zeros(cv.segments,numberMonths);
icorrCoupledAnode=ecorrCoupled;
icorrCoupledCathodeNoOxygen=ecorrCoupled;
icorrCoupledCathodeOxygen=ecorrCoupled;
icorrCoupled=ecorrCoupled;
ecorrUnCoupled=ecorrCoupled;
icorrUnCoupled=ecorrCoupled;
ecorr.uncoupled=zeros(cv.segments,1);
icorr.maxAnode=zeros(cv.segments,1);
icorr.maxCathodeOxygen=ecorr.uncoupled;
icorr.maxCathodeNoOxygen=ecorr.uncoupled;
chlorideBar=ecorr.uncoupled;
```

```
chlorideSample1=zeros(numberMonths,1);
chlorideSample2=chlorideSample1;
chlorideSample3=chlorideSample1;
barOxygen=ecorrCoupled;

%Initialize coupled flag.

cflag.cathodicCouplingLocation=zeros(cv.segments,1);

%Setup coefficients for the pde.

[c,a,f,d]=coefficients(corrosion);

%Develop boundary matrix for the chloride conditions.

[b]=boundarySlab(1,cv.segments,0,corrosion);

%Call parabolic subroutine to solve pde.

result.uChl=parabolic(result.u0(:,1),time.tlist_chl,b,...
          pdemesh.p,pdemesh.e,pdemesh.t,c(1)*31536000,a(1),...
          f(1),d(1),perror.rtol,perror.atol);

%Create chloride distribution array for each timestep
%including the initial conditions.

result.u=[result.u0(:,1),result.uChl];

%Send chloride array to routine where results around the bar are selected
%and checked for continuity.  If any continuity issues arise, data is
%smoothed.

result.chlBar=chlorideMod(result.u,cv,nodes);

%Start loop to check oxygen demand around bar given the
%chloride concentration for each year combination.  Stop
%loop when the maximum chloride value has reached the
%bottom of the bar.

while result.chlBar(cv.segments,year+1)<corrosion.MaxChl

   %Establish chloride profile around the bar for each
   %month of this year.

   barResultMonth=linspaceNDim(result.chlBar(:,year+1),...
         result.chlBar(:,year+2),13);
   sampleResultMonth=linspaceNDim(result.u(:,year+1),...
         result.u(:,year+2),13);

   for month=1:12
```

```
cflag.year=year;
cflag.month=month;

if year==2 && month==10

   display (month);

end

fprintf('Bar Diameter = %d mm\n',barDiameter);
fprintf('Bar Spacing= %d mm\n',spacing);
fprintf('Cover = %d mm\n',cover);
fprintf('Humidity = %d%%\n',humidity);
fprintf('Year = %d, Month = %d \n',year,month);

%Establish average chloride load for this time period.

result.bar_seg(:,1)=barResultMonth(:,month+1);

%Generate kinetic geometry information for each
%bar segment with the current chloride values.

[kg,corrosion]=tafelSlab(corrosion,result.bar_seg);

%Set g for the current conditions.

g.working(:,2)=kg.g;

%Call pde to solve for [O2] concentrations.

result=pdeResolveSlab(2,cv,g,result,pdemesh,c,a,...
   f,d,perror,time,nodes,corrosion);

%Call routine to adjust erev for O2.  If negative
%values result, oxygen limitations will be
%evaluated at the same time.

[g,result,corrosion,cflag,ecorr,icorr,kg]=...
   eRevAdjustUnCoupled(g,result,nodes,time,...
   pdemesh,c,a,f,d,perror,cv,corrosion,cflag,...
   ecorr,icorr,kg);

%Set dissolved oxygen concentration to the final
%result obtained in this algorithm as this will be
%used to determine if changes occur in the future.

corrosion.currentDissolvedO2=...
   bulk2dissolved(corrosion,result.bar_seg);

%Update uncoupled g with the new value of g after
%it has been checked for O2 concentrations.
```

```
g.uncoupled=g.working;

%Determine ecorr and icorr around the bar and
%throughout the model space using the final values
%for g at the timestep under consideration.  This
%step assumes uncoupled potentials.

[ecorr,icorr,g]=potential_bar(g,kg,corrosion,...
   ecorr,icorr,result,cv);

%Check if a potential difference exists at some
%point around the bar circumference at the end of
%this timestep.  If there is, then re-set to the
%beginning of the timestep with the final value of
%g calculated and then pass to the mass-transport
%and coupling algorithm.

[cflag]=find_transition(cv,ecorr,cflag);

%If a potential difference exists at the end of
%this time step evaluate the coupling effect that
%is created.

if cflag.type>1

      %A potential difference exists so pass all
   %species data to the mass-transport model to
   %determine the extent of coupling on the bar
   %surface.

   [g,result,ecorr,icorr,cflag,corrosion]=...
      mass_transport(result,g,time,corrosion,...
      cflag,ecorr,cv,perror,pdemesh,nodes,c,a,...
      f,d,kg,icorr);

else

   %No coupling occurs so set coupled to be the
   %same as uncoupled.

   icorr.coupled=-g.uncoupled(:,2)*...
      corrosion.faraday*corrosion.o2_number;
   ecorr.coupled=ecorr.uncoupled;

   %Set coupled currents to zero.

   icorr.maxAnode=zeros(cv.segments,1);
   icorr.maxCathodeOxygen=ecorr.uncoupled;
   icorr.maxCathodeNoOxygen=ecorr.uncoupled;
```

```
end

if numel(find(imag(ecorr.coupled)>0)==0)>0

  display 'found an imaginary number';

end

%Establish the corrosion potentials on the concrete
%surface.

ecorr=potential_surface(nodes,cv,pdemesh,ecorr,...
   corrosion);

%Determine ecorr and icorr around the bar and
%throughout the model space using the final values
%for g at the timestep under consideration.

monthTotal=(year)*12+month;

ecorrCoupledSurface(:,monthTotal)=...
   ecorr.coupledSurface;
ecorrUnCoupledSurface(:,monthTotal)= ecorr.unCoupledSurface;
ecorrUnCoupled(:,monthTotal)=ecorr.uncoupled;
ecorrCoupled(:,monthTotal)=ecorr.coupled;
icorrCoupledAnode(:,monthTotal)=icorr.maxAnode;
icorrCoupledCathodeNoOxygen(:,monthTotal)=….
                                        icorr.maxCathodeNoOxygen;
icorrCoupledCathodeOxygen(:,monthTotal)= icorr.maxCathodeOxygen;
icorrUnCoupled(:,monthTotal)=icorr.uncoupled;
barOxygen(:,monthTotal)=result.barOxygen;
icorrCoupled(:,monthTotal)=icorr.maxAnode+...
   icorr.maxCathodeOxygen+icorr.uncoupled;

%Identify chloride concentrations around the bar
%and at the sample depths.

chlorideBar(:,monthTotal)=barResultMonth(:,month+1);
chlorideSample1(monthTotal)=...
   mean(sampleResultMonth(nodes.sample_1,month));
chlorideSample2(monthTotal)=...
   mean(sampleResultMonth(nodes.sample_2,month));
chlorideSample3(monthTotal)=...
   mean(sampleResultMonth(nodes.sample_3,month));

%Save last time step results for the beginning of
%the next time step.

result.u0(:,2)=result.uO2(:,time.step_rem);

%Reset coupled flag.
```

```
                cflag.cathodicCouplingLocation=zeros(cv.segments,1);

            end

            %Increment year.

            year=year+1;

            %Break out if year exceeds 200.

            if year>200

                break;

            end

        end

        %Create file name for saving results

        fileName=strcat(num2str(barDiameter),'d',...
            num2str(spacing),'s',num2str(cover),'c',...
            num2str(humidity),'h','.mat');

        save(fileName,'barDiameter','spacing','cover','humidity',...
            'ecorrCoupledSurface','ecorrUnCoupledSurface',...
            'ecorrCoupled','ecorrUnCoupled',...
            'icorrCoupledAnode','icorrCoupledCathodeNoOxygen',...
            'icorrCoupledCathodeOxygen',...
            'icorrUnCoupled',...
            'chlorideBar','chlorideSample1','chlorideSample2',...
            'chlorideSample3',...
            'barOxygen');

       %Reset year counter to zero.

        year=0;

    end

    countHumidity=0;

end

countCover=0;

end

countSpacing=0;
```

```
end

end
```

C.24 find_transition

```
function [cflag]=find_transition(cv,ecorr,cflag)

%Function to establish the how many cells are present and the locations of
%where the last cathode segment will be.  Round potentials to the nearest
%1/10th of a millivolt in order to eliminate some of the early calculations
%where potentials differences are created due to oxygen differences but at
%a very small value.

ecorrRound=floor(ecorr.uncoupled*10000)/10000;

%Identify if potential differences exist around the bar circumference.

largestEcorrUncoupled=find(max(ecorrRound)==ecorrRound);
smallestEcorrUncoupled=find(min(ecorrRound)==ecorrRound);

%Identify the number of values in each largest and smallest ecorruncoupled.

numberLargestEcorr=numel(largestEcorrUncoupled);
numberSmallestEcorr=numel(smallestEcorrUncoupled);

%Identify which condition exists.

if numberLargestEcorr==cv.segments

   %Condition 1 - There are no potential differences around the bar.

   cflag.type=1;
   cflag.transitionAnodeOverCathode=0;
   cflag.transitionCathodeOverAnode=0;
   cflag.lastCathodeCathodeOverAnode=0;
   cflag.lastCathodeAnodeOverCathode=0;

else

   %We have potential differences that are present. Using the largest
   %ecorr.uncoupled determine if the maximum corrosion potential exists at
   %the top, bottom, or side of the bar.  Depending on the answer, one of
   %the following four corrosion cell types can be present:
      %Type 2 - Maximum corrosion potential at the top of the bar.  This
      %creates a single corrosion cell with the cathode near the top of
      %the bar and the anode near the bottom.
      %Type 3 - Maximum corrosion potential occurs at the bottom of the
      %bar.  This creates a single corrosion cell with the cathode near
      %the bottom of the bar and the anode near the top.
      %Type 4 - Maximum corrosion potential occurs between the extreme
```

```
        %top and bottom of the bar.  This condition creates two corrosion
        %cells with the anodes near the top and bottom of the bar and
        %the cathode along the side.
        %Type 5 - A combination of Type 2 and 4 where the maximum chloride
        %values are reached at the top of the bar resulting in maximum
        %corrosion potentials occurring at the top and somewhere along the
        %side.  This creates three corrosion cells with the middle
        %corrosion cell sharing the anodic region with the top cell and the
        %middle corrosion cell sharing the cathodic region with the bottom
        %cell.
        %Type 6 - Two cells are created configured as a
        %cathode/anode/cathode.

    if largestEcorrUncoupled(1)==1 &&
        smallestEcorrUncoupled(numberSmallestEcorr)==cv.segments

        %We have a Type 2 cell with once corrosion cell oriented with the
        %anode at the bottom.  Cathode over anode.

        cflag.type=2;

        %Set anode over cathode transition to 0 as this cell configuration
        %doesn't exist.

        cflag.transitionAnodeOverCathode=0;

        %Set cathode over anode transition to the bottom as we always start
        %at the extreme end of the anode and increment to the cathode side.
        %Check if we have constant potentials at the cathodic end
        %representing a flat spot on the corrosion potential curve.  If
        %this is present, take the first segment towards the anode which is
        %outside of the flat spot as the transitionCathodeOverAnode.


cflag.lastAnodeCathodeOverAnode=largestEcorrUncoupled(numberLargestEcorr)+1;

        %Set transition between the cathode and anode to the last segment.

        cflag.transitionCathodeOverAnode=cv.segments;

        %Set last cathodic segment for each cell.

        cflag.lastCathodeAnodeOverCathode=0; %No anode over cathode cell.
        cflag.lastCathodeCathodeOverAnode=1; %Allow cathode to go upto the top of the
bar.

    elseif largestEcorrUncoupled(numberLargestEcorr)==cv.segments &&
        smallestEcorrUncoupled(1)==1

        %We have a Type 3 cell with one corrosion cell oriented with the
        %anode at the top.  Anode over cathode.
```

```
    cflag.type=3;

    %Set anode over cathode transition to 1 as this cell configuration
    %has the anode at the top.

    cflag.transitionAnodeOverCathode=1;

    %Set last anode at one less the last segment or one less where the
    %first maximum constant corrosion potential occurs.

    cflag.lastAnodeAnodeOverCathode=largestEcorrUncoupled(1)-1;

    %Set cathode over anode transition to zero as this configuration
    %doesn't exist for this cell type.

    cflag.transitionCathodeOverAnode=0;

    %Set last cathodic segment for each cell.

    cflag.lastCathodeAnodeOverCathode=cv.segments;
    cflag.lastCathodeCathodeOverAnode=0;

elseif largestEcorrUncoupled(1)>1 &&
    largestEcorrUncoupled(numberLargestEcorr)<cv.segments

    %We have a Type 4 or 5 which are configured as follows:
       %Type 4 Cell - anode/cathode/anode.
       %Type 5 Cell - 3 cells with cathode/anode/cathode/anode

    %Check to see if a minimum value exists between the top and the
    %maximum value location.

    minimumValueBetweenTopAndMax=…
         find(min(ecorr.uncoupled(1:largestEcorrUncoupled(1))...
         ==ecorr.uncoupled(1:largestEcorrUncoupled(1))));

    %Check the first value found and if it is greater than 1 then we
    %have at Type 5 cell.  If it is equal to 1 then we have a Type 4
    %cell.

    if minimumValueBetweenTopAndMax(1)>1

       %We have a Type 5 cell with Cathode/Anode/Cathode/Anode
       %configuration.  Therefore we have two Cathode over Anode cells
       %and one Anode over Cathode cell.

       cflag.type=5;

       %Set anode over cathode transition to minimumValueBetweenTopAndMax
       %as this cell configuration occurs between the top and bottom
```

```
    %cell.  If more than one segment is at the same minimum take
    %the median segment value.

    largestSegmentAtMinimum=middle(minimumValueBetweenTopAndMax);

    cflag.transitionAnodeOverCathode=largestSegmentAtMinimum+1;

    %Two cathode over anode cells exist therefore two transitions
    %must be set.

    cflag.transitionCathodeOverAnode(1)=largestSegmentAtMinimum;
    cflag.transitionCathodeOverAnode(2)=cv.segments;

    %Set last cathodic segment for each cell.  For the anode over
    %cathode cell configuration the last cathode will be at the
    %segment where the maximum ecorr.uncoupled occurs.

    lastCathode=middle(largestEcorrUncoupled);

    cflag.lastCathodeAnodeOverCathode=lastCathode;

    %For the first cathode over anode cell, the last cathode will
    %be at the top of the bar.

    cflag.lastCathodeCathodeOverAnode(1)=1;

    %For the second cathode over anode cell, the last cathode will
    %be at the next segment adjacent to the last cathode for the
    %anode over cathode cell.

    cflag.lastCathodeCathodeOverAnode(2)=lastCathode+1;

    %Set last anode to one less than the last cathode for the anode
    %over cathode cell.

    cflag.lastAnodeAnodeOverCathode=lastCathode-1;

    %Set last anode to one more than the last cathode for the
    %cathode over anode cell.

    cflag.lastAnodeCathodeOverAnode(1)=2;
    cflag.lastAnodeCathodeOverAnode(2)=lastCathode+2;

else

    %We have a Type 4 cell so we have 2 cells one Anode over
    %Cathode, the other Cathode over Anode.

    cflag.type=4;

    %Set anode over cathode transition to 1 as this cell configuration
```

```
        %has the anode at the top.

        cflag.transitionAnodeOverCathode=1;

        %Set cathode over anode transition to the bottom as the second
        %cell has the anode at the bottom of the bar.

        cflag.transitionCathodeOverAnode=cv.segments;

        %Identify the middle segment for the cathodic region.

        middleCathode=middle(largestEcorrUncoupled);

        %Set last cathodic segment for each cell. For the cathode in
        %the anode over cathode cell, allow the last cathode to be the
        %the segment where the middleCathode resides.  For the cathode
        %in the cathode over anode cell, the last cathode will be the
        %middleCathode plus 1.

        cflag.lastCathodeAnodeOverCathode=middleCathode;
        cflag.lastCathodeCathodeOverAnode=middleCathode+1;

        %Set last anode to one less than the last cathode.

        cflag.lastAnodeAnodeOverCathode=middleCathode-1;
        cflag.lastAnodeCathodeOverAnode=middleCathode+2;

    end

elseif smallestEcorrUncoupled>1 && smallestEcorrUncoupled<cv.segments

    %We have a type 6 cell with two corrosion cells configured as
    %cathode/anode/cathode

    cflag.type=6;

    %Find the segments with the most minimum ecorr.uncoupled.

    middleAnode=middle(smallestEcorrUncoupled);

    %Set the cathode/anode cell transition to occur at the segment
    %which has the smallest ecorr.uncoupled.

    cflag.transitionAnodeOverCathode=middleAnode+1;

    %Set the anode/cathode cell transition to the segment adjacent to
    %the smallest ecorr.uncoupled.

    cflag.transitionCathodeOverAnode=middleAnode;

    %Set last cathodic segment for each cell.
```

```
        cflag.lastCathodeAnodeOverCathode=cv.segments;
        cflag.lastCathodeCathodeOverAnode=1;

    else

        display ('No matching cell configuration');

        pause;

    end

end

end
%
%
%
function middleValue=middle(middleArray)

%Routine to find the middle value of the array passed.  If the array has 1
%or 2 values it returns the first value.  If the array has more than 2
%values it returns the integer value of the average number of array
%components as follows:
    %numberArray=5
    %middleValue occurs at 5/2 = 2.5 so 2.

%Find the number of values passed in the middleArray.

numberArray=numel(middleArray);

if numberArray>2

        %We have multiple points with the same value so take the middle one.

    middleValue=middleArray(floor(numberArray/2));

else

        %We have 2 or 1 segments with the same value so use the first one.

    middleValue=middleArray(1);

end

end
```

C.25 geometrySlab

```
function [gd,sf,ns]=geometrySlab(slab)
```

```
%Program to establish geometry of a PDE.

%Define Grid Matrix
%   gd(i,j)=i by j matrix that describes each geometrical element used in
%   future algorithms to generate the mesh and boundary conditions.
%      i=each row describes a specific characteristic of each element.
%      j=number of unique geometrical elements.
%   gd(1,j)=Geometry Type
%      1 = Circle
%      2 = User Defined Shape
%      3 = Rectangle
%      4 = Elipse
%   For circles
%      gd(2,j)=x-coordinate of centre.
%      gd(3,j)=y-coordinate of centre.
%      gd(4,j)=Radius
%      gd(5 to n,j)= Not used for circles so set to 0
%   For User Defined Shape
%      gd(2,j)=Number of sides
%      gd(3 to n+1,j)=x-coordinate of first thru n corners.
%      gd(n+1 to n+n+1,j)=y-coordinate of first thru n corners
%   For rectangles
%      gd(2,j)=Number of sides if rectangle
%      gd(3,j)=corner 1 x-coordinate
%      gd(4,j)=corner 2 x-coordinate
%      gd(5,j)=corner 3 x-coordinate
%      gd(6,j)=corner 4 x-coordinate
%      gd(7,j)=corner 1 y-coordinate
%      gd(8,j)=corner 2 y-coordinate
%      gd(9,j)=corner 3 y-coordinate
%      gd(10,j)=corner 4 y-coordinate
%   For ellipses
%      gd(2,j)=x-coordinate of centre.
%      gd(3,j)=y-coordinate of centre.
%      gd(4,j)=x-radius of ellipse
%      gd(5,j)=y-radius of ellipse
%      gd(6,j)=rotational angle of the ellipse
%      gd(7 to n,j)=Not used for elipses so set to 0

%   sf=text string that describes the relationship between each element in
%   terms of adding or subtracting ie: R1-C1.
%   ns=element name array in ascii format.  Each column represents the
%   element name.

%Define first element (Rectangle)

width=slab.bar_spacing/2;
height=slab.thickness;
lower_left_corner_x=0;
lower_left_corner_y=0;
```

```
j=1;

gd(1,j)=3;
gd(2,j)=4;
gd(3,j)=lower_left_corner_x;
gd(4,j)=lower_left_corner_x+width;
gd(5,j)=lower_left_corner_x+width;
gd(6,j)=lower_left_corner_x;
gd(7,j)=lower_left_corner_y;
gd(8,j)=lower_left_corner_y;
gd(9,j)=lower_left_corner_y+height;
gd(10,j)=lower_left_corner_y+height;

ns(1,j)='R'; %Defines a rectangle.
ns(2,j)='1'; %Identifies this element as the first of its kind.

%Define second element (Circle)

radius=slab.bar_diameter/2;
circle_centre_x_coordinate=width;
circle_centre_y_coordinate=height-slab.cover-radius;

j=2;

gd(1,j)=1;
gd(2,j)=circle_centre_x_coordinate;
gd(3,j)=circle_centre_y_coordinate;
gd(4,j)=radius;

ns(1,j)='C'; %Defines a circle.
ns(2,j)='1'; %Identifies this element as the first of its kind.

%Define the sample region for chloride.
%First region is 10 mm to 25 mm below the top surface a the extreme left
%side of the model and 10 mm wide.

j=3;

gd(1,j)=3;
gd(2,j)=4;
gd(3,j)=lower_left_corner_x;
gd(4,j)=lower_left_corner_x+10;
gd(5,j)=lower_left_corner_x+10;
gd(6,j)=lower_left_corner_x;
gd(7,j)=lower_left_corner_y+height-25;
gd(8,j)=lower_left_corner_y+height-25;
gd(9,j)=lower_left_corner_y+height-10;
gd(10,j)=lower_left_corner_y+height-10;

ns(1,j)='R'; %Defines a rectangle.
ns(2,j)='2'; %Identifies this element as the second of its kind.
```

```
%Define the sample region for chloride.
%Second region is 50 mm to 65 mm below the top surface a the extreme left
%side of the model and 10 mm wide.

j=4;

gd(1,j)=3;
gd(2,j)=4;
gd(3,j)=lower_left_corner_x;
gd(4,j)=lower_left_corner_x+10;
gd(5,j)=lower_left_corner_x+10;
gd(6,j)=lower_left_corner_x;
gd(7,j)=lower_left_corner_y+height-65;
gd(8,j)=lower_left_corner_y+height-65;
gd(9,j)=lower_left_corner_y+height-50;
gd(10,j)=lower_left_corner_y+height-50;

ns(1,j)='R'; %Defines a rectangle.
ns(2,j)='3'; %Identifies this element as the third of its kind.

%Define the sample region for chloride.
%Third region is 100 mm to 110 mm below the top surface a the extreme left
%side of the model and 10 mm wide.

j=5;

gd(1,j)=3;
gd(2,j)=4;
gd(3,j)=lower_left_corner_x;
gd(4,j)=lower_left_corner_x+10;
gd(5,j)=lower_left_corner_x+10;
gd(6,j)=lower_left_corner_x;
gd(7,j)=lower_left_corner_y+height-115;
gd(8,j)=lower_left_corner_y+height-115;
gd(9,j)=lower_left_corner_y+height-100;
gd(10,j)=lower_left_corner_y+height-100;

ns(1,j)='R'; %Defines a rectangle.
ns(2,j)='4'; %Identifies this element as the fourth of its kind.

%Define relationship between each element.
%For our case we want the circle subtracted from the rectangle.

sf=strcat('(',ns(1,1),ns(2,1),'+',ns(1,3),ns(2,3),'+',ns(1,4),ns(2,4),...
      '+',ns(1,5),ns(2,5),')','-',ns(1,2),ns(2,2));

ns=abs(ns);

end
```

C.26 kineticSlabOxygen

```
function [corrosion]=kineticSlabOxygen(corrosion,cv)

%Subroutine to establish the kinetics of corrosion for the two half cell
%reactions that occur on the bar embedded in concrete:

%Anode - Fe==Fe2+ + 2e-
%Cathode - 02 + 4H20 + 4e-==4OH-

%The first step is to determine ecorr and icorr as these are the limiting
%reactions within this system.

%Terms and abbreviations.
%   eo=half cell electrode potential at standard conditions - volts reference to CSE.
%   io=exchange current density - A/mm2.
%   tafel=tafel slope volts/decade of current.

%Fe - Information obtained from Moreno et al "Corrosion of reinforcing steel
%in simulated concrete pore solutions.  Effect of carbonation and chloride
%content".

%Select pH for calculation of ecorr and icorr.
%pH available is either 12.5 or 13.9.

%eclx = volts relative to the standard hydrogen electrode which are
%converted to the CSE reference cell.
%chloride = g/100ml of solution (or mass volume percentage)
%iclx = current density in A/mm2.

%Create ereversible for each point on the bar surface.

corrosion.erevO2=corrosion.eoO2Std*ones(cv.segments,1);

switch corrosion.pH

   case {12.5};

      %Cl- content at 0%
      ecl1=[-0.040, -0.01, 0.40];
      icl1=[2.5e-11, 3.1e-9, 8e-9];

      %Cl- content at 0.02%
      ecl2=[-0.040, -0.01, 0.40];
      icl2=[2.5e-11, 3.1e-9, 8e-9];

      %Cl- content at 0.05%
      ecl3=[-0.06,-0.045,0.400];
      icl3=[2e-11,3e-9,1.1e-8];

      %Cl- content at 0.10%
```

```
    ecl4=[-0.145,-0.115,0.1];
    icl4=[2.5e-11,1.1e-8, 2.9e-8];

    %Cl- content at 0.20%
    ecl5=[-0.145,-0.115,0.1];
    icl5=[2.5e-11,1.1e-8, 2.9e-8];

    %Combine ecorr and icorr into on array for analysis.

    ec=[ecl1;ecl2;ecl3;ecl4;ecl5];
    ic=[icl1;icl2;icl3;icl4;icl5];

    %Convert potential to reference CSE rather than SHE.

    ec=ec-corrosion.SHEconvert;

    %Establish slopes and y-intercepts of both portions of the test data curve.

    m1=(ec(:,2)-ec(:,1))./(log10(ic(:,2))-log10(ic(:,1)));
    b1=ec(:,2)-m1.*log10(ic(:,2));

    m2=(ec(:,3)-ec(:,2))./(log10(ic(:,3))-log10(ic(:,2)));
    b2=ec(:,3)-m2.*log10(ic(:,3));

    %Chloride data points.
    chloride_label=[0,0.02,0.05,0.10,0.20];

    %Convert chloride from g/100ml (%) in solution to mmmol/mm3
    %determined by acid based extraction.

    chloride=chloride_conversion(chloride_label);

    corrosion.trigger=chloride(2); %This value is used in the transition finding algorithm.

    %Establish cathodic reaction kinetics.

    corrosion.erevO2=nernst(corrosion.dissolvedO2,corrosion);

case {13.9};

    %Cl- content at 0%
    ecl1=[-0.145, -0.115, 0.475];
    icl1=[3e-11, 5.5e-9, 3.1e-8];

    %Cl- content at 1%
    ecl2=[-0.145, -0.115, 0.475];
    icl2=[3e-11, 5.5e-9, 3.1e-8];

    %Cl- content at 3%
    ecl3=[-0.155, -0.150,0.20];
    icl3=[3e-11, 8e-9, 3.1e-8];
```

```
        %Cl- content at 5%
        ecl4=[-0.21, -0.195, 0.12];
        icl4=[3e-11, 3.1e-8, 7e-8];

        %Cl- content at 10%
        ecl5=[-0.32, -0.295, -0.09];
        icl5=[3e-11, 1e-8, 2e-8];

        %Combine ecorr and icorr into an array for analysis.

        ec=[ecl1;ecl2;ecl3;ecl4;ecl5];
        ic=[icl1;icl2;icl3;icl4;icl5];

        %Convert potential to reference CSE rather than SHE.

        ec=ec-corrosion.SHEconvert;

       %Establish slopes and y-intercepts of both portions of the test data curve.

        m1=(ec(:,2)-ec(:,1))./(log10(ic(:,2))-log10(ic(:,1)));
        b1=ec(:,2)-m1.*log10(ic(:,2));

        m2=(ec(:,3)-ec(:,2))./(log10(ic(:,3))-log10(ic(:,2)));
        b2=ec(:,3)-m2.*log10(ic(:,3));

        %Chloride data points.
        chloride_label=[0,1,3,5,10];

        %Convert chloride from g/100ml (%) in solution to mmol/mm3
        %determined by acid based extraction.

        chloride=chloride_conversion(chloride_label);

        corrosion.trigger=chloride(2); %This value is used in the transition finding algorithm.

        %Establish cathodic reaction kinetics.

        corrosion.erevO2=nernst(corrosion.dissolvedO2,corrosion);

end

%Find the slope and y-intercept for the oxygen reaction.

mo2=-corrosion.tafel_o2;

bo2=corrosion.erevO2-mo2*log10(corrosion.irev_o2);

%Calculate icorr for the anodic reaction for each chloride concentration.

%icorr=(10.^((corrosion.erevO2-ec(:,2)-
```

```
mo2*log10(corrosion.irev_o2)+m2.*log10(ic(:,2))./(-mo2+m2)));

%Calculate Ecorr for the anodic reaction for each chloride concentration.

%ecorr=(ec(:,2)+m2.*(log10(icorr)-log10(ic(:,2))));

%Round Ecorr to the nearest mV.

%ecorr=round(ecorr*1000)/1000;

%Flip ecorr and icorr to align with remainder of programming.

%ecorr=ecorr';
%icorr=icorr';

%Combine ecorr, icorr, and chloride data.

%corrosion.ecorr=ecorr;
%corrosion.icorr=icorr;
corrosion.chloride=chloride;
%corrosion.ec=ec;
corrosion.m1=m1;
corrosion.m2=m2;
corrosion.b1=b1;
corrosion.b2=b2;
corrosion.b_o2=bo2;
corrosion.m_o2=mo2;

end
```

C.27 mass_transport

```
function
[g,result,ecorr,icorr,cflag,corrosion]=mass_transport(result,g,time,corrosion,cflag,ecorr,...
                        cv,perror,pdemesh,nodes,c,a,f,d,kg,icorr)

%Subroutine to model the electrochemistry at the bar surface.  Theory based
%on Kennel, G., Evitts, R., Heppner, K., 2008, A critical crevice solution
%and IR drop crevice corrosion model, Corrosion Science, 50:1716-1725.

%This theory includes diffusion, electromigration, diffusion potential,
%charge density, and a sink or source term which is given by:

%dCi/time.dt = -zi ui F^2 Ci/e x Sum(zj Cj)   --------- Charge density Term.
%        -zi ui del (Ci) i/(F x Sum(zj^2 uj Cj) ---- Electromigration Term.
%        -zi ui del (Ci)/(sum(zj^2 uj Cj) x Sum(zj Dj del(Cj) ---- Diffusion potential.
%        +Di del^2(Ci) ---------------------------- Diffusion
%        +S ---------------------------------------- Sink or source.

%where:
%   zi=charge number for the species under consideration.
```

```
%   ui= ionic mobility (m2 mol/J s).  Estimated with:
%                           u=D/RT - D = Diffusion coefficient
%                                 R = Gas constant = 8.314472 J/mol/K
%                                 T = Temperature (kelvin)
%   Ci/j=concentration of species i or j.
%   F = Faraday's constant.

%Species under consideration include:
%   1 = Hydroxide (OH-).
%   2 = Fe2+.

%Variables.
%   k = segment number.
%   i or j = species.
%   n = time step.

%Variables being passed to the routine:
%   segments = number of control volumes developed around the bar.
%   nodes = a structured variable which includes:
%         nodes.bar = nodes along the bar perimeter starting on the top
%               and ending on the bottom of the bar.
%         nodes.distance = location of each node on the perimeter of the
%               bar starting on the top at "0" and ending on the bottom.
%         nodes.surface= sorted array of nodes along the top surface.
%         nodes.sample_x=range of nodes which are used to determine chloride
%               concentrations at the typical sampling depths used in practice.
%   result_store=species concentrations produced by the diffusion model.
%   c = diffusion coefficients for all species.
%   cycle_duration = length of time step used in the FEM.
%   icorr = corrosion rates for various chloride concentrations.
%   g = oxygen consumption rate at this time step and chloride
%   concentration.

%Set constants for this algorithm.

icorr.max=ones(cv.segments,1);
firstTimeThrough=1;
oldErevO2=ones(cv.segments,1);
cflag.condition=1; %We are at a coupled condition.

%Create arrays for error checking.

erevOldAll=zeros(cv.segments,20);
erevAll=erevOldAll;

%Determine z and u for all species.

ionic_mobility=c(1:corrosion.number_species)/(corrosion.r*corrosion.temp);

%Determine zi x ui.
```

```
coef.zi_ui=repmat(ionic_mobility.*corrosion.charge_transfer,cv.segments,1);

%Determine zj2 x uj.

coef.zj2_uj=(ionic_mobility.*corrosion.charge_transfer.^2)/corrosion.surfDiffusion;

%Determine zj x Dj

coef.zj_dj=corrosion.charge_transfer.*c(1:corrosion.number_species);

%Create coefficients that don't change due to species or concentration.

dx=cv.dx;
time.dt=time.year/time.month_rep;

%Store segment results to compare with segment results after coupling
%and mass transport effects are considered.

%result.old=result.bar_seg;

%Send concentration data to subroutine that will evaluate whether
%coupling is occurring between the anode and cathodes on the bar and
%whether there is an increase in current density caused by this coupling.
%Since coupling may increase the corrosion rate in areas where oxygen is
%present ie: O2 consumption will increase, we will need to check if [O2]
%concentrations have fallen below zero due to increased consumption.  If
%they have then we will need to loop through this process ie: couple, check
%[O2], then couple until we have achieved a balance between coupling and
%[O2] consumption on the bar surface.

g.working=g.uncoupled;

%Start loop to establish the effects of coupling around the bar perimeter.
%As coupling occurs, the oxygen concentrations around the bar circumference
%will change, sometimes causing areas to become negative.  When oxygen
%concentrations change, erevO2 changes so we must loop until the old and
%new erevO2 are within our error limit.

while numel(find(abs(oldErevO2-corrosion.erevO2)>perror.pot))>0

   %Increment firstTimeThrough as this will be used as a counter to exit
   %if we get stuck in finding a root.

   firstTimeThrough=firstTimeThrough+1;

   %Call routine to evaluate coupling.

   [icorr,ecorr,g,cflag]=coupling_multi(result,corrosion,cflag,coef,dx,...
                        g,ecorr,perror,kg,cv,icorr);

   %Identify locations where coupling has occurred in the cathodic region
```

```
%where oxygen is present.  These areas are the locations where coupling
%will change the local oxygen concentrations which will cause changes
%in erevO2

cflag.cathodicCouplingLocation=icorr.maxCathodeOxygen>0;

%Check if coupling caused an increase in g in oxygenated areas.

if numel(find(cflag.cathodicCouplingLocation==1))>0

   %Set the oldErevO2 to the current erevO2 as coupling has caused an
   %increase in oxygen consumption around the bar which will result in
   %a change to erevO2 or ilim.

   oldErevO2=corrosion.erevO2;

   %Set g.working to g.coupled as we want to evaluate the coupled
   %condition on the oxygen concentrations around the bar.

   g.working=g.coupled;

   %Call pde to solve for new [O2] concentrations.

   result=pdeResolveSlab(2,cv,g,result,pdemesh,c,a,f,d,perror,...
                         time,nodes,corrosion);

   %If some values are negative, set to the o2 bulk limit in order to
   %update the kinetics and erevO2.  Use the average of the o2
   %consumption rate.

   averageOxygenDepletion=mean(g.working(result.bar_seg(:,2)<perror.o2Bulk,2),2);

   result.bar_seg(result.bar_seg(:,2)<perror.o2Bulk,2)=-averageOxygenDepletion;

   %Update kinetics for the uncoupled condition using the updated
   %[O2]b.

   [kg,corrosion]=tafelSlab(corrosion,result.bar_seg);

   %Update g.uncoupled using the new kinetics.  Use a blended approach
   %so that we don't jump around too much.

   g.uncoupled(:,2)=0.2*kg.g+0.8*g.uncoupled(:,2);

   %Update g.coupled with new g.uncoupled at all locations where
   %coupled cathodic reactions are not occurring.

   g.coupled(cflag.cathodicCouplingLocation==0,2)=…
      g.uncoupled(cflag.cathodicCouplingLocation==0,2);

   %Update oxygen concentrations around the bar.  Set gworking to
```

```
%the modified gcoupled.

g.working=g.coupled;

%Call pde to solve for new [O2] concentrations.

result=pdeResolveSlab(2,cv,g,result,pdemesh,c,a,f,d,perror,...
                      time,nodes,corrosion);

%Check if negative [O2] is present.

if numel(find(result.bar_seg(:,2)<-perror.o2Bulk))>0

   %Store current cflag.depletion as this represents the uncoupled
   %condition.  When we pass the new variables to o2_adjust a new
   %cflag.depletion will be created which we don't want as it does
   %not represent the uncoupled condition...rather it represents
   %the coupled condition.

   depletionTemp=cflag.depletion;

   %Call o2AdjustSlab to reduce g to find our limiting corrosion
   %current density under coupled conditions.

   [g,cflag,corrosion,result,ecorr,icorr,kg]=o2AdjustSlab(g,result,nodes,time,...
                      pdemesh,c,a,f,d,perror,cv,cflag,corrosion,ecorr,icorr,kg);

   %Identify locations where coupling caused increased O2
   %consumption resulting in a reduction in g so that O2 remains
   %within the error tolerances.

   coupledCurrentChange=g.working(:,2)<g.coupled(:,2);

   modifyIcorrMax=coupledCurrentChange & cflag.cathodicCouplingLocation;

   icorr.max(modifyIcorrMax)=…
       g.working(modifyIcorrMax,2).*corrosion.faraday.*corrosion.o2_number;

   %Reset cflag.depletion to the stored values as these represent
   %the uncoupled condition while the new values represent the
   %coupled condition.

   cflag.depletion=depletionTemp;

   %Update guncoupled to reflect changes caused by coupling.

   [kg,corrosion]=tafelSlab(corrosion,result.bar_seg);

   g.uncoupled(:,2)=0.2*kg.g+0.8*g.uncoupled(:,2);

end
```

```
    else

        %We don't have any oxygen being used in the cathodic regions so we
        %can break out of this loop.

        break;

    end

    %Update currentDissolvedO2.

    corrosion.currentDissolvedO2=bulk2dissolved(corrosion,result.bar_seg);

    %Update corrosion potentials around the bar for the new g uncoupled.

    [ecorr,icorr,g]=potential_bar(g,kg,corrosion,ecorr,icorr,result,cv);

    %Update location of potentials around the bar for the new g uncoupled.

          [cflag]=find_transition(cv,ecorr,cflag);

    %Allow the routine to go for 10 repetitions.  If no minimum is achieved
    %exit as we are likely close to a solution.

    display (firstTimeThrough);

    message=['Year = ',num2str(cflag.year),' Month = ',num2str(cflag.month)];

    display (message);

    erevOldAll(:,firstTimeThrough)=oldErevO2;
    erevAll(:,firstTimeThrough)=corrosion.erevO2;

    if firstTimeThrough==10

        %We are caught in a local minima so exit and use the values
        %obtained as they are very close to where we want to be.

        display (firstTimeThrough);

        break;

    end

end

%O2 concentrations are within the set limits or we haven't changed
%gO2.  Due to smoothing of the gO2 curve we sometimes get regions
%of the bar which have O2 concentrations that are slightly outside
%of the O2 target.  These small variations do not change
```

```
%ecorr.uncoupled or icorr.coupled therefore just zero them out.

result.bar_seg(result.bar_seg(:,2)<0,2)=perror.o2Bulk;

end
```

C.28 modify_geometry

```
function [dm]=modify_geometry(d,n_elements)

%Routine to add more boundary segments to the bar area.

%d=original decomposed geometry matrix.
%dm=modified decomposed geometry matrix.

%Original decomposed geometry matrix has x elements the last 2 are related
%to the bar. First find the number of columns in the matrix as the last 2
%are the only ones related to the bar.

number_columns=size(d,2);
start_column=number_columns-2;

%Increase the bar elements.

angle_increment=(pi)/n_elements;

%Store current boundary segments for the geometry as these will be written over
%when the new segments are calculated.

dm=d;

%Obtain geometry of bar from column x-2.

x_centre=d(8,number_columns);
y_centre=d(9,number_columns);
radius=d(10,number_columns);

%Set old starting position.

x_start_old=x_centre;
y_start_old=y_centre+radius;

%Loop through the number of new elements and create new elements.

for i=1:n_elements

   x_end=x_centre-radius*sin(angle_increment*i);
   y_end=y_centre+radius*cos(angle_increment*i);

   dm(1,i+start_column)=1;
   dm(2,i+start_column)=x_start_old;
```

```
    dm(3,i+start_column)=x_end;
    dm(4,i+start_column)=y_start_old;
    dm(5,i+start_column)=y_end;
    dm(6,i+start_column)=0;
    dm(7,i+start_column)=1;
    dm(8,i+start_column)=x_centre;
    dm(9,i+start_column)=y_centre;
    dm(10,i+start_column)=radius;

    x_start_old=x_end;
    y_start_old=y_end;

end

end
```

C.29 nernst

```
function [e]=nernst(concentration,corrosion)

%Function to modify the standard potentials according to the concentrations
%in the electrolyte.  Currently only two electrochemical reactions are
%considered.

%Anodic Reaction - Fe2+ + 2e- == Fe
%Cathodic Reaction - O2 + 2 H20 + 4e- == 4OH-

%Nernst Equation takes the following form:
%         2.303 RT     [A]^a [B]^b
%E = Eo + -------- log -----------
%           nF         [C]^c [D]^d
%Where:
%   a[A] + b[B] == c[C] + d[D]

%Convert concentrations of mmol/mm3 to mol/litre.

concentration=concentration.*1000;

e=corrosion.eoO2Std+((2.303*corrosion.r*corrosion.temp)/...
          (corrosion.fe_number*corrosion.faraday)).*...
          log10(concentration/(10^(corrosion.pH-14))^4);

end
```

C.30 node2Seg

```
function seg=node2seg(segments,res)

%Function to average the node results within each control segment for
%comparison in later routines.
```

```
%Determine size of the results matrix.

node_incr=size(res,1);
node_incr=floor((node_incr-1)/(segments));
time=size(res,2);
seg=zeros(segments,time);

%Create a matrix labelling number of segments

list=linspace(1,segments,segments);

%Identify low index for each segment.

low=list*node_incr-node_incr+1;

%Identify the high index for each segment.

high=list*node_incr+1;

%Take the mean from each node value that resides between the low to high
%index for each segment.

for year=1:time

   for segment=1:segments

      seg(segment,year)=(res(low(segment),year)+res(high(segment),year))/2;

   end

end

end
```

C.31 o2AdjustSlab

```
function
[g,cflag,corrosion,result,ecorr,icorr,kg]=o2AdjustSlab(g,result,nodes,time,pdemesh,c,a,f,
d,...
                              perror,cv,cflag,corrosion,ecorr,icorr,kg)

%If oxygen has been depleted at some point around the bar this function is
%called to adjust the oxygen consumption rate at the bar surface (g_o2) so
%that an approximation of the ilim condition is identified. The rules that
%are used in this routine are as follows:
%   if [O2]>0 and g=gmax- No change to g.
%   if [O2]>0 and g<gmax - Increase g.
%   if [O2]<0 and g<=gmax - Lower g.

%Identify the starting g at each segment (including chloride effects) as
```

```
%this is used to ensure the algorithm doesn't cause g in locations to
%exceed the maximum kinetic condition.  If the kinetics change due to
%changes in oxygen concentration then gWorkingOld will be modified in those
%locations accordingly.  erev is taken care of in earlier algorithms, all
%we are interested in here is to make sure that the oxygen consumption on
%the bar surface results in oxygen concentrations that are positive with
%gworkingOld or are above zero with g at some value smaller than
%gworkingOld.

gWorkingOld=g.working(:,2);

%Initialize matrices used in this algorithm.

count=1;
exitCount=1000;
negOxLoc=result.bar_seg(:,2)<-perror.o2Bulk;
posOxLoc=ones(cv.segments,1);
adjFactorAll=zeros(cv.segments,exitCount);
resultAll=adjFactorAll;
gAll=adjFactorAll;
adjFactor=ones(cv.segments,1);
adjustmentModifier=10;
adjustment=ones(cv.segments,1);
adjFactorAll(:,count)=adjFactor;
gAll(:,count)=g.working(:,2);
resultAll(:,count)=result.bar_seg(:,2);

%Check if we are coupled and if so, set the parameters which sort the
%result in the proper sequence.

if cflag.condition==1

   %We are coupled so find the locations where coupling has occurred.

   coupledLocations=g.working(:,2)~=g.uncoupled(:,2);

   if cflag.type==2 || cflag.type==3

      %We have a single cathode.  Identify the point around which all
      %sorting occurs.

      coupledToBottom=find(coupledLocations==1,1,'first');
      coupledToTop=coupledToBottom-1;

   elseif cflag.type==4

      %We have two cathodes.  First identify the first cathode and the
      %points around sorting occurs.

      firstCathodeToBottom=find(coupledLocations==1,1,'first');
      firstCathodeToTop=firstCathodeToBottom-1;
```

```
        %Now identify the second cathode.

        secondCathodeToBottom=…
find(coupledLocations(cflag.lastCathodeAnodeOverCathode:cv.segments)==1,1,'first');
        secondCathodeToTop=secondCathodeToBottom-1;

    end

end

%Start loop to find maximum g with minimum [O2] on the bar surface.

while (numel(find((result.bar_seg(:,2)<-perror.o2Bulk)==1))>0 ||...

numel(find((abs(g.working(:,2))<abs(gWorkingOld))&(result.bar_seg(:,2)>perror.o2Bulk)=
…
    =1))>0) && count<exitCount

    %Start counter which tracks the number of loops and the precision of
    %the changes to g.

    count=count+1;

        %Identify locations where we have gone from positive O2 to negative O2
        %as when this happens we reduce the adjustment factor.

    segPos2Neg=posOxLoc&negOxLoc;

    %Update adjustment factor at locations where we have changed sign.

    adjustment(segPos2Neg)=adjustment(segPos2Neg)/adjustmentModifier;

    %Identify segments which have [O2] more positive than our error limit.

    posOxLoc=result.bar_seg(:,2)>0;

    %Locations where g is less than gmax.

    segLessGmax=abs(g.working(:,2))<abs(gWorkingOld);

    %Locations where g is less than gmax but [O2] is positive.

    segIncreaseG=posOxLoc&segLessGmax;

    %Identify segments which are adjusted.

    segCriteria=segIncreaseG|negOxLoc;

    %Set size of adjustment based on how close we are to the target and the
```

```
%number of times we have passed through this routine.
      closeToTarget=abs(result.bar_seg(:,2)/perror.o2Bulk);

if count<100

   %Set modification factor to the following values:
      %closeToTarget>10 - adjustment=0.01;
      %closeToTarget<10 but > 1 - adjustment=0.001;
      %closeToTarget<1 - adjustment=0.0001;

   greaterThan=closeToTarget>8;
   betweenValues=closeToTarget<=8 & closeToTarget>=1;
   lessThan=closeToTarget<1;

   %Increments that are increasing.

   adjustment(greaterThan & posOxLoc)=0.1;
   adjustment(betweenValues & posOxLoc)=0.01;
   adjustment(lessThan & posOxLoc)=0.001;

   %Increments that are decreasing.

   adjustment(greaterThan & negOxLoc)=0.01;
   adjustment(betweenValues & negOxLoc)=0.001;
   adjustment(lessThan & negOxLoc)=0.0001;

elseif count>=100 && count<200

   %Set modification factor to the following values:
      %closeToTarget>10 - adjustment=0.01;
      %closeToTarget<10 but > 1 - adjustment=0.001;
      %closeToTarget<1 - adjustment=0.0001;

   greaterThan=closeToTarget>8;
   betweenValues=closeToTarget<=8 & closeToTarget>=1;
   lessThan=closeToTarget<1;

   %Increments that are increasing.

   adjustment(greaterThan & posOxLoc)=0.01;
   adjustment(betweenValues & posOxLoc)=0.001;
   adjustment(lessThan & posOxLoc)=0.0001;

   %Increments that are decreasing.

   adjustment(greaterThan & negOxLoc)=0.001;
   adjustment(betweenValues & negOxLoc)=0.0001;
   adjustment(lessThan & negOxLoc)=0.00001;

elseif count>=200 && count<400
```

```
    %Set modification factor to the following values:
       %closeToTarget>10 - adjustment=0.01;
       %closeToTarget<10 but > 1 - adjustment=0.001;
       %closeToTarget<1 - adjustment=0.0001;

    greaterThan=closeToTarget>8;
    betweenValues=closeToTarget<=8 & closeToTarget>=1;
    lessThan=closeToTarget<1;

    %Increments that are increasing.

    adjustment(greaterThan & posOxLoc)=0.001;
    adjustment(betweenValues & posOxLoc)=0.0001;
    adjustment(lessThan & posOxLoc)=0.00001;

    %Increments that are decreasing.

    adjustment(greaterThan & negOxLoc)=0.0001;
    adjustment(betweenValues & negOxLoc)=0.00001;
    adjustment(lessThan & negOxLoc)=0.000001;


end

%Increase adjustment factor for segments where g is less than gmax and
      %[O2] is positive.

adjFactor(segIncreaseG)=adjFactor(segIncreaseG)+adjustment(segIncreaseG);

%Decrease adjustment factor for segments where negative oxygen is
%present.

adjFactor(negOxLoc)=adjFactor(negOxLoc)-adjustment(negOxLoc);

%Limit adjustment factor to values between 1 and a minimum value

adjFactor(adjFactor>1)=1;
adjFactor(adjFactor<0.00001)=0.00001;

%Reduce g progressively at each segment.  Once a segment reaches its
%target value, no further changes are allowed unless subsequent changes
%to adjacent segments cause the held segment to fall out of the target
%value.

g.working(segCriteria,2)=gWorkingOld(segCriteria).*adjFactor(segCriteria);

%Ensure g does not exceed the initial values which represent the maximum.

g.working(g.working(:,2)<gWorkingOld,2)=gWorkingOld(g.working(:,2)<gWorkingOld);

%Force curve to fit one of the three basic geometries at the beginning
```

```
%of the analysis.

if count<=50

   %Force fit g.working into one of the three base corrosion potential
   %configurations.

   gTemp=ecorrGeometry(g.working(:,2),corrosion,kg,result,cv);

   %Update g.working with the new smoothed values created by
   %ecorrGeometry.  Identify which segments are being modified and only
   %modify those segments which are negative.

   segmentsUpdate=segCriteria & negOxLoc;

   g.working(segmentsUpdate,2)=gTemp(segmentsUpdate);

end

%Check if uncoupled or coupled.  If uncoupled sort from top to bottom.
%If coupled condition, don't sort for now.

if cflag.condition==0

   %We are uncoupled so sort from top to bottom.

   g.working(:,2)=sort(g.working(:,2),'ascend');

   %Update adjustment factor after the curve fitting and ascending is
   %completed.

   adjFactor=g.working(:,2)./gWorkingOld;

end

if cflag.condition==1 && count<300

   %We are coupled so break the bar into two components as follows:
      %Coupled area to bottom of bar - Sort low to high.
      %Coupled are to top of bar - Sort low to high.

   %Find where the first coupled segment is located.

   if cflag.type==2 || cflag.type==3

      %Sort from the first coupled to the bottom of the bar.
            g.working(coupledToBottom:cv.segments,2)=…
                  sort(g.working(coupledToBottom:cv.segments,2),'ascend');

      %Sort from the first coupled to the top of the bar.
```

```
                g.working(1:coupledToTop,2)=…
                        sort(g.working(1:coupledToTop,2),'ascend');

        elseif cflag.type==4

            %We have 2 cathodic regions so sort the top region first.

            g.working(firstCathodeToBottom:cflag.lastCathodeAnodeOverCathode,2)=…

            sort(g.working(firstCathodeToBottom:cflag.lastCathodeAnodeOverCathode,2),…
                'ascend');

g.working(1:firstCathodeToTop,2)=sort(g.working(1:firstCathodeToTop,2),'ascend');

            %Sort the bottom region.
            g.working(secondCathodeToBottom:cv.segments,2)=…
              sort(g.working(secondCathodeToBottom:cv.segments,2),'ascend');
            g.working(cflag.lastCathodeAnodeOverCathode:secondCathodeToTop,2)=…
                sort(g.working(cflag.lastCathodeAnodeOverCathode:…
                 secondCathodeToTop,2),'ascend');

        end

        %Update adjustment factor after the curve fitting and ascending is
        %completed.

        adjFactor=g.working(:,2)./gWorkingOld;

    end

        %Limit adjustment factor to values between 1 and a minimum value

    adjFactor(adjFactor>1)=1;
    adjFactor(adjFactor<0.00001)=0.00001;

    %Reduce g progressively at each segment.  Once a segment reaches its
    %target value, no further changes are allowed unless subsequent changes
    %to adjacent segments cause the held segment to fall out of the target
    %value.

    g.working(segCriteria,2)=gWorkingOld(segCriteria).*adjFactor(segCriteria);

    %Call pde to solve for new [O2] concentrations.

    result=pdeResolveSlab(2,cv,g,result,pdemesh,c,a,f,d,perror,time,nodes,corrosion);

    %Update which segments are now negative.

    negOxLoc=result.bar_seg(:,2)<0;

    adjFactorAll(:,count)=adjFactor;
```

```
   gAll(:,count)=g.working(:,2);
   resultAll(:,count)=result.bar_seg(:,2);

end

%Identify locations where g<kg.g as these are the locations where g is
%at an ilim condition.

cflag.depletion=result.bar_seg(:,2)<10*perror.o2Bulk;

%In some conditions, the coupled oxygen consumption that results from this
%calculation becomes less than the uncoupled oxygen consumption rate. When
%this occurs, fix the coupled oxygen consumption to the uncoupled oxygen
%consumption.  This condition can only be applied when we are in the
%coupled condition.

if cflag.condition==1

g.working(g.working(coupledLocations,2)>g.uncoupled(coupledLocations,2),2)=g.uncou
pled(g.working(coupledLocations,2)>g.uncoupled(coupledLocations,2),2);

end

%Display an oops if we exceed 1000 calculations....this is for my
%de-bugging.

if count==1000

   display 'oops';

end

%Once passing criteria is met, set all oxygen concentrations on the bar
%surface that are near the error limit to the oxygen consumption rate as
%this value represents the minimum oxygen concentration that will sustain
%the corrosion process ie: 0 concentration will not occur as oxygen moves
%into the control volume at the same rate it moves out ie: the control
%volume concentration is constant.  Before changing oxygen concentrations,
%store the oxygen results around the bar for later comparison.

result.barOxygen=result.bar_seg(:,2);

%Now update results to the oxygen depletion rate by setting all oxygen
%concentrations in the areas which are oxygen limited to the oxygen
%consumption rate for that area.

result.bar_seg(cflag.depletion,2)=-g.working(cflag.depletion,2);

%Update erev.

[kg,corrosion]=tafelSlab(corrosion,result.bar_seg);
```

```
%Update dissolved oxygen in the electrolyte.

corrosion.currentDissolvedO2=bulk2dissolved(corrosion,result.bar_seg);

display (count);

message=['Year = ',num2str(cflag.year),' Month = ',num2str(cflag.month)];

display (message);

end
```

C.32 oxygenConsumption

```
function [g,result,corrosion,cflag]=oxygenConsumption…
      (g,result,corrosion,cflag,nodes,time,pdemesh,c,a,f,d,perror,cv)

%Routine to take the bulk oxygen results, convert them to dissolved oxygen
%and then evaluate whether negative oxygen concentrations have occurred or
%whether oxygen concentrations have moved away from the starting
%conditions.  Both scenarios result in ecorr.uncoupled being changed.

%Establish current dissolved oxygen concentrations.

currentDissolvedO2=bulk2dissolved(corrosion,result.bar_seg);

%Check if the new dissolved o2 is different than the old.  If it is, update
%erev accordingly.

if numel(find(currentDissolvedO2~=corrosion.oldDissolvedO2))>0

   %Set all negative values to error limit to see if it results in a lowering
   %of erevO2 which lowers icorr and hence g causes the negative oxygen
   %concentrations to disappear.

   result.bar_seg(result.bar_seg(:,2)<0,2)=perror.o2;

   %Call routine to adjust erev for O2.

   [g,result,corrosion]=…
         eRevAdjust(g,result,nodes,time,pdemesh,c,a,f,d,perror,cv,corrosion);

   %Check if results have negative oxygen values.

   if find(result.bar_seg(:,2)<0)>0

      %Negative values exist so reduce g until O2 is within our error
      %limits.
```

```
        [g,cflag,corrosion]=o2AdjustSlab(g,result,nodes,time,...
              pdemesh,c,a,f,d,perror,cv,cflag,corrosion);

    end

end

%Set old dissolved oxygen concentration to the final result obtained in
%this algorithm as this will be used in future calculations.

corrosion.oldDissolvedO2=result.bar_seg(:,2);

end
```

C.33 pdeResolveSlab

```
function [result]=pdeResolveSlab(species,cv,g,result,pdemesh,c,a,f,d,perror,...
                time,nodes,corrosion)

%Routine that takes the boundary conditions and runs the pde module which
%is then processed to return the final concentrations within the model
%space.

%Update boundary conditions using the revised g.

[b]=boundarySlab(species,cv.segments,g.working,corrosion);

%Call parabolic function to solve PDE for the updated boundary conditions.

result.uO2(:,:)=parabolic(result.u0(:,species),time.tlist,...
    b,pdemesh.p,pdemesh.e,pdemesh.t,c(species),a(species),f(species),...
    d(species),perror.rtol,perror.atol);

%Store species results from the nodes which represent the interface between
%the concrete and bar.

result.bar_node(:,species)=result.uO2(nodes.bar,time.step_rem);

%Average the results of the nodes which makup each segment.

result.bar_seg(:,species)=node2seg(cv.segments,result.bar_node(:,species));

end
```

C.34 PotentialBar

```
function [ecorr,icorr]=potentialBarSlab(g_o2,kg,corrosion)

%Function to convert the oxygen consumption rate to icorr and ecorr at each
%point along the bar.

%Conversion based on the following paper.  Moreno, M., Morris, W., Alvarez,
```

```
%M., Duffo, G., 2004, Corrosion of reinforcing steel in simulated concrete pore
%solutions.  Effect of carbonation and chloride content, Corrosion Science,
%46:2681-2699.
%g_o2 = oxygen consumption rate in mmol/mm3/s.
%corrosion = variable that includes ecorr, icorr, slope, y-intercept and chloride test data.

%Find icorr using g which is proportional to the current density as per
%Kennell, G., Evitts, R., Heppner, K., 2008, A critical crevice solution
%and IR drop crevice corrosion model, Corrosion Science, 50:1716-1725.
%Control volume height is deleted from the calculation as this volume
%does not exist within the finite element model.  So we are only
%interested in the rate of current on the bar surface which is
%proportional to the rate of oxygen consumption.

%g=i/(F x n)

%   g = oxygen consumption rate in mols/mm2/s.
%   i = current density in A/mm2.
%   F = Faradays constant = 96500 Coulomb/mol
%   n = number of electrons consumed in reduction of oxygen

icorr=-g_o2*corrosion.o2_number*corrosion.faraday;

%Chloride levels will be different at each point around the bar so
%determine the potential at each point using the two different slopes.

ecorr=kg.m1.*log10(icorr)+kg.b1;
pot_curve2=kg.m2.*log10(icorr)+kg.b2;

%Select the correct potential based on whether icorr occurs higher or lower
%than i_int.

ecorr(icorr>kg.i_int)=pot_curve2(icorr>kg.i_int);

end
```

C.35 TafelSlab

```
function [kg,corrosion]=tafelSlab(corrosion,barResult)

%Function to determine the tafel slopes and io for each kinetic of
%corrosion curve at each node using the chloride concentrations that exist
%at each location.
%Output is organized as follows:
%   - m1, m2 is the slope of curve 1 and curve 2 respectively.
%   - b1, b2 is the y-intercept of curve 1 and curve 2 respectively.
%   - i_int is the current flow at the intersection between curve 1 and
%     curve 2.
%   - ecorr is the mixed corrosion potential assuming no oxygen limitations.
%   - icorr is the mixed corrosion current density assuming no oxygen
```

```
%     limitations.

segments=size(barResult,1);

%Preallocate arrays for speed.

m1=zeros(segments,1);
b1=m1;
m2=m1;
b2=m1;
i_int=m1;
e_int=i_int;

%Convert bulk oxygen content to dissolved oxygen content.

dissolvedO2=bulk2dissolved(corrosion,barResult);

for seg=1:segments

    %Update iron dissolution curves for each segment given the current
    %chloride conditions.
    [m1(seg),b1(seg),m2(seg),b2(seg),i_int(seg),e_int(seg)]=…
        chloride_slope(corrosion,barResult(seg,1));

    %Update the oxygen reduction curve for each segment given the current
    %oxygen conditions.

    corrosion.erevO2(seg,1)=nernst(dissolvedO2(seg),corrosion);

end

%Update oxygen reduction curve for the new erev.

corrosion.b_o2=corrosion.erevO2-corrosion.m_o2*log10(corrosion.irev_o2);

%Find intersection between the cathodic reaction and the anodic reaction
%ie: what is icorr assuming no ilim conditions. Since there are 2 iron
%kinetic corrosion curves two intersections will be derived.  Select the
%lower of the two as that represents the correct intersection.

icorr_1=10.^((b1-corrosion.b_o2)./(corrosion.m_o2-m1));
icorr_2=10.^((b2-corrosion.b_o2)./(corrosion.m_o2-m2));

icorr=min(icorr_1,icorr_2);

%Determine oxygen consumption rate based on icorr.

kg.g=-icorr./(corrosion.faraday*corrosion.o2_number);

%Place remainder of results in a structured array for future re-call.
```

```
kg.m1=m1;
kg.b1=b1;
kg.m2=m2;
kg.b2=b2;
kg.i_int=i_int;
kg.e_int=e_int;
kg.ecorr=corrosion.m_o2.*(b2-corrosion.b_o2)./...
                    (corrosion.m_o2-m2)+corrosion.b_o2;
kg.icorr=10.^((corrosion.b_o2-b2)./(m2-corrosion.m_o2));

end
```